A study of some aspects of extensive air showers at sea level

Mark John Enderby

A STUDY OF SOME ASPECTS OF EXTENSIVE AIR SHOWERS AT SEA LEVEL

By

Mark John Enderby, B.Sc. (Durham)

A thesis submitted to the University of Durham
for the degree of Doctor of Philosophy

Department of Physics,
Durham University, U.K.

DECEMBER, 1982

CONTENTS

ABSTRACT

An experiment to search for tachyons, associated with extensive air showers, using an unshielded plastic scintillator is described. No evidence for their existence has been found. A review of tachyon theory and previous searches is given.

The design and implementation of an automatic data collection system for the Durham Air Shower Array, using a PET microcomputer, is described. In addition various improvements to the array are described. The performance of the array and the methods of data analysis are discussed.

The array has been operated with five detectors and the results compared to those expected by simulation. The power of the zenith angle distribution has been determined and found to correspond to previous determinations. The size spectrum has also been determined in the range 2.10^4 to 10^6 electrons. Although the slopes are in agreement with other measurements the absolute rate is low. It is concluded that this is mainly due to the lack of redundancy in the array and that more detectors are required.

PREFACE

This thesis describes the work performed by the author at Durham University, while under the supervision of Dr. F. Ashton, during the period 1978 to 1982.

During this time, the author has carried out an experiment to search for tachyons. Also he has been responsible for the design and implementation of an automatic data collection system as well as other improvements to the Durham Air Shower Array. The array was run for a short time and various air shower parameters were measured for showers of size 2.10^4 to 10^6 electrons.

The results of the tachyon experiment have been previously reported by Abdullah et al (1979) in the Proceedings of the XVIth International Conference on Cosmic Rays (Kyoto 1979).

ACKNOWLEDGEMENTS

I would like to thank Professor A. W. Wolfendale F.R.S. for the use of the Physics Department's laboratories and his interest and encouragement with this work.

I am grateful to my supervisor, Dr. F. Ashton, for his help, guidance and invaluable suggestions throughout this work. I would like to thank all the members of the group, both past and present for their friendly co-operation and assistance. In particular I would like to thank Dr. M. Abdullah and Dr. J. Fatemi for many constructive discussions. Mr. K. Tindale, Mr. W. Leslie and the staff of the main workshop, Mr. T. Jackson and the staff of the electronics workshop and Mr. D. Jobling and the staff of the student workshop are thanked for their help during the period of this work.

The Science and Engineering Research Council are thanked for the provision of a Studentship and for the facilities provided by the Northumbrian Universities Multiple Access Computer.

Finally I am indebted to my wife for her help and encouragement during this research and her assistance in typing and in drawing the diagrams.

CHAPTER 1

INTRODUCTION

1.1 DISCOVERY

It was the discovery of an unknown, highly ionising agency by Elster and Geitel (1900) and Wilson (1901), during experiments concerning the conduction of electricity in the atmosphere, which started investigation into what have become known as Cosmic Rays. Their experiments with shielded electroscopes led to the conclusion that there must be some external ionising agency of great penetrability. Though Wilson speculated on an extraterrestial source, the lack of evidence for a reduction of the effect, even under ' many feet of rock ' led him to agree with Geitel that it seemed to be a property of the air itself. However, no matter what precautions were taken to isolate these detectors, some residual ionisation was shown to be present. If γ-rays from the earth were indeed to blame, then investigation of the change of ionisation with height would confirm it. So Hess (1911,1912) made balloon ascents to 5km. Upto about 1km a slight decrease was noted, but above this, the ionisation increased rapidly. From these experiments the extraterrestial origin for the ionising agency was evident. Hess's work was confirmed by Kolhörster (1913) who extended the data to 9km.

Further confirmation came from Millikan and Cameron (1926) who measured the absorption of the radiation in water and found it to be similar to that in an equivalent mass of air. This indicated a radiation which is absorbed by air on its downward path with no local generation. It was Millikan who first called the radiation Cosmic Radiation.

1.2 NATURE OF THE COSMIC RADIATION

Once the existence of the cosmic radiation had been confirmed, the next question was its nature. Further work in this field had to await the development of two new instruments. Skobeltzyn (1927), while using a cloud chamber between the poles of a magnet to observe β-radiation, noticed other tracks which were hardly deflected by the magnetic field. He attributed these to Compton recoil electrons, secondary to the supposed primary γ-radiation. At the same time, Bothe and Kolhörster (1928,1929) were developing a technique using Geiger-Muller counters. Using a counter, single charged particles could be detected, but background radiation remained a problem. However, if two or more counters, placed in a straight line, fired simultaneously, then it indicated that a particle of high penetrating power had passed through all of them. This 'coincidence' method attained great importance in further investigations. It was concluded that the radiation consisted of charged particles of very high energy, ie. greater than 10^9eV.

Clay (1927) set out to observe the variation of intensity of cosmic rays with latitude, on a voyage from Amsterdam to Java. Further measurements in 1932 enabled him to confirm that the intensity varied with the geomagnetic field strength and conclude that primary cosmic rays were indeed charged particles.

The theoretical explanation of this latitude effect was carried out by Lemâitre and Vallarta (1933) using the calculations of Størmer (1930), which he had used to, unsuccessfully, describe the aurora. Using this theory, the measurement of intensity could be used to determine the ratio of momentum to charge of the particles. Another outcome of the theory was that it predicted an excess of radiation from the west, if the particles were mostly

positively charged and vice-versa if they were mostly negative charged. Johnson (1935) concluded that the majority of primary cosmic rays were positively charged due to the stronger intensity from the west and suggested that they were protons. This effect is known as 'East-West' asymmetry. This was unexpected because most of the recognisable particles, observed in cloud chambers, had been electrons.

Other experimenters set about investigating the interactions of cosmic rays with matter in the hope of shedding light on their nature. Rossi (1935) observed the counting rate of three aligned Geiger-Muller counters in coincidence, with absorbers being placed between them. An increase in absorber thickness at first led to a rapid decrease in count rate but this became slower at greater thickness. This was interpreted as being due to the radiation consisting of two components, 'soft' and 'hard'. The former is rapidly absorbed while the latter is absorbed gradually. Rossi also discovered the phenonemon of groups or 'showers' of particles when a triangular arrangement of counters, under a lead absorber, triggered simultaneously.

This was also observed by Blackett and Occhialini (1933) using a counter controlled cloud chamber. They concluded that the positive particles were not protons due to their low specific ionisation and long range and it was determined that their mass must be nearer to that of an electron. However the development of a more exact theory of the interactions of charged particles with matter, by Bethe and Heitler (1934), indicated that radiation losses were much more important than those due to ionisation. This meant that the observed particles, to travel through large amounts of absorber as they are seen to do, could not be electrons.

It had been noted by Auger et al (1939) and others that showers also occured in the absence of absorbers and this was taken to mean that showers could be initiated in the atmosphere. Bethe and Heitler's theory enabled a model of this shower process to be developed. Either an electron undergoes bremsstrahlung to produce a photon or a photon undergoes pair production and produces an electron-positron pair. These products then undergo similar interactions. The resulting cascade then builds up until each particle's energy is too low to allow further interaction except by Compton scattering, photo-electric absorption and ionisation.

In order to identify the unknown, highly penetrating, particles various researchers investigated the energy loss of cosmic ray particles in lead and iron plates, as observed in a cloud chamber. Street and Stevenson (1937) observed tracks which stopped in the chamber and determined the mass of the particles to be about 130 times that of an electron. This was later refined to be about 200 times. This particle is now known as the muon.

Independently of this, Yukawa (1935) had suggested the existence of a meson as the intermediary of the strong nuclear interaction, and the similarity was eventually taken up. However, difficulties arose as the muon did not undergo strong interaction and also had a different lifetime.

It was not until 1947 that, using the recent development of nuclear emulsions, Lattes et al observed one meson decaying into another. The strongly interacting mesons were called pi-mesons or pions and it was shown that these decayed into muons with the associated production of neutrinos.

Finally, to complete the basic picture of the cosmic ray processes in the atmosphere, was the discovery, in accelerators and cosmic rays, of the neutral pion which decays into two photons. This is the link whereby primary protons can initiate the electron-photon cascade mentioned above. In addition the hard component of muons is produced from charged pions which are also produced when protons interact with nuclei in the atmosphere. This process is fully described in Chapter 8.

1.3 COMPOSITION AND ENERGY SPECTRUM OF THE PRIMARY RADIATION

The primary radiation has been discovered to consist of three components, nuclear (ie nuclei), electronic (ie electrons and positrons) and electromagnetic (ie χ-rays and γ-rays). It is the nuclear component which is of greater interest in the study of extensive air showers (EAS).

With the advent of satellites, direct measurements of the primary energy spectrum and composition can be made and have confirmed the results from previous balloon flights at very high altitudes ($\sim 5 g cm^{-2}$). The principal detectors used in these experiments are nuclear emulsions, scintillation counters and plastic detectors (which can be etched to reveal the particle tracks). However the size of these detectors is limited, as is their exposure time. This means that for energies greater than about 10^{13}eV the flux is too low to provide reliable data. Study of EAS has allowed the energy spectrum to be extended to about 10^{20}eV but they cannot shed much light on the composition because of the lack of knowledge of particle interactions at such high energies. The basic form of the energy spectrum for various components is shown in figure 1.1.

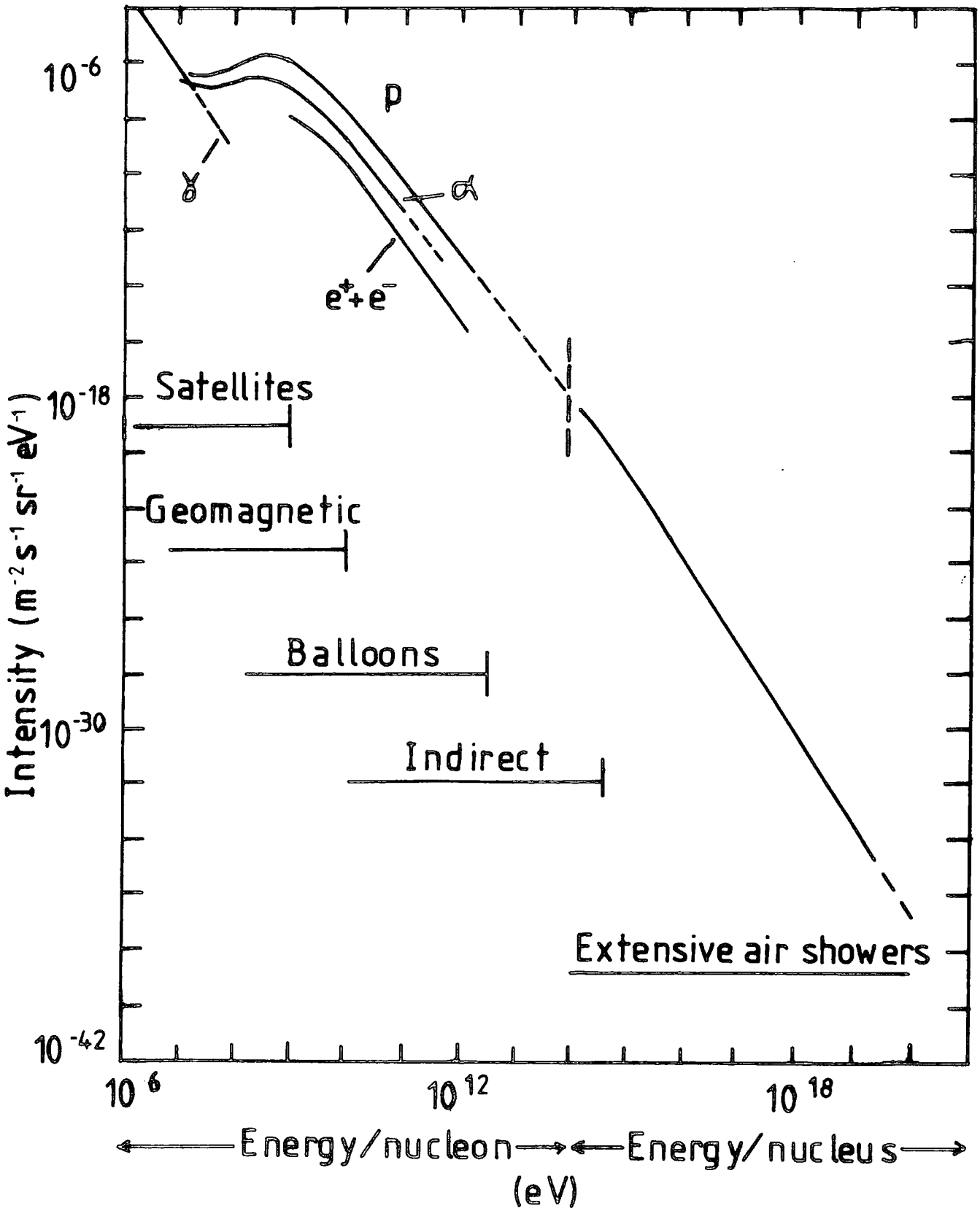

FIGURE 1.1 : Primary Cosmic Ray Spectra (after Wolfendale 1973)

Table 1.1 shows the composition of the primary radiation for various energies (after Juliusson (1975)) normalised to a percentage of the total. A number of interesting points are raised by these results. Firstly, when compared to the universal abundance of elements, the primary cosmic rays have an excess of Li, Be and B nuclei. It is believed that this is due to the fragmentation of heavier nuclei as they pass through the small amount of matter between their source and the Earth. On this basis, the amount of this matter has been estimated as about 4 to 5 gcm^{-2} of hydrogen and hence the average travelling time of the cosmic ray nuclei is around three million years which is significantly smaller than the age of the Universe. Secondly there is a paucity of hydrogen, helium and possibly oxygen and a noticable enhancement of iron (and elements just lighter) when compared with the universal abundance. However this appears not to be due to preferential acceleration for highly charged nuclei since nuclei of charge greater than iron are thousands of times less abundant. Instead, it is suggested that it is a property of the source itself which indicates highly evolved stars. Whether composition changes in the region above 10^{13}eV is very much an open question and longer exposures of detectors on satellites are required.

The overall primary energy can be characterised over a wide range of energies by a power law of the form

$$I(>E) = KE^{-\gamma}$$

where K is a constant, E is the primary energy, I is the intensity and γ is the slope of the spectrum. Figure 1.2, giving recently reported spectra (Hillas 1981) superimposed on the review of Hillas (1975), shows the presently accepted form of the integral

TABLE 1.1 : Composition of Cosmic Rays at High Energies

(after Juliussen 1975)

ATOMIC NUMBER (Z)	ELEMENTS	KINETIC ENERGY PER NUCLEUS (eV)			
		10^{10}	10^{11}	10^{12}	10^{13}
1	Hydrogen	58±5	47±4	42±6	24±6
2	Helium	28±3	25±3	20±3	15±5
3-5	Light Nuclei	1.2±0.1	1.1±0.1	0.6±0.2	
6-8	Medium Nuclei	7.1±0.4	12.2±0.8	14±2	
10-14	Heavy Nuclei	2.8±0.2	6.7±0.5	10±1	
16-24	Very Heavy Nuclei	1.2±0.2	3.6±0.4	4±1	
26-28	Iron Group Nuclei	1.2±0.2	4.5±0.5	10±2	24±7
30	VVH Nuclei		0.007±0.004		

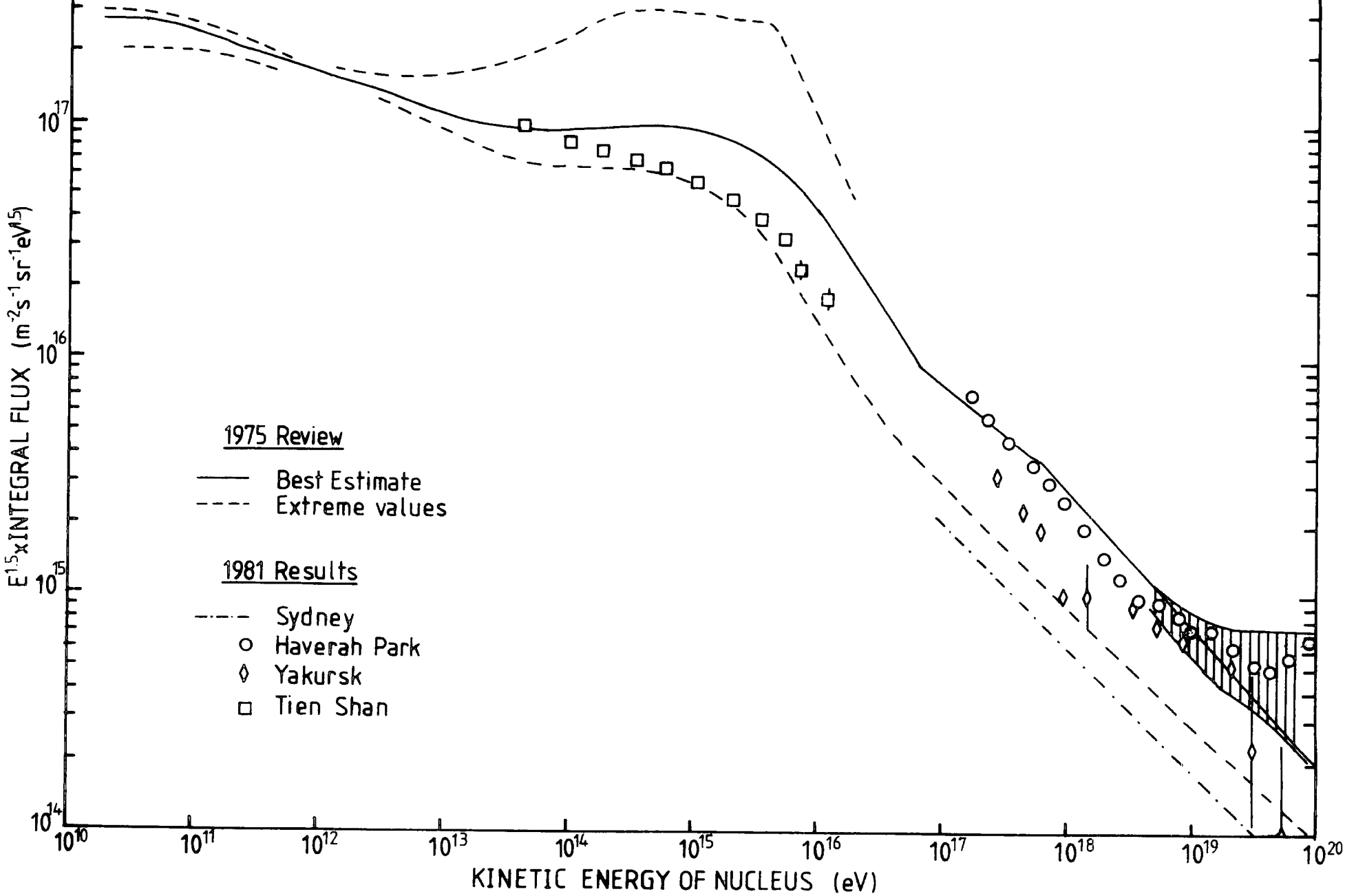

FIGURE 1.2 : Integral Energy Spectrum of the Primary Radiation

energy spectrum. Between 10^{10}eV and 10^{15}eV the slope is given by $\gamma \simeq 1.6$, but around 3.10^{15}eV this changes to $\gamma \simeq 2.0$. This 'knee' has been attributed to a number of phenonema. One suggestion is that this is due to the inability of the galactic magnetic fields to contain various types of particles as their containment rigidities are exceeded. However there is evidence that the proton spectrum steepens at higher rigidities than for heavy nuclei (Hillas 1979) so casting doubt on this explanation. Karakula et al (1974) have suggested that there is a contribution from pulsars in this region of the spectrum. Another explanation has been put forward by Hillas (ibid) who suggests that the steepening may arise nearer the source and be a result of photodisintigration. Other workers are sceptical about the existence of this 'knee'. A detailed determination of the composition in this region would enable clarification of this problem.

It has been suggested by Greisen (1966) and others that there should be a cut-off in the spectrum at around 10^{20}eV. This is due to attenuation, by pair production, of the proton flux by the 2.7K black body relict radiation. No evidence for this has been seen up to the highest energies observed, ie around 3.10^{20}eV (Hillas 1975). However recent results from Haverah Park (Bower et al 1981) have indicated a dip in the flux at around 10^{19}eV which would correspond to the onset of pair production losses, though an alternative explanation would be the rapid escape of particles from the galaxy. One main problem, in explaining the lack of a cut-off, is that the spectrum at these high energies may well be directional since magnetic deflections, at these energies, should be greatly reduced.

1.4 ORIGIN OF THE PRIMARY RADIATION

The questions of the source of cosmic rays and the methods by which they are accelerated to such high energies are still very much open. The main problems that have to be addressed are as follows:

(i) What are the charge spectra and energy at source.

(ii) What is the possibility of acceleration outside the source.

(iii) Is there trapping in an acceleration region by magnetic fields.

(iv) Are there changes of charge spectra due to interactions with the interstellar medium.

(v) Need to account for the remarkable degree of isotropy and constancy of the primary radiation.

The observed primary spectrum has to be a result of a combination of ideas about the above.

The question of the charge spectra has been noted in the previous section, which suggested that the observed primary energy spectrum pointed to sources which are highly evolved. This has led to the idea of supernovae as sources (eg Ginzburg 1964). Taking the energy of particles produced by a supernova to be $\sim 2.10^{49}$erg, distributed uniformily over the whole galactic disc, and the mean time between supernovae to be 40 yr then the rate of ejection of energy is about 2.10^{40}erg s^{-1}. Taking the local cosmic ray density (~1eV) spread over the volume of the galactic disc and the lifetime for particles in the disc of 3.10^{6}yr gives the required energy input of about 2.10^{41}erg s^{-1}. Since there is good agreement between these figures the suggestion is highly attractive. However this would require a high acceleration efficiency. Also the primary spectrum up to about 10^{15}eV, which follows a single

power law, would seem to require a single source, since no fundamental process would give the same power law spectrum in every discrete source, and the power law spectra from many sources, with any dispersion in the spectral index, would not sum to give a power law spectrum.

Other discrete sources have been suggested, eg pulsars, but none can account for the total cosmic ray flux. The high degree of isotropy is also evidence against them.

Fermi (1949) had suggested a diffuse origin of cosmic rays, accelerated stochastically by collisions with moving magnetic fields. This theory has been developed and general opinion now seems to favour a mixture of diffuse and discrete sources.

At high energies, ie above 10^{18}eV, galactic models fail and extragalactic cosmic rays from the local supercluster have been shown to be consistent with present observations (Wdowczyk 1979). However very high power would be required. The question of whether the cosmic ray flux is confined to the galaxy, in whole or in part, is still open to question. However some extragalactic contribution is probably needed to explain the lack of a high energy cut-off and electrons, most likely come from the galaxy due to inverse Compton losses with the microwave background radiation. A summary of evidence is given by Longair (1981) and reproduced in table 1.2.

Among attempts to clarify the position are investigations of anisotropy of very high energy cosmic rays above 10^{17}eV, which would be expected to be little deflected from source and the abundance of Be^{10} in sea sediments (Tanaka 1979). In the latter, it is pointed out that Be^{10} nuclei are produced in the atmosphere by cosmic ray interactions and that variations in intensity should show up by investigating the abundance of Be^{10}

	Galactic Theories		Extragalactic Theories	
	Confinement Volume			
Evidence	Disc	Halo	Supercluster	All Space
1 Cosmic ray electrons	Consistent	Probably consistent	Inconsistent	Inconsistent
2 Chemical composition of light cosmic ray nuclei	Consistent	Consistent	Consistent	Consistent
3 Spectra of cosmic ray sources	Consistent	Consistent	Consistent	Consistent
4 Cosmic ray clocks	Consistent	Consistent	Inconclusive	Inconclusive
5 Transuranic elements	Consistent	Consistent	Inconclusive	Inconclusive
6 γ-rays from π° decays	Consistent	Consistent	Inconclusive	Inconclusive
7 Isotropy of cosmic rays				
10^{11}eV	Consistent	Consistent	Consistent	Consistent
10^{15}eV	Consistent	Consistent	Consistent	Consistent
$\gtrsim 10^{19}$eV	Inconsistent	Inconsistent	Consistent	Consistent
8 Photo-pion and photo-pair production	Consistent	Consistent	Probably consistent	Probably inconsistent for protons. Consistent for Fe nuclei
9 Energy sources for cosmic rays	Consistent with supernovae	Consistent with supernovae	Very powerful sources needed	Extremely powerful sources needed

TABLE 1.2 : Summary of Cosmic Ray Origin Theories (after Longhair 1981)

as a function of depth in ocean sediments. Any departure from a monotonic decrease with depth with a half-life of 1.6 10^6 yr would indicate discrete sources. No evidence was found but improved experiments are now under way.

1.5 SIGNIFICANCE OF COSMIC RAYS

As has been indicated in the previous sections, cosmic ray physics has been responsible for many important discoveries in elementary particle, nuclear and astro- physics. Until the advent of particle accelerators, cosmic rays were the sole source of high energy particles and in this flux were discovered such elementary particles as the positron, muon, pion as well as strange particles. Much information on nuclear interactions has also been found in this manner. Despite the development of large accelerators capable of producing large fluxes of energies up to 10^{12}eV, the cost of constructing much larger ones will ensure that cosmic rays at energies in excess of 10^{12}eV will remain an important source for very high energy nuclear physics. For example, a comparison of ground level observations with the primary spectrum can be used to extend interaction models to above accelerator energies as it is apparent that well established rules governing nuclear interactions below 10^{12}eV (eg Feynman's 'scaling hypothesis') are not as successful as expected at cosmic ray energies.

Another important feature is their bearing on astro-physical phenonema. Many questions have still to be answered about their origin, acceleration and propagation. They can also provide information on the interstellar medium, magnetic fields and

nature of their sources aswell as being a probe into the far reaches of the galaxy and beyond. Thus it can be seen that cosmic rays still retain an important place in future research into nuclear physics and the nature of the universe.

CHAPTER 2

THE AIR SHOWER ARRAY

2.1 INTRODUCTION

The air shower array was built over the period 1973 to 1976 by members of the MARS research group under the supervision of Dr. M. G. Thompson. It was handed over in 1977, minus the digitisation electronics and computer, in order to allow its continued use to trigger the group's flash tube chamber.

The basis of the array is formed by fourteen plastic scintillator detectors arranged in a geometric pattern, modified by the availability of suitable sites. They are supplemented by eight liquid scintillator detectors. However these have not been used and, therefore, are not described here. The layout of the array is shown in figure 2.1.

Each detector is supplied with EHT for the photomultiplier tubes (PMT) and 24V DC for the head amplifiers (which amplify the output of the PMTs) from the laboratory. A third cable is provided to carry the PMT outputs to the laboratory. A fourth cable is kept as a spare. The arrangement of the detector supply cables is given in figure 2.2.

Once the signal has been returned to the laboratory, it is passed to an analogue multiplexer and on to an oscilloscope where the output is displayed and photographed. The outputs of seven of the detectors are discriminated and passed to a coincidence unit which produces a trigger pulse for operation of the recording equipment and other apparatus.

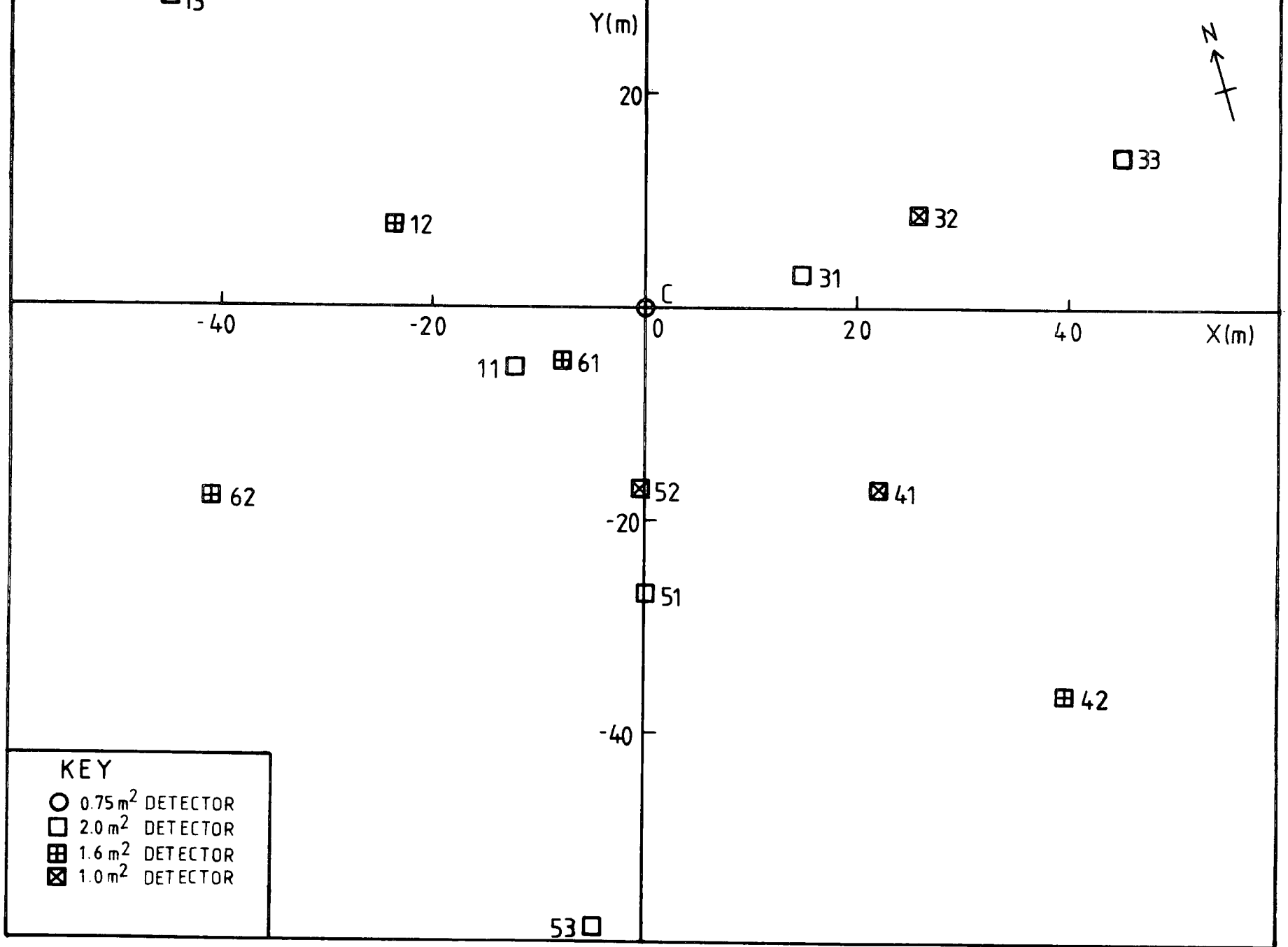

FIGURE 2.1 The Durham Air Shower Array

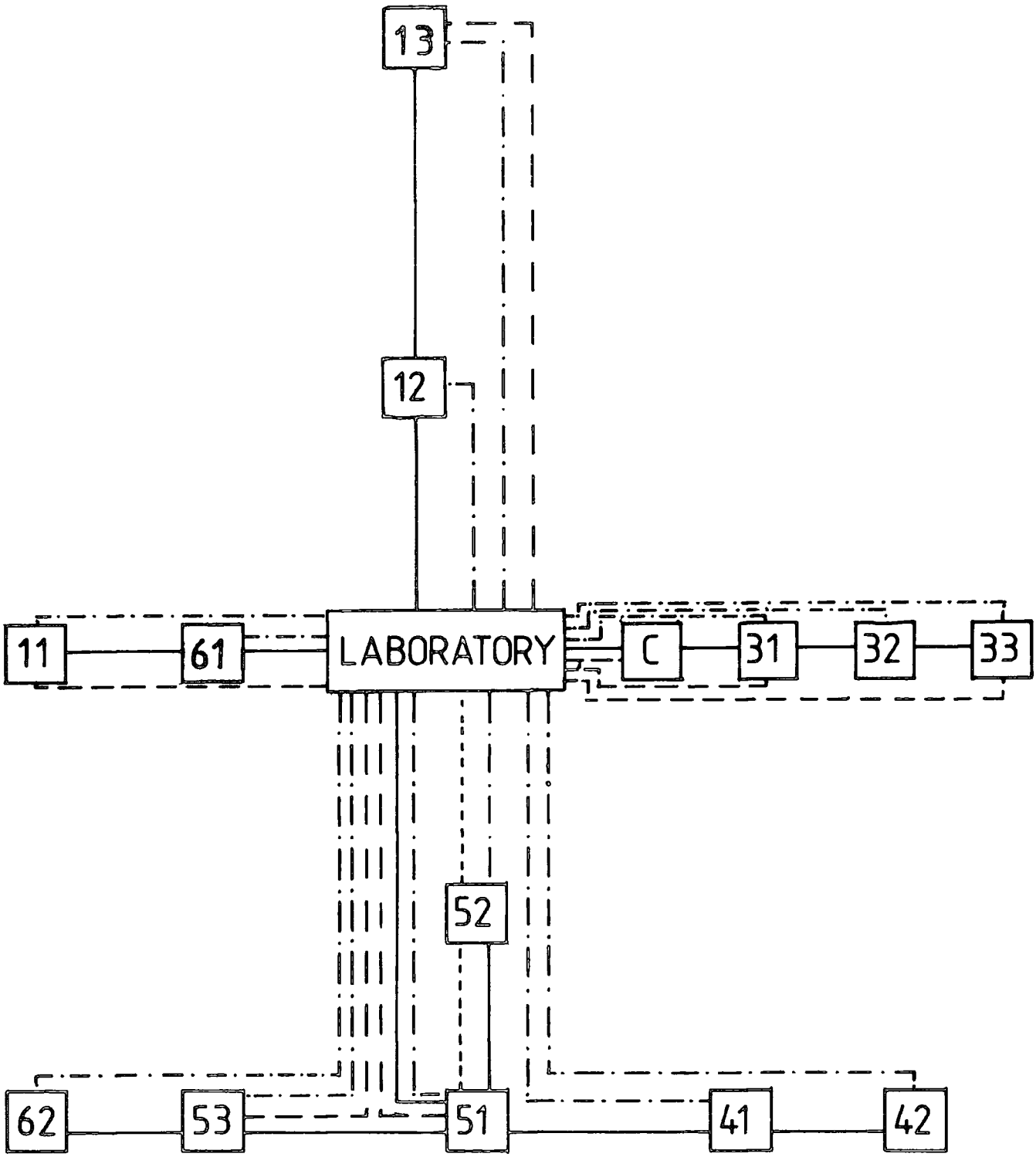

FIGURE 2.2 : Layout of cables supplying detectors

DETECTOR	AREA (m^2)	COORDINATES		
		X	Y	Z
C	0.75	0	0	0
11	2.0	-12.30	-5.64	-4.83
31	2.0	14.80	3.10	0.16
51	2.0	0.30	-26.80	0.18
13	2.0	-45.0	29.5	-13.5
33	2.0	45.0	14.0	0.2
53	2.0	-5.0	-58.5	-8.7
12	1.6	-24.0	7.5	-12.8
42	1.6	39.5	-36.5	-8.3
61	1.6	-7.9	-5.1	-4.9
62	1.6	-41.0	-18.2	-11.1
32	1.0	25.5	8.5	0.7
41	1.0	22.0	-17.0	-11.4
52	1.0	-0.5	-17.0	0.67

TABLE 2.1 : Areas and coordinates of detectors

Seven detectors are used for determining timing information. These detectors have an extra PMT, supplied with EHT, separately from the density PMTs. Each output is returned to the laboratory and processed through a fast amplifier, a fast discriminator and a time-to-amplitude converter (TAC) before being passed to the analogue multiplexer along with the density information.

2.2 DESCRIPTION OF THE ARRAY

2.2.1 The Plastic Scintillator Detectors

The fourteen detectors are identified as C, 11, 12, 13, 31, 32, 33, 41, 42, 51, 52, 61, 62 the first digit denoting the arm of the array and the second is the number of the detector on that arm. There are four types of detectors, these being of area $2m^2$ (11,31,51,13,33,53), $1.6m^2$ (12,42,61,62), $1m^2$ (32,41,52) and $0.75m^2$ (C). The positions had been chosen so as to enhance the symmetry of the array. Each scintillator is housed in a wooden box, the head amplifiers being located in aluminium boxes recessed into the scintillator box. These boxes are covered in aluminium foil to shield against electrical interference, except for C which is housed in an aluminium box. The detector box rests on an angle iron bed to prevent damp and assist in the circulation of air. A weatherproofed wooden hut covers the whole detector as shown in figure 2.3. Each hut has a panel at one end to allow access to the electronics.

The central detector, C, consists of two separate, rectangular slabs of 5cm thick NE102A plastic scintillator and the PMTs are arranged as shown in figure 2.4(a). Each slab has two Philips 53AVP PMTs, viewing via perspex light guides, one at each

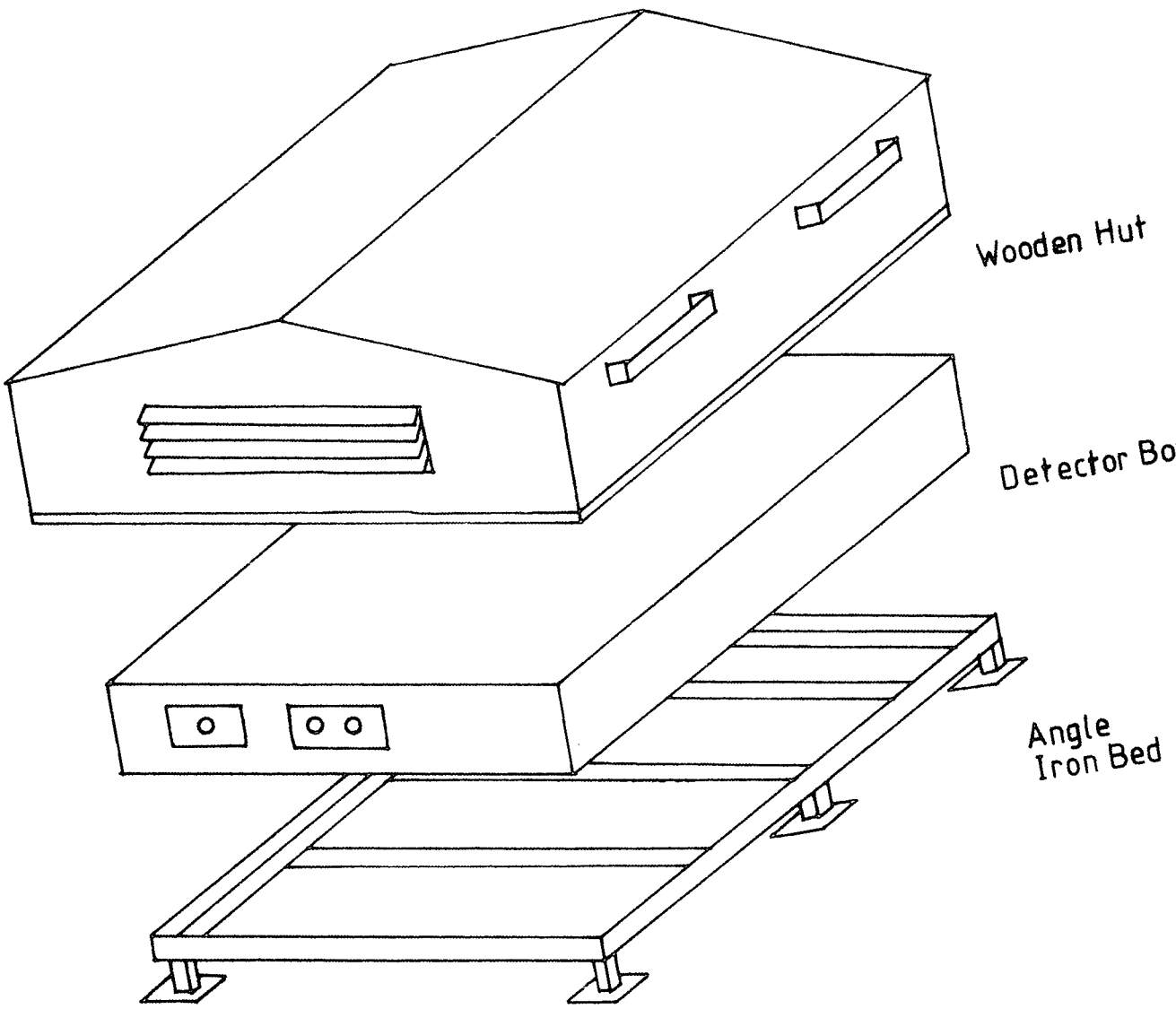

FIGURE 2.3 : A typical detector arrangement

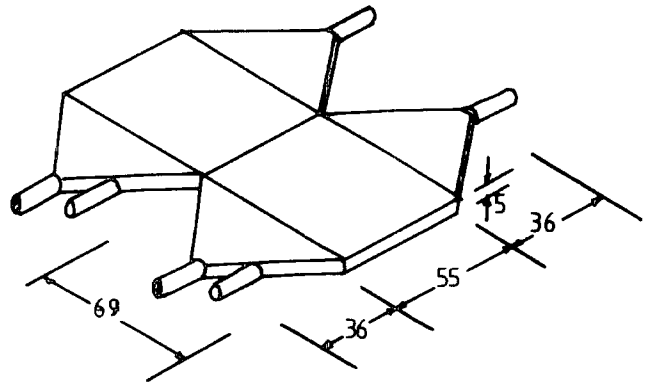

(i) 0.75 m^2 detector

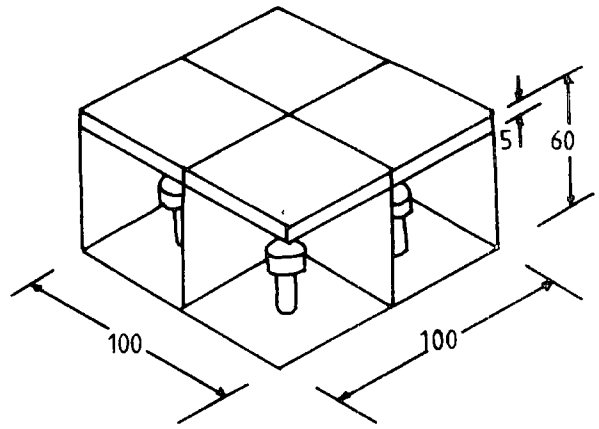

(ii) 1.0 m^2 detector

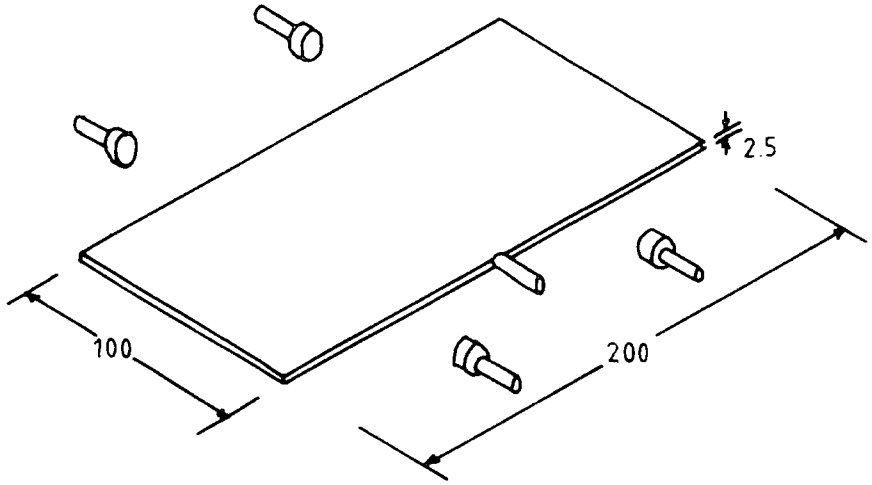

(iii) 2.0 m^2 detector

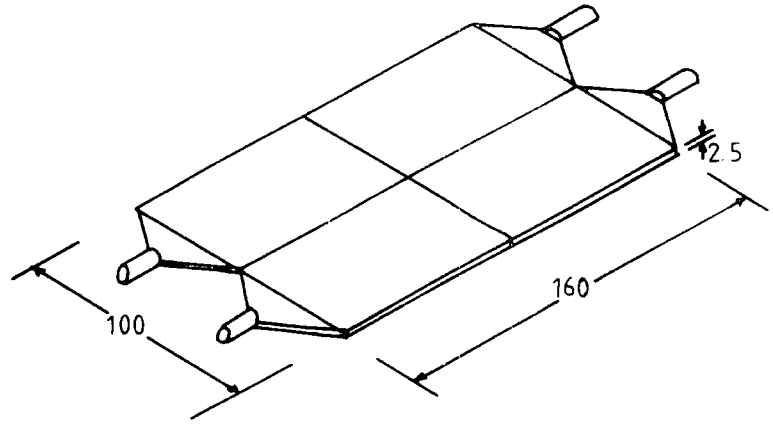

(iv) 1.6 m^2 detector

FIGURE 2.4 : Arrangement of scintillators in detectors (all dimensions in cm)

end, these being used to obtain density information. Also attached to the light guide at one end is a Philips 56AVP PMT which is used to provide the timing pulses. This detector acts as both the spatial and temporal origin for the array.

The $2m^2$ detectors are the only other ones, besides C, to provide timing information and be used in trigger selection. They consist of a 2m x 1m x 2.5cm slab of NE110 scintillator. Density information is provided by four EMI 9579B PMTs, two each viewing the 2m sides of the slab from a distance of about 3cm. One of the 2m sides has a Philips 56AVP PMT attached to it (using NE580 optical cement) to provide timing pulses. This is shown in figure 2.4(b).

The $1.6m^2$ detectors consist of four identical light-proofed quarters (figure 2.4(c)). The slabs are 2.5cm thick NE102A plastic scintillator. Each quarter is viewed by a Philips 53AVP PMT through a perspex light guide.

The $1m^2$ detectors, again, consist of four light-proofed slabs, but, here, they are viewed on their broad face by an EMI 9579B PMT. The slabs are 5cm thick and of unknown composition. The arrangement increases the response of the detector to almost unity over all of its area and is necessitated by the scintillator's unknown composition and not being of the highest quality.

2.2.2 The Photomultiplier Tubes

There are three types in use, these being the EMI 9579B with a 12cm photocathode, the Philips 53AVP with a 5cm photocathode and the Philips 56AVP also with a 5cm photocathode. These were chosen as they have a spectral response which is in the same region as that of the plastic scintillator and also

broader so that the number of photons from the scintillator resulting in an electrical signal is maximised (figure 2.5).

The tubes are supplied with negative EHT and their base circuits are shown in figure 2.6. These are of the high current design for good linearity and to reduce saturation effects. The output is negative with an exponential decay time constant of 20μs. The timing tubes also give a negative output and use a negative EHT supply but the output has a f.w.h.m. of about 5ns and are semi-gaussian. Operating voltages are about 1kV for the density PMTs and 2kV for the timing PMTs. Tube linearity for the operating conditions described above have been investigated by Smith (1976) and found to be good.

Two EHT supply units are used. One for the 'slow' (density) PMTs and the other for the 'fast' (timing) PMTs. The former was set at 2.4kV and the latter at 2.7kV. This is then dropped to the tube operating voltage in distribution units, at the detector, as shown in figure 2.7. This allows the voltage applied to individual tubes to be adjusted without affecting the voltage at the others.

2.2.3 The Head Amplifiers

The outputs from each of the 'slow' PMTs in a detector are summed, amplified and inverted in the head amplifier. The circuit, shown in figure 2.8, consists of an emitter-follower for each channel, whose outputs are summed and amplified by a μA702 operational amplifier feeding into an emitter-follower to drive the signal down the cable to the laboratory. The gain is nominally set to five and the response of the amplifier is shown in figure 2.9. The temperature dependence has been investigated

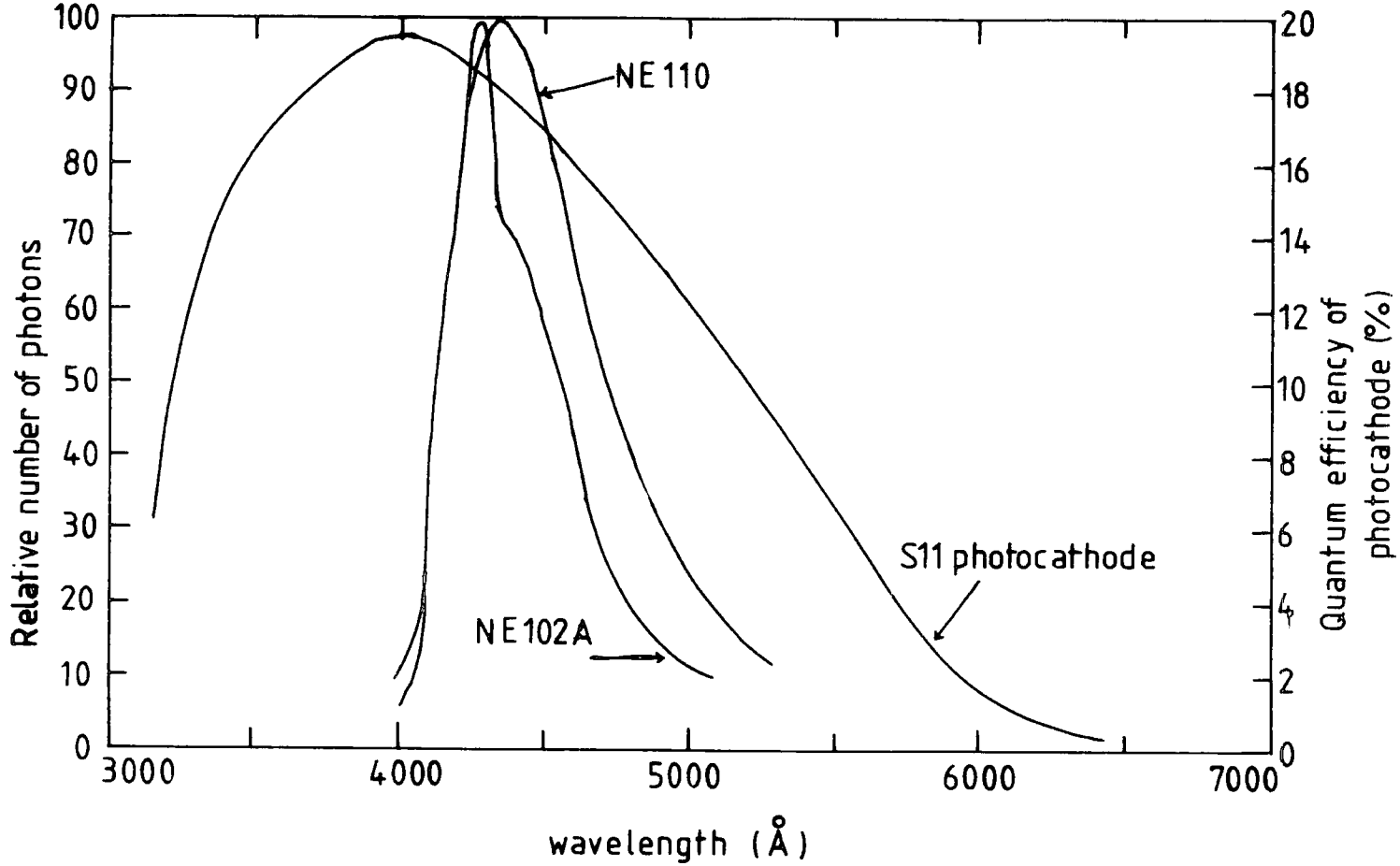

FIGURE 2.5 : Spectral response of scintillators and photomultiplier tubes (after Smith 1976)

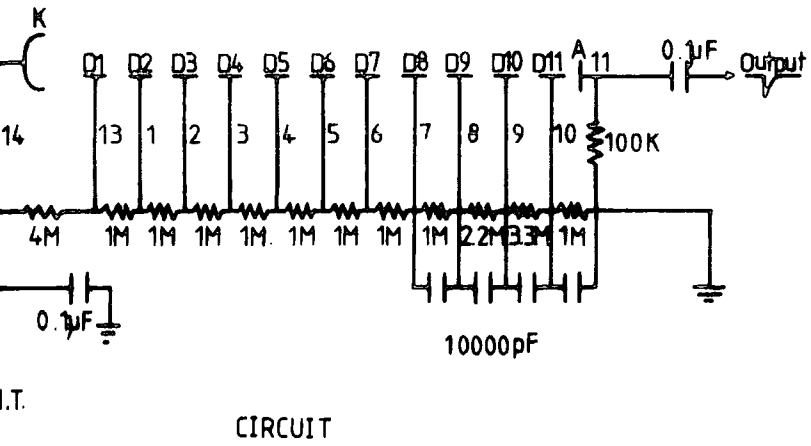

CIRCUIT

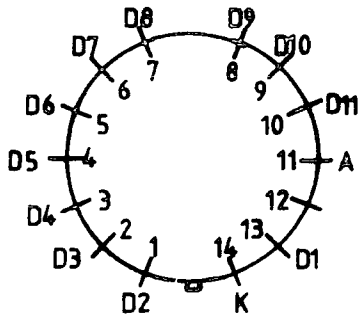

BASE

EMI 9579B

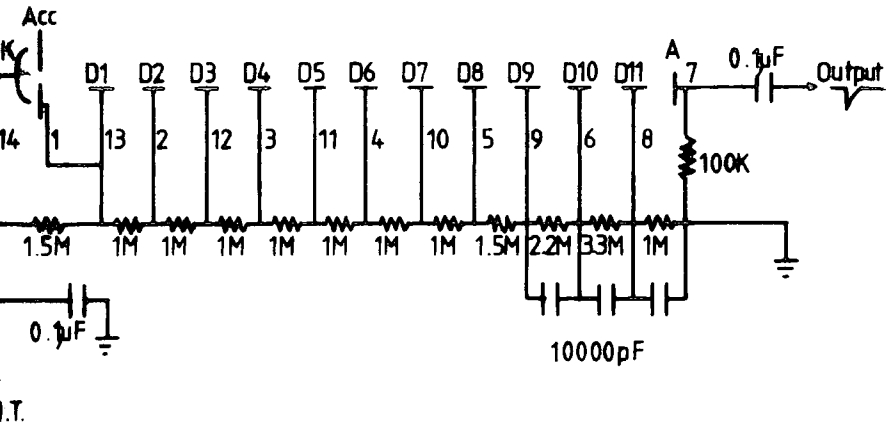

CIRCUIT

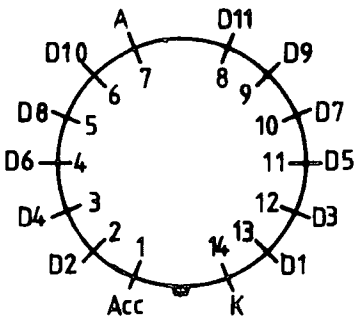

BASE

PHILIPS 53AVP

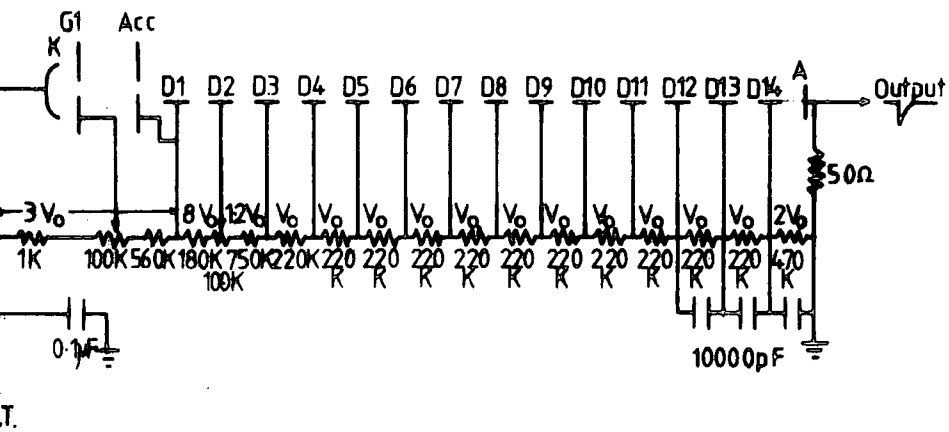

CIRCUIT

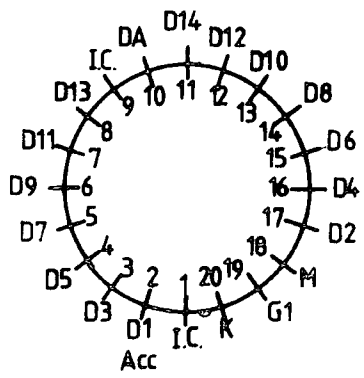

BASE

PHILIPS 56AVP

FIGURE 2.6 ; The Array photomultiplier base circuits

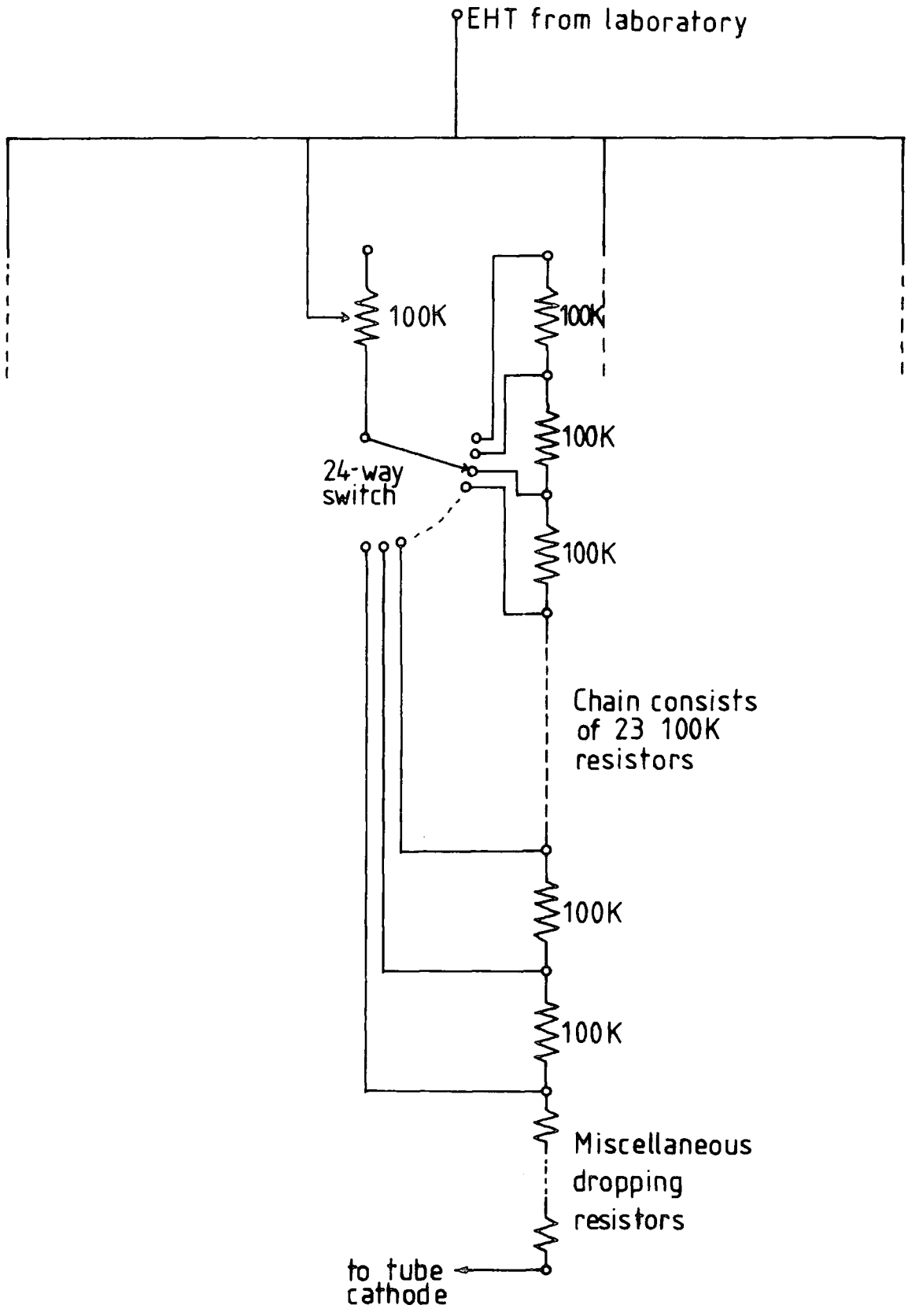

FIGURE 2.7 : EHT distribution at detectors

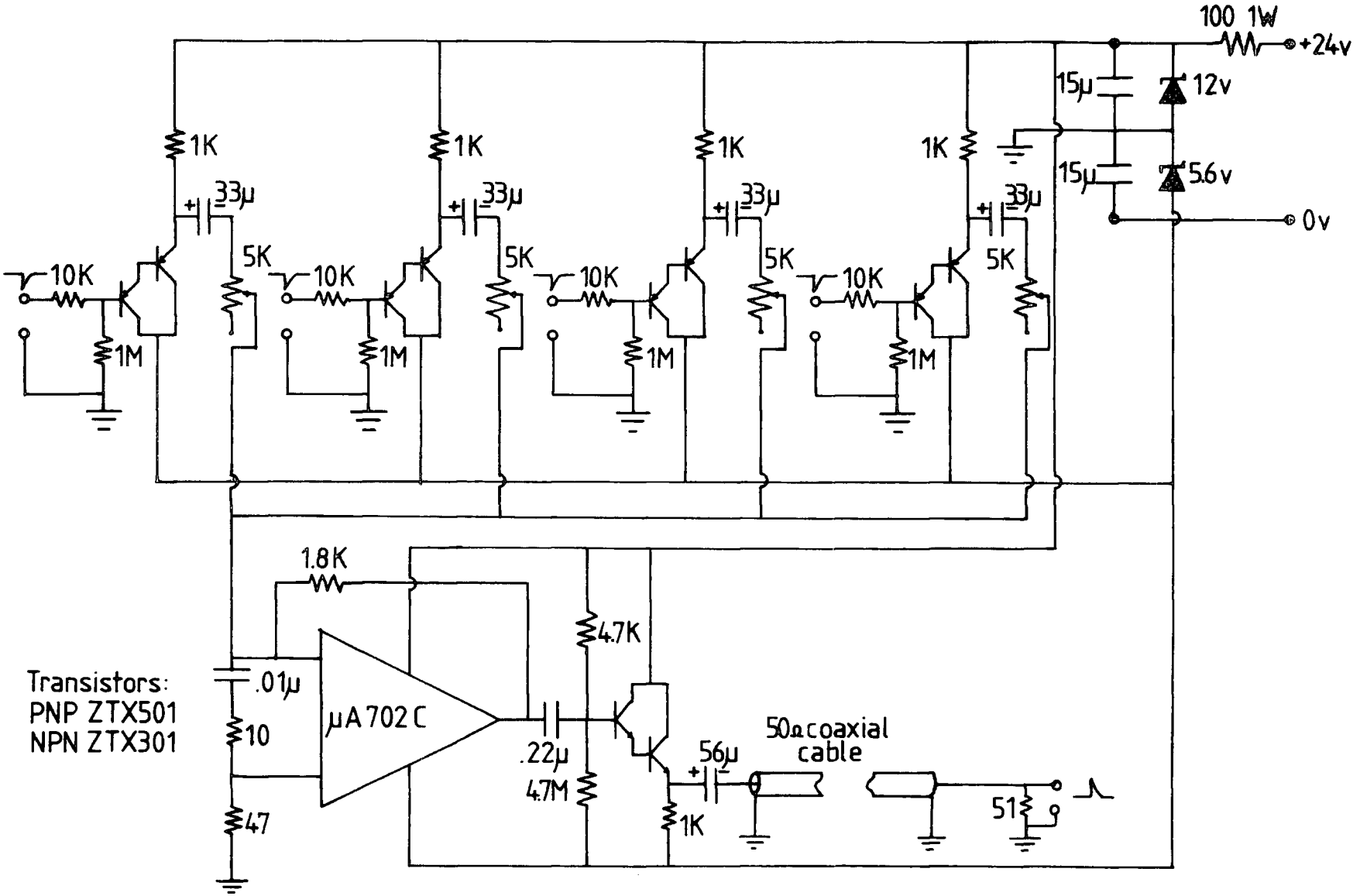

FIGURE 2.8 : Four input head amplifier

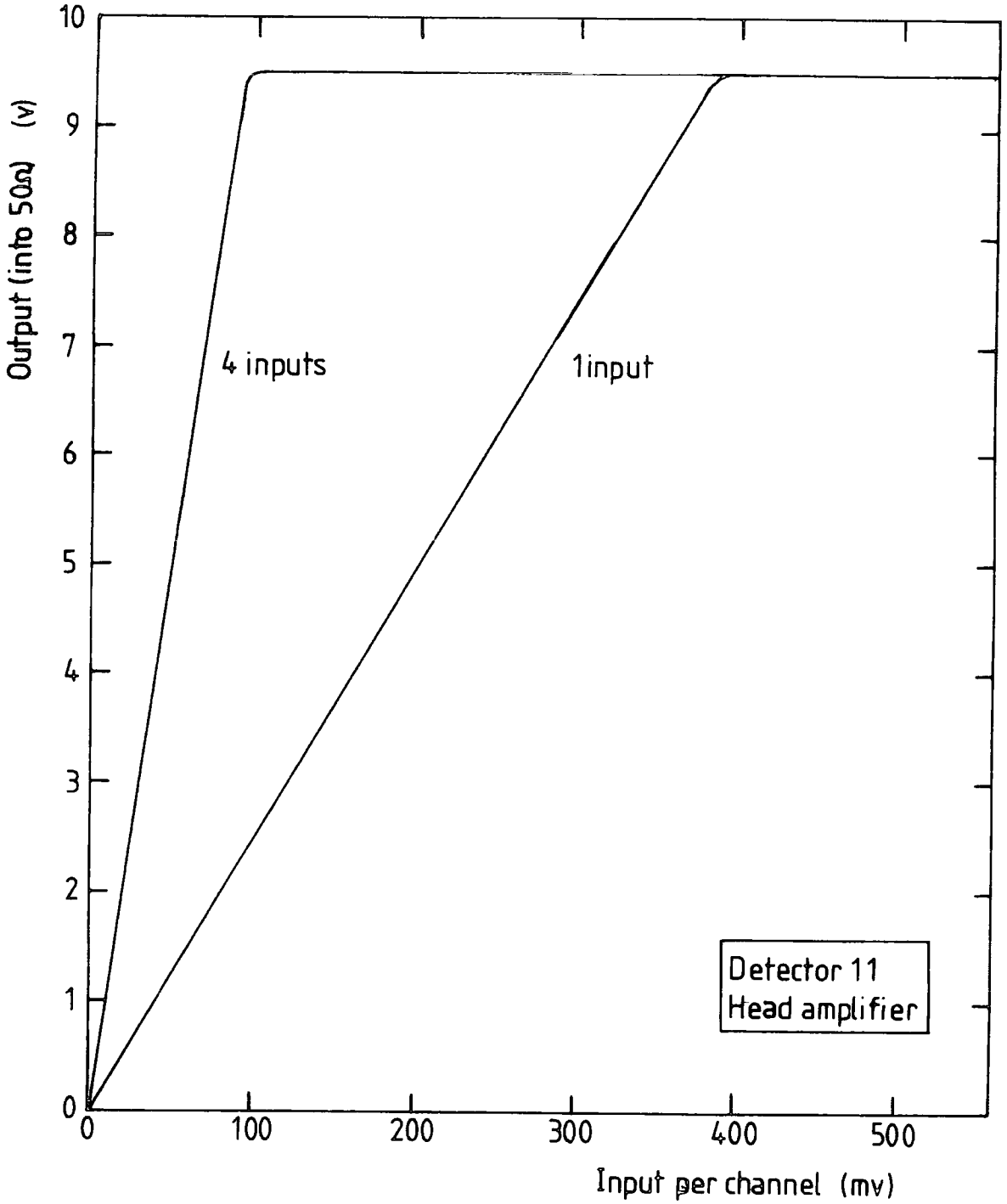

FIGURE 2.9 : Typical head amplifier gain characteristic

(Smith, ibid) and shown to have negligible effect on the gain. Power for the amplifier is supplied by a 24V 3A stabilised power supply in the laboratory.

2.2.4 Cabling

To economise on cable, the 'slow' EHT and the LT run from detector to detector along the arms as shown in figure 2.2. The coaxial cable is RG58 c/u 50 in which the pulse information propagates with 0.9dB per 100m loss which is compensated for by an increase in the PMT EHT. The frequency response does not significantly alter the shapes of either the density or timing pulses. The 24V LT cable is screened 4-core BICC 16.2.4C with two of the cores spare. The propagation time of the coaxial cable and its dependence on humidity and temperature has been investigated by Smith (ibid). It was found that humidity had no effect, the cables being waterproof, and the temperature coefficient is $(-6.0\pm0.2)\ 10^{-4}$ ns m^{-1} $^{o}C^{-1}$ over the range 15^{o}C to 47^{o}C. No correction need therefore be applied.

2.3 CALIBRATION OF THE DETECTORS

2.3.1 Introduction

The number of photons reaching the PMTs will depend on the energy of the particle, the angle at which it passes through the detector and the point at which it passes through the detector (as the scintillator is not uniform and the photons are attenuated as they pass through it). Since no two detectors are the same, each has to be individually calibrated.

One main problem of scintillators is the light attenuation length, ie the distance over which light is attenuated by e^{-1} of

its original intensity. The non-uniformity caused by this has to be taken into account. Therefore contour maps of each type of detector's response have been obtained (Smith, ibid) and from these, calibration points have been obtained (figure 2.10). The pulse height obtained at this point can then be converted to a parameter defined as the 'mean pulse height per particle per detector' which is then used in the calibration.

2.3.2 Calculation of the Calibration Pulse Height

The aim of the calibration is to adjust the EHT supply to the PMTs in a detector so that the output, in mV, at the laboratory, when divided by 100, will give the number of particles per square metre at the detector, ie. the density at the detector.

Let D = particle density at detector (ptles m^{-2})

A = area of detector (m^2)

H = pulse height (mV)

n = number of PMTs viewing a single scintillator slab

S = calibration pulse height (mV $ptle^{-1}$ PMT^{-1} m^{-2})

Calibration pulse height for detector is SA (mV $ptle^{-1}$ PMT^{-1} det^{-1})

Calibration pulse height for a PMT is nSA (mV $ptle^{-1}$ det^{-1})

which is defined to be 100mV.

$$S = \frac{100}{An} \quad \text{mV ptle}^{-1} \text{ PMT}^{-1} \text{ m}^{-2} \qquad (2.1)$$

However two corrections require to be made to this value of S. These are as follows:

(i) It is found to be more convenient to measure the mode, not the mean, of the distribution of output pulse heights, which are aquired on a pulse height analyser (PHA). The relationship between the mean and the mode varies between

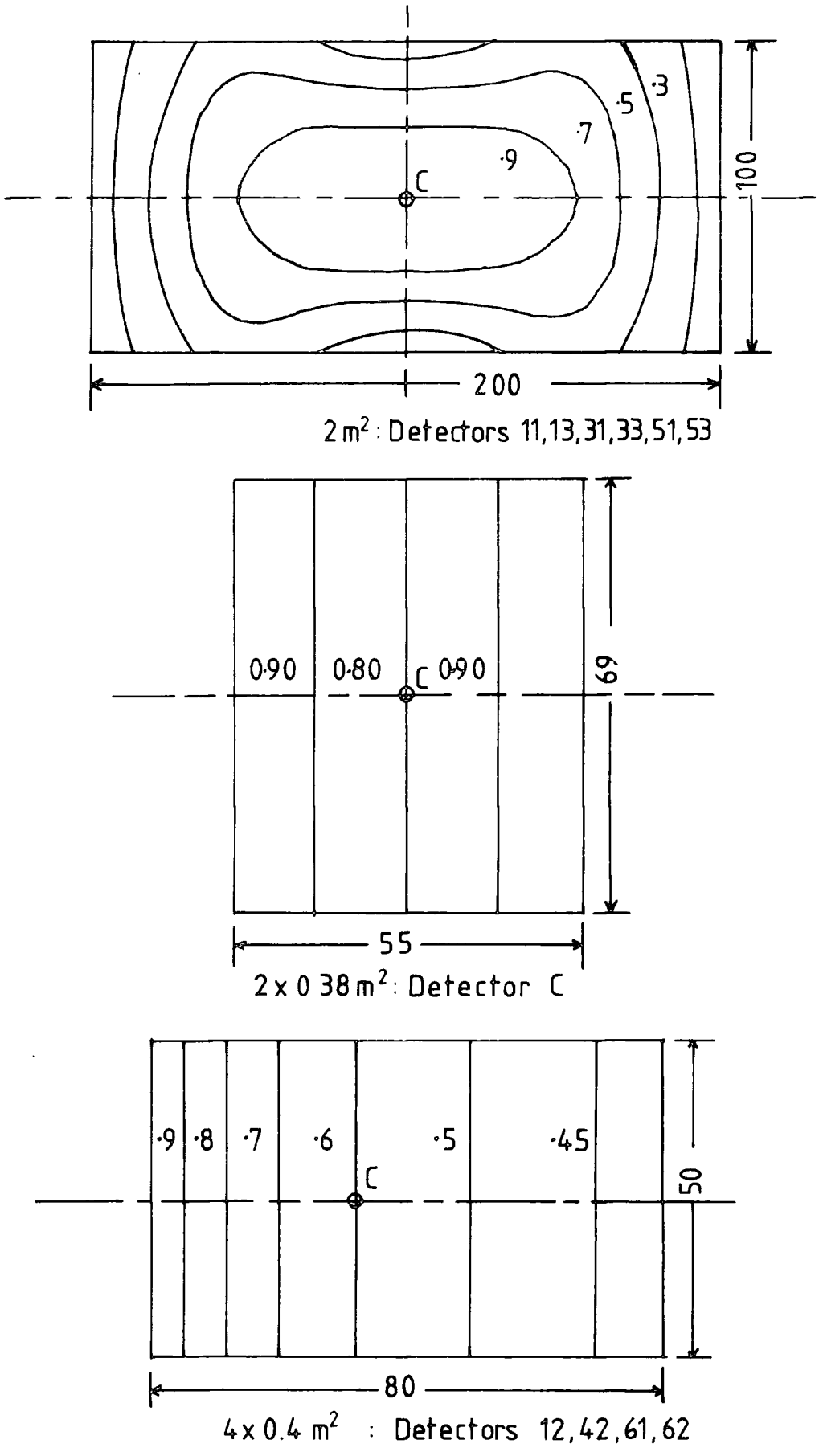

FIGURE 2.10 : Pulse height contour map of the Array's scintillators (after Smith, 1976)

C represents the calibration points

detector types and has been determined at the calibration point by Smith (ibid). The ratio, R, was found to vary by no more than 4% over the total scintillator of any detector.

(ii) A number of the detectors have a calibration point which is not at the same spot where the mean pulse height occurs and a further correction has to be applied. This ratio, g, is given by the pulse height at the calibration point divided by the pulse height at the mean pulse height coordinate and has been determined by Smith (ibid).

Including these corrections in the pulse height calibration equation gives :

$$S = \frac{100g}{AnR} \quad mV\ ptle^{-1}\ PMT^{-1}\ m^{-2} \qquad (2.2)$$

at the mode of the single particle distribution at the calibration point. The values for R and g are given in table 2.2.

2.3.3 Calibration Procedure

In practice, when the detector output is displayed on the PHA, the single particle peak is not observed as it is masked by noise, due, in the main, to PMT noise and light leaking into the detector. In order to reduce the noise a particle telescope is used.

The telescope consists of a 23 x 23 x 3 cm^3 slab of NE102A plastic scintillator, viewed from one edge by two Philips 53AVP PMTs. Each of these is supplied with +1.9kV from the laboratory via a charge sensitive amplifier (CSA). This enables the cable requirement to be reduced, only two (one for each tube) being installed for each arm of the array. The scintillator and tubes are sealed in an aluminium box.

The signals from the CSAs are passed to a dual discriminator

DETECTOR	A	N	n	R	g	S
C	0.75	4	2	1.53±0.01	0.89	38.3
11,31,51, 13,33,53	2.0	4	4	1.83±0.01	1.41	9.6
12,42,61,62	1.6	4	1	1.60±0.01	1.00	39.1
32,41,52	1.0	4	1	1.40±0.01	1.00	71.4

A = Total area of detector (m^2)

N = Total number of photomultiplier tubes in detector

n = Number of photomultiplier tubes viewing each piece of scintillator

R = Mean of pulse height distribution divided by its mode

g = Pulse height at calibration point divided by mean pulse height

S = Calibration pulse height (mV)

TABLE 2.2 : Calibration parameters for density measurement

(figures 2.11 and 2.12) , set at a level of 100mV to remove a large proportion of the noise, and from these into a coincidence unit which produces a 2μs, -5V rectangular pulse for gating the 100 channel Laben PHA. In this way the majority of pulses recorded by the PHA are particle pulses. Because the analogue multiplexer (MUX) has an input resistance of 50Ω , a 50Ω termination has to be applied to the PHA input.

To calibrate each tube the other tubes have, first, to be disconnected from the head amplifier. The telescope is placed with the centre of its scintillator over the calibration point and the PHA started. After approximately ten minutes a sufficiently accurate distribution is obtained in order to decide whether the PMT EHT supply is too low or too high. The EHT is then adjusted and the process repeated. As the calibration value is approached the calibration time requires increasing. The tube is considered calibrated if within ±4% of the required value.

When this is reached, the PHA is run overnight to obtain a more accurate distribution. The resulting distribution can then be drawn and the mode determined. A typical single particle peak is shown in figure 2.13.

2.4 SIGNAL PROCESSING

2.4.1 Timing Information

Pulses from each of the fast PMTs is passed, first, to a NE4634 Fast Amplifier, where necessary, and then to a NE4635 Fast Discriminator. It is essential that the pulse from C arrives first. The distance of the outer detectors (13,33,53) from the laboratory ensures this, but for the inner detectors (11,31,51) a large coil of cable is put into the line to delay the pulse. The pulse from

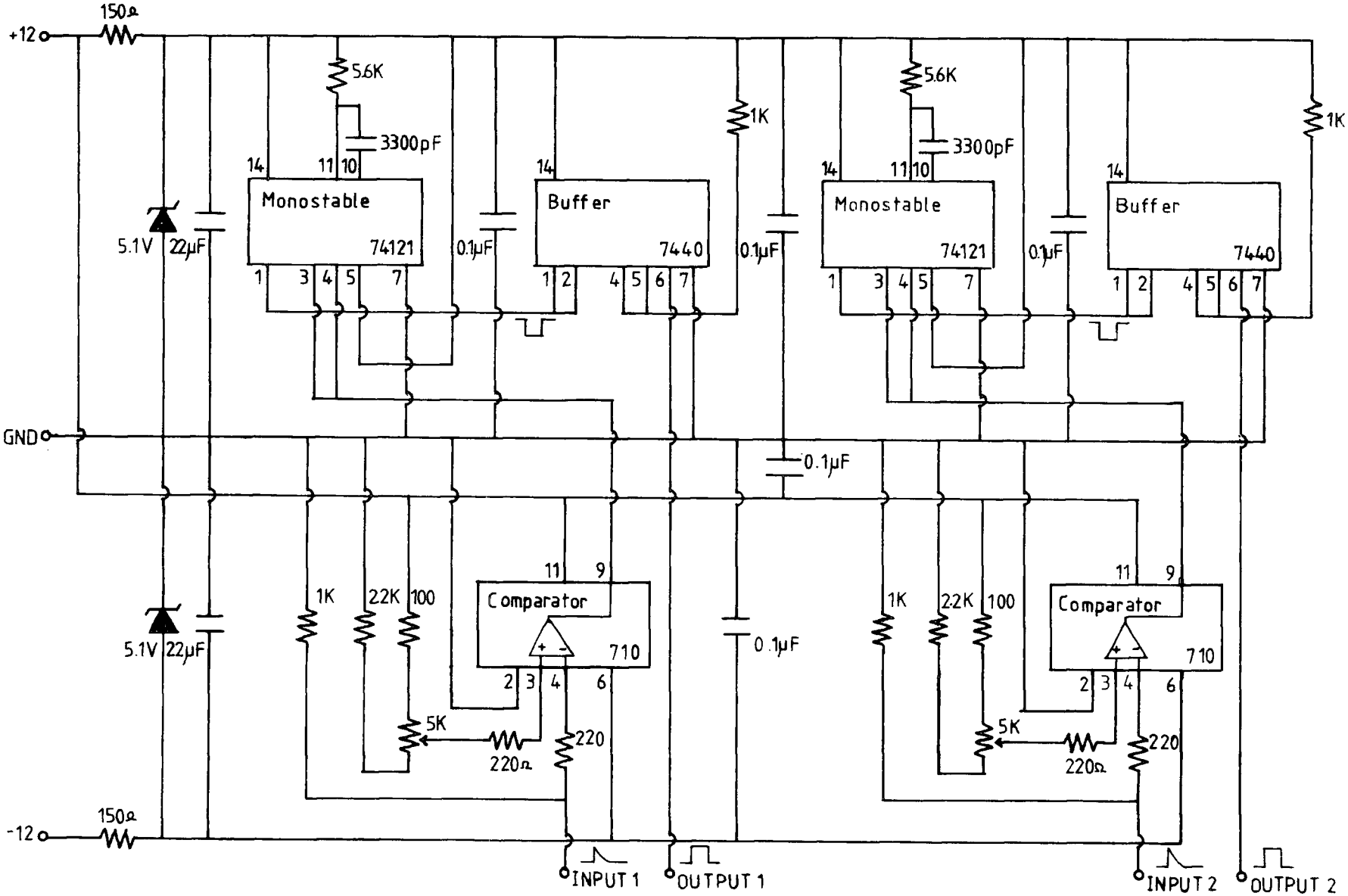

FIGURE 2.11 : Circuit diagram of dual discriminator used in detector calibration

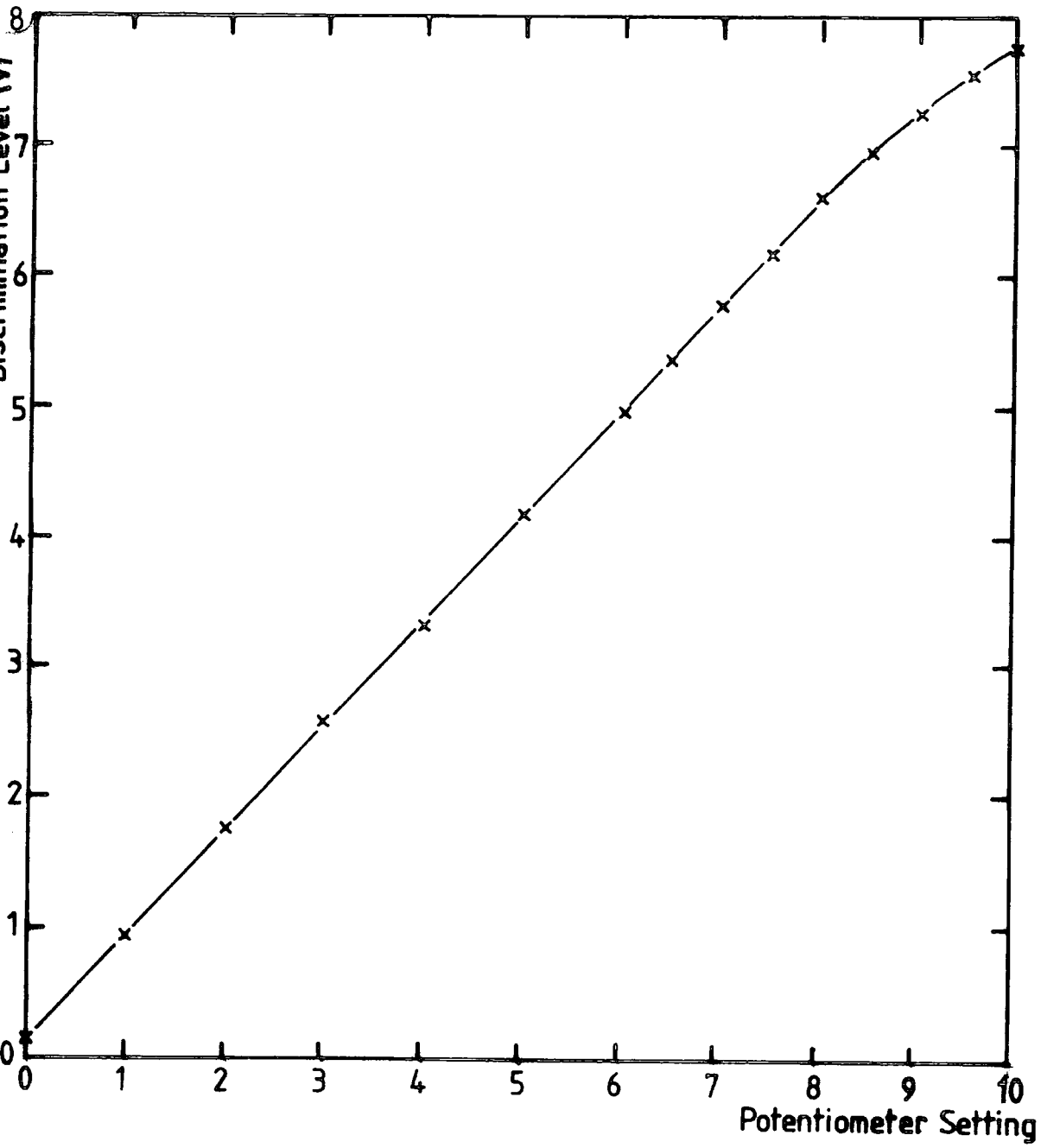

FIGURE 2.12 : Characteristic of circuit shown in figure 2.11

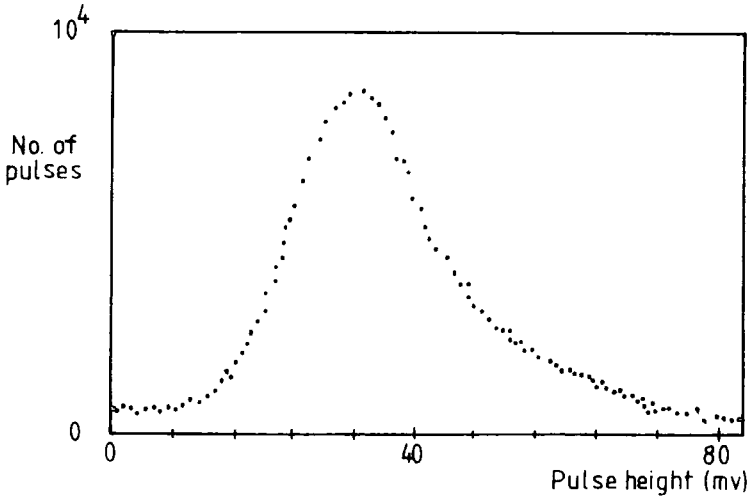

FIGURE 2.13 : Typical single particle peak as displayed on pulse height analyser

C is then used to start each of six NE4645 TACs (which produce a rectangular output of height proportional to the time difference between the start and stop pulses, and width 5μs), the pulses from the individual timing detectors stopping them. The output of a TAC is then proportional to the time the shower front passes through the detector, relative to the time it passes through C, plus the differences in cable and electronics delays. This pulse is then passed to the MUX and held if a shower trigger occurs.

It is thus necessary to ensure timing information is received for all shower fronts but noise should not be high enough to give false signals. A suitable indicator is the rate of pulses from the discriminator of each channel. A rate of around $200s^{-1}$ has been found to fit the requirement. However this can only be a rough guide as the rate fluctuates markedly with variations in atmospheric conditions. Adjustment of this is made daily during operation of the array by altering the amplification and/or discrimination levels.

2.4.2 Density Information

Density signals from C,11,31,51,13,33,53 are fed to buffer-discriminators. Each of these has an input of 10KΩ impedance and three outputs. One output is direct (for output to the PHA), the second is buffered (for general use) and the last is discriminated. The discriminator is of the leading edge type, using a μA710 high speed comparator and the level is adjustable between 40mV and 7V. The discriminated outputs are then fed to a coincidence unit. This allows any combination of the above detectors to form a trigger. Usually only two combinations are used. These are the inner ring trigger, consisting

of C,11,31,51, and the outer ring trigger, consisting of C,13, 33,53. The trigger pulse is then fed to a buffered fan out to allow it to trigger the data recording electronics and any ancilliary equipment (eg the flash tube chamber). The threshold for triggering was set at 4 particles m^{-2} for C and 2 particles m^{-2} for the other detectors.

2.4.3 Data Recording

All channels, both 'slow' and 'fast', are fed to the MUX where the pulse heights are held by sample and hold circuits (SH) on application of the trigger pulse. The trigger also actuates a strobe which produces a series of 24 TTL pulses. These are fed to the MUX and the stored pulse heights are dumped, serially, to a Tektronix 5102 dual beam oscilloscope at a spacing dictated by the strobe spacing. The operation of the strobe and MUX are described in greater detail in Chapter 5.

The oscilloscope is externally triggered by the trigger pulse. In order to extend the pulse height range that can be measured the MUX output was fed to one beam on $1Vcm^{-1}$ and to the other beam on $0.1Vcm^{-1}$. Since the saturation output of the head amplifiers is approximately 9.5V, the maximum particle density that can be recorded is about 95 particles m^{-2}. The first beam allows densities in the range 2 to 100 ptles m^{-2} to be recorded while the second covers the 0.2 to 10 ptles m^{-2} range.

In order to establish the time of the event, a digital clock, which has a triggerable six digit light emitting diode display, is placed adjacent to the oscilloscope screen.

A camera was used to record the event. It is contained

in a light-tight box, together with the oscilloscope, and the shutter remains open. A 'camera drive unit' was built to control the film wind on. This is triggered by the trigger pulse and after a delay of approximately one second closes a relay in the power supply line to the camera motor for a time sufficient to wind on one frame. This circuit is shown in figure 2.14. Figure 2.15 shows the form of the output and figure 2.16 is a block diagram of the data recording system.

2.5 CONCLUSIONS

The array, in this form, was run in conjunction with the tachyon search experiment, which is described in Chapter 4. As such, its main purpose was to provide a shower trigger.

However, during its use, it was found to be very unreliable, and unsuited to use for long periods as a shower trigger on a 'one man operation' basis. The problems encountered included the following:

(i) Failures of EHT supply due to failure of the dropping resistors, potentiometers and capacitors. This resulted in a shift of calibration factor, excessive noise or total failure.

(ii) Light leaks into boxes which caused excessive noise.

(iii) Detectors not built for ease of maintenance.

A number of electronic and mechanical alterations were made to attempt to alleviate the problems.

Also the photographic method of data recording was obviously unsuitable for analysing large amounts of data, especially if these results are to be ancilliary to another experiment. A microcomputer was used to automate the data collection and analysis. The modifications and the data collection are described in Chapter 5.

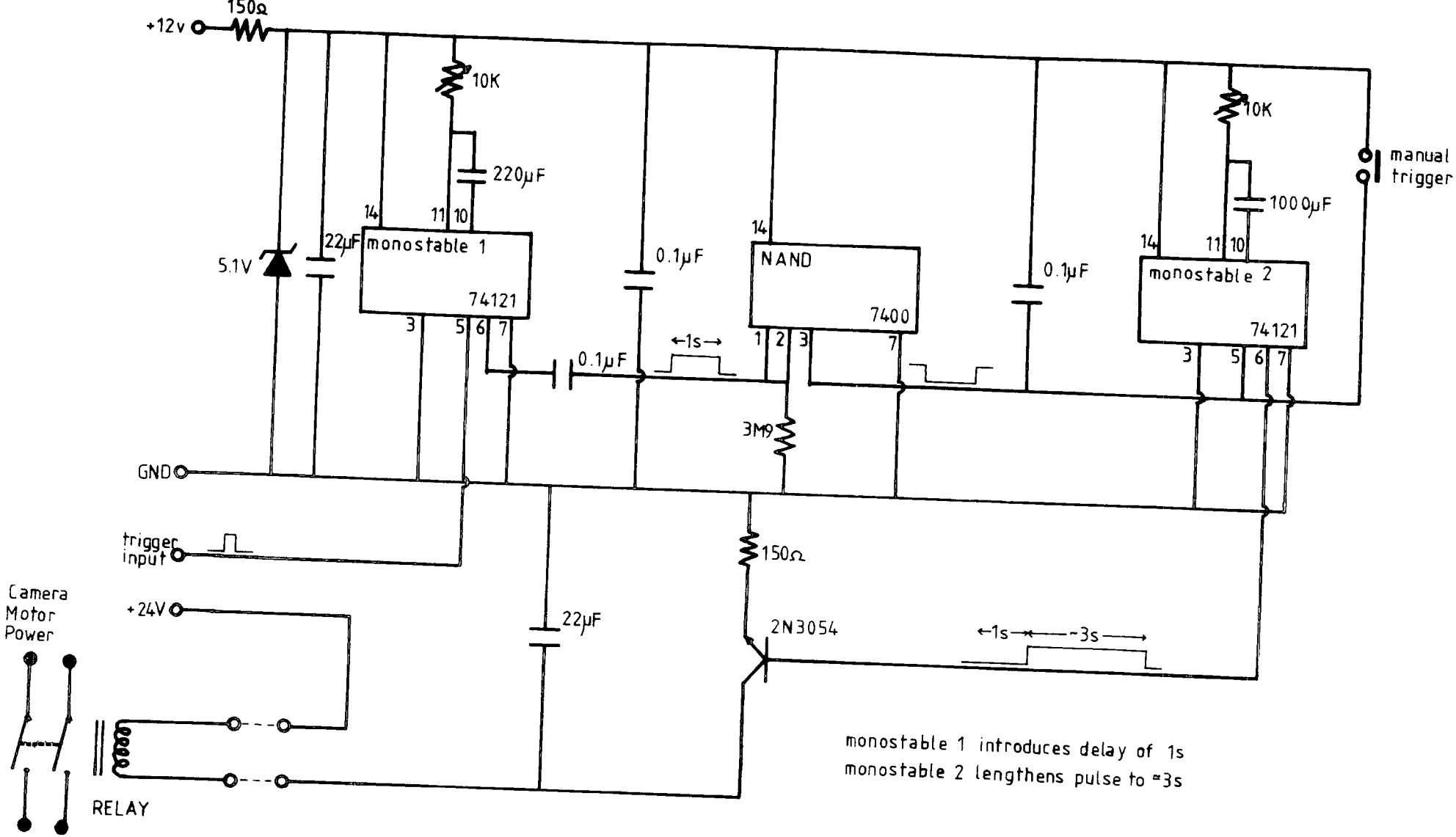

FIGURE 2.14 : Camera drive unit

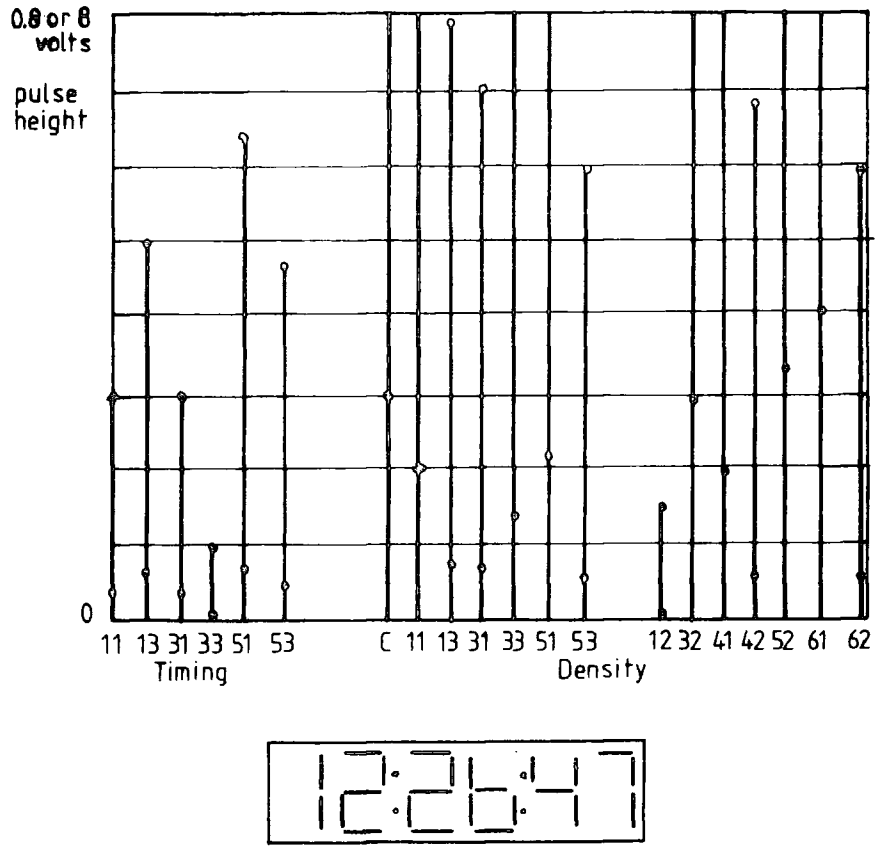

FIGURE 2.15 : Diagrammatic representation of a shower as recorded on the oscilloscope
(The top of a pulse appears as a bright spot)

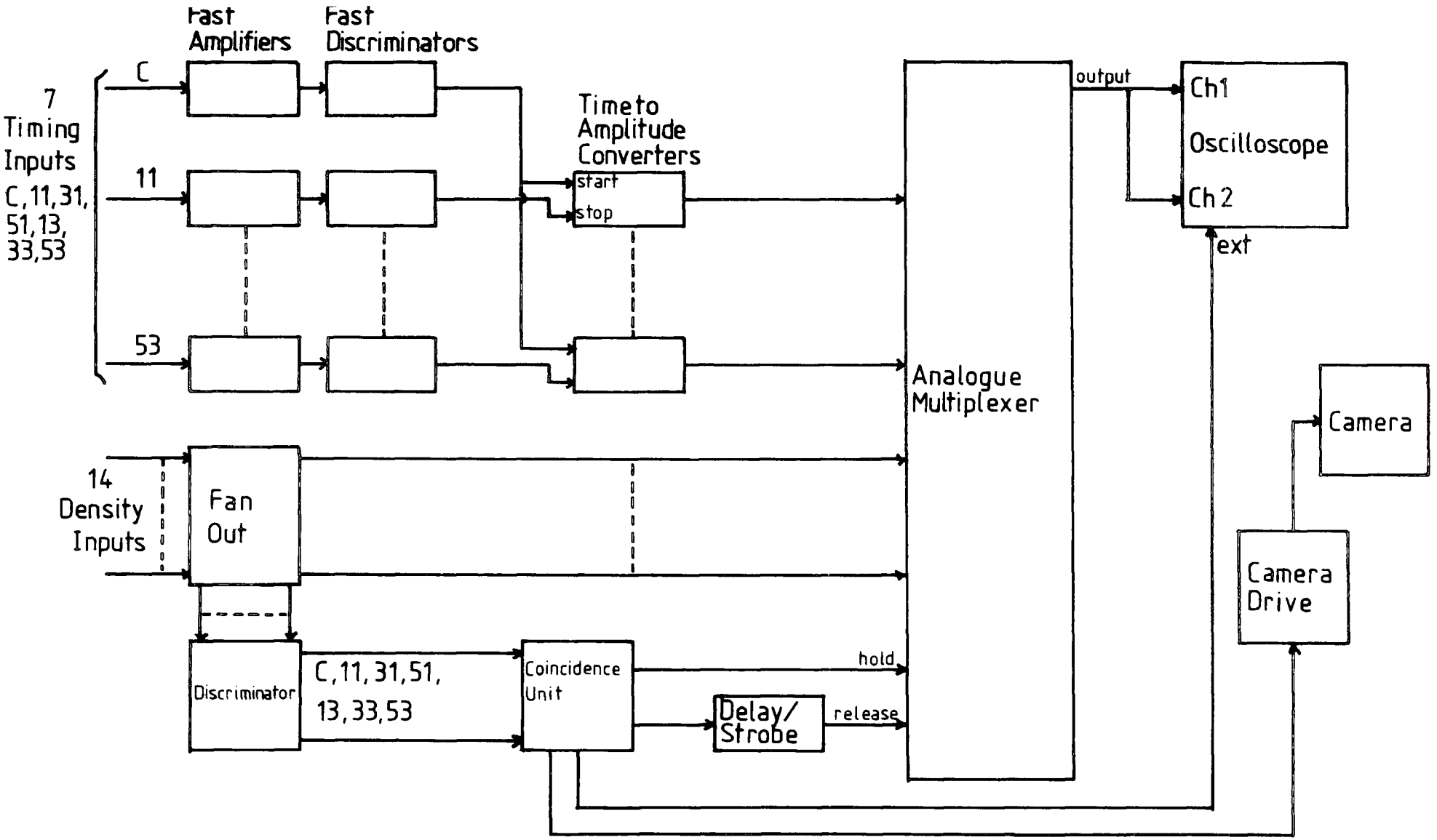

FIGURE 2.16 : Block diagram of output electronics

CHAPTER 3

INTRODUCTION TO TACHYON THEORY

3.1 TACHYON PHYSICS

3.1.1 Tachyons and Relativity

The first point that has to be discussed in any account of tachyon theory is that of their acceptability in the framework of relativity. Since the formulation of the special theory of relativity by Einstein, objections to superluminal particles have been based on the fact that particles cannot be accelerated to velocities greater than c, the velocity of light in a vacuum. In fact Einstein, himself, had concluded that 'velocities greater than that of light .... have no possibility of existence'.

This view prevailed until Bilaniuk and Sudarshan (1962) re-examined the problem. They pointed out that, although the theory disallowed acceleration of subluminal particles (ie. particles with velocities less than c) to superluminal velocities (ie. velocities greater than c), there was nothing in the theory which prevented the production of particles with superluminal velocities, provided that their velocities were always greater than that of light.

The existence of superluminal velocities would therefore introduce a new class of particles to physics in addition to 'normal' subluminal particles and luminal particles, eg. photons and neutrinos. Particles of these groups can only exist in their respective velocity domains.

3.1.2 The Second Postulate and Emission Theories

The above discussion is on the basis that the second

postulate of the special theory of relativity (ie. c is independent of the velocity of the source) holds. That it does, is not now in dispute, though experiments of increasing accuracy are still being carried out. However it is appropriate to mention some of the experimental tests of the postulate and alternative theories to explain the observations (emission theories).

3.1.2.1 Ritz Emission Theory

The only serious attempt at an emission theory was produced by Ritz (1911) as an alternative to relativistic electromagnetic theory. However he did not consider it to be a true theory but used it only to show that Lorentz invariance was not a necessary concept. It used as its basic assumption that every electric charge continually emits infinitely small, fictitious, particles in all directions. These particles were assumed to leave the charge with a relative velocity c and travel at constant velocity, independent of the subsequent motion of the charge. The force exerted by this charge on another depends on the distribution and relative velocities of these particles at the second charge. Using classical kinematics, Ritz was then able to calculate a formula for the force of one charge on another which depended only on the relative positions, velocities and accelerations. He had thus created a theory which was relativistic in the Galilean sense. However the development of a more general theory was terminated by his death.

3.1.2.2 Experimental Verification of the Second Postulate

If the velocity of light is dependent on the source velocity then binary star systems would show unusual effects (DeSitter, 1913). The most obvious to occur would be event time-order reversal and the appearance of multiple images of a star.

However it was pointed out by Fox (1965) that optical observations may not be valid as the radiation is scattered during its propagation through the interstellar medium. For λ=5000Å a characteristic extinction length, χ, of about 2 l.yr is obtained - less than the distance to the star.

This prompted a number of experimenters (Alvager et al, 1963 : Sadeh, 1963) to measure the velocity of γ-rays, whose extinction length, it was argued, would be negligible, produced in various interactions. None of these appeared to disprove the postulate. However Filippas and Fox (1964) noted that, though χ appeared to be negligible, the amounts of material put in the path of the γ-rays was $\simeq\chi$ thus invalidating the results. They carried out a similar experiment with much reduced extinction but came to the same conclusion as the others.

It was not until recently that improved techniques allowed stars to be observed in high wavelength regions. Using this data, the binary star problem is overcome as χ is now large, ~20 kpc for 70keV X-rays. Brecher (1977) studied three binary, regularly pulsing, X-ray sources which were close enough for extinction effects to be negligible. From their distances, orbital periods and Döppler velocities he determined the constant k, in $c'=c+kv$ (where c' is the velocity of the radiation and v is the velocity of the source. k=0 for Einstein's theory and k=1 for Ritz theory). A value of k of less than 2.10^{-9} was obtained, a factor of 10^5 smaller than laboratory determined values, thus establishing the second postulate to much greater accuracy.

3.1.3 Basic Properties of Tachyons

Having shown that the existence of tachyons must be

contained in the framework of special relativity we now look at the basic energy-momentum relationships of tachyons. Firstly we consider the energy-mass relation,

$$E = \gamma m_o c^2 \quad (\text{where} \quad \gamma = \left[1 - (\tfrac{v}{c})^2\right]^{-\frac{1}{2}}) \tag{3.1}$$

The energy must be real. This is true for v less than c as γ is real and positive. It also holds for v equal to c, provided m_o is set to zero. The latter is shown to be true by the existence of photons and neutrinos. We can now extend this argument to include tachyons. In order to keep the energy real, m_o must be imaginary when γ is imaginary.

$$\text{ie. we set} \qquad m_o = i m_* \tag{3.2}$$

where m_* is known as the meta-mass.

What is the meaning of an imaginary proper mass ? The same can be said of the zero mass of a luxon (a particle with velocity of c). In both cases it is impossible for us to travel in the same rest frame as the particle and measure its mass. Therefore any objection is invalid. (Also the proper time and proper length relating to a superluminal particle are imaginary).

3.1.4 Geometrical Considerations and Symmetry

The solutions of the energy-momentum vector ($E^2 = p^2c^2 + m^2c^4$), invariant under Lorentz transformation, can be displayed in E - p space as shown in figure 3.1. There are a total of six solutions. The upper branch describes particles with velocity less than c (known as ~~tardyons~~ bradyons). The velocity, v_x, is given by

$$v_x = \frac{dE}{dp_x} \tag{3.3}$$

It can be seen that the velocity of a ~~tardyon~~ bradyon can never reach c even if it is transformed to a frame where the energy is very

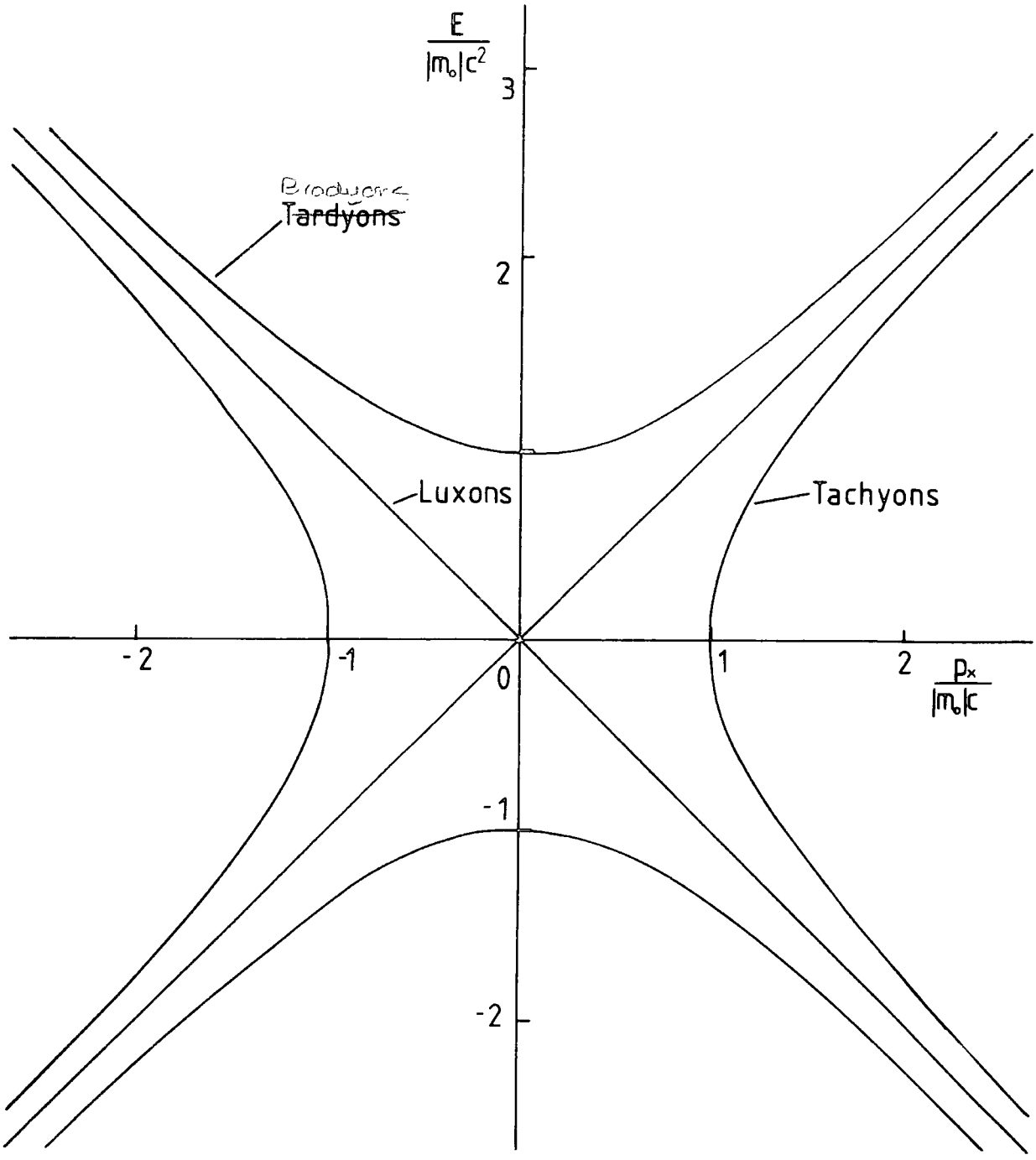

FIGURE 3.1 : Plot of the energy-momentum vector invariant, showing the solutions for particles in each of the three velocity domains

large.

If we set m_o to zero then we get straight lines above the x-axis. These describe luxons and everywhere on this line the velocity is c irrespective of the Lorentz-transformation (LT) that may be performed.

The left and right branches, above the x-axis, describe particles whose velocities are always greater than c, ie. tachyons, and it can be seen that their existence would complete the symmetry of the solutions.

The branches below the x-axis describe particles (of all three types) which have negative energy and these can be associated with anti-particles.

3.1.5 Causality and the Reinterpretation Principle

One of the more serious objections to the existence of tachyons is the causality problems that would ensue. This is because, for certain observers, their energy would be negative (as can be seen from figure 3.1).

Firstly consider the Minkowski time-space diagram, in one-dimension, shown in figure 3.2. Now the world line of a luxon is shown by the line v = c, with gradient 1.

$$v = \frac{dx}{dt} = c \qquad \text{or} \qquad \frac{dx}{cdt} = 1$$

The world lines of all subluminal particles must have,

$$v < c \quad \text{or} \quad \frac{dx}{cdt} < 1 \qquad \text{ie. gradient} > 1$$

Similarly superluminal particles must have world lines with gradient < 1. Also simultaneous events occur on the x-axis and

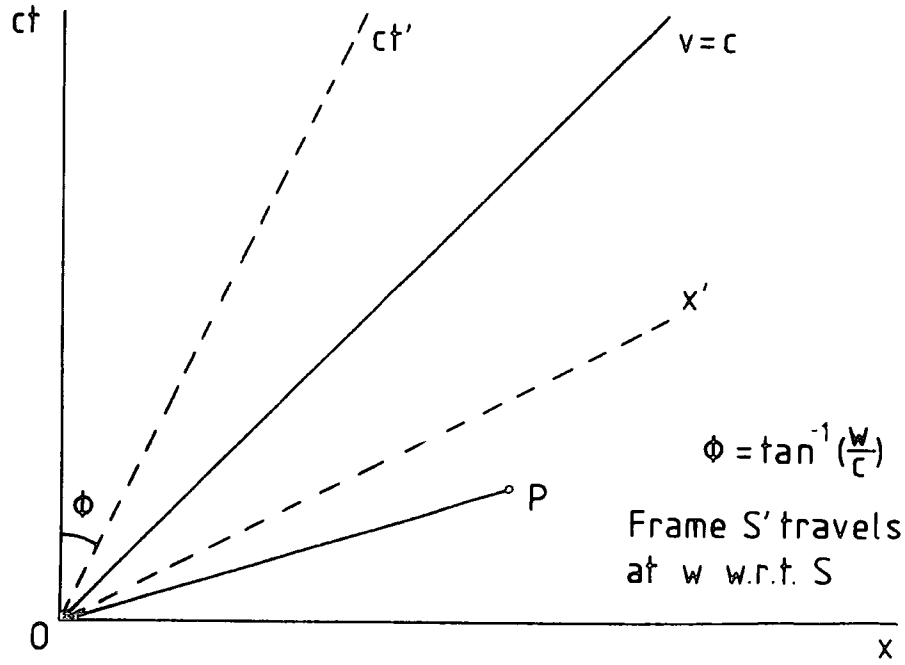

FIGURE 3.2 : Minkowski time-space diagram

the world line for stationary objects coincides with the ct-axis. For an observer in the primed frame moving at a velocity ω, with respect to the unprimed frame, these two conditions, ie. the limits of x=0 and t=0, are represented by different world lines in the unprimed frames. The angle, ϕ, which the primed axes make with their respective unprimed axes is given by $\phi = \tan^{-1}(\frac{\omega}{c})$.

Now consider the world line of a tachyon which passes O. The angle with the x-axis, α, must be less than 45^{o} for its velocity to be greater than c in the unprimed frame. To an observer in the primed frame, the situation will be different. If $45^{o} > \alpha > \phi$ then nothing out of the ordinary is observed. However if $0 < \alpha < \phi$ the particle will appear to be going back in time to O'. This paradox will occur when the condition $v\omega > c^{2}$ is satisfied.

This is, apparently, an untenable state of affairs. Bilaniuk and Sudarshan have noted that this time reversal also occurs at the point where the energy of the particle becomes negative. Using this they produced a principle which allowed a consistent theory of tachyons to be developed. This is known as the Reinterpretation Principle (RIP) and states that a negative energy particle which is observed first and later emitted is equivalent to a positive energy particle which is absorbed after emission (a normal situation). Although two observers will now disagree about the direction of travel, the laws of physics remain the same and this is all that is required by special relativity. The idea of the RIP is similar to the idea of anti-particles and the Stückelberg-Feynman interpretation of positrons as negative energy electrons running backwards in time (Feynman, 1949).

3.1.6 Tolman's Paradox

More subtle arguments against tachyons are based on the

possibility of faster-than-light communications. Most modern arguments are developments of the paradox of Tolman (1917).

Consider two observers, P in frame S and Q in frame S' (as shown in figure 3.3). P sends a superluminal signal to Q. It can be seen that it is possible for Q to send a superluminal signal to P which arrives before P had sent out the original signal, resulting in an apparent paradox. Again the paradox can be resolved by the use of the RIP. The interpretation which can now be given to the situation is that both observers believe that they are sending both signals and, as a result, there is no flow of information.

3.1.7 Basic Tachyon Kinematics

If we take equation 3.1 we can plot energy as a function of $\frac{v}{c}$ (β) as shown in figure 3.4. Tardyons can be seen to exist only within the bounds of $-1<\beta<+1$ irrespective of the amount of energy supplied. The minimum energy occurs when the particle is at rest and this energy is just the rest mass.

In contrast, if we provide energy to a tachyon it will slow down to c (but never reach this velocity). Moreover the minimum energy for a tachyon will be zero when its velocity is infinite. This has led to the suggestion that if electrically charged tachyons exist which spontaneously loose energy by radiation, a sea of transcendental (ie. with infinite velocity) tachyons will result. A transcendental tachyon will have the property of existing everywhere on its world line at any point in time. This leads to another interesting link with subluminal physics. In the latter we have the quantum mechanical situation of total uncertainty of position when a particle is brought to rest. For a tachyon the same occurs when its velocity is infinite.

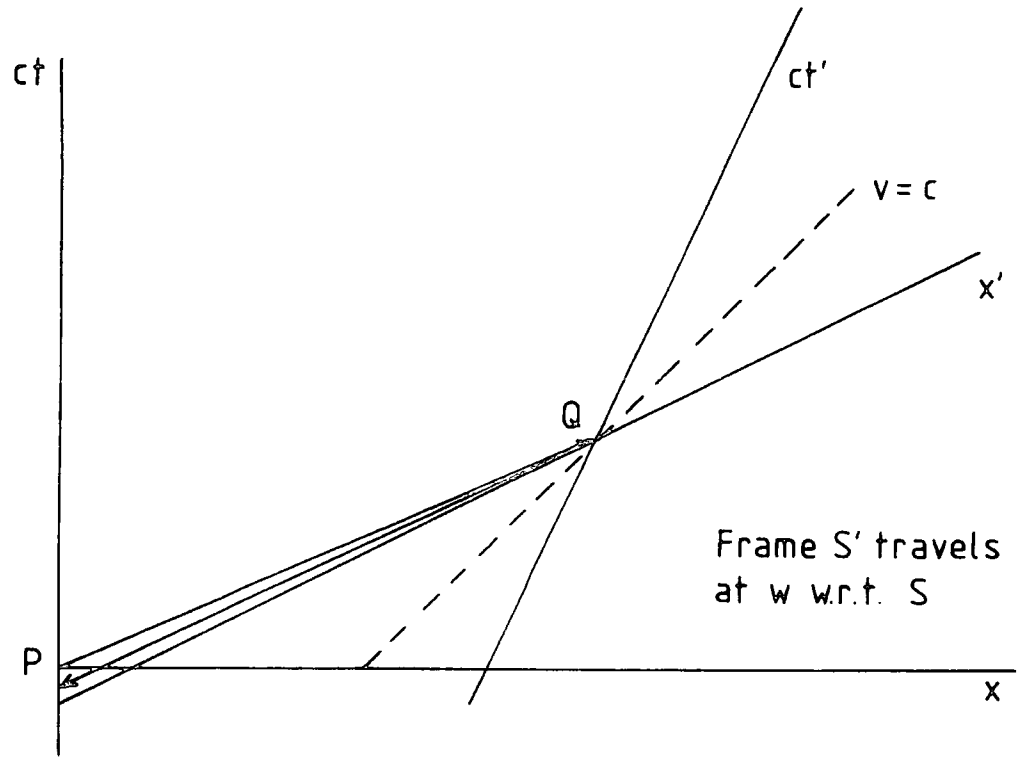

FIGURE 3.3 : Minkowski time-space diagram demonstrating Tolman's paradox

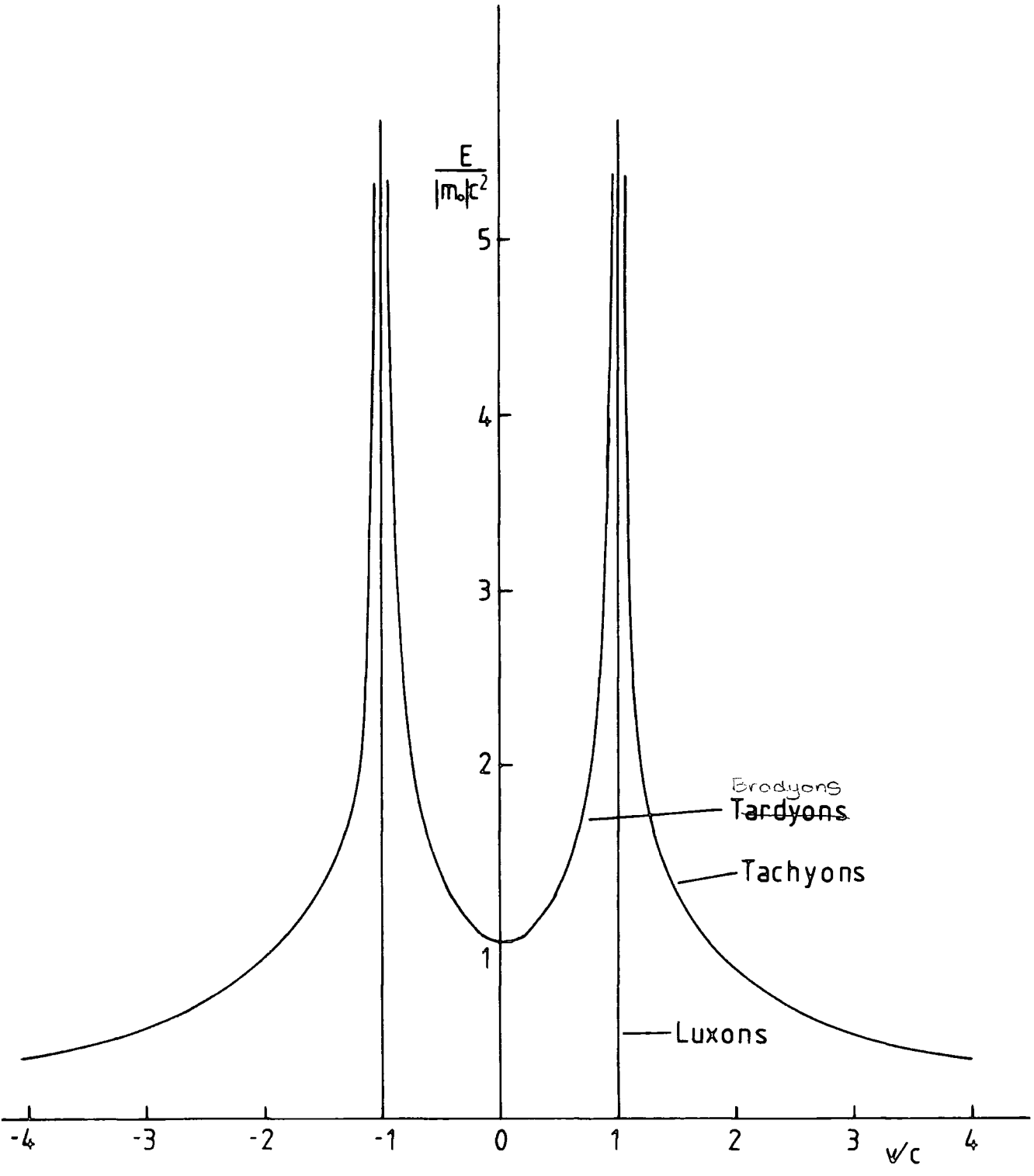

FIGURE 3.4 : Relativistic energy versus velocity

The momentum, as a function of β , is plotted in figure 3.5. Here, it can be seen that, the momentum of a transcendental tachyon is finite and equal to $m_* c$, compared to zero momentum for a ~~tard~~broad yon.

3.2 FURTHER PROPERTIES

3.2.1 Introduction

If tachyons are shown to exist then the above basic properties, in most physicist's eyes, are likely to hold. However further properties are much more contentious. The lack of progress in searches for tachyons and activity in other branches of theoretical physics has meant that little work has been done in the development of a consistent theory of tachyons in General Relativity and Quantum Theory. The main contributions have been due to Feinberg (1967) and Recami and Mignani (1974). The latter have produced many papers on all aspects of tachyon theory and are, perhaps, the most vigorous proponents of tachyons. Other contributors have, in general, concerned themselves with only limited topics, primarily related to the question of the existence of superluminal particles. There are basically two trains of thought. These are that tachyons are the same as ordinary particles (except for their velocity) and that tachyons are fundamentally different from ordinary particles.

Because of the limited amount of work done and the lack of a consensus on advanced theories, I will only discuss certain topics, concentrating on those which directly affect the ability to detect tachyons.

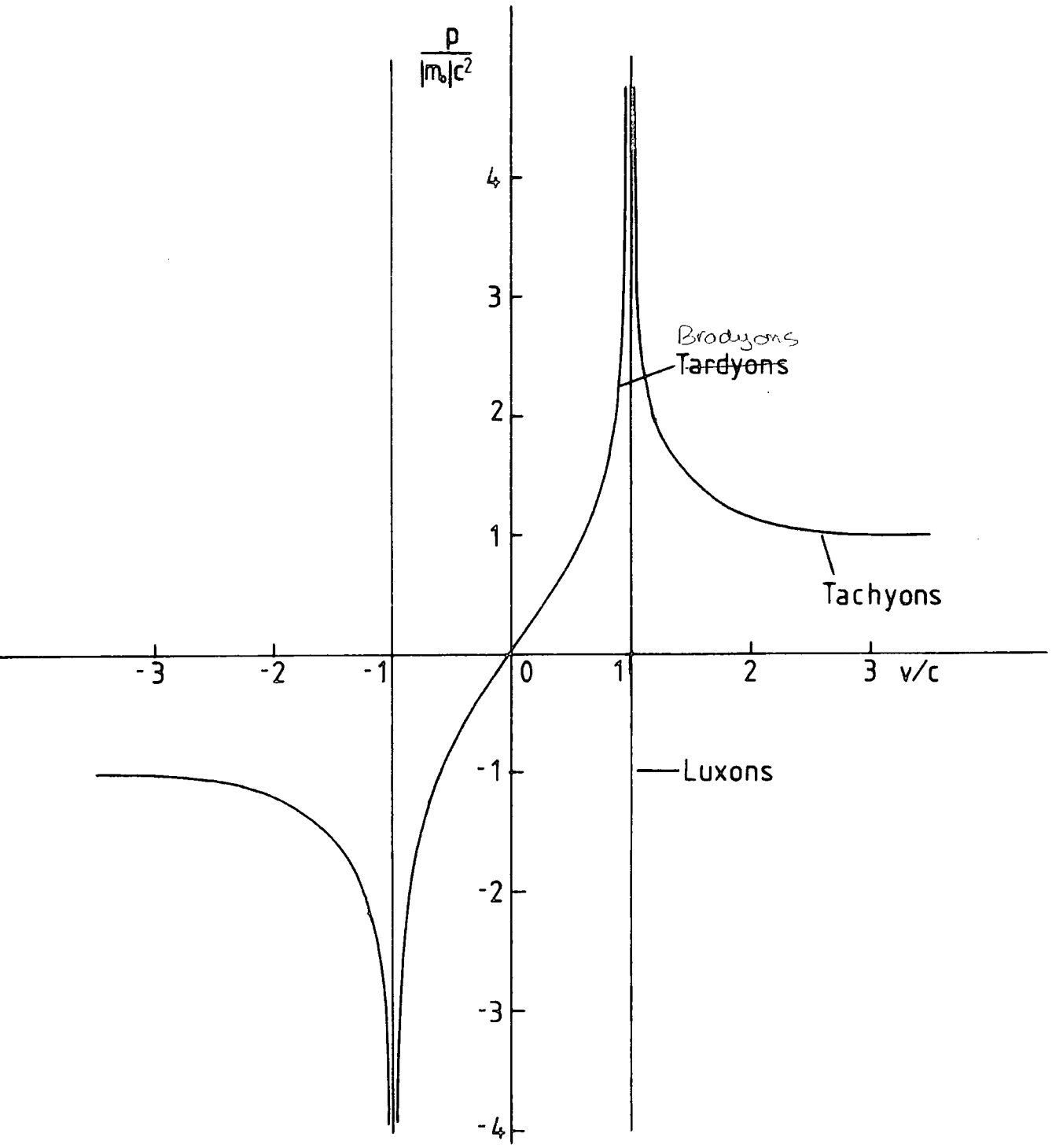

FIGURE 3.5 : Relativistic momentum versus velocity

3.2.2 Superluminal Frames of Reference and Extended Relativity

Mignani and Recami have developed special relativity (SR) to include tachyons. This so-called extended relativity (ER) includes an extra, third, postulate. 'Negative-energy objects or particles, travelling forward in time, do not exist (and physical signals are carried only by objects that appear to carry positive energy)'. This is, in effect, equivalent to the RIP. From these postulates they derive a revised SR. Also from this third postulate, the existence of anti-particles can be inferred. Application of the RIP will yield the anti-particles except for the helicity which is obtained from application of the complete LT. If we wish to include tachyons in SR, superluminal LTs (SLT) must be derived, as normal, subluminal, LTs are inadequate. Mignani and Recami have combined LTs and SLTs to form the generalised LTs (GLT). From the three postulates it can be seen that a tachyon in a subluminal frame is equivalent to a bradyon in a superluminal frame and vice-versa. Also a luxon is the same in either frame.

3.2.3 Quantum Field Theory

Much effort has been expended in trying to place tachyons in the framework of a quantum field theory (QFT). However a reasonable theory has not yet been formulated.

3.2.3.1 Feinberg (1967,1978)

Feinberg investigated a QFT of non-interacting, spinless, tachyons by considering the Klein-Gordon equation with virtual mass ($m=i\mu$). For its solutions to represent particles with real energy, a restriction that $|k| \leq \mu$ has to be imposed and the

implication of this is that tachyons cannot be localised in space, resulting in difficulties in describing propagation and thus velocity becomes a loosely defined parameter. Annihilation and creation operators are defined and a LT changes from one to the other, thus describing the interchanging roles of emission and absorption implied by the RIP. Subjecting the commutation relations of these operators to LTs produces the result that tachyons must be fermions.

The number of tachyons in a given reference frame is determined from a conserved current which is found to exist. Particle states can then be determined from the action of creation and annihilation operators and an inferred vacuum state. However this vacuum state is not Lorentz invariant and corresponds to causal anomalies which can be reinterpreted.

He also considers the production and scattering processes of tachyons and produces selection rules on the basis of energy and momentum conservation. He concludes that,

(i) any system of normal particles is energetically unstable against emission of tachyons.

(ii) tachyons can emit massless particles (eg . photons and neutrinos) without changing their own mass. Thus he allows the emission of Cerenkov radiation by tachyons in free space.

(iii) single tachyons can decay into several tachyons with the same μ^2 so that if the self-interaction is very weak there will be a rapid degradation of the energy spectrum.

3.2.3.2 Aarons and Sudarshan (1968), Dhar and Sudarshan (1968)

The theory of Feinberg was critisised for being incompatible with Lorentz invariance so a different form of quantisation is

used. This involved writing the scalar field in terms of the annihilation operators only. Thus anti-commutation rules are not necessary for quantisation and tachyons obey Bose statistics. However one result is that negative energy states can be created so that a physical postulate is required to deal with these. It is given as 'the only physically relevant quantities are the transition amplitudes. Any transition amplitude is to be interpreted as the amplitude for transition between positive-energy particles where all negative-energy particles (of momentum p) in the initial state are interpreted as outgoing positive-energy particles (of momentum -p); similarly for negative-energy particles in the final state'. This is just the RIP in another form.

3.2.3.3 Robinett (1978)

Solutions of the Klein-Gordon equations with imaginary mass have been investigated. He found solutions which show that the imaginary mass Klein-Gordon field propagates at no faster than the speed of light and thus concludes that this is an incorrect basis for the description of a tachyon, if such a particle exists.

3.2.3.4 Schwartz (1982)

It is suggested that Feinberg, and others, were wrong in using the conservation of four-momentum as the basis of a QFT for tachyons. Instead he considers the stress-energy-momentum tensor which is differentially conserved. The four-momentum can then be derived from this. This leads to a different quantisation of the field theory which does not require negative-energy states or the RIP.

3.2.4 Preferred Direction Theories

In order to overcome difficulties involved in the interpretation of imaginary quantities and acausality, several authors have discussed the idea of a preferred direction . Antippa (1972), Antippa and Everett (1971, 1973) add, to the postulates given by Recami and Mignani, one which states that 'the time axis is unidirectional with respect to bradyons but isotropic with respect to tachyons. The space direction is unidirectional with respect to tachyons but isotropic with respect to bradyons'. This removes the Lorentz invariance problem as only tachyons with positive or negative momenta need exist. For tachyons in a preferred reference frame, ie. having relative velocity along the preferred direction (the tachyon corridor), the GLTs hold with $\xi=\frac{1}{\beta}$ substituted for β. Thus a transform consists of general frame to preferred frame via a LT, preferred frame to preferred frame with relative motion via a GLT and finally to the new general frame via a LT. Another consequence of the preferred direction is that causal loops are removed since the world line of a tachyon always increases and the RIP is, therefore, not required. There are three experimental consequences,

(i) Flux will be unidirectional and hence detector orientation is important.

(ii) GLTs only operate in the preferred frame, so electromagnetic fields need not propagate at c when observed from another frame. Therefore Maxwell's equations are not obeyed and nothing can be implied about the tachyon-field coupling.

(iii) The violation of rotational invariance leads to directionality.

3.2.5 Lorentz Invariance

Many attempts have been made to solve the problems of

Lorentz Invariance (LI) violation. Pavlopulus (1967) proposed that LI is only approximate and valid in regions of space accessible to experiment. These regions are characterised by a universal length which is in the same order as the diameter of a proton. He concludes that, for very short wavelengths, the group velocity of an electromagnetic wave can exceed c. Consequently tachyons can only exist $\leq 10^{-15}$m away from a bradyon and thus only take part in strong interactions between bradyons confined to such regions.

Broido and Taylor (1968) investigate whether LI necessarily implies causality. They show that non-causal effects are impossible in a large class of theories which involve Lorentz invariant Green's functions and conclude that there are many difficulties in tachyon theories which aspire to relativistic invariance.

3.2.6 Electromagnetic Properties

This is an important area for investigation because of its implication for detection of tachyons. Recami and Mignani (1974), in their review, apply their GLTs to Maxwell's equations in order to describe the electromagnetic properties of tachyons as viewed from subluminal frames of reference. It is noted that the RIP is required to remove anomalies and that it has the effect of changing the sign of the charge of any particle which is 'reinterpreted'. Looking from a subluminal frame at a tachyon, requires the components of the four-vectors to be multiplied by i and it is noted that this is equivalent to rotating the Minkowski space-time diagram through $\frac{\pi}{2}$. They conclude that electromagnetic fields are changed in such a way that charged tachyons would appear as magnetic monopoles.

Lemke (1975, 1976a, b) used the SLTs of Antippa and Everett to derive the electrodynamics of tachyons. He had two critisisms

of Recami and Mignani's work,

(i) the transformation of the electromagnetic potential leads to the implication that tachyons produce Cerenkov radiation, which contradicts their prediction .

(ii) this also implies that a tachyon produces infinite radiation energy and hence must immediately lose all its energy.

He assumes the law of light speed invariance is not valid in its most general form and space is isotropic. He therefore does not imply the existence of a tachyon corridor but he uses a preferred direction along the instantaneous direction of motion of the tachyon. Though he obtains GLTs similar to those of Recami and Mignani, he choses different solutions of Maxwell's equations. Despite this, his conclusions are similar and his results agree with the magnetic monopole theory.

Marchildon et al (1979) discuss electromagnetic interactions on the basis of tachyon-bradyon reciprocity. They claim that Lemke's preferred direction argument is inconsistent. However their formulation produces the same results but disagree with his interpretation since he fails to take into account that the superluminal field doesn't satisfy Maxwell's equations, so that it cannot be identified with the ordinary, subluminal, field, nor can its coupling to bradyons be identified with the unit of electric charge. They investigate superluminal electromagnetic fields, derive Maxwell's equations and suggest the electromagnetic interactions of tachyons. A consequence of this is that they find that Cerenkov radiation should not be emitted unless there is an effective coupling of tachyons to the subluminal electromagnetic field. In their theory this must be very weak and the radiation would be very much less than that expected for a

charged particle of charge e and velocity greater than c, as assumed in searches for tachyons. They also suggest that tachyons can only couple very weakly to bradyons as in subluminal reference frames, superluminal electromagnetic fields obey equations different to Maxwells' and are not invariant. Finally they find that the electromagnetic behaviour is not exactly analagous to that of electric charges or magnetic poles. It is, loosely speaking, more like that of an electric charge.

3.2.7 Cerenkov Radiation

As will be mentioned in §3.3, the question of whether Cerenkov radiation is emitted by a tachyon travelling in a vacuum is fundamental to its detection. As has been seen from the previous sections, it is still very much an open question as to whether the quantum theories of tachyons allow the radiation, either in a vacuum or in a medium. However it is noted that the radiation is produced by the relaxation of a medium which has been polarised by the transverse component of the particle's electric field. One difficulty is that if, as has been suggested, the electric field is produced in a narrow cone along the direction of motion, then a very high density medium is required which would then provide high absorption for any radiation produced. Another difficulty is that for the radiation to be produced in vacuum, the vacuum must be polarised. This requires a vacuum structure which, though applicable in quantum mechanics, does not correspond to a real, physical, vacuum. Thus it is concluded that tachyons do not emit Cerenkov radiation in any situation.

3.2.8 Other Approaches to Tachyons

Many papers have been published which diverge from the

'mainstream' theories, in the main stimulated by those trying to dispose of tachyons once and for all. However the most interesting are due to those who believe in the tachyon's existence and have produced more original theories to support their belief.

3.2.8.1 Bludman and Ruderman (1968)

The classical physics of very dense matter was investigated, especially the case where the medium becomes 'ultrabaric'. This occurs when the pressure exceeds the total energy density, at which point a compressional wave in the medium will propagate at a velocity exceeding c, which is usually given as a reason for ignoring this state. They discuss two models which show this behaviour and suggest a link with quasars, the redshifts of which cluster around 1.95. They calculate limiting gravitational redshifts of just under 2 for their models.

3.2.8.2 Goldoni (1972, 1973)

It is pointed out that, according to Recami and Mignani, the four-momentum of a subluminal particle is not invariant under SLT. Hence two or more body interactions between bradyons and tachyons can only involve exchanges between those state vectors which are invariant under SLT, ie. they can only interact by changes in internal quantum numbers, eg. strangeness. By demanding invariance under SLT, the introduction of tachyons can only be justified if we hypothesise suitable interactions between tachyons and bradyons which allow one to interpret the breakdown of 'slow' symmetries as a process in which some quantum numbers are exchanged between the slow and fast worlds. He shows that a bradyon field and a tachyon field can only interact if massless

and deduces the existence of two massless particles - the 'slow' spurion and 'fast' tadpole - which are associated on a Feynman graph of massless field interactions.

3.2.8.3 Everett (1976)

He proposed an alternative, to special relativity, with preferred reference frames and deviations from LTs. For velocities close to c there are departures from relativistic physics. The dependence of mass and lifetime on velocity is determined and, in principle, acceleration past c is allowed.

3.2.8.4 Narlikar and Sudarshan (1976)

The propagation of tachyons in an expanding universe is discussed. A primordial tachyon, produced in the 'big-bang', would need a very large energy to survive. In an indefinately expanding universe the trajectory will turn back in time and a mass limit can then be set on the tachyon on the basis of its survival ($\frac{M}{m_e} \lesssim 1.8\ 10^{-11}$ for the Einstein-deSitter model and $\frac{M}{m_e} < 1.6\ 10^{-16}$ for the empty Friedmann model). It is suggested that photons and neutrinos are tachyonic. Finally the existence of tachyons may remove the space-time singularity of the 'big-bang' and provide a mechanism for homogenising the universe over large distances.

This area was further investigated by Walstad (1979). He chooses a preferred frame in which the microwave background and expansion appear isotropic. Together with the requirement that the cosmological model is completely causal, a preferred frame can be produced in general relativity. In addition to the conclusions drawn by Narlikar he suggests that tachyons might explain the 'missing mass' required to close the universe. However such paradoxes remain.

3.2.8.5 Kowalczyński (1978, 1979)

Solutions of the Einstein-Maxwell equations of general relativity, for a tachyon are studied. He shows that a moving tachyon would produce electromagnetic shockwave surfaces which could be detected by its effect on photons. The shapes of these surfaces are considered and it is suggested that, if they are strong enough to blacken the grains of nuclear emulsion, the shape could be used as a tachyon signature. He concludes that existing exposures should be examined for such surfaces.

3.2.8.6 Basano (1980)

He suggests that, while the RIP may be applicable at the microscopic level, it does not apply at the macroscopic level. The transition between the two is investigated statistically by using multiple causal loops. He also suggests that the RIP fails and symmetry violations occur when free will is taken into account.

In reply Maccarrone and Recami (1980) point out that this free will argument is incorrect but agree in part with the statistical argument. They conclude that further work in this area is required.

3.2.8.7 Santilli (1982)

The propagation of ordinary, massive, particles or physical signals under strong and electromagnetic interactions is considered. He states that $v_{max} = c$ is not 'universal', ie. not valid under all possible physical conditions of particles, eg. under strong interactions as a member of a nuclear structure; entering into deep inelastic collisions with other hadrons; moving within the core of a star. A generalisation of the v_{max} law depending on local quantities is produced and from this he concludes that,

in such cases, tachyons are normal physical particles and v_{max} can exceed c.

3.3 SEARCHES FOR TACHYONS

3.3.1 Introduction

Given the above theories one can proceed on the basis of Gellman's Totalitarian Principle: 'Anything which is not prohibited is compulsory'. The question is how to conduct the search, given that there is no consensus on the properties of tachyons. It is apparent that the most 'reliable' method is to measure the time of flight as this is fundamental to the particle's definition. Two further, more contentious, methods have been used, these being observation of Cerenkov radiation in a vacuum and observation of particle production in bubble chambers. The most popular method, though, has been to search for tachyons produced by cosmic ray interactions in the upper atmosphere. However the question remains as to how tachyons can be detected, if they can be detected at all.

3.3.2 Cerenkov Searches

Experiments of this sort assume that a tachyon will emit Cerenkov radiation in a vacuum (see §3.2.7), their variation being in how potential tachyons are generated.

3.3.2.1 Alväger and Kreisler (1968)

They used a 5 mCi Caesium 134 source to produce γ-rays with which it was hoped to produce tachyon pairs by using a lead target. A $3kVcm^{-1}$ field was applied, to resupply energy lost to radiation, and a photomultiplier tube used to detect photons. No peak in the observable range of 0.1e to 2e (where e is the

height of a pulse due to an electron) was observed and an upper limit on cross-section for production by 0.8keV photons in lead of $3\ 10^{-30} cm^2$ was determined. Two further assumptions required were that tachyons gain energy in an electric field as ordinary particles and they have a small probability of being captured in matter.

3.3.2.2 Davis et al (1969)

A similar experiment to that described above was conducted but using a 129 mCi cobalt 60 source of energy ~1.2 MeV. Two photomultipliers were used and a coincidence required. Again a negative result was found and an upper limit of $1.67\ 10^{-23} cm^2$ for the production cross-section determined.

3.3.2.3 Bartlett and Lahana (1972)

The same apparatus as Davis et al was used, but a magnetic field replaced the electric field, on the supposition that a tachyon should act as a magnetic monopole (§3.2.6). From the negative result it was determined that the upper limit for the cross-section for tachyon production by 1 MeV γ-rays in lead and water were $0.6\ 10^{-36} cm^2$ and $2\ 10^{-36} cm^2$ respectively.

3.3.2.4 Bartlett, Soo and White (1978)

In this experiment the assumptions were: monopole behaviour; production in cosmic rays; they would be influenced by the magnetic field in Fermilab's 15ft bubble chamber. However, in addition to looking for Cerenkov photons using photomultipliers, they had Lexan plastic detectors on the assumption that tachyons might produce tracks in them. An upper limit on the tachyon flux of $5\ 10^{-12} cm^{-2} s^{-1}$ was determined.

3.3.3 Bubble Chamber Searches

3.3.3.1 Baltay et al (1970)

Neutral tachyons produced from negative kaons and anti-protons interacting with protons in a bubble chamber were looked for, ie. reactions as follows :

$$\begin{aligned} &K^- p \to \Lambda^0 t^0 \to p\pi^- t^0 && \bar{p}p \to \pi^+\pi^- t^0 \\ &K^- p \to \Lambda^0 t^0 \bar{t}^0 \to p\pi^- t^0 \bar{t}^0 && \bar{p}p \to \pi^+\pi^- \bar{t}^0 t^0 \end{aligned} \qquad (3.4)$$

The spacelike four-momentum property is used. For single particle production, the 'missing mass' technique is employed, a tachyon's signature being a negative missing mass squared. For tachyon pairs the missing mass squared can be positive or negative, which causes difficulties. However it is sensitive for pairs with mass greater than a minimum value. The resulting production rates are given as :

$$\begin{aligned} &\frac{K^- p \to \Lambda^0 t^0}{K^- p \to \Lambda^0 \pi^0} \leqslant 2\ 10^{-3} && \frac{\bar{p}p \to \pi^+\pi^- t^0}{\bar{p}p \to\ 3\pi} \leqslant 2\ 10^{-3} \\ &\frac{K^- p \to \Lambda^0 t^0 \bar{t}^0}{K^- p \to \Lambda^0 \pi^0} \leqslant 2.5\ 10^{-3} && \frac{\bar{p}p \to \pi^+\pi^- \bar{t}^0 t^0}{\bar{p}p \to\ 4\pi} \leqslant 1\ 10^{-3} \end{aligned} \qquad (3.5)$$

It is concluded that if tachyons exist then they must be very weakly interacting with ordinary matter.

3.3.3.2 Danburg et al (1971, 1972)

The first experiment was a search for tachyon pairs produced by 2.2 GeV/c $K^- p \to \Lambda t^+ t^-$ interactions. It assumed that,

(i) the tracks were visible so the particle's velocity can be determined from the curvature.

(ii) tachyons behave as ordinary particles in magnetic fields.

(iii) Cerenkov radiation is suppressed so that it is not the

dominant energy loss.

No events were found and the upper limit on the cross-section for the production of t^+t^-, having 'rest mass' between ~100 MeV and 1 GeV, of 0.2 μbarn was determined.

The second involved decays of the form $p \rightarrow pt^o$ and $p \rightarrow pt\bar{t}$, ie. the observation of a proton recoil without an incoming particle. The experiment could distinguish recoil protons of kinetic energy as low as 4 MeV. None were found and the lower limit for the lifetime of free protons for elastic, tachyonic, decay via the above reactions is $2\ 10^{21}$ yr.

3.3.4 Indirect Methods

3.3.4.1 Cohen et al (1977)

Using very long baseline interferometry measurements, they have shown that nearly half of strong compact extragalactic radio sources appear to be expanding with velocities in the range 4c to 10c. The sources take the form of two components receding from each other along some preferred direction. Explanations for this phenomena, eg. Blandford et al (1977), run into difficulty since the expansion is not spherically symmetric. Much better measurements are required in order to clarify the position.

3.3.4.2 Cooper (1978)

A reanalysis of the experiment by Chamberlain et al (1955) in which the anti-proton was discovered was conducted. The experiment involved negative particles being scattered in the forward direction when the Bevatron proton beam impinged on a copper target. In addition numerous mesons were detected. The spectrum of velocities of these mesons was found to exceed c, the

mean being 1.053c, and this led to a probability of 0.9972 that meson velocities exceeded c. Since the time of flight was critical to measure the anti-proton mass the original experiment would be invalidated if the data was adjusted to remove the super-luminal velocity (which would mean greater than 5% error in the 40 ft distance). Even working back from a more accurate anti-proton mass determination results in a probability in excess of 0.863.

3.3.4.3 Andreyev et al (1979)

A scintillation telescope was used for time of flight measurements and the time resolution determined. Particles with anomalous velocities were found and it was concluded that an upper limit on the intensity of penetrating particles with anomalous velocity of less than 8 $10^{-12}cm^{-2}s^{-1}sr^{-1}$ for $\beta>2$ and $\beta<0.66$ was determined with a 90% confidence level.

3.4 EXTENSIVE AIR SHOWER SEARCHES

3.4.1 Principle

This type of search assumes three properties of tachyons to be true :

(i) They travel faster than light (true by definition).

(ii) They are detectable. Usually this means that they should give up energy to a scintillator.

(iii) They are produced in the interaction of very high energy cosmic ray primary particles at the top of the atmosphere, and are not absorbed by the atmosphere.

The latter two properties are considered reasonable in the light of the, previously discussed, theory.

The shower front moves with a velocity very close to that of light. A tachyon will therefore arrive at the observer before the shower front. One would expect the most likely tachyon production to be a tachyon-antitachyon pair created with the production threshold energy and zero kinetic energy giving an infinite velocity. For large kinetic energies the velocity tends to the velocity of light. On average a primary undergoes its first interaction at an atmospheric depth of 97 gcm^{-1} (17 km above sea level). For a vertical shower a tachyon would, therefore, arrive within a period of 57 μs before the shower front. For a shower with an axis inclined at 60^{o} to the vertical (less than 1% of all showers at sea level have zenith angles greater than 60^{o}) then this rises to 114 μs. So if tachyons exist one would expect to observe a number of events, within a period of 120 μs prior to the shower front, in excess of that expected due to the random background.

A review of experimental searches using this principle are given in the following sections.

3.4.2 Ramana Murthy (1971)

In this experiment a period of 19 μs previous to an extensive air shower (EAS) was examined for potential tachyon signals. The procedure was to open a 20 μs long gate on arrival of a potential signal and look for the arrival of an EAS in this period. This was then to be compared with the number of EAS expected to arrive by chance, an excess of actual events would then indicate the presence of tachyons.

A potential tachyon signal was derived in one of two ways. Firstly using a photomultiplier viewing a liquid scintillator

which may detect charged or neutral tachyons interacting with the scintillator medium (mode 1). Secondly using a method similar to Alväger and Kreisler (1968) where a coincidence was required from a pair of photomultipliers viewing the gap between two electrodes for the production of Cerenkov radiation (criticism of this method was given in a previous section) by charged tachyons (mode 2).

The EAS signal is produced using a coincidence from four photomultipliers viewing four scintillators situated at the corners of a square of side 10 m. The electron density requirement was 1 m^{-2} and the trigger rate was 20 min^{-1}. The experiment was run for 5079 hr in mode 1 and 2597 hr in mode 2. In both cases the number of coincidences fell within one standard deviation on the expected number of chance coincidences. It was concluded that the frequency of occurrence of tachyons is less than 3 10^{-4} to 1 10^{-5} relative to that of electrons.

3.4.3 Clay and Crouch (1974)

A plastic scintillator was used as the tachyon detector. The output of a photomultiplier was fed into a digital transient recorder which digitises to six bit accuracy. Each word is then put into a 256 word store (representing a 128 μs delay). This was then output to a chart recorder which reduced the effective delay to 114 μs.

The EAS trigger was obtained from five 1x1x0.005 m^3 plastic scintillators, arranged in a square array of side 30 m, one at each corner and one at the centre. A coincidence between the central detector and any three of the others produced a trigger which was then used to trigger the transient recorder.

In analysis, the observed time period was reduced to 97.5 μs. The position, in time, of the largest pulse which occurs in this period was noted and plotted on a histogram. This was then compared with a histogram produced using a random trigger. The resulting distribution was found not to be uniform and it was concluded that non-random events, preceding the arrival of an EAS, had been observed and it was suggested that this was a result of particles travelling with an apparent velocity greater than c.

3.4.4 Prescott (1975)

Prescott followed up the work of Clay and Crouch by re-analysing their data and performing new experiments. His reanalysis consisted of comparing the number of pulses in the 0 to 105 μs previous to the shower front with that in the 105 to 210 μs region. No excess of pulses were seen in the former interval, thus contradicting the previous results. This discrepency was traced to the large overshoot (~30%) generated in the transient recorder. This meant that any pulses in the first and second bins would be substantially lowered if a large pulse arrived just prior to them. This led to a deficiency in 'largest pulse' counts in these bins and hence an erroneous χ^2.

The Clay and Crouch apparatus was modified to reduce the overshoot and the results from this produced no evidence for a non-uniform distribution in the time interval preceeding the shower front. Also an independent experiment was devised. This consisted of a 50x50x10 cm^3 plastic scintillator, viewed by a two inch photomultiplier, located 17.5 m from the centre of the Buckland Park array. The signal was amplified and delivered to a

transient recorder with output to a chart recorder. Signal to noise was improved by two orders of magnitude, from ~0.1 of the mean single particle energy release in the scintillator to $5\ 10^{-4}$. Overshoot was reduced to less than 0.5%. 4315 showers of energy greater than $5\ 10^{15}$eV were observed and produced a negative result. An upper limit on the tachyon/electron flux, at the 90% confidence limit, was determined as $5\ 10^{-5}$.

3.4.5 Fegan et al (1975)

A search was conducted at sea-level, using a 250x5 cm^3 plastic scintillator, placed at the centre of an array of three 500x0.5 cm^3 plastic detectors, to provide the air shower trigger. This produced a rate of about 1 hr^{-1} which corresponded to a mean shower energy of $2\ 10^{15}$eV. The output of the two, five inch, photomultipliers ,viewing the detector in coincidence, was fed to a 200 bit static shift register which produced an 800 μs record of the time distribution of detected events.

Two modes of operation were used. The first, mode A, demanded coincidence between the photomultipliers and corresponded to an energy deposit in the scintillator of $\geq$1 MeV. The second, mode B, took an output from only one of the photomultipliers and corresponded to a deposit of $\geq$0.5 MeV. The EAS trigger was used to inhibit the shift register clock 380 μs after the trigger and so retain a record of its contents from 420 μs before the front to 380 μs after.

A statistical analysis of the interval 12 μs to 408 μs before the front produced no evidence for a deviation from a random distribution. Upper limits for the tachyon flux, at the 3σ level, were determined as $2.06\ 10^{-2} m^{-2} shr^{-1}$ in mode A and

6.58 $10^{-2}m^{-2}shr^{-1}$ in mode B, at the mean shower energy.

3.4.6 Emery et al (1975)

An array of four 1x1 m^2 trays, each with 24 Geiger-Muller counters, were set up with three evenly spaced on a circle of radius 21.2 m and one at the centre. The air shower trigger was such as to produce a rate of 357 per day corresponding to an energy of about 10^{15}eV. The outputs of all tubes were connected in parallel to a shift register which allowed an interval of 108 μs to be recorded. 27449 showers were recorded, during which 3512 GM pulses preceeded them in the 108 μs. A χ^2 test produced a 0.9 probability that the time distribution was the same as a uniform one.

A second experiment involved a 75 cm diameter, 2.5 cm deep, liquid scintillator at the centre of the array. This was used because of the possibility that tachyons might not trigger GM counters but be capable of producing pulses in scintillators. The system was set to record pulses greater than 0.1 of a muon pulse. 3766 precursor pulses were seen in 9521 showers, which gave a 0.15 probability of the distribution being uniform. It was concluded that there is no positive evidence for tachyons in association with air showers.

3.4.7 Hazen et al (1975)

The tachyon detectors consisted of plastic scintillators of dimensions 1.2m x 1.2m x 38mm with an output to a transient recorder (which recorded pulses between 0.03 and 0.1 of the height due to a single muon and in a time domain of 170 μs). The trigger from the array produced a rate of 10 hr^{-1} corresponding to a minimum shower size of around 10^5 particles. The first run

consisted partly of using two detectors and partly using one. The number of largest pulses detected in the interval prior to the shower front was compared with that from a run using a random trigger, generated by very small showers. No evidence for a significant difference was found.

A second run involved the use of two detectors placed one above the other. The time distribution of coincident pulses in the 160 μs prior to the front were found, using a χ^2 test, to not be significantly different from a uniform distribution. They concluded that the upper limit on the flux of tachyons at sea-level, associated with EAS of size 10^5 is $10^{-8} cm^{-2} s^{-1} sr^{-1}$.

3.4.8 Smith and Standil (1977)

A cosmic ray telescope, consisting of five scintillators of area 0.7 m^2, was used. Each element could register particles which deposited energy greater than a fifth of that due to a muon and the detector registered charged particles at a rate of 27.5 s^{-1}. Air showers were detected by an array of three detectors which triggered on showers of energy $6\ 10^{14}$eV at a rate of $10^{-2} s^{-1}$.

The detection of a tachyon candidate caused three independent measurements of the ionisation of the initiating particle to be digitised and stored. If an air shower arrived within 290 μs of this event, the data, along with the pulse heights from the array detectors and the time, would be saved on paper tape.

The apparatus was run for 223 days, during which numerous checks on the stability of the detecting system were carried out. 204702 showers were recorded, along with 1519±39 tachyon candidates. When the number of expected coincidences were subtracted, an excess of 46±40 events were found. It was concluded that these

could be explained as random coincidences between the start and stop signals at the time to amplitude converter.

3.4.9 Ashton et al (1977b)

Air shower triggers were provided by the Durham Array outer ring, as described in chapter 2, with a rate of (8.53 ± 0.46) hr^{-1} and a minimum shower size of about $8\ 10^4$ particles. The tachyon detector consisted of a layer of scintillation counters, each of thickness 5 cm, with a total sensitive area of 2.1 m^2. The equipment consisted of, from top to bottom, 15cm of lead, 8 layers of neon flash tubes, 15cm of iron, the tachyon detectors and 108 layers of flash tubes. The outputs from the scintillators were summed, passed through a 240 μs delay line and displayed on an oscilloscope, the screen of which was photographed. The flash tubes allowed the tracks of tachyon candidates to be recorded. However they also introduced the possibility of high voltage pick-up pulses in the detector electronics.

In 341 showers, six precursors were observed with pulse heights greater than three times the height of that due to a relativistic muon. Moreover these all occurred in the time interval 0 to 120 μs preceeding the shower front. No anomalous tracks were seen to be associated with the events. The number of such pulses expected was calculated to be 0.81. In addition a χ^2 test gave a probability of $4.5\ 10^{-6}$ that six events would occur in this region and none in the 120 to 220 μs region. It was concluded that a possible flux of tachyons existed but that better statistics were required to establish if the effect is real or not.

3.4.10 Bhat, P. N. et al (1979)

A search was conducted using a tachyon detector 10m from the centre of an array of 24 detectors. The tachyon detector consisted of two plastic scintillators each 80x80x1 cm^3, located in a stack of 14 gcm^{-2} iron plates which form the multi-plate assembly of a large bubble chamber. A 48 gcm^{-2} layer of lead shields the chamber from low energy particles. The output of the detector is discriminated at the three muon level. The apparatus was operated in two modes. In the first the two scintillators were operated in coincidence and a period of 1 to 401 μs after a tachyon candidate was scanned for the arrival of an air shower. If one arrived, then the delay time and the air shower data were recorded. The rate of air showers was 12 hr^{-1} and the estimated minimum size of the showers was 2 10^5. 20988 showers were observed in 1749 hr and four events were observed. Since the number expected was seven, there was no excess of events.

In the second mode only one detector was used. The trigger was adjusted and gave a rate of 42 hr^{-1} with a minimum shower size of around 10^5. 78624 showers were observed and 27 events occurred compared with 31 expected. The events were also uniformly distributed over the time interval. From the experiment they concluded that the upper limit on the tachyon flux, at the 95% confidence level, is 2.3 $10^{-10} cm^{-2} s^{-1} sr^{-1}$.

3.4.11 Fegan (1981)

Three plastic scintillators of 0.05 m^2 area, at the vertices of an equilateral triangle of side 20 m, constituted the air shower selector. The minimum shower energy which would produce a trigger was 10^{16}eV which corresponded to a rate of 0.17 hr^{-1}.

The tachyon detector consisted of a 0.5 m^2 x 0.025 m sheet of NE102 plastic scintillator with two five inch photomultipliers attached. The signals from both tubes were summed and fed to a transient recorder. This allowed a period 480 μs before the shower to 24 μs after to be recorded. The detector was shielded by 15 cm of lead. Amplitude integrated histograms were produced, both for the real data and the random data, which was from triggers injected throughout the experiment as a system check. Grouping the data into 12 bins revealed no significant excess in any time bin. However there was some evidence for clustering between 48 and 60 μs when 960 bins were used, the peak deviating by 5.33σ from the mean at 57 μs. This remained despite re-analysis to remove noise fluctuations. Fegan suggested that the excess is not inconsistent with tachyons but could be caused by correlated showers (Gerasimova et al, 1960). However Gerasimova determines the cores of associated showers to be separated by a distance of about 1 km which makes this explanation unlikely.

3.5 CONCLUSIONS

The existence of tachyons has been shown to be still very much open to doubt. Attempts to form a reasonable, theoretical, framework from which their interactions and properties can be formulated are also shown to be somewhat confused. This has meant that searches have had to cover a wide variety of possible behaviour and negative results are difficult to interpret since they test for two things, ie. the production mechanisms and sources of tachyons and the ability to detect them. Thus in bubble chamber searches the conclusions can be that the production threshold is high and/or that their interactions with matter

are so weak that they cannot be detected. As has been discussed it is believed that Cerenkov experiments are invalid.

Cosmic ray searches, a review of which are given in table 4.2, allow a higher production threshold to be investigated but rely on the detection of tachyons by scintillation counters or Geiger-Muller tubes, either directly or indirectly through the production of secondaries. Nevertheless they are the most promising of existing methods of search.

CHAPTER 4

THE TACHYON SEARCH EXPERIMENT

4.1 INTRODUCTION

The lack of tachyon detection at laboratory energies suggests that, if tachyons are produced, then some reasonably high threshold energy for production must exist. So recent searches have been conducted in extensive air showers. The method used for the search is that first used by Ramana Murthy (1971) and since used by others (see chapter 3).

It is assumed that tachyons are produced as particle-antiparticle pairs in interactions of the sort that occur when a high energy cosmic ray primary proton collides with a nucleus in the upper atmosphere, ie. a reaction of the type :

$$p + N \rightarrow N + N + t + \bar{t} + \text{mesons} \qquad (4.1)$$

Alternatively, if tachyons are produced in cosmic ray sources and have an interaction length comparable with that of a proton primary, thus initiating an extensive air shower, then these, too, can be detected by this method.

A second assumption is that a tachyon will lose energy in a scintillator and give rise to photons or will be detectable by the production of secondary particles which can be detected. In the absence of a consistent theory these assumptions are considered reasonable.

On average a primary proton undergoes its first interaction at an atmospheric depth of 97 gcm^{-2} (17 km above sea-level). If it has sufficiently high energy ($\gtrsim 10^6$ GeV) it will then

produce an extensive air shower, the front of which propagates at a velocity very close to that of light. The most likely kinetic energy for a tachyon is zero, ie. it is created at the production threshold energy. In this case its velocity will be infinite. Also, if the initial kinetic energy is greater than zero, any interaction with the atmosphere will lower its kinetic energy and its velocity will increase.

For this case, a tachyon would arrive within a period of 57 μs before the shower front. For showers inclined at 60^{o} (less than 1% of showers have zenith angles greater than 60^{o}) this is increased to 114 μs. For finite velocity tachyons or for tachyons produced in secondary hadron interactions, low in the atmosphere, the delay time would be smaller.

The events in the 240 μs preceeding a shower are studied and the distribution in the region 0 to 120 μs compared, statistically, with that in the region 120 to 240 μs. This should indicate any excess of particles in the first region which could be tachyons.

4.2 EXPERIMENTAL ARRANGEMENT

4.2.1 Introduction

The tachyon detector was the 2x1x0.025 m^3 plastic scintillator, designated 31, in the air shower array. This is unshielded except for approximately 2 gcm^{-1} of wood, which is negligible. The electronics used in conjunction with this detector have been described in chapter 2. The signal from this detector was taken from the buffer/fan-out unit and fed through 264 μs of delay line. The delay line output is fed to an oscilloscope which is triggered and photographed in an identical manner

to that used for recording the air shower data. A block diagram of the system is given in figure 4.1.

4.2.2 The Delay Lines

Hackenthall 1600 delay line was used, which has a delay of 1 μs per foot. The losses in the line are such that severe attenuation is caused. Thus a 240 μs length could not be used. The delay line was divided into three 80 ft lengths, each followed by a buffer-amplifier. The buffer-amplifiers were adjusted so as to restore the pulse height to its original value before entering the next section of line. They consist of three 741S operational amplifiers which perform as two inverting amplifiers and a buffer (figure 4.2). The overall gain of the system is thus set equal to unity. To prevent reflection of pulses at the ends of each delay line, each was terminated by its characteristic impedance (1.65K) so as to make the lines appear to be of infinite length.

It was found that coiling the delay lines and putting them in trays was impracticable. This was because the electromagnetic field, due to the pulse travelling down the line, interacts with adjacent sections of the line and produces noise and reflection of pulses. To overcome this, each was wound round a wooden former of 75 cm length and 45 cm diameter, which was found sufficient to space each loop and make the interaction effects negligible. The total delay was measured and found to be 264 μs since the figure of 1 μs per foot for the delay line is only approximate.

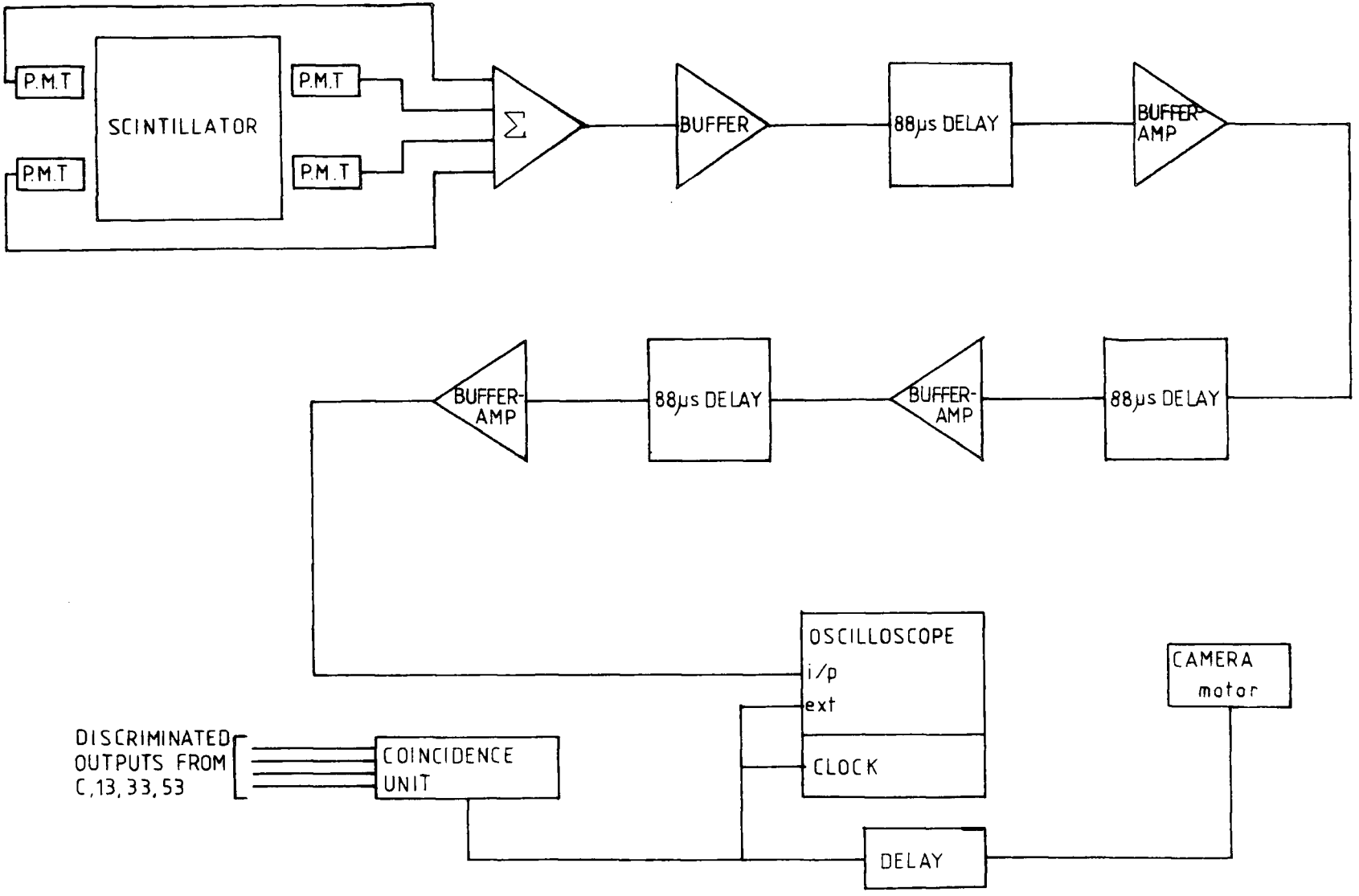

FIGURE 4.1 : Block diagram of tachyon search experiment

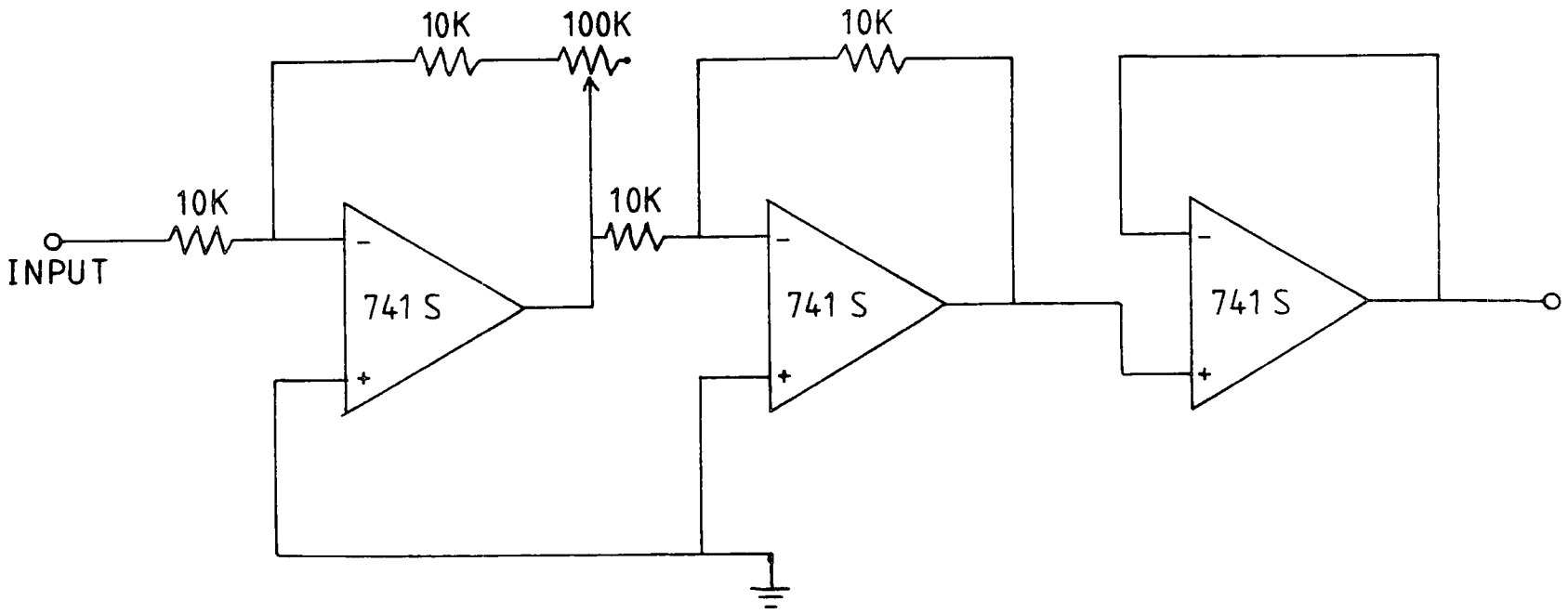

FIGURE 4.2 : Circuit diagram of delay line amplifiers

4.2.3 Display of the Delay Line Output

The delayed signal was fed to one channel of a Tektronix 5102A dual beam oscilloscope, the other beam being used as a base line marker in case of pulse undershoot. The timebase was adjusted to be 300 μs to enable all the delay period and the shower front pulse to be recorded. The maximum recordable height was set to 400 mv (equivalent to fourteen particles passing through the detector). The oscilloscope was triggered and photographed (along with a digital clock) in the same manner as that described for the air shower array output.

4.2.4 Triggering

The air shower trigger front was established using the outer ring detectors, ie. C,13,33,53. The triggering thresholds used were as follows : ΔC (≥ 20.2 m^{-2}), $\Delta 13$ (≥ 4.2 m^{-2}), $\Delta 33$ (≥ 4.6 m^{-2}), $\Delta 53$ (≥ 4.6 m^{-2}), which gave a trigger rate of 3.9 hr^{-1}. The theoretical range of shower sizes and the core distances which can be detected with these thresholds were calculated, as described in appendix B, and the results shown in figures 4.3 and 4.4. The minimum detectable shower size was found to be $2.5\ 10^5$ particles which is equivalent to a primary energy of about 10^{15}eV.

4.3 DATA AND CHECKS ON CONSISTENCY

The experiment was run for 1660 hours and in this time 6461 shower triggers occurred. During this time the normal air shower array checks were made. In addition the gain of the delay line system was monitored, but it was not found to change significantly during the experiment.

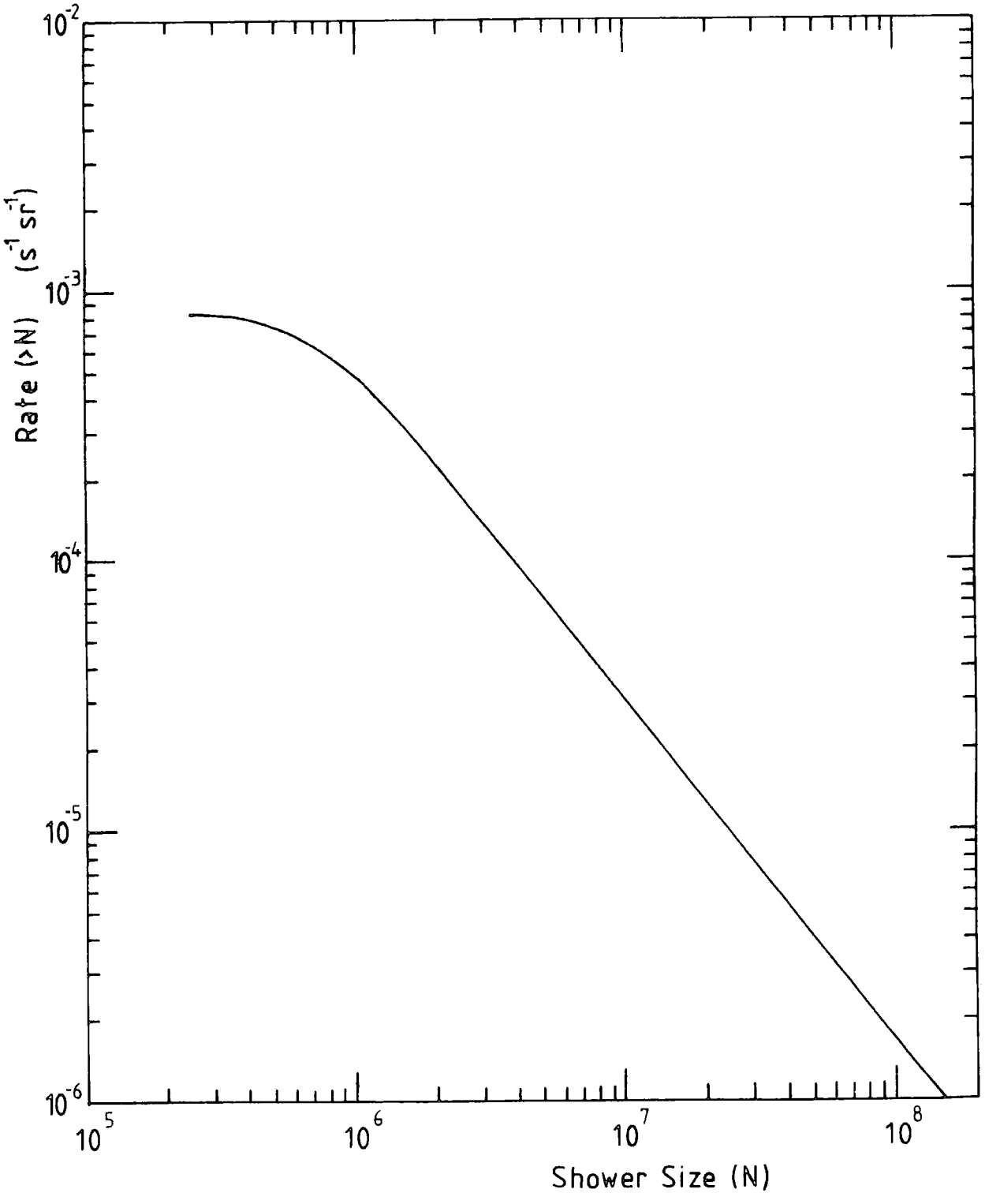

FIGURE 4.3 : Rate of showers of size greater than N which trigger the array. ($\Delta_c \geq 20.2m^{-2}$, $\Delta_{13} \geq 4.2m^{-2}$, $\Delta_{33} \geq 4.$ m^{-2}, $\Delta_{63} \geq 4.$ m^{-2})

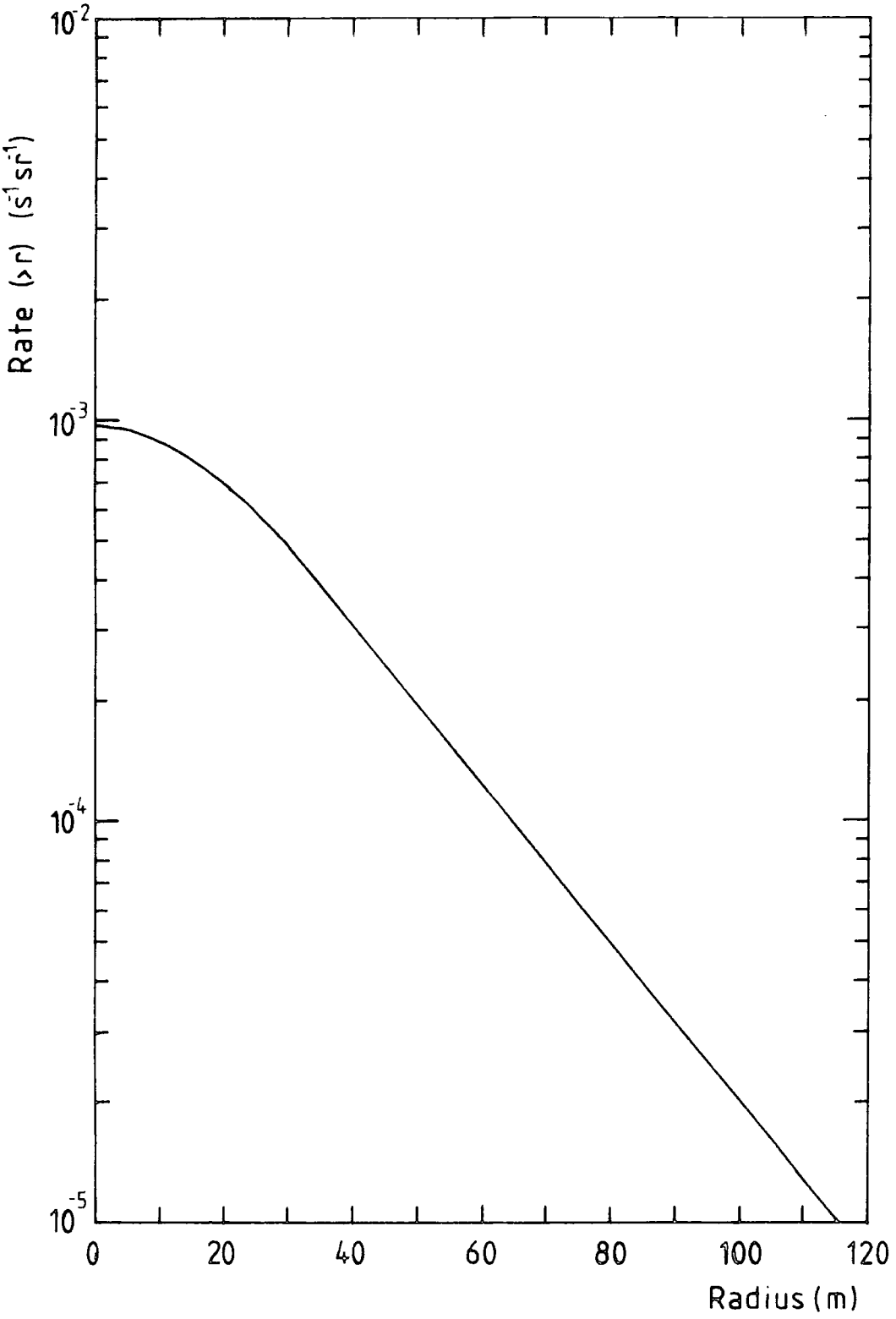

FIGURE 4.4 : Rate of showers which trigger the array and whose cores fall at a distance greater than r from the centre of the array. ($\Delta_c \geq 20.2m^{-2}$, $\Delta_{13} \geq 4.2m^{-2}$, $\Delta_{33} \geq 4.6m^{-2}$, $\Delta_{53} \geq 4.6m^{-2}$)

Figure 4.5 serves to illustrate the salient features of the oscilloscope trace. Actual traces are shown in figures 4.6a and 4.6b. The extensive air shower front pulse is preceded by a 'hump' of width approximately 80 μs and a region of high frequency oscillation which extends for a region of about 20 μs prior to the arrival of a shower front pulse and both are instrumental in nature.

The height of the hump was investigated as follows. The integral distribution of particle densities in detector 31 is plotted in figure 4.7. These were determined from a run of the air shower array, using the same trigger levels. This has to be done because the dynamic range of the recording system could not include both the shower front pulses and the much smaller single particle pulses. It is seen that the median particle density is $26m^{-2}$ corresponding to 52 particles traversing the 2 m^2 detector. In the present experiment, the average pulse height produced by relativistic particles traversing the detector at normal incidence is 28.7 mv. Using this figure we can compare the integral distribution of hump heights and these are plotted, assuming them to be proportional to the shower front pulse heights (ie. proportional to the particle densities) and fitting this to the density distribution. It was found that the two fitted if the hump was $7.7\ 10^{-3}$ the height of the shower front pulse. Although the hump is not serious in reducing the efficiency of detecting shower precursors, the high frequency oscillation which occupies the 20 μs time domain prior to the shower front pulse is, and will be discussed later.

It is to be noted that shielding the detector, just sufficient to absorb the electron-photon component of the

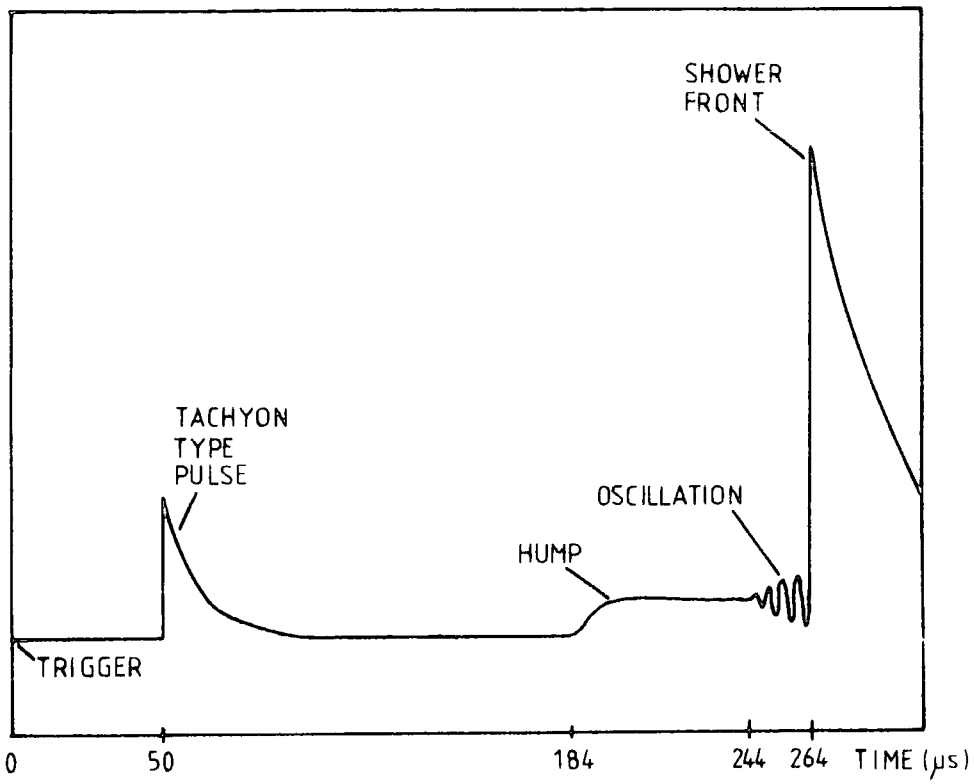

FIGURE 4.5 : Typical oscilloscope photograph showing a tachyon type pulse. Normally the air shower front pulse height is off-scale. Tachyon pulses are expected to occur in the 120 μs time domain preceeding the EAS front pulse. The tachyon type pulse in the diagram is drawn outside this time domain for clarity of presentation.

FIGURE 4.6 :

a) Trace showing two precursor pulses (one being too small to measure), occurring at 210 and 118 μs prior to the shower front, associated with a small shower.

b) Trace showing a very large air shower with associated 'hump' and oscillation. A precursor pulse has occurred on the 'hump'.

The time between the start of the timebase and the arrival of the shower front is 264 μs. The vertical scale is approximately 1cm : 25mv.

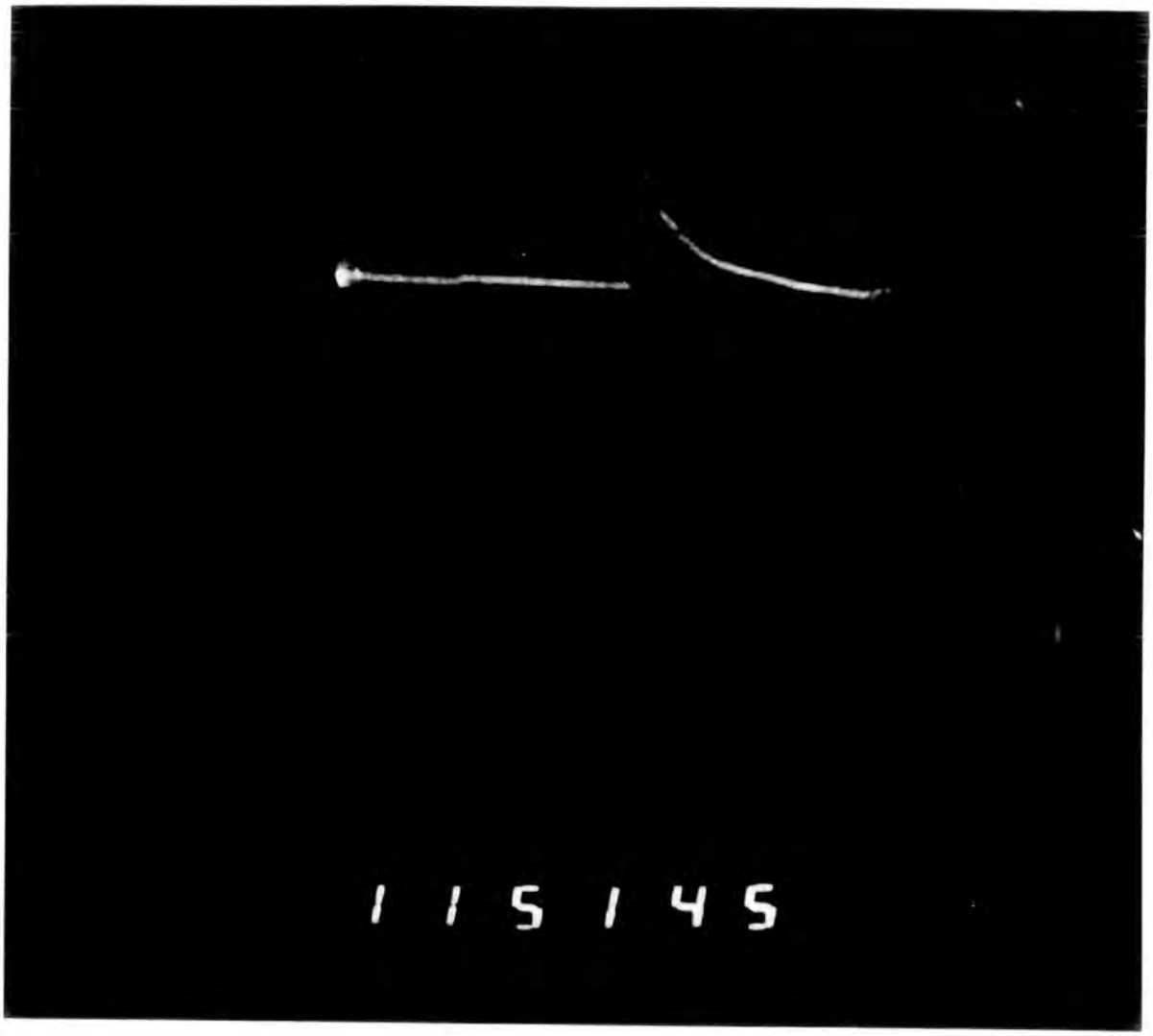

FIGURE 4.6a

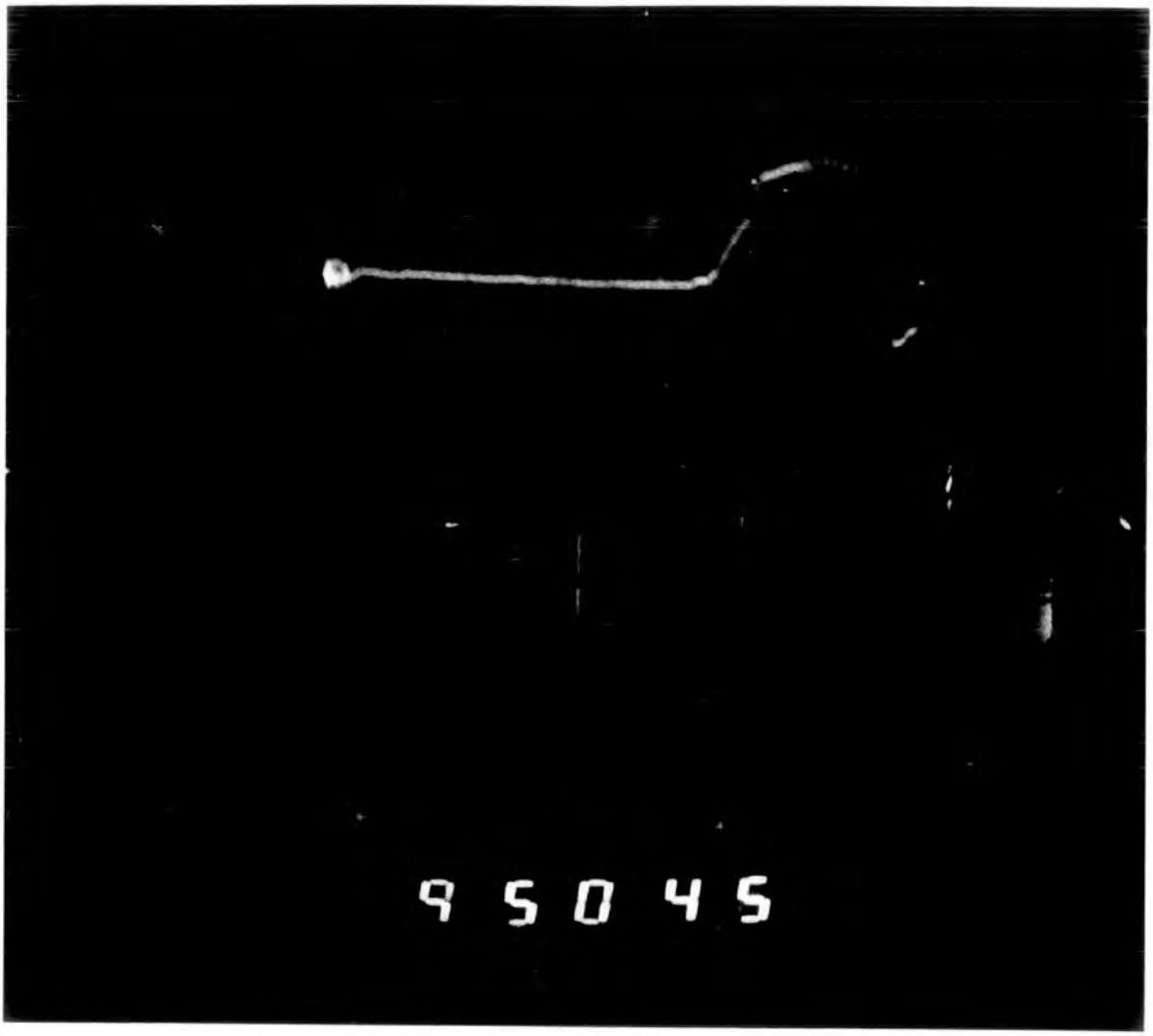

FIGURE 4.6b

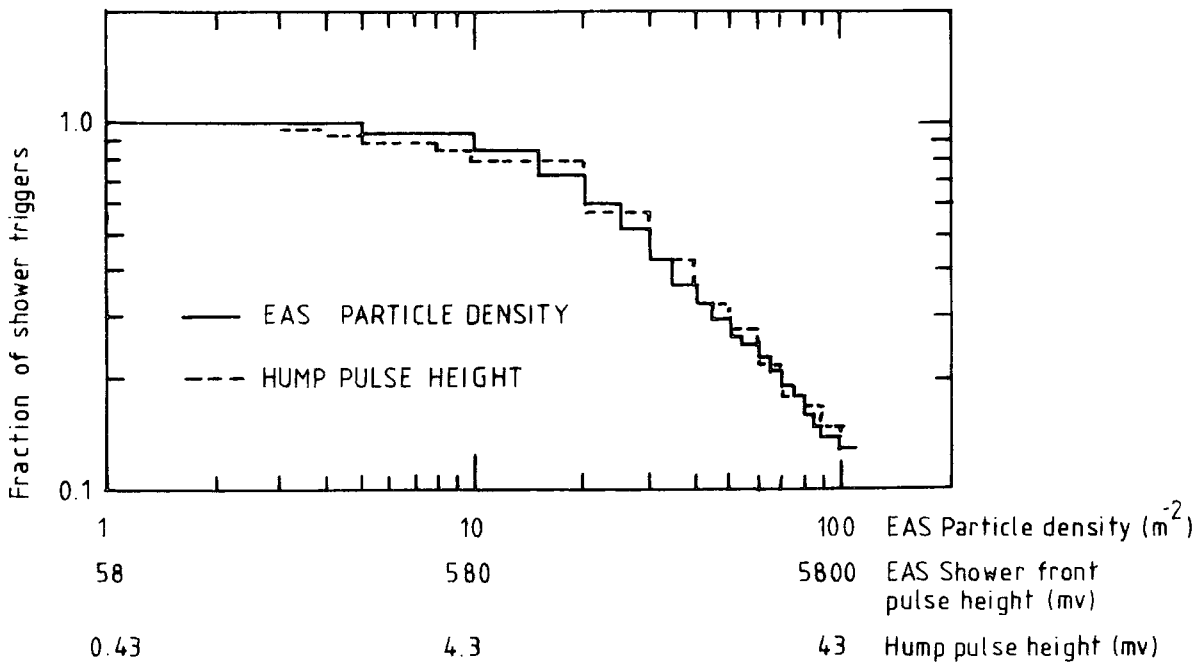

FIGURE 4.7 : Fraction of shower triggers that produce a density > $\Delta\, m^{-2}$ in the tachyon detector for the air shower selection requirement in the text.

extensive air shower would certainly reduce the shower front pulse by a large factor and hence also the amplitude of the oscillation, thus enabling measurements to be made, in the 20 μs region, with the present apparatus. The minimum pulse height that could be determined with accuracy was 20 mv.

4.4 RESULTS

For each event, the time of occurrence, the height and time before the shower front of every pulse was recorded. For the 6461 shower triggers, 3439 pulses of 10 mv or greater (equivalent to 0.35e, where e is the pulse height due to a relativistic electron) were observed. Figure 4.8 shows the time distribution of particles traversing detector 31 for threshold energy losses in the detector of 10,20,30,40,50,100,200 mv. It can be seen that there is a depletion of observed events in the 20 μs period prior to the arrival of the shower front and this is due to the obscuration produced by the high frequency oscillation already mentioned. For this reason analysis was performed over 20 to 260 μs only.

If all the events recorded are produced by background (ie. thermal noise from the photomultipliers at small pulse heights and cosmic ray particles not associated with the air shower trigger at large pulse heights) then it expected that the time distribution of events in the 20 to 260 μs time domain would be flat. If, however, a significant tachyon flux is associated with the air shower triggers and detected by the system, then an excess of events in the 20 to 120 μs region would be expected. For small threshold energy losses in the detector ($\leq$1.7e) there are sufficient events to test whether the distrib-

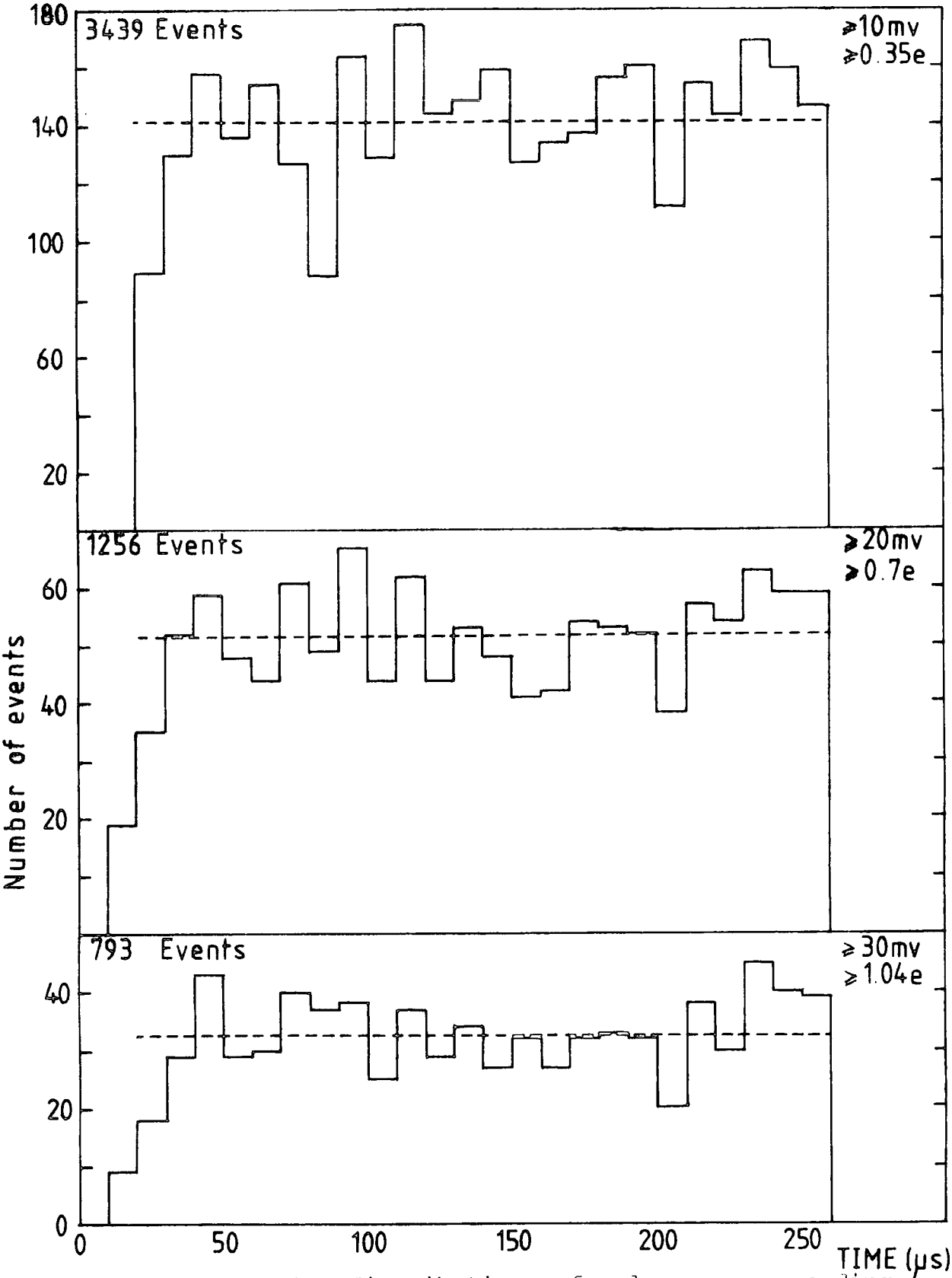

FIGURE 4.8 : Time distributions of pulses corresponding to different threshold energy losses in the tachyon detector obtained from a sample of 6461 triggers. --- is the mean calculated over the range 20-260 μs.

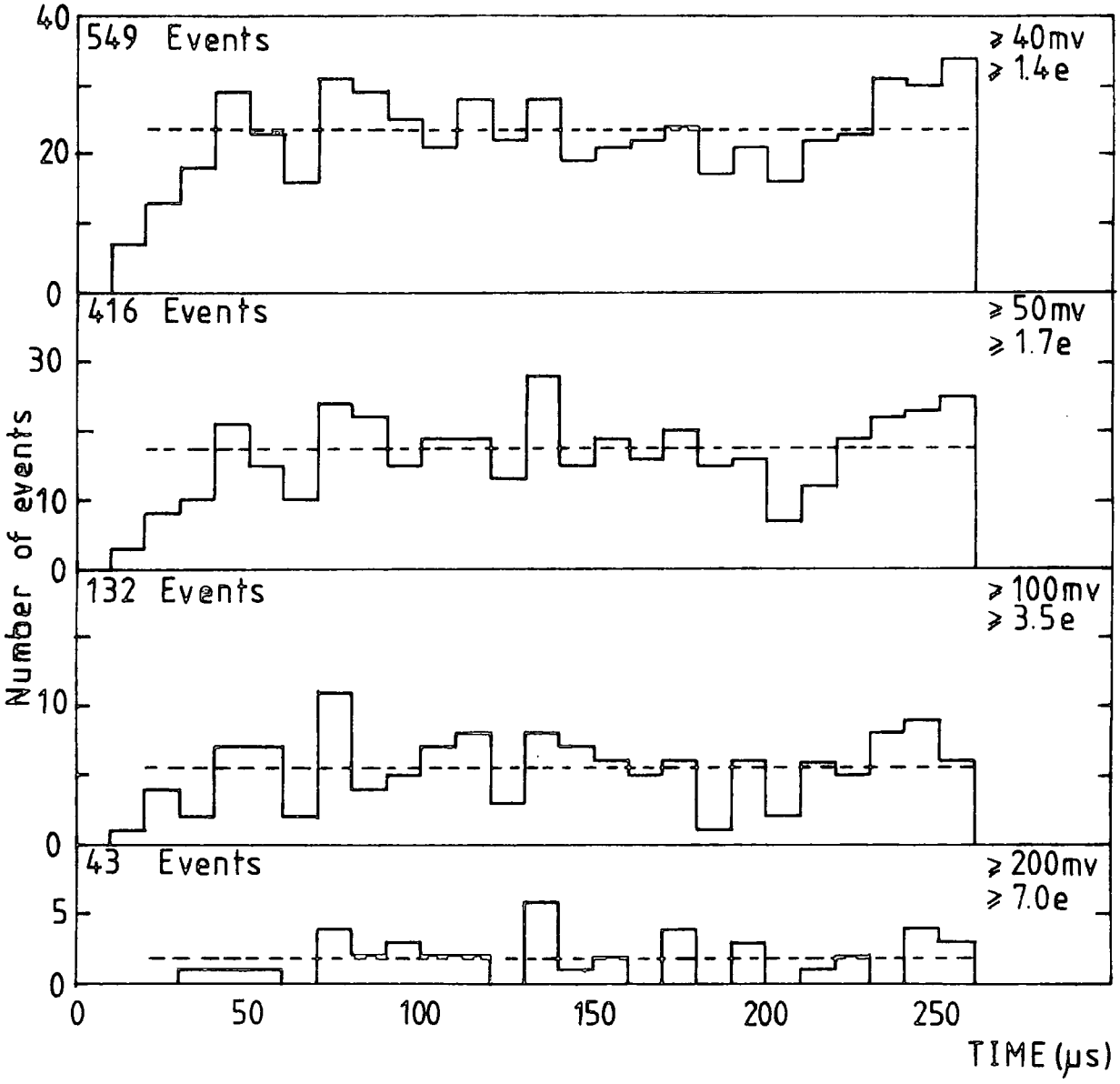

FIGURE 4.8 : Continued

utions correspond to a uniform distribution by using a chi-square test. The probability, P, of the distribution being uniform are given in table 4.1. In addition, the test was applied to each half of the distribution ie. 20 to 140 μs and 140 to 260 μs, their respective probabilities P_1, P_2 also being shown in the table.

It is possible that tachyonic pulses might be predominantly similar heights. To investigate this, time distributions are also drawn for pulse heights in various bands. These are shown in figure 4.9 and the probabilities given in table 4.1.

From this analysis it can be seen that there is no evidence for a significant number of events being produced by tachyons associated with extensive air showers. For large energy losses in the detector (>7e) there are insufficient statistics to enable a chi-square test to be performed. However, comparing the number of events observed in the time domain 20 to 140 μs with the number observed in the 140 to 260 μs region the result is, again, that there is no evidence for a significant excess of events in the first interval, where tachyons are expected to occur, when compared to the second interval. It is noted that the distributions involving pulses in the 10 to 20 mv range give very low probabilities of approximating a uniform distribution. This is due to the difficulty of measuring such small pulses, especially on the leading edge of the hump. This manifests itself in a large dip in the distribution of pulses of height greater than 10 mv, at 80 μs.

Another method of testing the data to see whether there is evidence for a significant tachyon flux is to compare the rate of pulses of height greater than a given voltage, v, that

ange	Means			Standard Deviation			Probability of being from a Uniform Distribution		
	M_0	M_1	M_2	σ_0	σ_1	σ_2	P_0	P_1	P_2
10mv (>0.35e)	141.5	136.8	146.2	22.1	26.0	16.0	<0.0001	<0.0001	0.04
20mv (>0.7e)	51.5	51.5	51.6	8.3	8.9	7.7	0.10	0.06	0.25
30mv (>1.04e)	32.7	32.4	32.9	6.6	6.8	6.5	0.10	0.12	0.17
40mv (>1.4e)	23.5	23.6	23.3	5.4	5.5	5.4	0.15	0.18	0.17
50mv (>1.7e)	17.2	17.0	17.4	5.4	5.9	4.8	0.015	0.01	0.18
100mv (>3.5e)	5.6	5.7	5.6	2.4	2.7	2.1	0.60	0.40	0.50
200mv (>7.0e)	1.8	1.8	1.7	1.6	1.7	1.5			
)mv - 20mv).35e - 0.7e)	90.0	85.4	94.6	17.7	21.7	10.9	<0.0001	<0.0001	0.18
)mv - 30mv).35e - 1.04e)	108.8	104.5	113.1	19.3	23.5	12.3	<0.0001	<0.0001	0.17
)mv - 40mv).35e - 1.4e)	118.1	113.3	122.8	21.1	25.0	14.7	<0.0001	<0.0001	0.035
)mv - 50mv).35e - 1.7e)	123.9	119.1	128.8	21.2	25.2	14.7	<0.0001	<0.0001	0.05
)mv - 30mv).7e - 1.04e)	18.9	19.1	18.7	4.2	4.6	3.7	0.50	0.25	0.68
)mv - 40mv).7e - 1.4e)	28.1	27.9	28.3	5.8	6.2	5.3	0.20	0.13	0.35
)mv - 50mv).7e - 1.7e)	34.3	34.5	34.2	7.0	8.0	5.9	0.07	0.02	0.35
)mv - 40mv L.04e - 1.4e)	9.2	8.8	9.6	3.7	3.3	4.0	0.40	0.40	0.27
)mv - 50mv L.04e - 1.7e)	15.5	15.4	15.5	5.0	5.4	4.6	0.17	0.02	0.14
)mv - 50mv ..4e - 1.7e)	6.2	6.6	5.8	2.8	2.8	2.6	0.16	0.50	0.08
)mv - 100mv ..4e - 3.5e)	17.8	17.9	17.8	4.2	4.1	4.2	0.45	0.40	0.50
)mv - 100mv ..7e - 3.5e)	11.6	11.3	11.8	4.1	4.3	3.8	0.05	0.15	0.05
10mv - 200mv .5e - 7.0e)	3.9	3.8	3.9	1.9	2.0	1.9	0.40	0.65	0.15

BLE 4.1 : Statistical analysis of pulse height distributions.

Range 0 : 20 - 260 μs
Range 1 : 20 - 140 μs
Range 2 : 140 - 260 μs

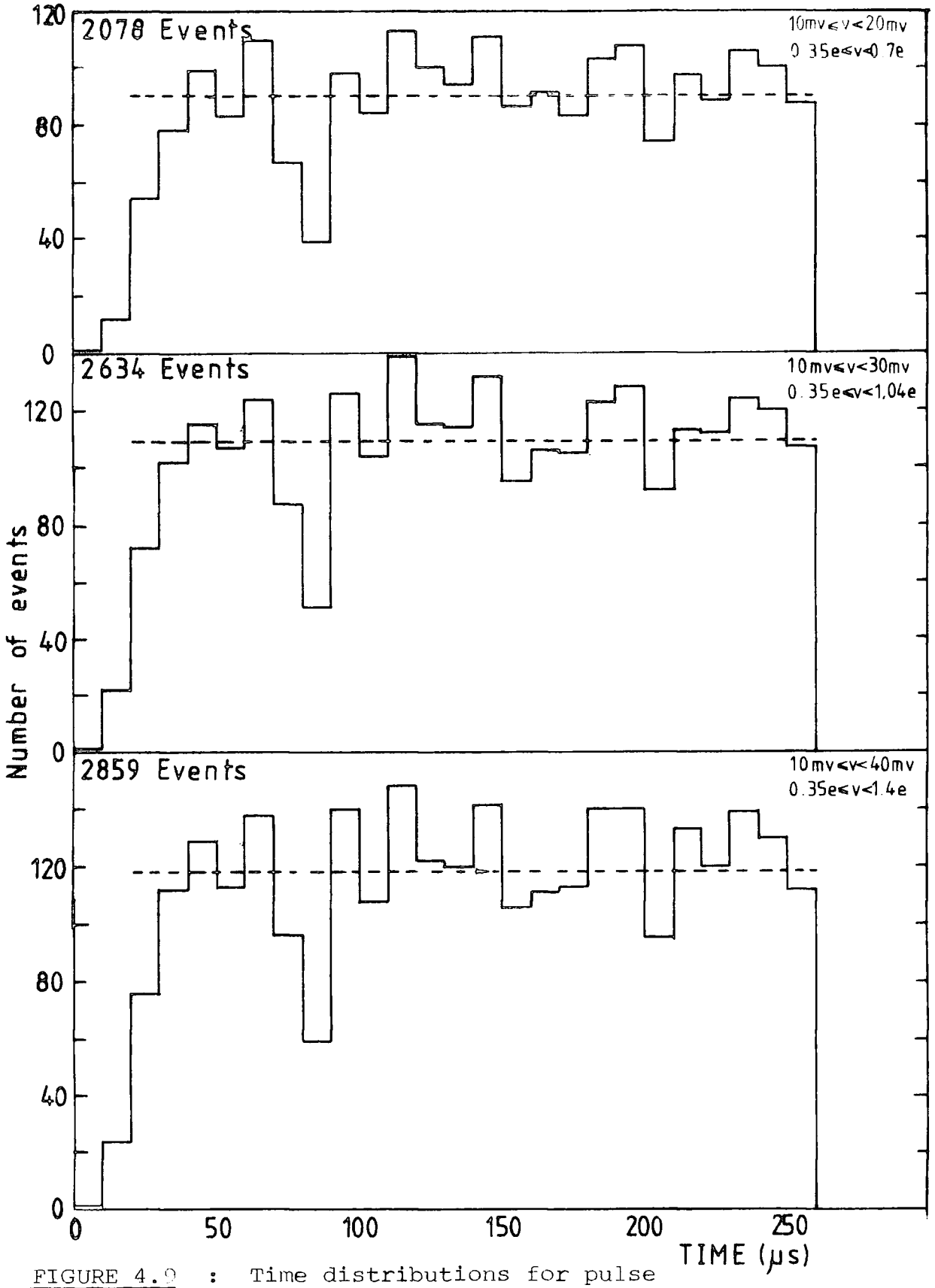

FIGURE 4.9 : Time distributions for pulse heights between two limits. --- is the mean calculated over the range 20-260 μs.

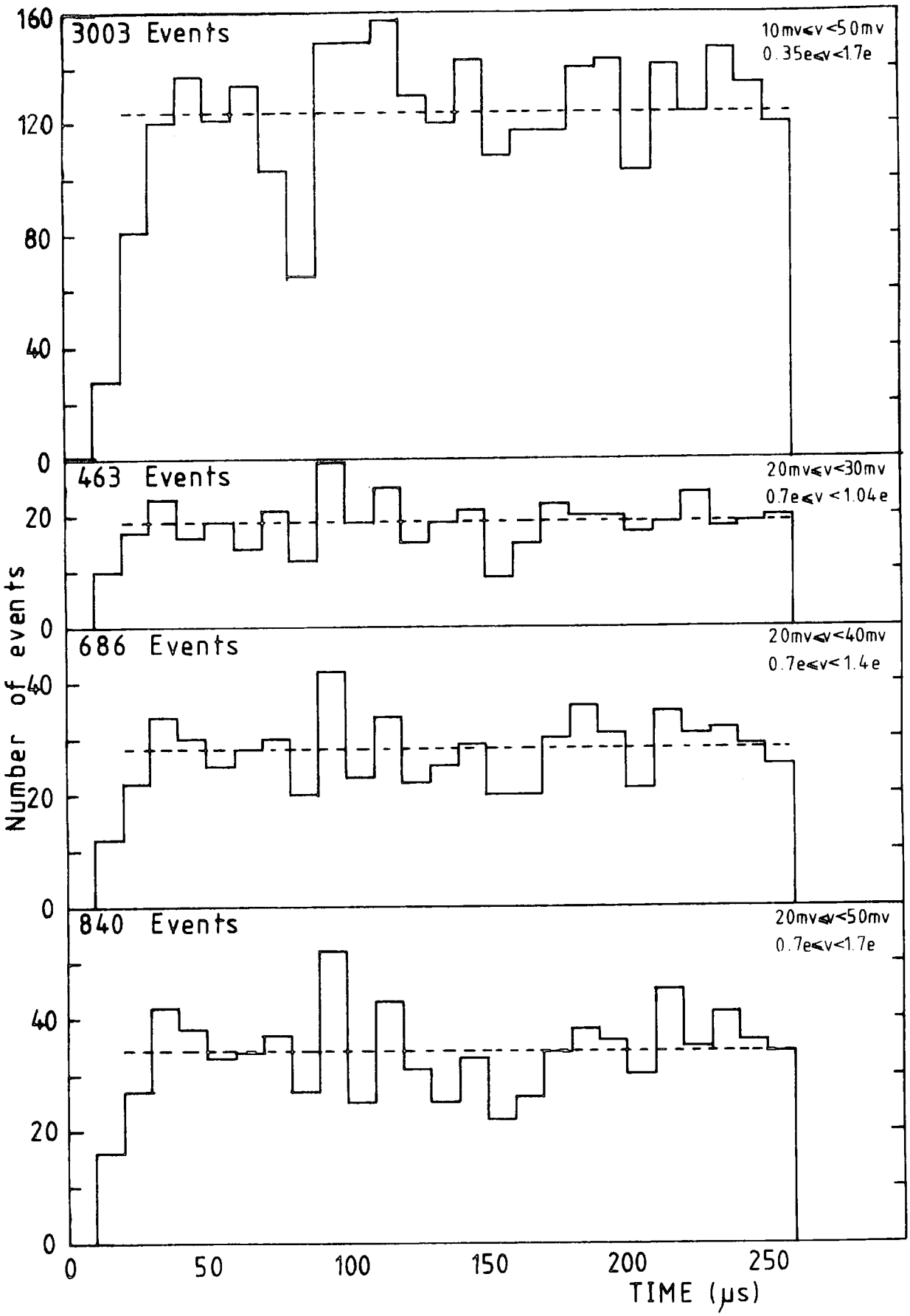

FIGURE 4.9 : Continued

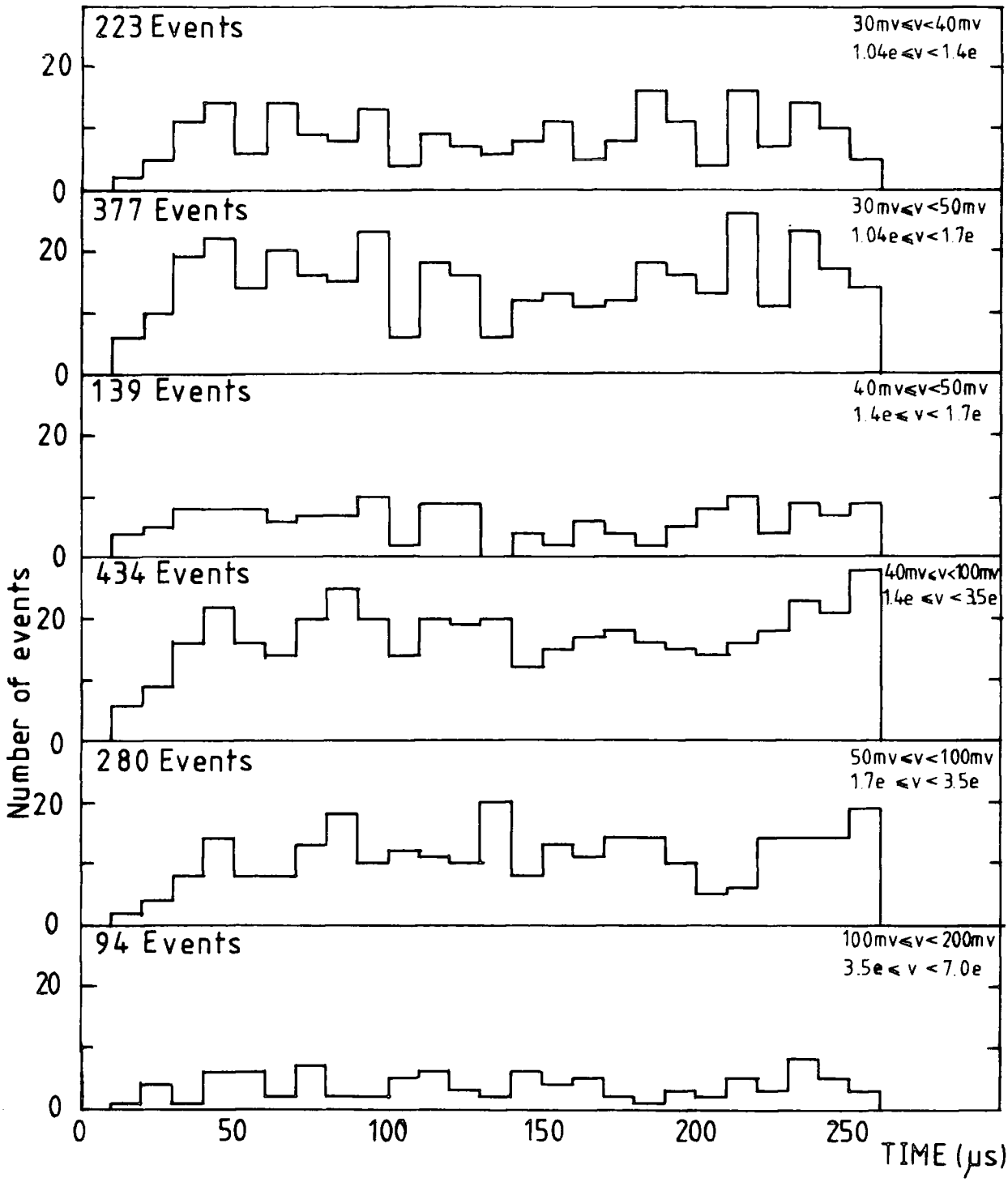

FIGURE 4.9 : Continued

are produced by the detector using an amplifier-discriminator-scalar combination, with that obtained from the oscilloscope measurements. If n(>v) pulses of height greater than v are measured in the time domain 20 to 260 μs during 6461 triggers then,

$$R\ (>v) = \frac{n\ (>v)}{240 \times 10^{-6} \times 6461} \quad s^{-1} \qquad (4.2)$$

Figure 4.10 shows such a comparison. The agreement between the two methods of measuring R(>v) is good, indicating again that there is no significant excess of events associated with extensive air showers.

Finally, multiple pulse events were investigated. A significant number of events have been observed in which more than one previous pulse was seen. If, for a given threshold energy loss, the average number of early pulses observed is Z, then the probability of observing r pulses, P(r) is expected to be Poissonian, provided that the pulses are randomly distributed in time, is given by,

$$P\ (r) = \frac{e^{-Z} Z^{r}}{r!} \qquad (4.3)$$

Table 4.2 gives the comparison between the observed and expected numbers for different threshold energy losses. The number of events with zero r increases with threshold energy loss because the rate of background pulses decreases rapidly with increasing threshold energy loss. If a tachyon signal is present in the data then an excess of events having multiple early pulses can be expected, as a real early tachyon pulse associated with some showers would mean that both early pulses are not randomly related with respect to the shower front pulse. It is seen from

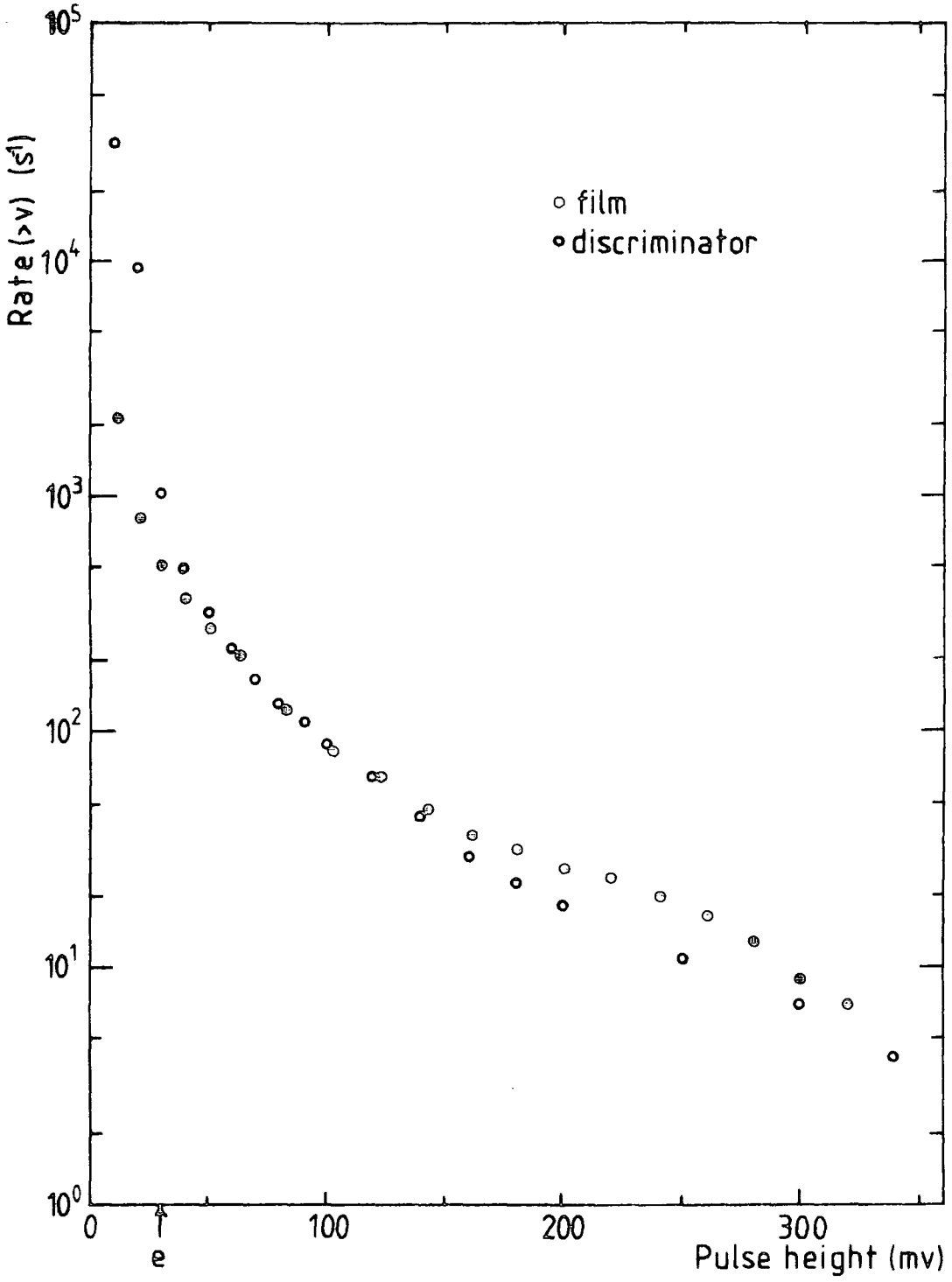

FIGURE 4.10 : Response of the tachyon detector to the total cosmic ray flux. Integral rate of pulses of height >v millivolts (measured at the input to the oscilloscope) versus pulse height v. The average pulse height produced by relativistic muons traversing the detector at normal incidence is 28.7 mv and is indicated by e on the graph.

Threshold 0.35e			
n	n_o	n_e	n_o-n_e
0	3780	3786.7	
1	2027	2023.2	
2	556	540.5	+16.5
3	84	96.3	
4	11	12.9	
5	2	1.4	
6	0	0.1	
7	1	0	
8	0	0	
	6461		

Threshold 0.70e			
n	n_o	n_e	n_o-n_e
0	5309	5310.5	
1	1053	1041.4	
2	86	102.1	-16.1
3	11	6.7	
4	1	0.3	
5	1	0	
6	0	0	
	6461		

Threshold 1.04e			
n	n_o	n_e	n_o-n_e
0	5708	5706.8	
1	709	708.4	
2	40	44.0	-4.0
3	3	1.8	
4	1	0.1	
5	0	0	
	6461		

Threshold 1.4e			
n	n_o	n_e	n_o-n_e
0	5913	5908.1	
1	518	528.5	
2	30	23.6	+6.4
3	0	0.7	
4	0	0	
	6461		

Threshold 1.7e			
n	n_o	n_e	n_o-n_e
0	6076	6072.2	
1	369	376.9	
2	16	11.7	+4.3
3	0	0.2	
4	0	0	
	6461		

Threshold 3.5e			
n	n_o	n_e	n_o-n_e
0	6334	6335.2	
1	127	124.5	
2	0	1.2	-1.2
3	0	0	
	6461		

Threshold 7.0e			
n	n_o	n_e	n_o-n_e
0	6422	6422.1	
1	39	38.8	
2	0	0.1	-0.1
3	0	0	
	6461		

TABLE 4.2 : Number of triggers showing n pulses in the tachyon detector in the time domain 20-260 us prior to the arrival of an EAS shower front for different threshold energy losses in the tachyon detector. n_o is the observed number of events and n_e is the expected number assuming the expected number obeys a Poisson distribution.

table 4.2 that an excess is observed for small threshold energy losses ($<0.7e$) in the detector, but these are subject to the errors previously mentioned. For larger threshold energy losses ($\geq 0.7e$) the agreement between the observed and expected number of double pulse events is remarkably good, indicating no evidence for a real tachyon flux.

4.5 CONCLUSIONS

A review of tachyon searches in air showers is given in table 4.3. All experiments, except those of Bhat et al and Ashton et al have very low thresholds for potential tachyon signals and hence the majority of these signals would be due to noise, with a consequent dilution of statistics. The two experiments with higher thresholds (ie. 3e) deny the possibility that tachyons may produce lower pulse heights in the detectors.

The present experiment allows various ranges of pulses to be individually investigated, since the pulse heights are recorded. This means that any threshold can be investigated with the minimum of noise contamination. Also, since there is a possibility that tachyon pulses might be predominantly of the same height, one can investigate pulse height bands.

It has been concluded that, using an unshielded plastic scintillator detector of 2 m^2 area and 2.5 cm thickness as a tachyon detector, no evidence has been found for a significant flux of tachyons (assuming that tachyons ionise at a rate $\gtrsim 24\%$ that of a relativistic muon) in a sample of 6461 extensive air showers, at sea-level, generated by primary cosmic rays of energy greater than 2.5 10^{15} eV. It should be noted that as the measurements described here were insensitive to tachyons arriving

		of expt. ($g\ cm^{-2}$)	energy (eV)	detector (m^2)		time (hr)	showers	height detectable (e)
RAMANA-MURTHY (1971)	MODE 1 MODE 2	800	$3\ 10^{13}$	0.75	-	5079 2597	$6.1\ 10^{6}$ $3.1\ 10^{6}$	
CLAY & CROUCH	(1974)	SL	$2\ 10^{15}$	1.0	-	181	1307	0.1
PRESCOTT	(1975)	SL	$5\ 10^{15}$	0.25	-	~600	4315	$5\ 10^{-4}$
FEGAN (1975)	MODE A MODE B	SL	$2\ 10^{15}$	2.5	-		2649 1514	0.1 0.05
EMERY (1975)	EXPT 1 EXPT 2	SL	$\sim 10^{15}$	4(GM tubes) 0.44	-	1840 640	27449 9521	0.36 0.1
HAZEN (1975)	RUN 1 RUN 2	SL	10^{15}	2.16 1.44	-	104 197	1039 2366	0.05 0.02
SMITH & STANDIL	(1977)	SL	$6\ 10^{14}$	~0.7	$7 gcm^{-2}$ steel	4695	204702	0.2
ASHTON et al	(1977)	SL	10^{15}	2.1	$170 gcm^{-2}$ Pb $118 gcm^{-2}$ Fe	40	341	3.0
BHAT (1978)	MODE 1 MODE 2	800	$6\ 10^{14}$ $3\ 10^{14}$	1.28	$45 gcm^{-2}$ Pb $112 gcm^{-2}$ Fe	1749 1872	20988 78624	3.0
THIS EXPT		SL	10^{15}	2.0	-	1660	6461	0.35
FEGAN	(1981)	SL	10^{16}	0.5	-	9768	1673	<1

TABLE 4.3 : Summary of EAS searches for tachyons. (e is the pulse height due to a single electron)

in the 20 μs before the arrival of the shower front it is estimated that only tachyons having velocity in excess of about $4.5\ 10^{8}\ ms^{-1}$ would have been detected in the present work.

A variation of this experiment, would be to shield the detector in order to reduce noise and provide a tachyon with a more substantial target, to allow the possibility of secondary particle production in nuclear interactions. If the secondaries included charged, subluminal, particles then they would be detected and the resulting data could be processed as described above. Of course, this still relies on the tachyon interacting with solid matter. Until a more reliable theory is developed, tachyon search methods will continue to be based on ideas which may be wrong, but an improved theory requires the spur of experimental results, unless it appears as a consequence of an 'established' theory.

CHAPTER 5

THE MODIFIED AIR SHOWER ARRAY

5.1 INTRODUCTION

As described in chapter 2, the air shower array was found to have many problems. Consequently a number of modifications were made to the detectors. These consisted of :

(i) improving the EHT distribution.

(ii) modifications to the huts and boxes.

(iii) fitting of light emitting diodes in the detectors to aid calibration.

To improve data collection and analysis, the necessary electronics were built to interface the analogue multiplexer (AM) to a PET microcomputer and the software written to allow automatic data collection.

Because of the extent of the modifications, only five detectors (C,11,31,51,52) were treated. However the electronics and computer programs were designed so that extra detectors could be added to the system with little effort.

5.2 MODIFICATIONS TO THE ARRAY

5.2.1 Huts and Boxes

The large weight of the weather-proofed huts prevented easy access to the scintillator box and precluded rapid repair of the detector, which is especially important when only a few detectors are available. To remedy this one end panel was made removable. Wheels were then attached, to the sides, which could be raised and lowered so that when lowered they lifted the hut off the ground, and with the end panel removed, the hut could

be rolled away from the detector.

The other main problem was light leaks. Black foam rubber strip was attached around the edges of the access panels on the scintillator box and, in addition, any potential gaps were sealed with aluminium foil tape. However this has to be replaced at every access but was necessary as even a very small amount of light would swamp the single particle peak, as displayed on the pulse height analyser.

5.2.2 EHT Distribution

There were two main problems. The first was that too high a voltage was being delivered from the laboratory and hence an unnecessarily large drop had to be made at each detector. The second was the switches and potentiometers used for the voltage dropping at the detectors. These were very susceptible to dirt and damp. Also the large drop in potential meant that the resistors were working close to the limits of their tolerance, thus resulting in frequent failure. The dropper units were rebuilt using fixed resistors only, located on tag strips. Where possible the dropper chain of each tube was made up of equal valued resistors to spread the load. Although this made it more difficult to adjust the voltage on each tube, once set up it was more unlikely that the voltage would require adjustment due to the greater reliability. This was found to be so.

With the rebuilding of the distribution units and a knowledge of the maximum tube voltage requirement (obtained from the calibration of the unmodified array) a much lower EHT supply voltage could be used. This was 1.6 kV, a reduction of a third on the original supply. During the operation of the modified array, no trouble was given by the EHT distribution.

5.2.3 Head Amplifiers

The old head amplifiers were located in boxes recessed in the scintillator box. To examine the individual photomultiplier tubes (PMTs), the amplifier had to be removed and the wires from the other PMTs had to be unsoldered.

Modifications were made so that the wires from the PMTs were terminated in sockets on a plate flush with the side of the scintillator box (thus also making the box more light-tight). New head amplifiers were made and placed in weather-proof plastic boxes which had an input lead for each tube. In addition to making it easier to examine a single PMT output, it made repair and substitution of head amplifiers simple.

5.2.4 Calibration Light Emitting Diodes

Previously, the only thorough check on the stability of the calibration was to keep recalibrating which is time consuming. It was decided to install a light emitting diode (LED) on each scintillator to produce light pulses of known size and shape and thus enable a quick check on system operation, when required.

In the 1 m^2 and 0.75 m^2 detectors the diodes were put at the centre of the top surface of each scintillator. On the 2 m^2 detectors one was placed at the centre of each end face of the scintillator. Pulses are sent from the laboratory, using the spare cable, and the output from the detector observed on an oscilloscope. If a significant change in the calibration was noted, the cause could be investigated and a new calibration made. However this did not occur during the period of operation.

5.3 DATA COLLECTION ELECTRONICS

5.3.1 Introduction

The electronic units, used previously, were retained with the exception of the camera drive unit. Instead of the camera/ oscilloscope combination, a PET microcomputer was used and this required the construction of an interface to digitise the data and present it to the PET in the required form. A block diagram of the electonics is shown in figure 5.1.

5.3.2 Burst Pulse Generator

This consists of a 555 timer IC which produces a continuous train of TTL pulses, enveloped by the output of a 74121 mono-stable IC, as shown in figure 5.2. Adjustment of the mark-space ratio of the timer and the output pulse length of the monostable allows the interval between pulses and the number of pulses to be altered. On arrival of a shower trigger pulse the unit is triggered and the pulse train output fed to the multiplexer. Data from the multiplexer is then output in serial form at a spacing governed by the pulse interval. This interval has to be small enough so that there is negligible loss in the multiplexer sample and holds but long enough to allow time for digitisation and recording.

5.3.3 Analogue Multiplexer

This consists of two types of units. The first, master, unit (NE 4509) provides the control function for holding the information. It has eight inputs, one being for the 'hold' pulse and the others (numbered 1 to 7) for the analogue input signals. The first six have an input impedance of 50Ω and the seventh

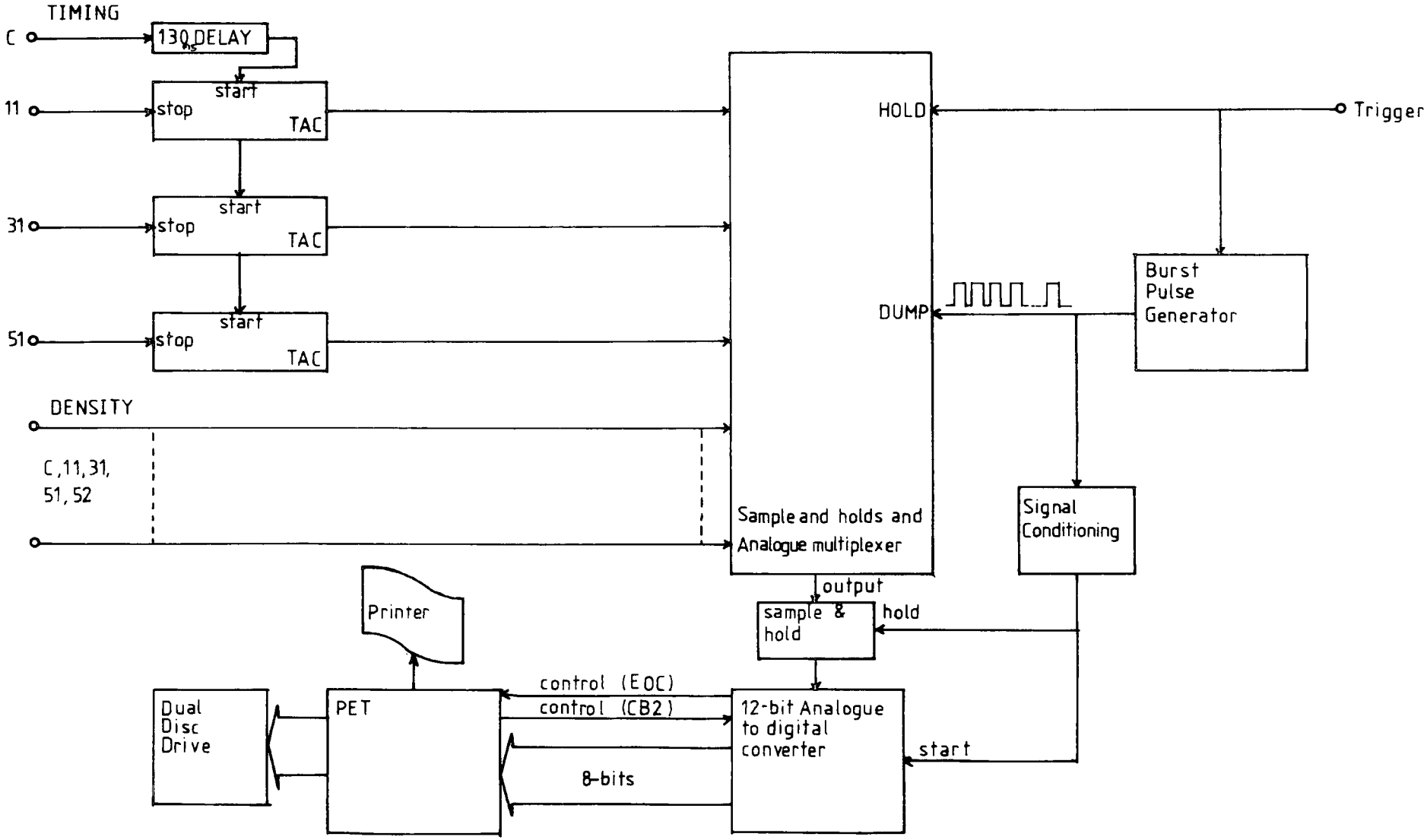

FIGURE 5.1 : The data recording system

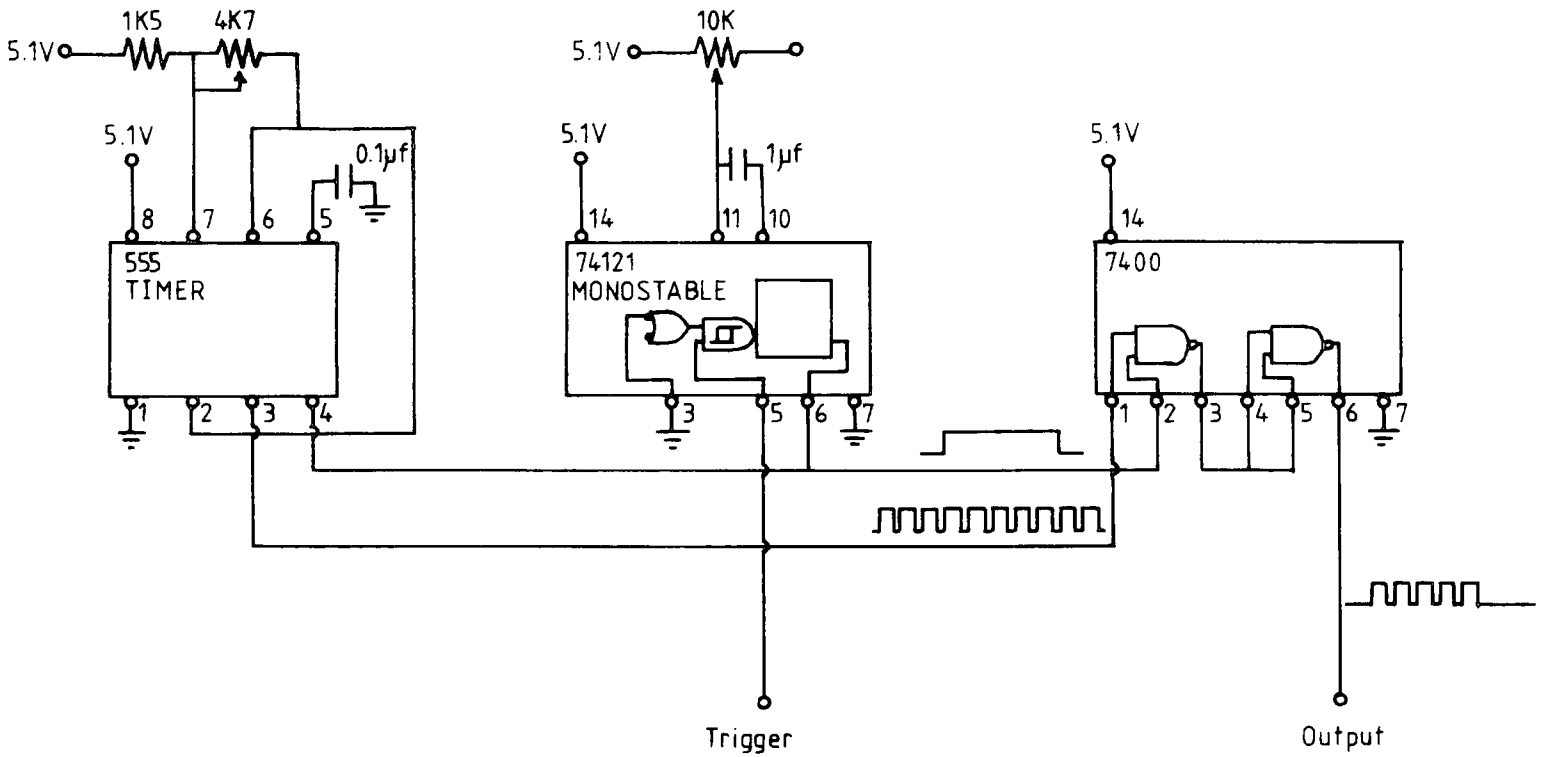

FIGURE 5.2 : Burst pulse generator

has one of 700Ω. The other unit is a slave (NE 4510), of which three are available for use but only one is required for the five density and three timing channels. These are similar to the master unit but lack the control circuitry. All units share a hold and release pulse which are input via the master unit. Each of the 50Ω input channels has a linear response, a gain of approximately 0.4 and a saturation input of about 9.5V.

On receiving the trigger pulse, the master unit generates hold pulses for each sample and hold, situated in the input lines. The train of pulses from the burst pulse generator then operates a counter in the master unit and releases each channel, in turn, by means of an AM 3705 analogue multiplexer IC.

The droop rate of the multiplexer sample and holds is approximately 250 mv V^{-1} s^{-1} and, therefore, it is necessary to release the data within 50 ms to prevent significant (~1%) degradation of the data. The other important parameter of the multiplexer is the width of the output pulses, this being 5 μs.

5.3.4 Multiplexer - PET Interface

A DATEL ADC-HX12BGC 12-bit successive approximation ADC was chosen to digitise the data. Choosing the digitisation rate is a compromise between cost and speed. The faster the digitisation, the less pulse height is lost in the sample and holds. Also the speed should be less than the time taken by the program between reading each pulse height. The maximum digitisation time of 20 μs was sufficient for this purpose. Because of the narrowness of the multiplexer output pulses, a sample and hold was required to preserve the pulse height long enough for digitisation. An LF398 sample and hold IC was used which has a droop rate of

50 mV $V^{-1}s^{-1}$.

The sample and hold and ADC are controlled by pulses derived from the burst pulse generator after small delays (~3μs) have been introduced to optimise pulse capture and digitisation by allowing the held pulse to settle. A timing diagram for the process is given in figure 5.3.

The other main component of the interface is a 74157 digital multiplexer. This is necessary because the PET is an 8-bit machine and the 12-bit ADC output has to be delivered in two parts. This is done under program control.

The operation of the interface is described in the next section and the circuit is given in figure 5.4.

5.4 MICROCOMPUTER DATA RECORDING

5.4.1 Introduction

The output of the burst pulse generator was set to twelve pulses at ~~2ms~~ 90μs intervals. Consequently not all channels were used. This was deliberate because the unused channels could be used as markers to check for channel 'dropouts' (infrequently, under certain, undetermined, conditions, one or more channels would not appear at the multiplexer output) and ADC gain. Also, the constant, hold pulse was processed through the system and could also be used as a gain check.

The speed required for data input ruled out a BASIC routine for data reading and therefore a machine code routine was required. A second requirement was for the permanent storage of data. The final requirement was that the data collection should be interrupt driven. This means that data is read only

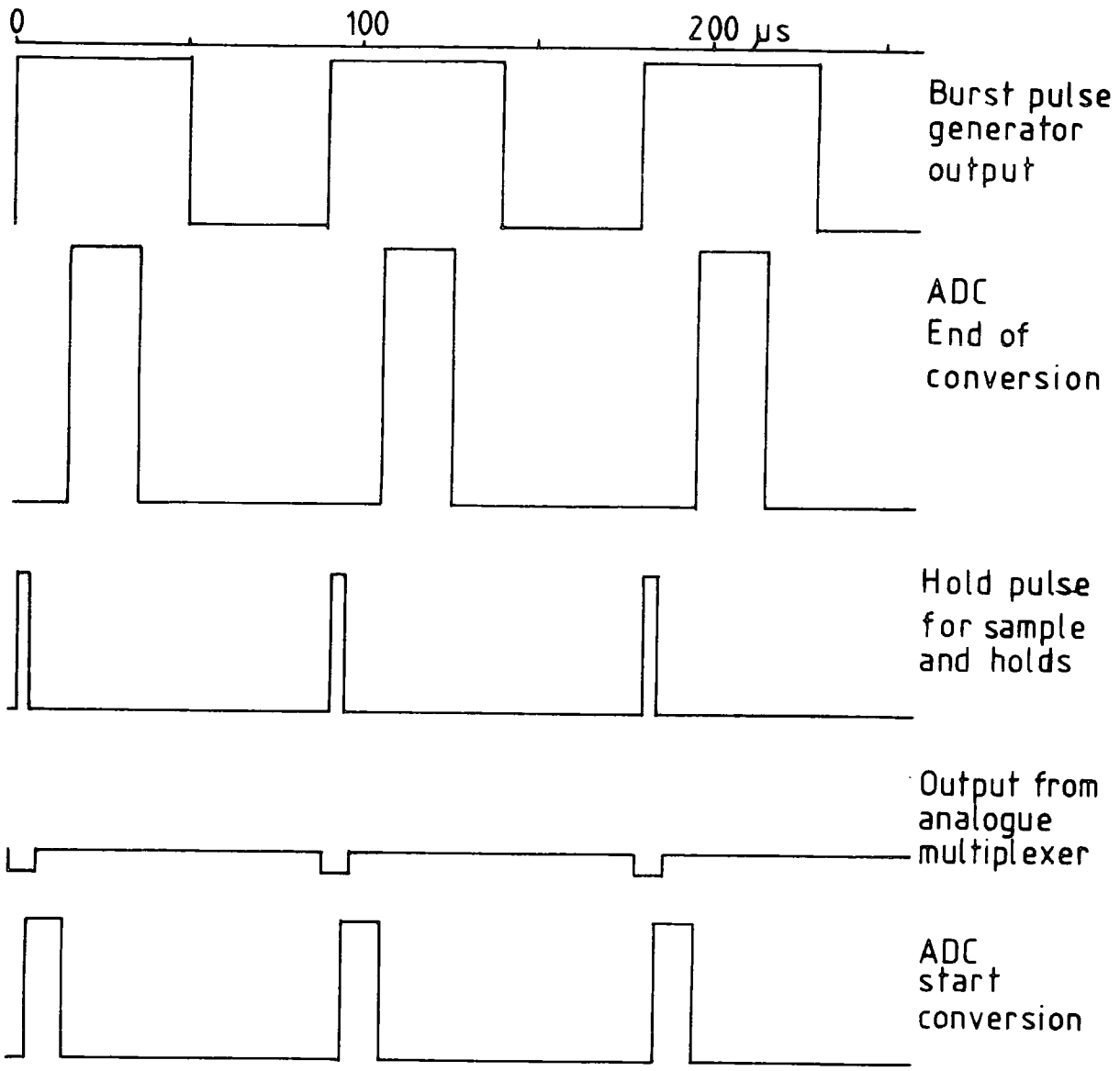

FIGURE 5.3 : Control Timing for data collection electronics

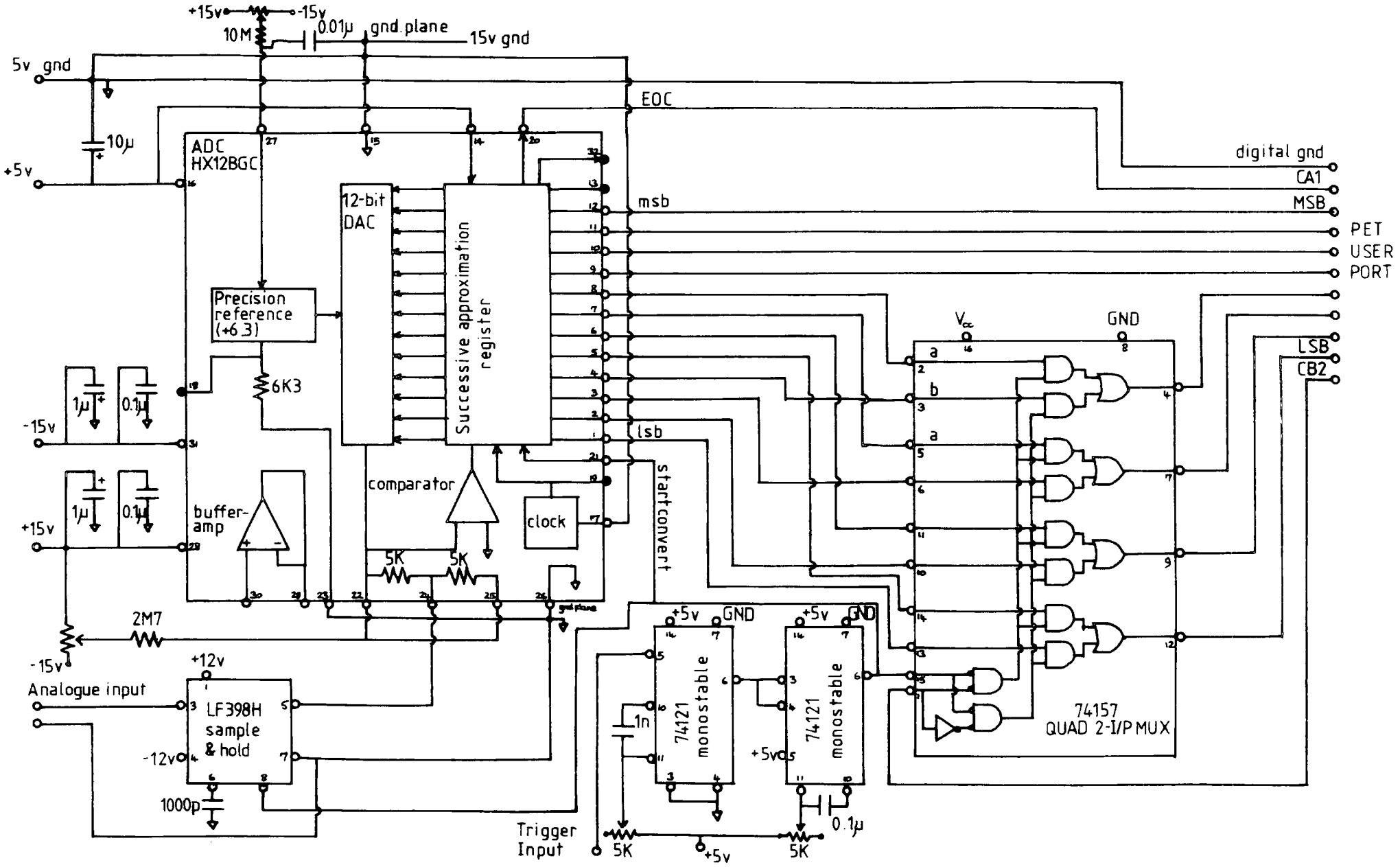

FIGURE 5.4 : The analogue to digital converter and interface electronics

when a signal is received from the ADC and allows programs (eg. for data processing) to be run while the array is in operation. Since the rate of showers is $\lesssim 20\ hr^{-1}$ for the inner ring trigger this provides a considerable time saving, in that processing can proceed simultaneously with data collection.

The microcomputer system consists of a Commodore PET 2001 with 32K bytes of memory, dual Computhink disc drives with 800K byte capacity and an Anadex DP8000 printer. The experiment was attached to the 'user' port, an 8-bit input/output port, with two control lines, which is memory-mapped. The cable from the interface consists of eight data lines, a control line along which the 'end of conversion' signal is sent from the ADC to initiate the data read sequence, and a control line from the PET to the digital multiplexer to enable all 12 bits to be read.

5.4.2 Control Software

There are three programs involved in the data collection process. Listings are given in appendix A.

a) STORE.GO : This is the main machine code program which reads and stores data. It is resident at the top of user memory while the array is in operation but is protected from interference from BASIC programs.

b) SET.GO : This is an initialisation program which sets up constants and registers used by STORE.GO.

c) SETUP : This is a BASIC initialisation program which asks the user various questions about how the data is to be stored and then sets up the relevant parameters.

The sequence of operation of STORE.GO is given in the flow chart which is shown in figure 5.5.

The output from the ADC consists of twelve 12-bit words at intervals of ~~2ms~~ 90μs. At the time each is produced an 'end of conversion' (EOC) pulse is also produced. Initially only the eight most significant bits (MSB) are presented to the user port, which is input on receipt of the EOC pulse. The PET then sends a pulse to the digital multiplexer which then outputs the other four, least significant, bits (LSB) to the user port. It is noted that the four MSBs are read again and these are removed by logically 'ORing' with 15 ($0F hexadecimal).

When the first EOC pulse is received, an interrupt is produced in the processor and this causes the STORE.GO routine to be executed. The first eight bits are read and stored in a buffer memory, reserved in the user memory just below the control program. A pulse is then sent to the digital multiplexer and the next eight bits are read., which are stored in the next location. This process is repeated for all twelve inputs. If too many or too few EOC pulses are received, then the data is ignored (eg. in the case of a spurious trigger). The shower number, time (from the PET's internal clock) and a delimiter ($FF), to denote the end of the data string, are then stored. Facilities are included to detect errors in the data input to prevent corruption of data.

The data can then be stored on floppy disc. This is done automatically at a predetermined interval which can be anything from 1 to 191 showers per file. This is chosen as a compromise between the dead time involved in storing the data on disc

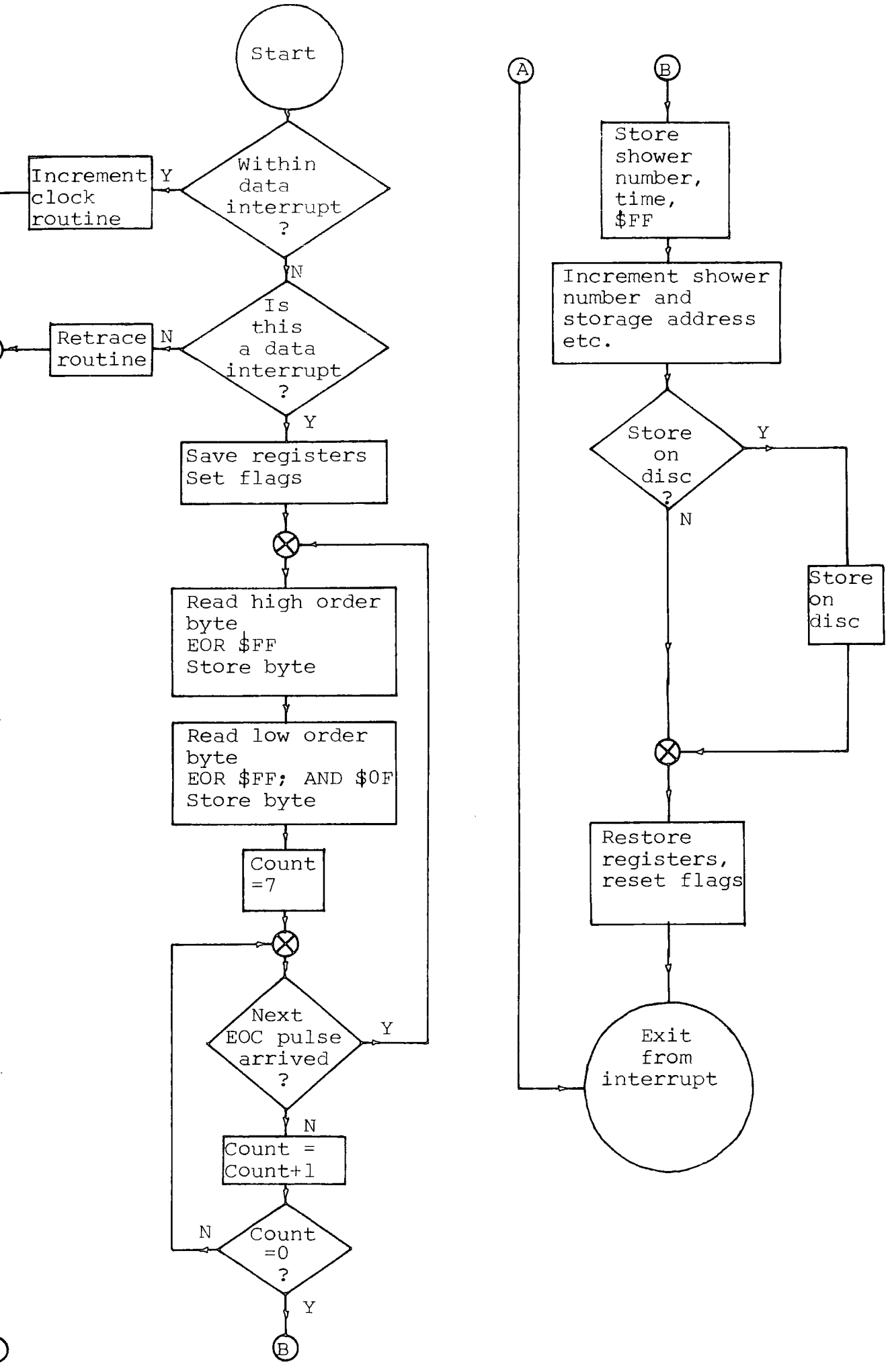

FIGURE 5.5 : Flowchart of operation of progaram STORE.GO

(upto 3s) and the risk of power dips or failure which would cause loss of data. When a file is full, another file is started and similarly for full discs. When both discs are full, a message is displayed to tell the operator to change discs and allows about 8 hours in which to respond. The dead time due to the whole process of reading and storing the data is about 1.5 ~~25~~ms (unless a disc save is executed) which is negligible when compared to the rate of showers. This method of storage allows 14898 showers to be stored before the discs require changing. This is equivalent to a period of about 30 days continuous running.

Another task performed by the program is to maintain the internal clock, which is disabled when the interrupt is operated. Also various memory locations have to be restored to their values prior to the interrupt when the data has been read in. Extension of the array can easily be accomodated by the changing of several variables in the program. The timing diagram for data being read into the PET is given in figure 5.6.

5.4.3 Running the Data Recording System

The three programs are loaded in the order : STORE.GO, SET.GO,SETUP. The latter is run. The user is asked for details of the data storage, eg. the time of starting; the number of showers per file (to a maximum of 191); the number of files per disc (to a maximum of 39 for an empty disc); disc drive number (1 or 2); the number of showers before a disc save is implemented. After these details have been entered, the scalar is reset and the system is then on-line. The microcomputer is still available for normal use. To terminate the data collection, the

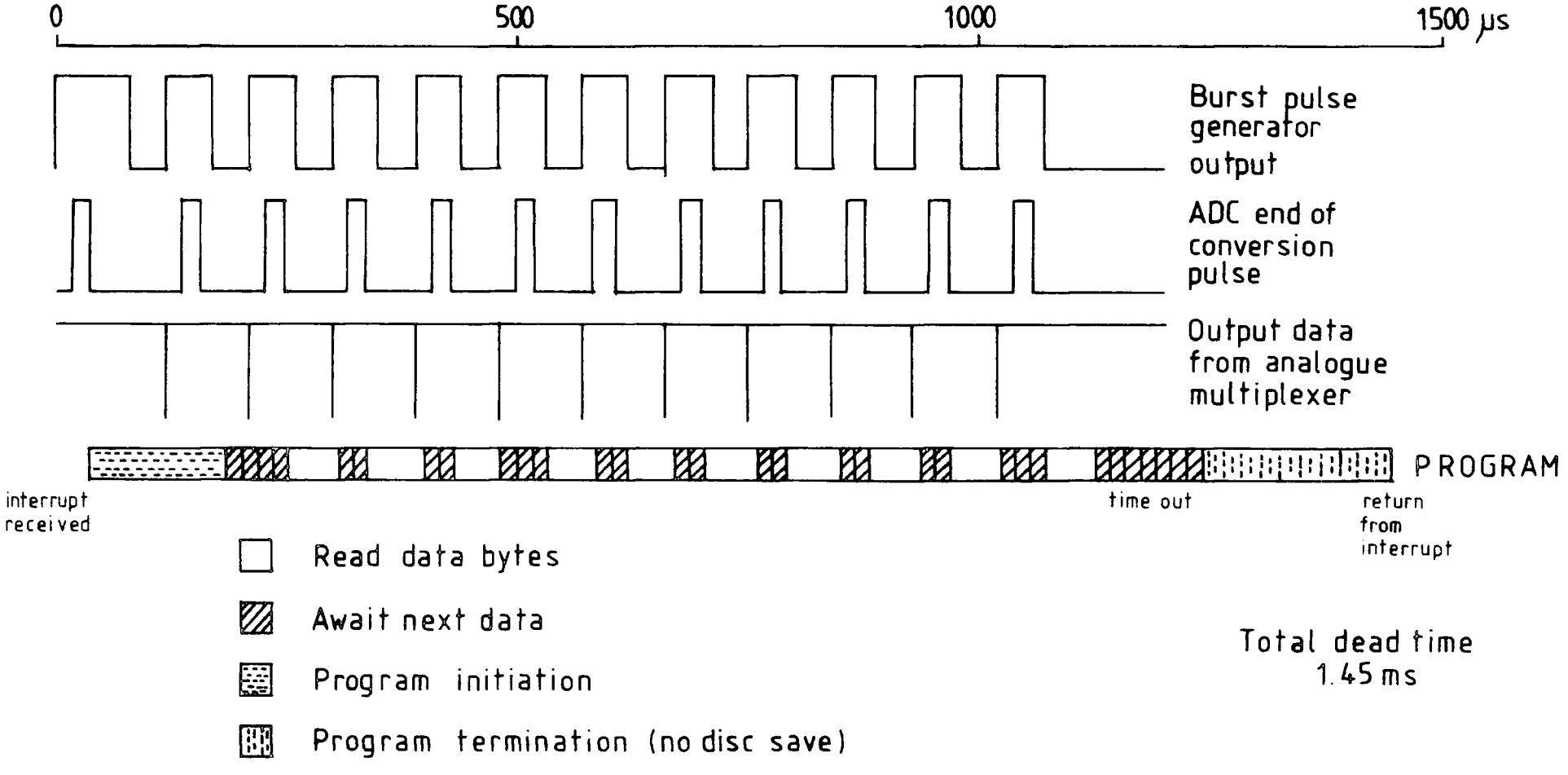

FIGURE 5.6 : Timing diagrams for STORE.GO operation

program RESET.GO is loaded and run which puts the data collection system off-line.

5.5 CALIBRATION OF THE RECORDING SYSTEM

Calibration of the system was done in total so that the result was a set of coefficients for each channel which allowed the 12-bit binary number to be converted directly to either time or density depending on which channel is under consideration.

For the timing channels the TACs were set to give their full output pulse height for 500ns delay. Harwell RL101 delay line units were used to produce a plot of delay versus ADC output. These could be represented approximately by two straight lines (see figure 5.7) and the coefficients obtained are given in table 5.1. It was found necessary, in order to centralise the timing distributions in the 500ns range, to introduce a 130 ns delay in the timing pulse from detector C. A Harwell unit was used to provide this.

Density channels were calibrated using a NE Precision Pulse Generator producing 10 μs decay time pulses. Plots obtained were a good fit to a straight line (figure 5.8) and the coefficients obtained are given in table 5.2. One problem in calibrating the density channels is that the time taken for the pulse to reach its maximum varies with the pulse height. One result of this is that the position of the hold pulse jitters. Measurements were carried out to determine the characteristics of the density pulses and the timing of the hold pulse. Using these allowed reconstruction of the pulse so that the maximum height could be obtained. This was carried out in the data processing.

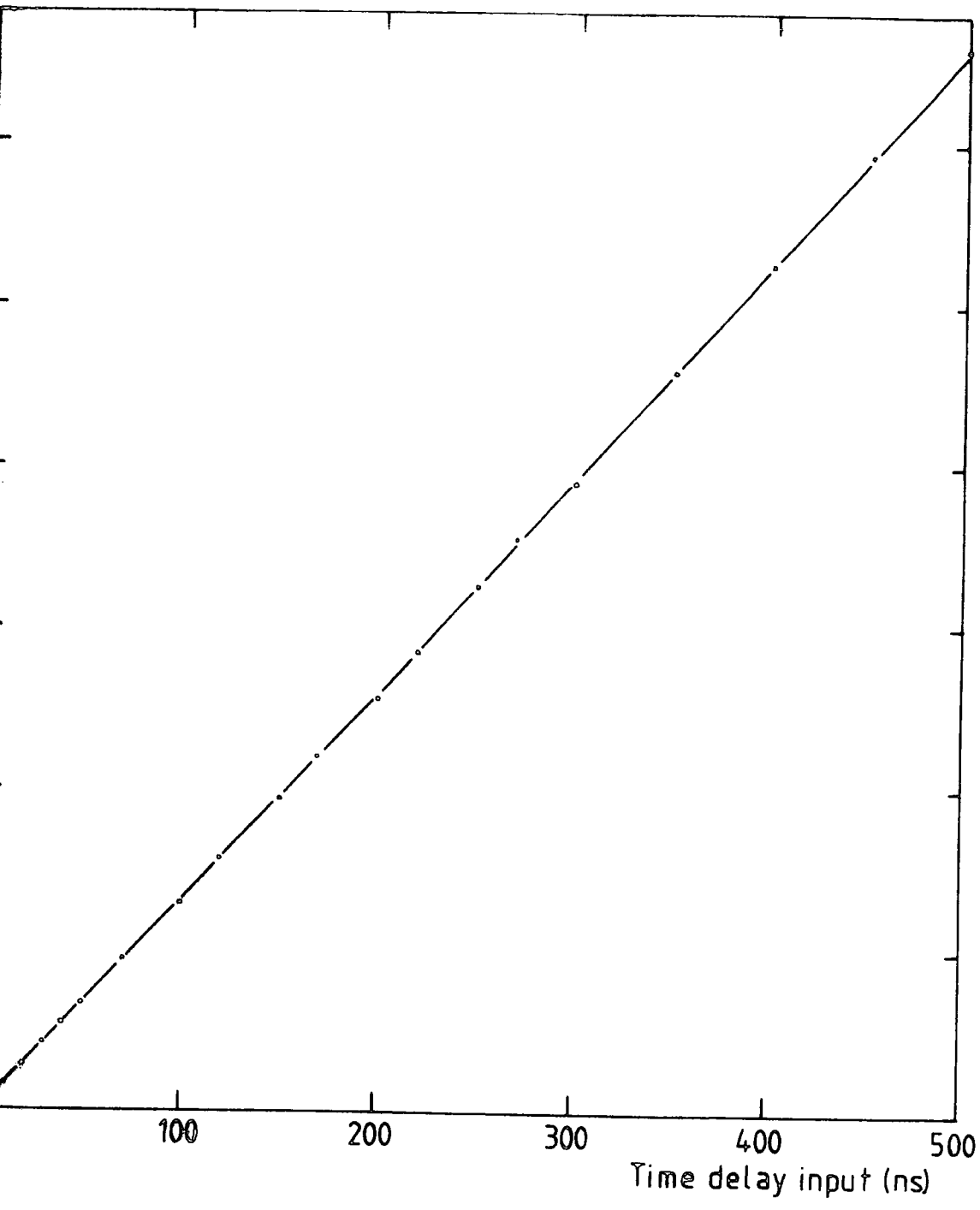

FIGURE 5.7 : Example of timing channel calibration (Ch 11)

DETECTOR	F Bytes 1500	F Bytes 1500	G Bytes 1500	G Bytes 1500
11	0.152	0.144	4.645	11.43
31	0.158	0.149	-2.962	7.681
51	0.156	0.148	-1.159	8.104

TABLE 5.1 : Time to amplitude converter coefficients

TIME(ns) = F×(BYTES) + G

DETECTOR	DA	DB
C	0.00284	0.1659
11	0.00272	0.1412
31	0.00272	0.1284
51	0.00281	0.1411
52	0.00274	0.1456

TABLE 5.2 : Density channel coefficients

Density Pulse Height = DA×(BYTES) + DB

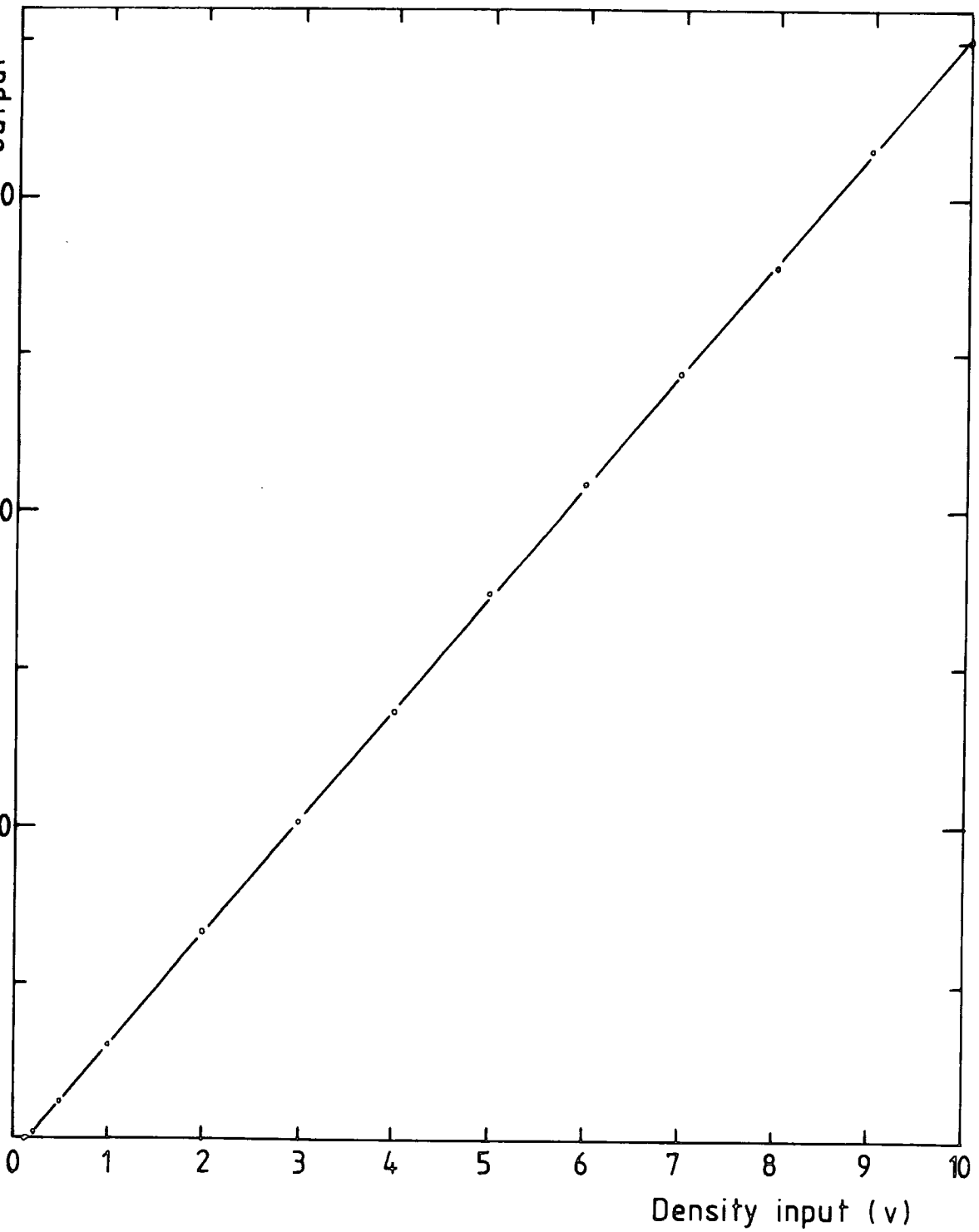

FIGURE 5.8 : Example of Density Channel Calibration (Ch 11)

5.6 CALIBRATION OF THE MODIFIED ARRAY

The array was calibrated as described in chapter 2. Each tube was tested by placing it in a light-tight box, in which a LED was placed, facing the tube. The diode was fed by a pulse generator with a 1.6V, 0.6μs width rectangular pulse at 1KHz. The output of each tube was measured as a function of the applied voltage. From the tube's response and the mode of the particle peak, at a given voltage, it was possible to estimate the voltage required for calibration. This considerably speeded up the calibration procedure.

The resulting PHA distribution modes and the coefficients obtained from them are shown in table 5.3 which also shows the voltages applied to individual tubes.

Besides the use of diodes, checks on the calibration could be obtained from the study of the distributions of output densities from each detector over the period of operation. However, as noted previously, no noticable shift occurred during the period of operation.

The response of the array was estimated following the method described in appendix B for the trigger used (ie. $\Delta_c = 4m^{-2}$, $\Delta_1, \Delta_3, \Delta_5$, all = $2m^{-2}$). The range of shower sizes and core distances over which the array is calculated to be sensitive are shown in figures 5.9 and 5.10.

5.7 CONCLUSIONS

The operation of the air shower array, as modified, has been described. Attempts to improve its reliability and ease of maintainance have been instituted with some success.

Detector Element	Tube	Operating Voltage (kV)	Mode of PHA Distribution (mV)	DC
C/1	1	1.230	83	10.8
	2	1.370		
C/2	3	1.385	63	
	4	1.527		
11	1	0.870	32.5	10.7
	2	0.800		
	3	0.999		
	4	0.850		
31	1	0.803	43.5	10.1
	2	1.256		
	3	1.248		
	4	1.510		
51	1	0.780	38	9.1
	2	0.903		
	3	1.455		
	4	1.270		
52/1		1.115	71	10.0
52/2		1.094	78	
52/3		0.900	72	
52/4		0.998	76	

TABLE 5.3 : Operating Voltages and Output Characteristics of Detectors. (Density = Density Pulse Height×DC)

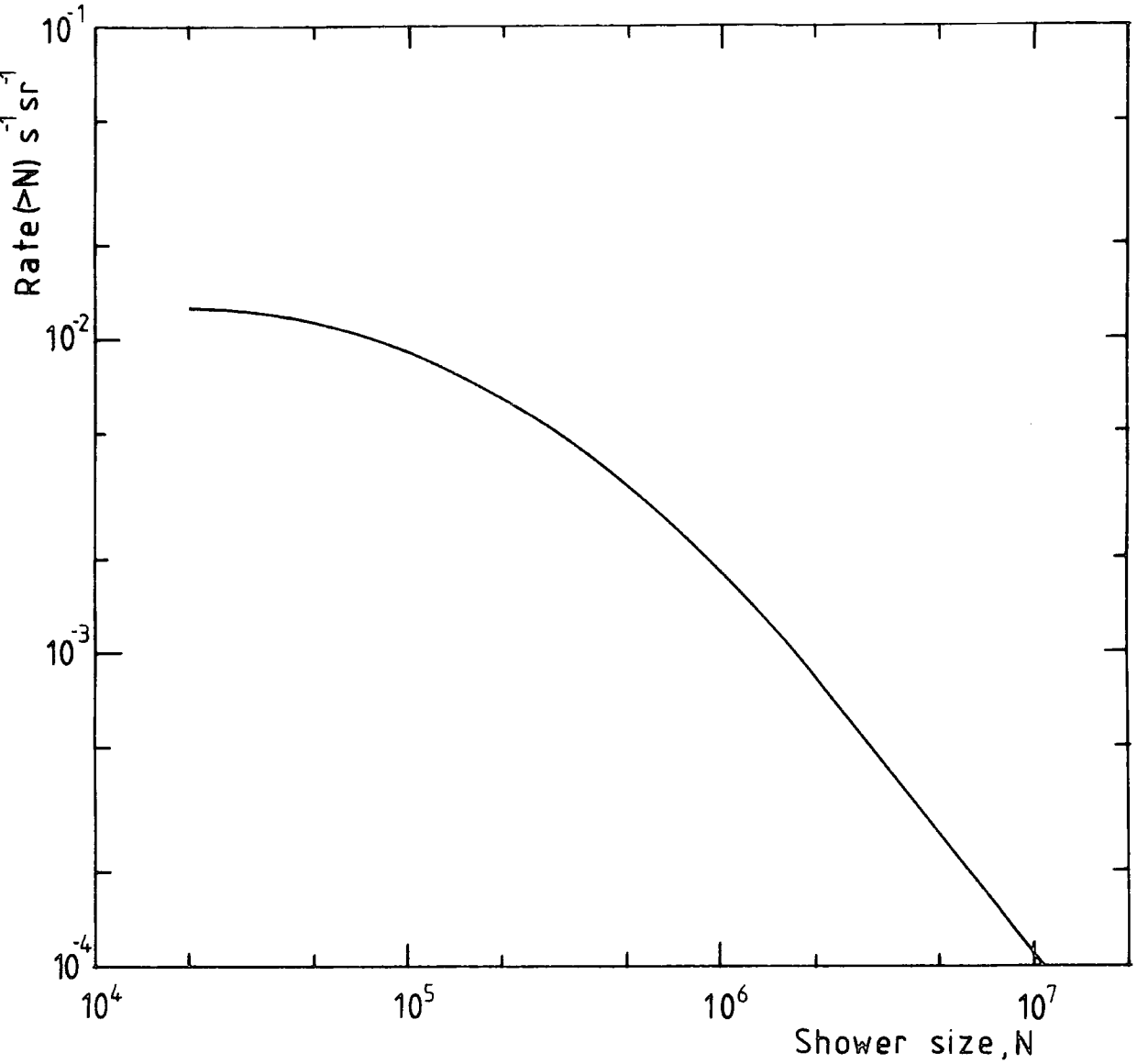

FIGURE 5.9 : Rate of showers of size greater than N which trigger the array. ($\Delta_c \geq 4m^{-2}, \Delta_{u,w,s} \geq 2m^{-2}$)

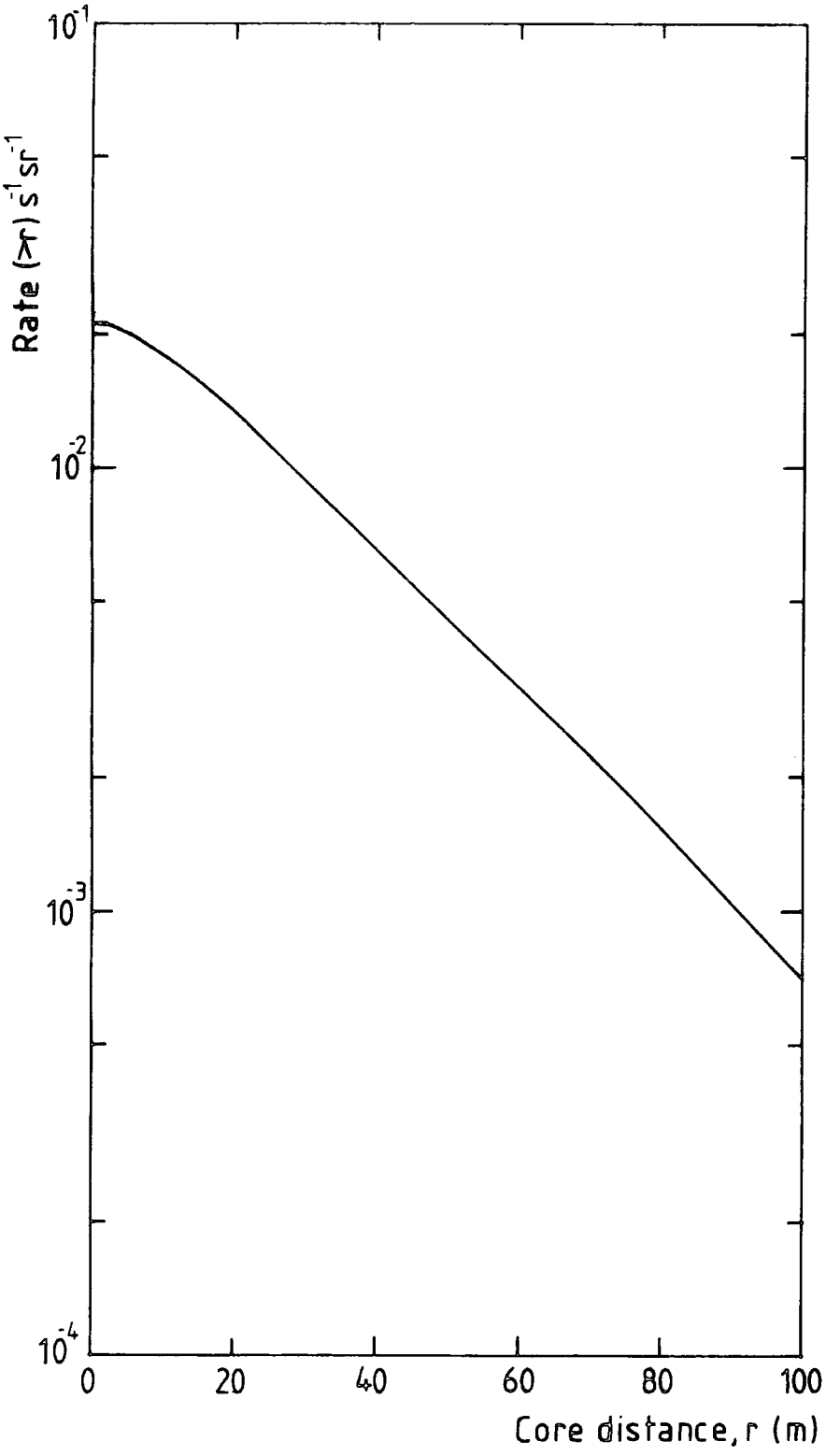

FIGURE 5.10 : Rate of triggering showers whose cores fall at a distance greater than r from the centre of the array. ($\Delta_c \geq 4m^{-2}, \Delta_{u,v,s} \geq 2m^{-2}$)

The collection of data has been automated and this results in the storage of raw data on floppy disc. The data can then be retrieved and used, in conjunction with the coefficients determined from the calibration, to produce the shower axis direction, the shower size and the core location. This processing can proceed at the same time as the array is in operation, thus saving the need for other computing facilities. This processing is described in the next chapter.

CHAPTER 6

DATA PROCESSING

6.1 INTRODUCTION

The data collection system has been described in chapter 5. The data for a shower consists of a string of bytes, stored in consecutive memory locations. It is from this data that the air shower parameters are determined. Two programs are used for data processing. The first retrieves the data, for each shower, from disc. Using the calibration coefficients for each channel, the particle densities in each detector and time delays are determined and the shower axis direction is calculated from the delays. This data is then stored on disc as well as being printed out. The second program takes the density information and the shower axis direction and determines the estimated core location and shower size which are stored and printed out. The basic shower parameters are then available for analysis.

6.2 PROGRAM 'DATAPROC'

A typical string of shower data is shown in figure 6.1. It consists of a string of 26 bytes, each formed of two hexadecimal digits. Table 6.1 shows the position of each piece of data in the string.

The first operation of the program is to load all the shower data of a given file into memory. Each shower is then processed consecutively. Data which is required by the program, initially, is the filename and the date that the file was started, this allows the date of occurrence of a shower to be determined. Also there are a number of output options which are described

0000 4C0D 3801 2C0B 680E 0000 1D0D 0D0D 010B 1006 A902 2109 01FF

FIGURE 6.1 : Data string for an example shower

Byte Pair	Data	Notes
1	NOT USED	
2	TIME DELAY FOR 11	
3	TIME DELAY FOR 31	
4	DENSITY FOR 52	
5	TIME DELAY FOR 51	
6	NOT USED	
7	HOLD PULSE	(i)
8	DENSITY FOR C	
9	DENSITY FOR 11	
10	DENSITY FOR 31	
11	DENSITY FOR 51	
12	TIME OF EVENT	(ii)
13	(SHOWER NUMBER (TERMINATOR	(iii) (iv)

(i) Should be of constant height. Used as a check on gain of system.

(ii) The internal PET clock consists of a three byte counter which increments every 1/60 s. It is the 2 msb bytes which are stored as the time of the event.

(iii) Maximum value is AA (hexadecimal) for a given file.

(iv) Set to FF (hexadecimal) to provide an integrity check on data.

TABLE 6.1 : Data Storage String

later. A flowchart is given in figure 6.2 and a program listing in appendix A.

6.2.1 Data Conversion

First, position 26 in the string is checked to see if it contains $FF, hence confirming whether the data string is complete. If it is not, an error flag is set, the string and error code stored in an array and the next data string processed. Very few failures of this type occurred and these were attributed to spurious triggers. Further checks on data integrity consist of checking that shower numbers are consecutive and that the gain is stable. Defective data strings are treated as described above.

The pairs of bytes associated with each time delay and density are then extracted, converted to decimal and then to absolute values (time in ns and density in particles per square metre), using the calibration coefficients derived as described in chapter 5.

Finally the shower number and event time are read and stored. The time is first converted to h.m.s. Using this and the date of run initialisation, the date of the shower can be determined.

6.2.2 Axis Determination

Besides the time the shower front passes through each detector relative to the central detector (the measured time delay), one also requires the line delay for each detector in order to determine the axis direction. This is the time the pulse takes to travel from the fast PMT, in a detector, to the laboratory. This can be determined by sending a pulse up the unterminated line and observing the delayed arrival of the reflected pulse on

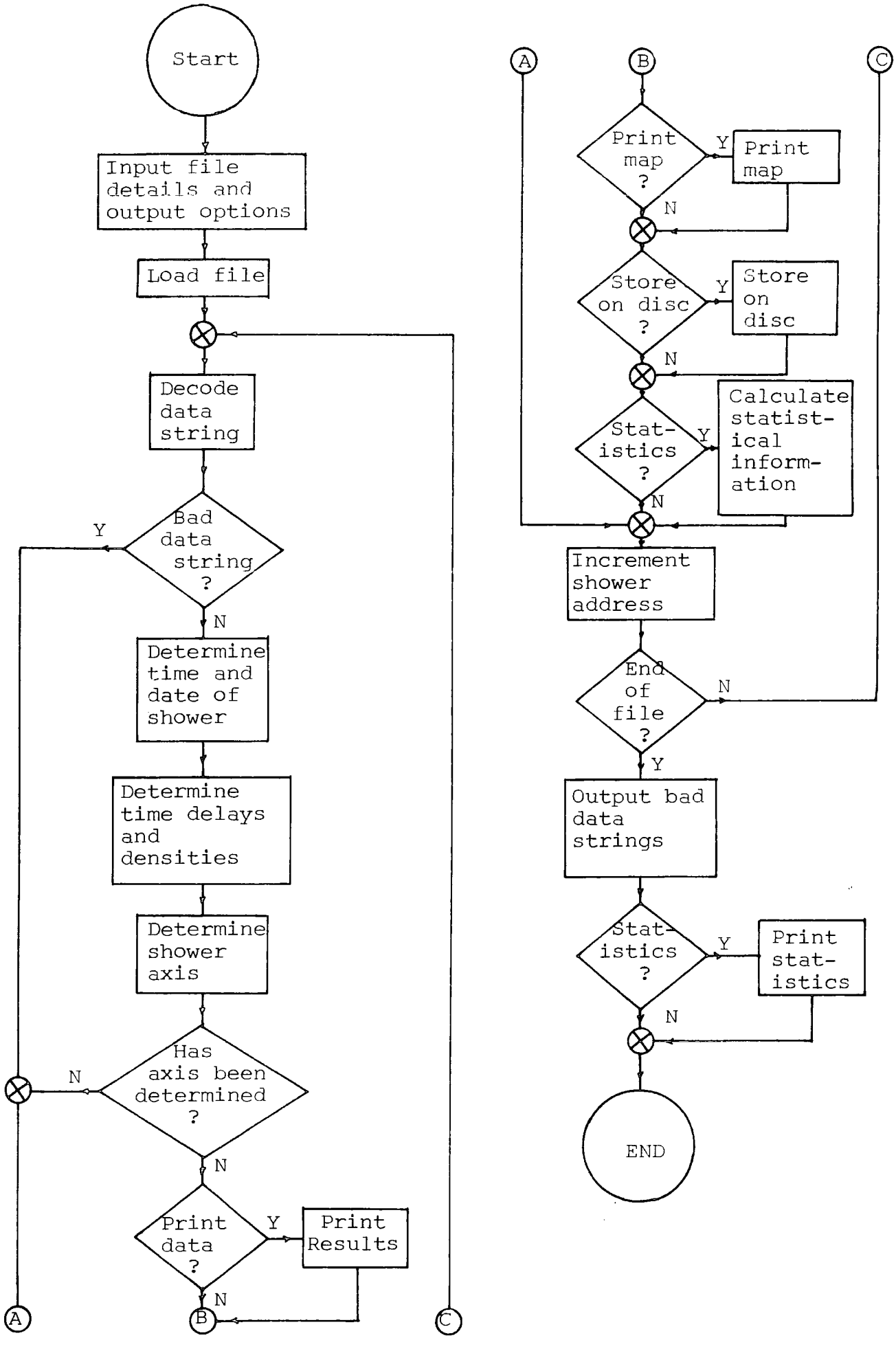

FIGURE 6.2 : Flowchart of DATAPROC program

an oscilloscope. However, a more accurate value, which includes any delay in the electronics, is found by taking the mean of the distribution of the timing data from each detector. From these, the 130 ns of the extra delay in the C channel has to be subtracted. Finally one must subtract the time taken for a vertical shower to pass from C to the relevant detector, ie. $\frac{z}{c}$. The form of the time distribution is shown in figure 6.3. These time distributions form a valuable check on the data collection and this is further described in appendix D. The actual time delay of the shower front, passing through a detector relative to C, is then given by the recorded time minus the modified line delay.

Given two of these time delays and the detector coordinates, the zenith (θ) and azimuthal (ϕ) angles of the axis can be uniquely determined by the equations :

$$\cos(\theta) = \left[-(AB+CD)+((AB+CD)^2-(A^2+C^2-1)(B^2+D^2+1))^{\frac{1}{2}}\right]/(B^2+D^2+1)$$

$$\tan(\phi) = (C+D\cos\theta)/(A+B\cos\theta) \qquad (6.1)$$

where $A = (y_2t_1-y_1t_2)/E$ $\qquad B = (y_2z_1-z_2y_1)/E$

$C = (x_1t_2-x_2t_1)/E$ $\qquad D = (x_1z_2-x_2z_1)/E$

$E = x_1y_2-y_1x_2$

The proof of the above equations is given in appendix C. It is to be noted that the azimuthal angle is defined in the anti-clockwise direction from the x-axis (figure 2.1).

Since three time delays are available, two determinations of the angles are made and then averaged. Examination of the results from the three possible pairs show a good agreement with each other.

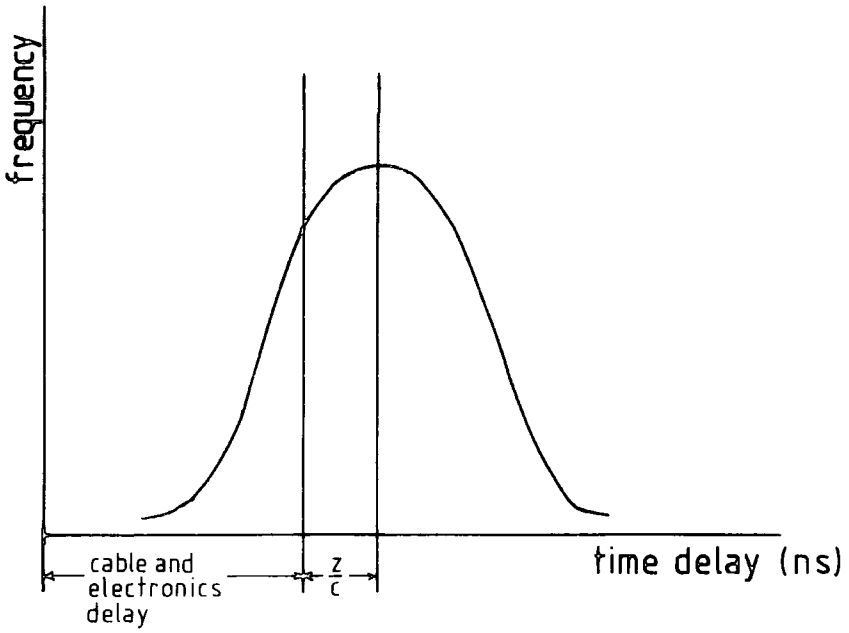

FIGURE 6.3 : Form of the time delay distribution

6.2.3 Data Output

A variety of forms of data output are available, either singly or in combination. These are as follows ;

(i) Printed list : The data is output to the printer as a table. Also printed is a list of failed data strings to allow manual retieval, if possible.

(ii) Map : Data is output in the form of a map. This is of value if a rough core determination is required to be made manually. However, in practice, its use is limited due to the time required to print the map for each shower.

(iii) Disc : Data is stored on floppy disc.

(iv) Statistics : The density distributions, for each detector, and the three time delay distributions are printed for the file being processed.

An example of the map output for the data of figure 6.1 is shown in figure 6.4.

6.3 PROGRAM 'CORELOC'

6.3.1 Introduction

The next stage in the processing is to determine the core location and the shower size. For this a lateral structure function is required, that due to Greisen (1960) being used, which assumes an average age parameter, s, of 1.25. The density of particles at a given distance from the core, r, is given by,

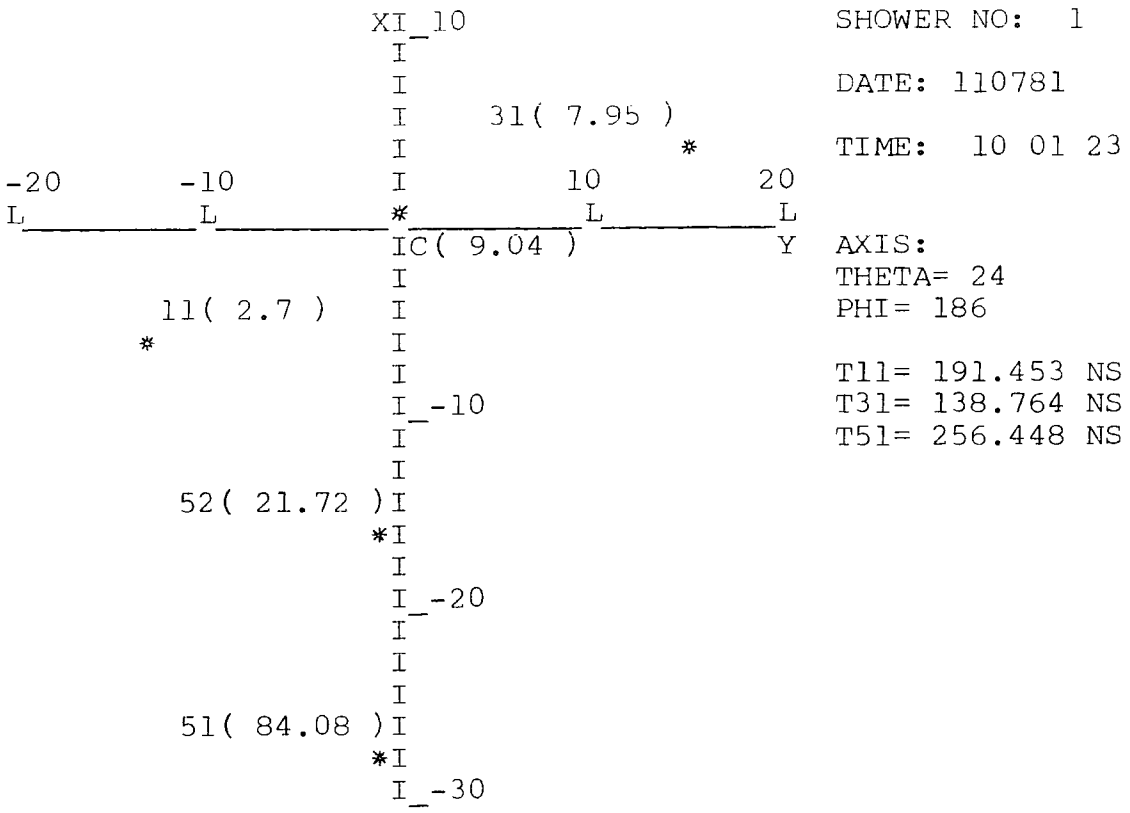

FIGURE 6.4 : Example output of DATAPROC with the data string of figure 6.1 as input

$$\Delta(r) = \frac{0.4\ N}{r_1^2} \left(\frac{r_1}{r}\right)^{0.75} \left(\frac{r_1}{r+r_1}\right)^{3.25} \left(1 + \frac{r}{11.4\ r_1}\right) m^{-2} \qquad (6.2)$$

where N is the shower size and r_1 = 79m at sea level.

Using this, the density information and the axis direction, a minimisation technique can be used to estimate the core location and shower size.

6.3.2 Minimisation Technique

First of all an approximate core location is required. Two methods were examined. First, from a map of the array with densities, an estimate can be made. However this is time consuming and even though a reasonably accurate estimate can be made it does not reduce the search time enough to counteract this. The alternative is to take the coordinates of the detector with the highest density. Since this can be easily done automatically and has been found to be more efficient in time, it is the method used.

The Greisen structure function is expressed as,

$$\Delta(r) = N\ f(r)$$

For a given core position and a single electron density sample the error on the estimated shower size is related to the error on the density estimate by,

$$d\Delta = f(r)\ dN$$

Now $\sigma_\Delta = f(r)\ \sigma_N$ or $\sigma_N = \frac{\sigma_\Delta}{f(r)} = \frac{\sigma_\Delta}{\Delta/N}$ or $\sigma_N = \frac{\sigma_\Delta N}{\Delta}$

σ_Δ is calculated assuming the sampling fluctuations on n particles are $1.2\sqrt{n}$.

$$\therefore \quad \Delta = \frac{n \pm 1.2\sqrt{n}}{A} \quad , \quad \Delta = \frac{n}{A} \quad , \quad \sigma_{\Delta} = \frac{1.2\sqrt{n}}{A} \quad , \quad \text{so} \quad \frac{\sigma_{\Delta}}{\Delta} = \frac{1.2\sqrt{n}}{n}$$

The weighted shower mean is, thus, given by,

$$\bar{N}_w = \frac{\sum_{i=1}^{n} N_i / \sigma_{N_i}^2}{\sum_{i=1}^{n} 1 / \sigma_{N_i}^2} \qquad (6.3)$$

From this and f(r), the expected number of particles through each detector can be determined and a chi-square test can be performed. Because the number of particles is low, the chi-square test has to be modified as follows (Smith, 1976),

$$\chi^2 = \sum_i \frac{(O_i - E_i)^2}{E_i + \sqrt{E_i} + 0.25} \qquad (6.4)$$

A square, of pre-defined size, is set up around the current core location. The chi-square is then calculated for cores set up on the corners and mid-points of the sides of this square. The approximate core is then moved to the point which produces the minimum chi-square and the process repeated. If the original chi-square remains the minimum, then the side of the square is reduced by a factor of two and the process repeated. The process is continued until the square side has reached a pre-defined limit. The resulting approximate core,mean shower size and chi-square are then taken as output.

6.3.3 Program Procedure

The initial and the minimum box side are normally set at 10m and 1m respectively, but can be adjusted if required. Also a limit on the search area is input, which is normally set at a box, of side 100m, about the initial core estimate. The density and axis information can be put in either manually or directly

from disc. Only showers with at least ~~four~~ three non-saturated, non-zero detectors are considered for processing and this selection is made initially.

During the search, if a detector is less than 5cm from the present core, it is ignored as the Greisen function is not valid in this case. An error message is printed to warn of this occurrence. Another error message is produced if the search area is exceeded. In this case the search is terminated and the present search parameters output. On completion of a search, the core location, shower size and chi-square are output, together with a list of saturated and zero density detectors. Once a file has been completely processed, the complete list of the shower parameters is stored on floppy disc for future processing. A flowchart for the program is shown in figure 6.5 and a listing is given in appendix A.

6.4 SIMULATION OF EAS

6.4.1 Introduction

Simulation allows the prediction of the properties of the air shower array and the data analysis in order to interpret the data correctly. In addition it allows the determination of limits on the parameters and hence the rejection of potentially inaccurate data.

In order to do this, a computer program was written which produces simulated air shower data. The simulated showers are then processed as if they are real showers and the resulting parameters compared to those input to the simulation program. From this comparison the limits within which showers can be considered as having been accurately analysed can be determined. These limits

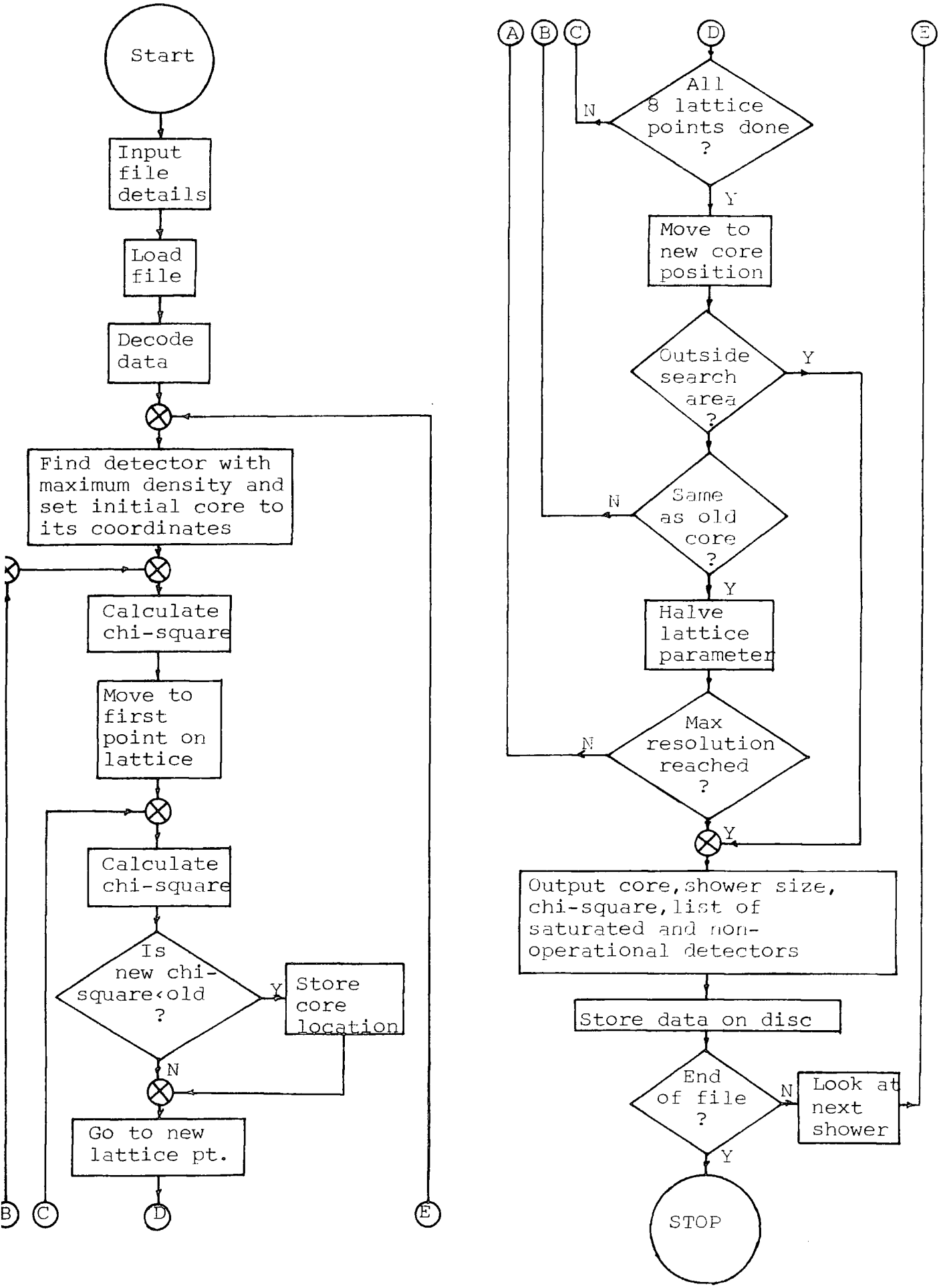

FIGURE 6.5 : Flowchart of CORELOC program

are placed on the shower size range, the axis zenith angle and the distance of the core from the centre of the array.

6.4.2 The Shower Simulation Routines

The program is required to be able to generate showers at random from the relevant distributions for shower size, axis direction and core position. In order to do this a technique is required to generate random numbers from a given distribution.

6.4.2.1 Generation of the Shower Size

The shower size, N, is randomly generated from the distribution of the form,

$$f(N) = AN^{-\gamma}$$

where A and γ are constants. The integral method (Knuth, 1981) is used. The actual distribution has a change in slope, so the size is actually generated from a two part distribution,

$$\begin{aligned} f_1(N) &= A_1 N^{-\gamma_1} \qquad N_L \leq N < N_B \\ f_2(N) &= A_2 N^{-\gamma_2} \qquad N_B \leq N < N_U \end{aligned} \tag{6.5}$$

where N_U, N_L are the upper and lower limits of size generated and N_B is the point where the slope changes.

Firstly the distribution is normalised by dividing by the total area, T, under the distribution, ie.

$$T = A_1 \int_{N_L}^{N_B} N^{-\gamma_1} \, dN + A_2 \int_{N_B}^{N_U} N^{-\gamma_2} \, dN \tag{6.6}$$

The integral distribution is then formed.

$$I_1 = \left[A_1 \int_{N_L}^{N} N^{-\gamma_1} \, dN \right] / T \qquad N_L \leq N < N_B$$

$$I_2 = \left[A_2 \int_{N_B}^{N} N^{-\gamma_2} \, dN + A_1 \int_{N_L}^{N_B} N^{-\gamma_1} \, dN \right] / T \qquad N_B \leq N < N_U \tag{6.7}$$

If a random number is generated from a uniform distribution between 0 and 1 and equated to the integral, then the relevant random shower size can be determined from equations 6.7. If the random number, R, is greater than,

$$(A_1 \int_{N_L}^{N_B} N^{-\gamma_1} \, dN)/T$$

then I_2 is used, otherwise I_1 is used. This procedure is carried out in the subroutine NGEN. Limits of $1.8\ 10^4$ and $1\ 10^9$ are placed on the size since outside this region the rate of triggering is very low or non-existant.

6.4.2.2 Generation of the Axis Direction

The relationship of shower intensity to the zenith angle of the axis is given by,

$$I(\theta) = I(0) \cos^n\theta \quad m^{-2}s^{-1}sr^{-1} \tag{6.8}$$

where n is a constant. The generation of the zenith angle is by the method described above, with,

$$I = \frac{K \int_0^{\theta} \cos^n\theta \sin\theta \, d\theta}{K \int_0^{\pi/2} \cos^n\theta \sin\theta \, d\theta}$$

$$\text{or} \qquad \theta = \cos^{-1} (R)^{1/(n+1)} \tag{6.9}$$

where R is a random number taken from a uniform distribution between 0 and 1. This is carried out in the THETAGEN subroutine with a value of n = 8.

The generation of the azimuthal angle, ϕ, is simply by the generation of a random number from a uniform distribution between 0 and 2π.

6.4.2.3 Generation of Core Position

Shower core coordinates are generated uniformily over a circular area. The area is restricted since the probability of a shower triggering the array, falls rapidly as the distance from the centre of the array increases, and a cut can be made beyond which it is considered unnecessary to generate cores. The justification for this is found by plotting the probability of a shower, falling within a distance, R, from the centre, of triggering the array. This is shown in figure 6.6. It can be seen that above 75m, showers have very little probability of triggering the array.

6.4.2.4 Fluctuations

Two further distributions are required for shower simulation. These are the Gaussian and Poissonian distributions which are used to impose statistical fluctuations on the various parameters.

Gaussian random numbers are generated using the following method (Knuth, 1981). Two uniformily distributed random numbers, between 0 and 1, are generated, r_1, r_2. The following are then formed,

$$v_1 = 2r_1 - 1 \ , \ v_2 = 2r_2 - 1 \ , \ s = v_1^2 + v_2^2 \qquad (6.10)$$

(if $s \geq 1$ then repeat)

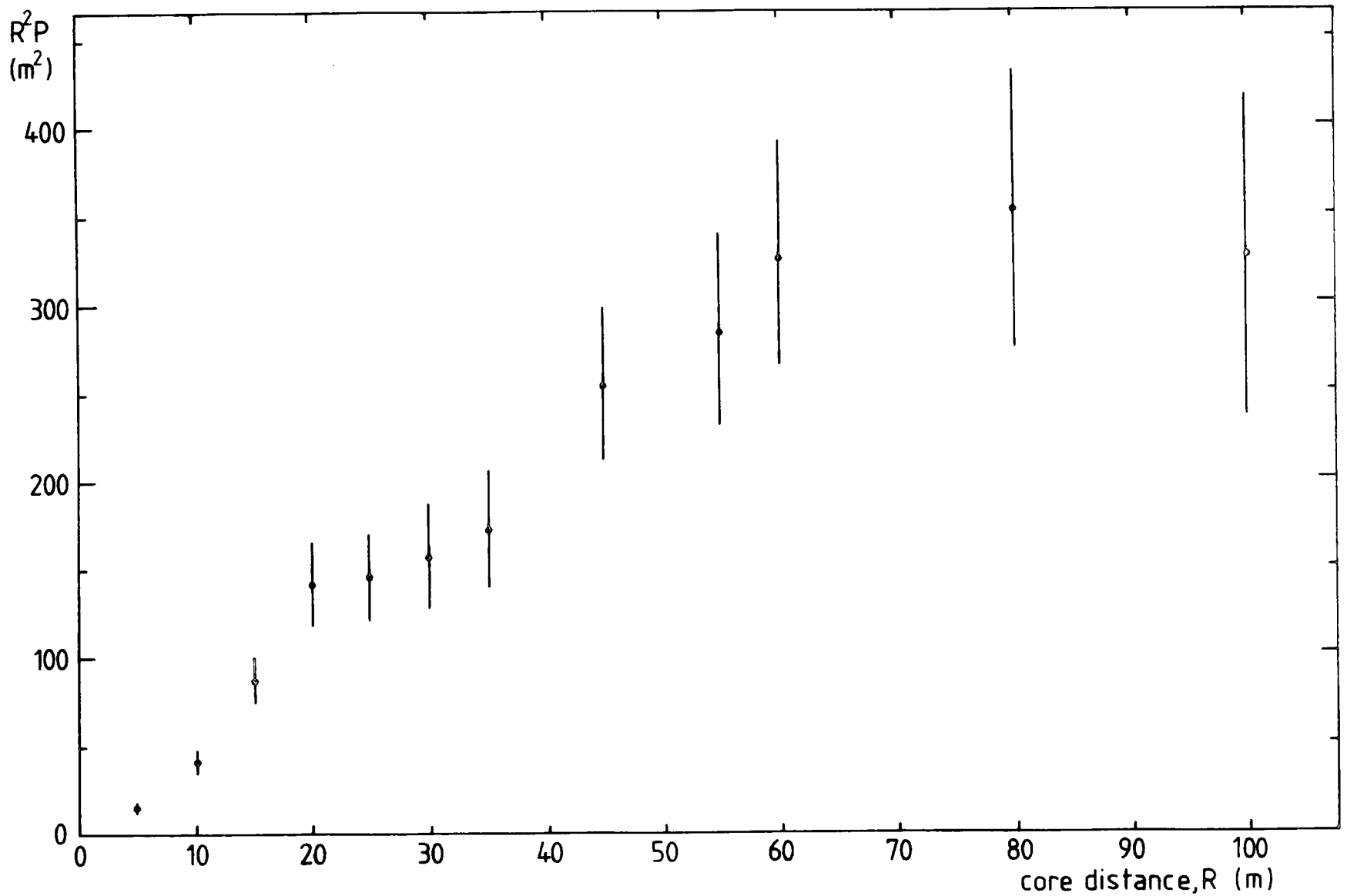

FIGURE 6.6 : Probability, P, that a shower of size $2\ 10^4 \leq N \leq 10^8$ will fall within a distance R from detector C. R^2P is proportional to the total number of successful showers.

The Gaussian random numbers are then given by,

$$x_1 = v_1\sqrt{-2\ln(s)/s} \qquad x_2 = v_2\sqrt{-2\ln(s)/s} \qquad (6.11)$$

This method gives approximately 100 pairs of x_1, x_2 for 127 pairs of r_1, r_2. The Gaussian distribution has a standard deviation, σ, of 1 and a mean, m, of 0, so the required values are,

$$X_1 = m + \sigma x_1 \qquad \text{and} \qquad Y_1 = m + \sigma y_1$$

To reduce any non-randomness due to any correlation that may exist between this pair only X_1 is used. (Subroutine GAUSSGEN).

For the Poissonian distribution, which is used for integers of less than 30, the following procedure is used (Knuth, 1981). The required number is given by the number of times, minus one, a uniformily distributed random number, between 0 and 1, must be generated before the product, of the random numbers, becomes less than $e^{-\lambda}$, where λ is the input integer. (Subroutine POISSGEN).

6.4.3 The Shower Simulation Program

The procedure of shower generation is shown in figure 6.7 as a flowchart. Firstly, the shower size, axis direction and core position are generated. From the axis direction, the time delay for each detector is determined. These are fluctuated with a Gaussian distribution of standard deviation 5ns, and the axis direction is then re-determined. Shower cores are then generated. Using this information, the densities at each detector can be determined using the Greisen function. These are then fluctuated with the Gaussian distribution, with standard deviation equal to the square root of the density, or the Poissonian, for means of less than 30. Finally the density is converted to the

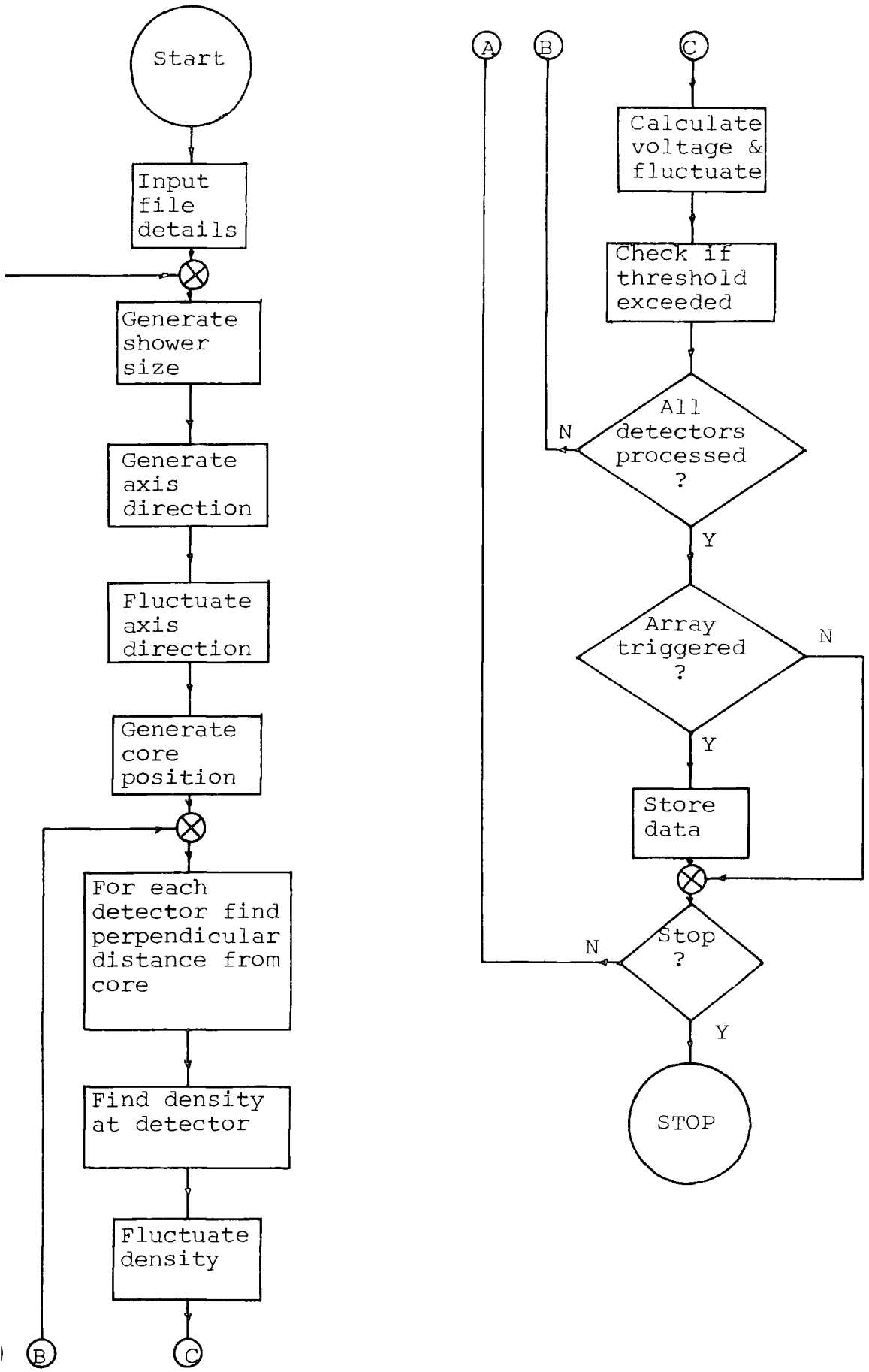

FIGURE 6.7 : Shower simulation program flowchart

voltage obtained from the detector. This value is fluctuated using the single particle voltage distributions. In order to do this, each of the distributions is approximated by a Gaussian distribution. The voltage is then converted back to a density. Finally the densities at each detector are checked against the discriminator threshold levels and the shower data only retained if these levels are exceeded for all the triggering detectors. The simulated data can now be processed as for real showers.

6.4.4 Results of the Simulation

Two different procedures are followed in the simulation. The first is to generate showers over the whole ranges of N, θ, ϕ and cores and then analyse them to compare them with real data. The other is to generate showers with one parameter fixed, eg. shower size or the distance of the core from the centre of the array, in order to investigate the limits in which showers can be analysed with reasonable accuracy. This latter procedure is the more important of the two.

Results from the general simulation are shown in figures 6.8 to 6.13. Figure 6.8 shows the input versus the output zenith angles. From this a limit on the zenith angle has been set to 30^{o}, above which scattering becomes more pronounced.

Figure 6.14 shows the variation of the mean core location errors with the analysed core distance from detector C. The errors shown indicate the spread of values obtained. From this, a cut of 50m on the analysed core distance, R_{anal}, has been chosen.

For investigation of the shower size spectrum, it is

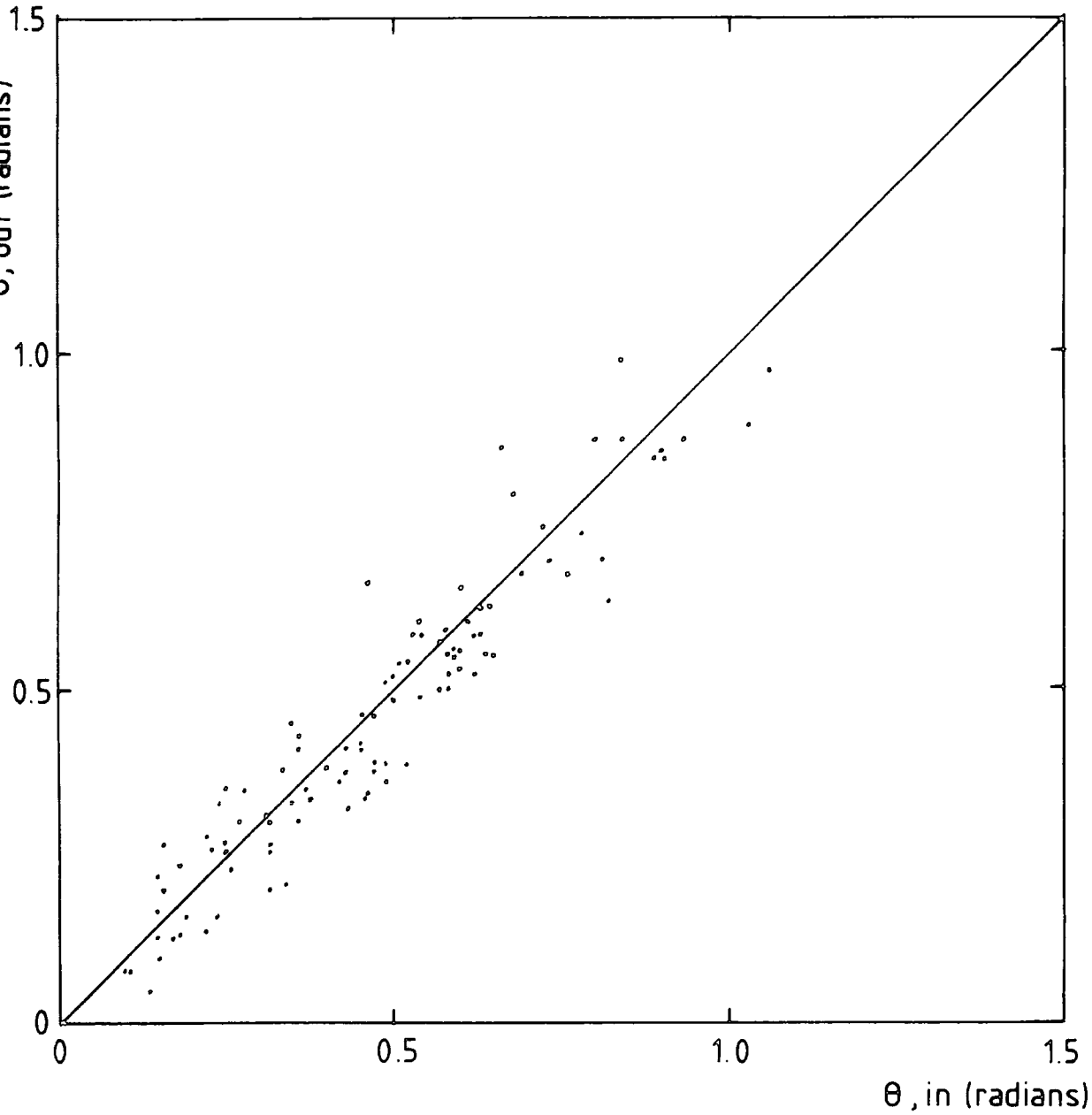

FIGURE 6.8 : Randomly generated zenith angles, fluctuated with a Gaussian distribution. (93 showers)

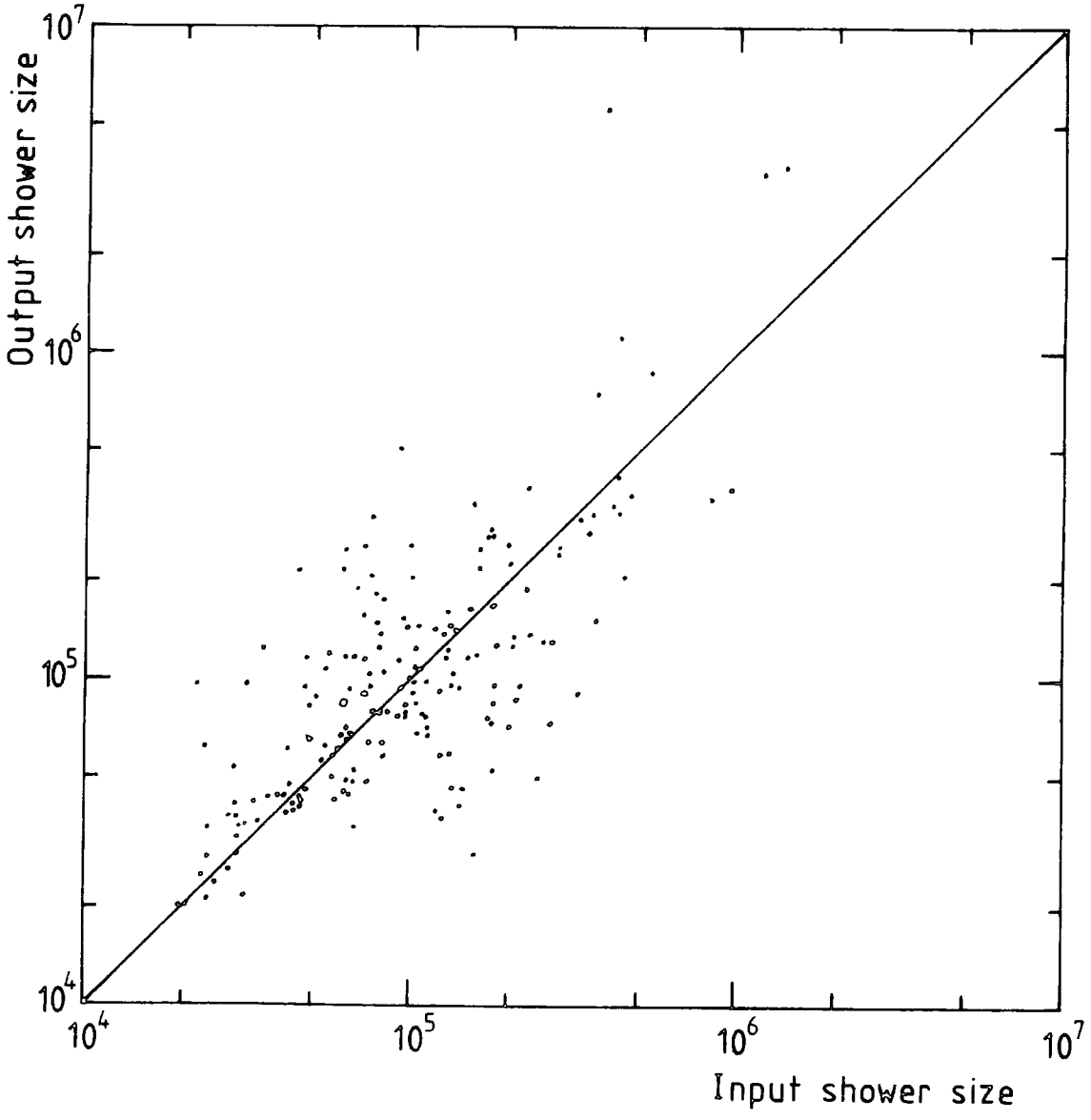

FIGURE 6.9 : Analysed shower size versus simulated shower size for 200 showers.

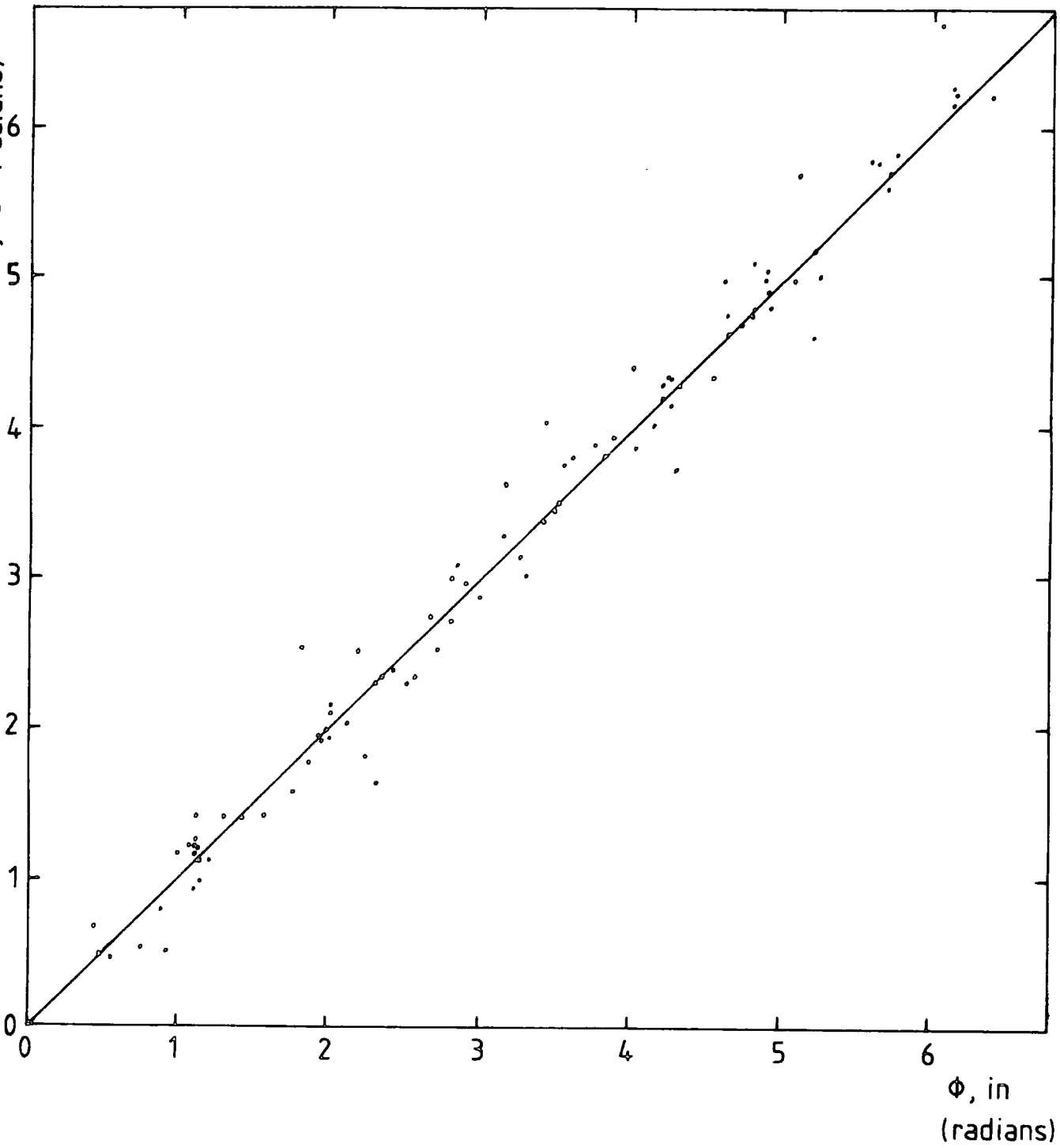

FIGURE 6.10 : Randomly generated azimuthal angles, fluctuated by a Gaussian distribution. (100 showers)

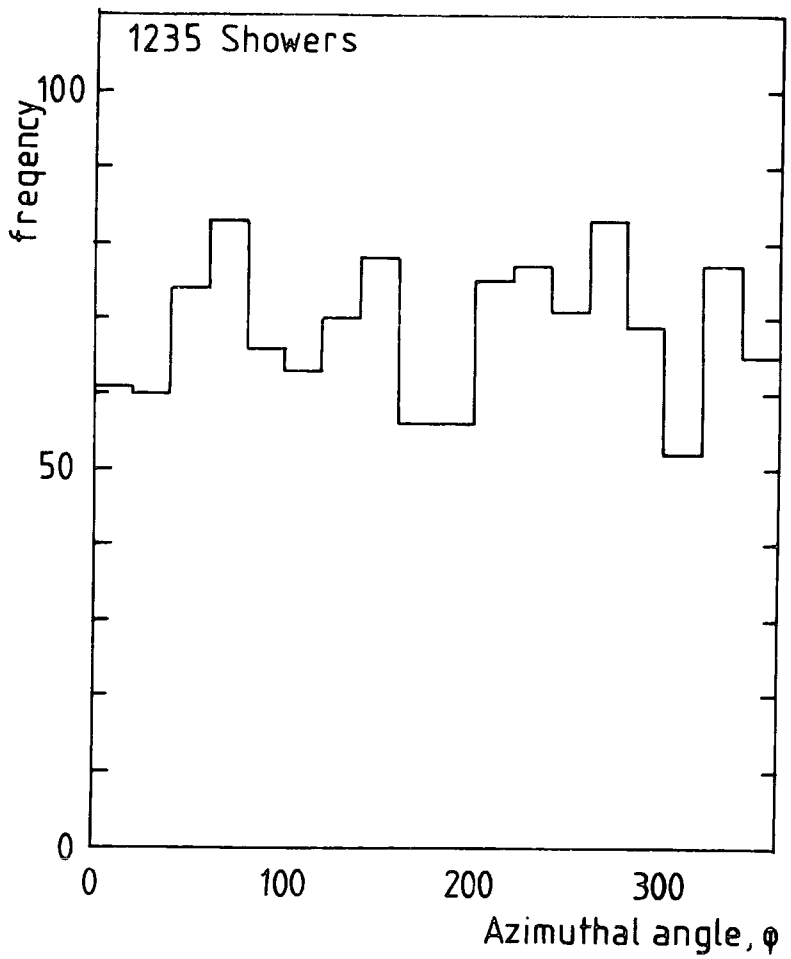

FIGURE 6.11 : Azimuthal angle distribution for simulated showers which trigger the array

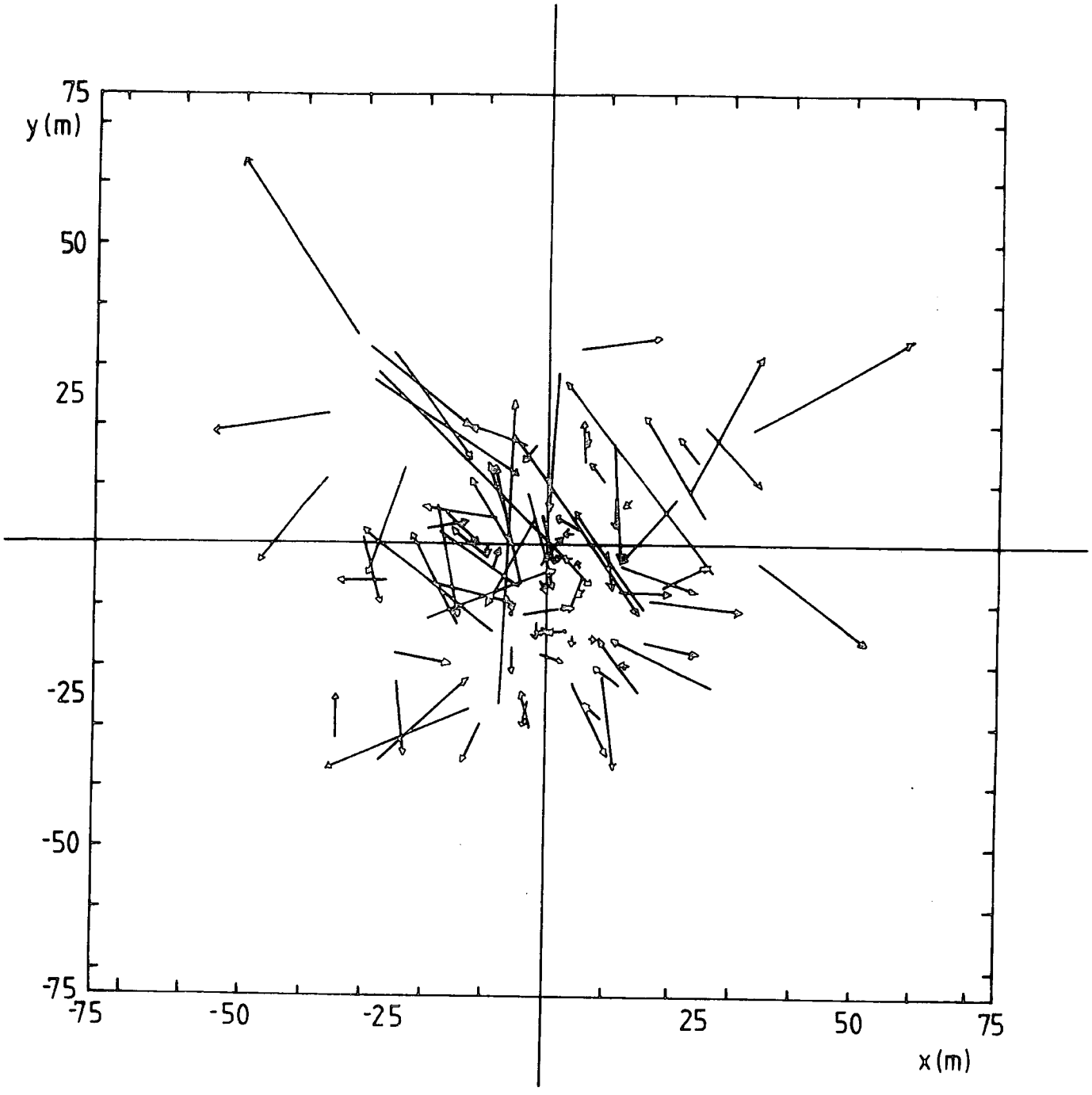

FIGURE 6.12 : Displacement of analysed cores with respect to cores of simulated showers for 90 showers. (arrow points to analysed core)

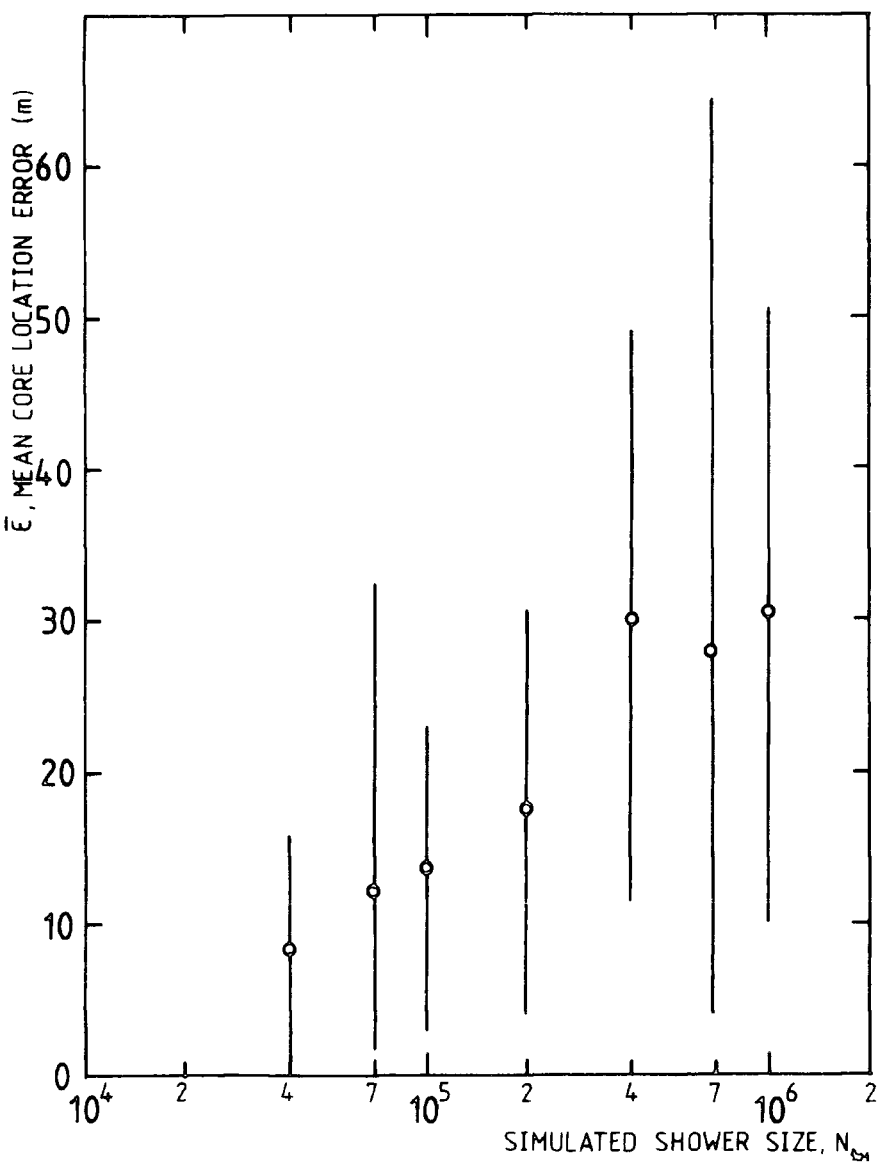

FIGURE 6.13 : Mean core location error versus simulated shower size. (Error bars indicate range of core location error)

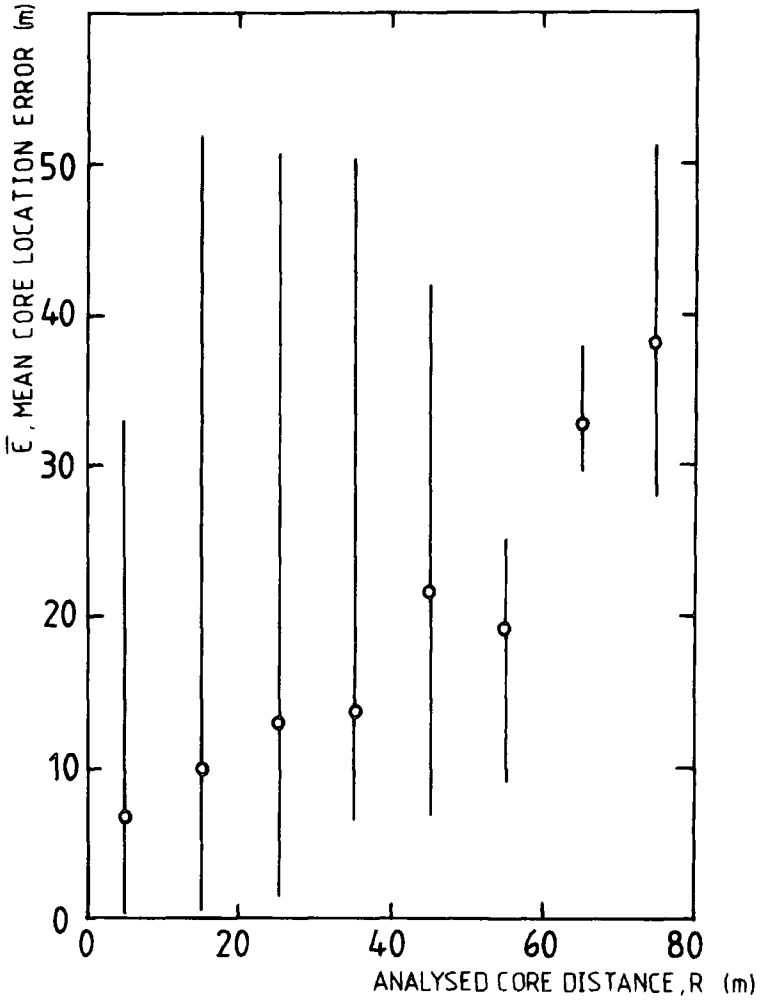

FIGURE 6.14 : Mean core location error versus analysed core distance from detector C. Error bars indicate range of core location error.

important to restrict the shower size to those which are most accurate. To estimate the lower limit, the probability of triggering the array for different shower sizes is determined for cores within 50m. For the upper limit, the saturation of detectors has to be taken into account. If more than two detectors are saturated, the shower is not analysed and therefore the probability of the shower being able to be processed is reduced. The resultant probability plot is shown in figure 6.15. For a greater than 90% probability, the shower size is restricted to the range $3\ 10^5$ to $7.5\ 10^5$.

Finally a plot is made of input shower size versus mean analysed size for simulated showers, subject to the above cut-offs. This is shown in figure 6.16, the error bars indicating the spread of analysed shower sizes. From this it is seen that the analysed shower size has a bias due to the processing. This plot is used to determine the correction required to be made to the analysed shower size.

6.5 CONCLUSIONS

The analysis of the data has been described. It can be seen that simulation plays an important part in the data analysis, by indicating the range of showers over which some confidence in the results can be maintained. However it can be seen that with the present array large errors occur, due to the small number of detectors. Simulation allows an estimate of the improvement in accuracy which would occur by increasing the number of detectors.

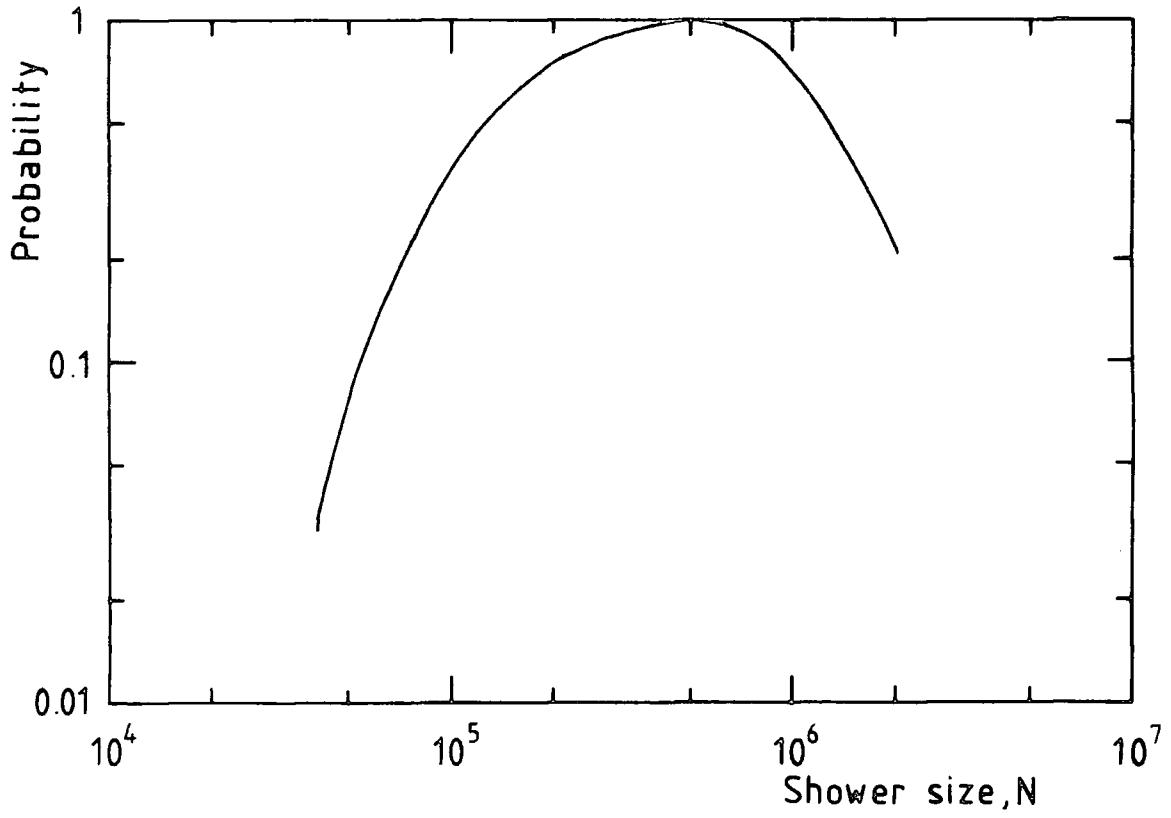

FIGURE 6.15 : Probability of a shower, R≤50, Θ≤30, triggering the array and being analysed (assumes small showers all analysable and that showers are not analysable when three or more detectors are saturated).

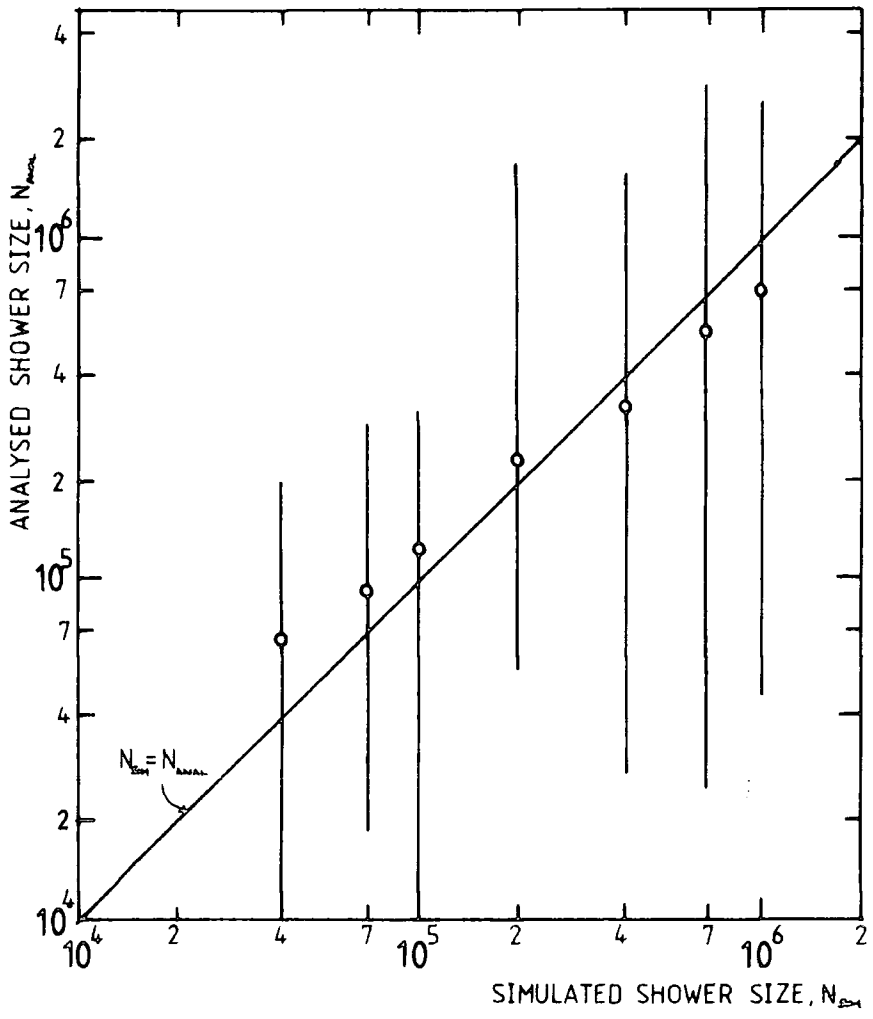

FIGURE 6.16 : Comparison of analysed shower sizes of simulated showers of fixed size.

CHAPTER 7

THE SINGLE SCINTILLATOR RESPONSE

7.1 INTRODUCTION

During the development of the data recording system, before the majority of array detectors were operational, it was decided to investigate the response of a single scintillator. This had two purposes. The first was to check the operation of the multiplexer, analogue-to-digital converter and microcomputer system and the second was to check on the apparatus as a whole by comparing the results with those due to other workers.

The response was investigated by determining the integral pulse height density distribution using two methods. In one the data recording system was used to record and bin every pulse height, above the threshold for the ADC, and the other was to use the conventional discriminator and scalar method.

7.2 EXPERIMENTAL ARRANGEMENT

The detector used was 11 which is $2m^2$ in area and 2.5cm deep and was calibrated as described in §2.3. It was connected to the data recording system as described in chapter 5. A number of changes to the system were made as follows. The discrimination level was adjusted so that any pulse from the detector, exceeding a threshold equivalent to 0.1 particles would produce a trigger. The output of the burst pulse generator was reduced to one pulse in order to reduce the dead time involved in recording unused multiplexer channels. Finally several parameters in the software were adjusted to facilitate reading and storing of a single channel. In order to output the data in a convenient form a

section of machine code was added to STORE.GO which binned the data and a BASIC program was written which allowed this data to be printed out in tabular form or as a histogram.

As an alternative, the detector output was taken via a discriminator to a scalar. This allowed the integral pulse height spectrum to be determined directly by measuring the rate of pulses greater than a given threshold set by the discriminator.

In order to extend the range of pulse heights investigated, the EHT supplied to the detectors' photomultipliers was adjusted as required, this allowed a range of particle densities from $2\ 10^{-2}m^{-2}$ to $10^{3}m^{-2}$ to be measured. For each value of EHT used a single particle peak was obtained, using the pulse height analyser, in order to calibrate the distribution in terms of particle density.

Some runs were also made with the photomultiplier tubes covered with black cloth. This allowed the electrical noise in the tubes to be determined so that it could be subtracted from the integral pulse height distribution. In the event, this correction was found to be small.

The resulting integral spectrum is shown in figure 7.1 where the curves are compared to the EAS density spectra of Greisen (1960), Ashton et al (1975) and McCaughan (1982). It is noted that the two methods used to determine the distribution are in good agreement, thus indicating that the data recording system is functioning correctly. For particle densities in excess of 50, the distribution is also in good agreement with the previous determinations of the density spectrum. However, below this density, there is a marked difference. A deviation is expected

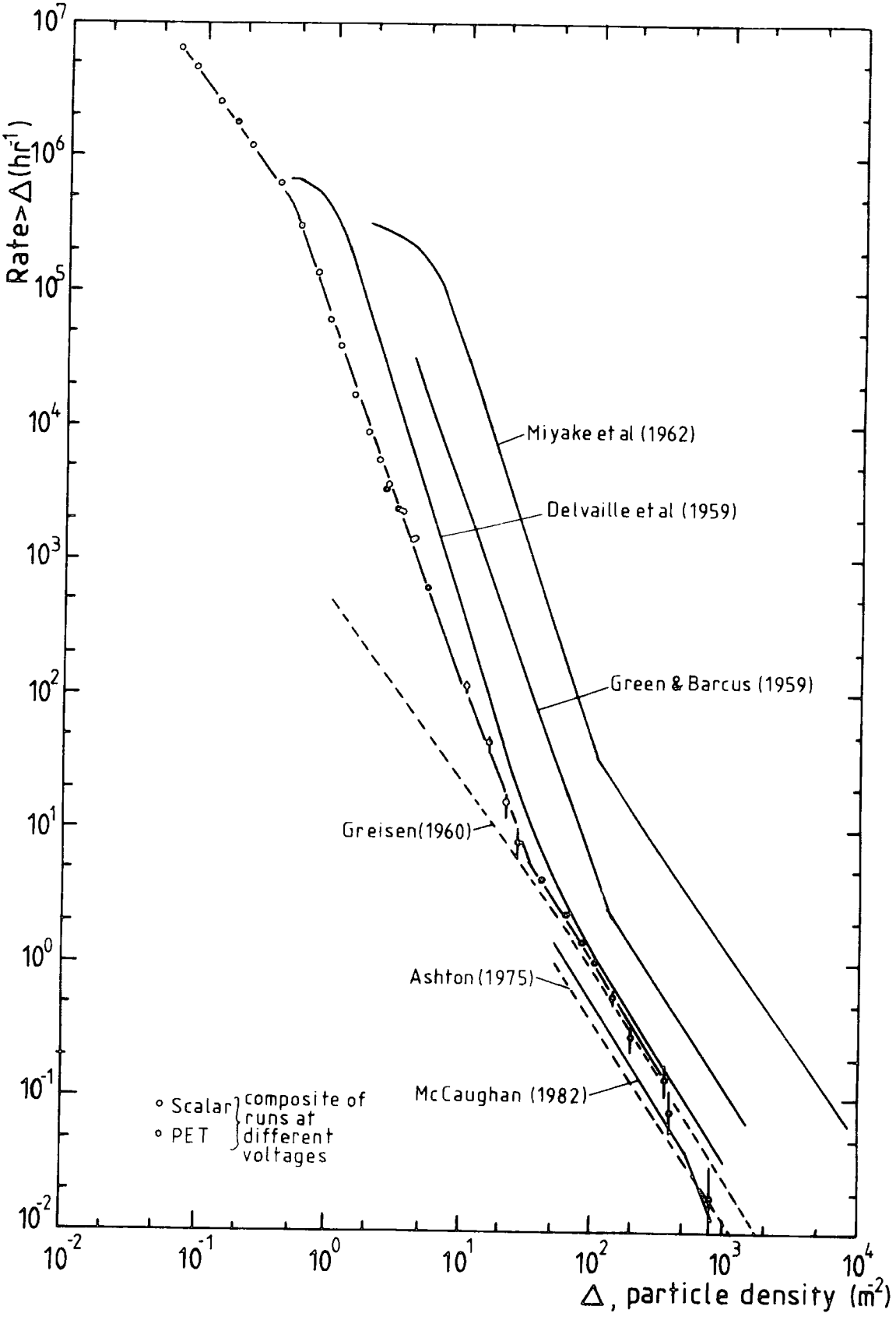

FIGURE 7.1 : Single scintillator response. (Detector 11, area = $2m^2$, thickness = 2.5cm)

due to the single particle peak, which EAS density spectrum measurements remove by requiring some form of coincidence. In addition to this there is a transition region apparent between 1 and 50 particles per square metre. The rate goes as the density to the power (-2.65±0.06) in this region and (-1.53±0.10) in the EAS density spectrum region. Figure 7.1 compares the results for a single scintillator of Delvaille et al (1959), using a $0.86m^2$ scintillator, and Miyake et al (1962), using $0.25m^2$ and $2.5m^2$ detectors at 2770 m.s.l. It is seen that agreement with Delvaille's result is good and also with the slope of the distribution of Miyake et al, their rate being higher due to the altitude.

7.3 INTERPRETATION OF THE TRANSITION EFFECT

7.3.1 Green and Barcus (1959)

A liquid scintillator of 10ft diameter and 5" depth at an elevation of 1575 m.s.l. was used to investigate the single scintillator response. The resulting integral spectrum (figure 7.1) can be described by two lines. The first is

$$Q(\geq p) = 22.0\ p^{-(1.514\pm0.022)}\ s^{-1},\ 3\ 10^{1} \leq p \leq 3\ 10^{3} \qquad (7.1)$$

where p is the number of particles in the scintillator. This was interpreted as the response due to EAS. Below 30 particles the gradient changes abruptly and the line corresponds to

$$R(\geq p) = 1.68\ 10^{3}\ p^{-2.76}\ s^{-1} \qquad (7.2)$$

Using the results of Teucher (1952), on the production of three-pronged stars in nuclear emulsions by cosmic radiation, they determined that the rate of star production in the detector was 1500 min^{-1}, on the assumption that the rates are simply proportional to the geometric cross-section. From this, and the average energy

lost by a particle traversing the scintillator, they conclude that the average energy for three-pronged star production is 90MeV. This is compared to the value of 100MeV determined by Camerini et al (1951) and thus they attribute the transition effect to nuclear interactions in the scintillator.

However, if these simple calculations are repeated for the present scintillator, which has about one twentieth of the volume and is at sea-level, where the star production rate is around a fifth of that at their elevation, then the average energy so determined is 5MeV. From this calculation, and other evidence mentioned later, it is suggested that Barcus and Green's conclusion was a result of their assumptions and coincidence.

7.3.2 Allan et al (1965)

In an experiment specifically designed to investigate the pulse spectrum of a single detector, Allan et al used detectors of two types, water Cerenkov tanks and scintillators. The Cerenkov detectors were of $2.25m^2$ area and 120cm depth (equivalent to 3.4 radiation lengths) while the plastic scintillators were of $1m^2$ area and 10cm thickness. Liquid scintillators of $2.2m^2$ area and 10cm depth were also used. In all cases the three regions were observed and the transition region was further investigated.

For water Cerenkov detectors the following was found:

(a) The counting rate (minus the EAS contribution) is proportional to area, which is what would be expected from some production process in the detector due to single particles.

(b) Observation of tracks produced in a flash-tube chamber, run in conjunction with the detector, in the transition region,

produce many events with only one or two tracks, thus implying a neutron, photon or charged particle entering from the side.
(c) The barometer effect coefficient of particles in the transition region was determined to be in the region 2-3% per cm Hg. This rules out the possibility of the effect being mainly due to nucleon interactions.
(d) The spectral shape was found to be essentially the same for detectors of different depths, which suggested that electron-photon cascading in the water, due to single muons, is not likely.
(e) Underground measurement indicated a reduction of intensity equivalent to that due to the reduction of intensity of the muon component.

For the scintillators it was found that:

(a) 2.5cm of steel shielding produced an increase in the number of larger pulses in the transition region, presumably due to the cascading of the soft component. However the lack of radiation between spectra when no shielding, 5cm or 15cm of lead were used implied that pulses are due to the penetrating component.
(b) The barometer coefficient was determined to be less than 5% per cm Hg, again too small for nucleons but compatible with muons.
(c) Calculations were made on nucleon-induced stars by considering nucleon flux and cross-sections, and it was concluded that the estimated response was much too small.

They concluded that the transition region is muon-induced but suggested that further work on the mechanism is required.

7.3.3 Maslin et al (1967)

Further investigations were conducted, following on from the work of Allan et al. Using flash tubes below a Cerenkov detector, they determined that pulses were due to cascade processes in the detector. They also produced calculations which allowed them to account for the pulse height spectrum almost entirely in terms of knock-on electrons.

7.3.4 De et al (1971)

Following the ~~contradictory~~ uncertainty in results of Allan et al and Maslin et al, the authors attempted to resolve the problem. They used two plastic (NE102) scintillators, one of dimensions 50x50x10 cm^3 and the other 50x50x20 cm^3, both at sea-level. The resulting gradients were -1.62 for the EAS region and -2.9 for the transition region. They found that the rate for larger pulses in the transition region increases as the scintillator thickness is increased, with a corresponding decrease in the rate of low energy pulses. They also confirmed the shielded results of Allan et al. These results confirm the interpretation of the transition region as mainly due to electromagnetic interactions in the scintillator.

7.4 CONCLUSIONS

The operation of the data recording system and the detector and its associated electronics have been determined to be satisfactory when tested by the determination of the single scintillator response.

Also, the shape of the pulse height spectrum has been discussed. It has been shown that it can be divided into three

regions, low pulses being due to single particles, high pulses being due to EAS and,in between these, a transition region exists which is most likely due to electron-photon cascades produced in the scintillator by single muons.

CHAPTER 8

EXTENSIVE AIR SHOWERS

8.1 INTRODUCTION

An extensive air shower (EAS) is the result of the collision of a primary cosmic ray with an air nucleus in the upper atmosphere. The collision initiates a cascade of particles which spread out to cover a large area at sea-level. This magnification of the effect of cosmic ray particles is invaluable as a tool for the study of those with high energy. For example, a primary with an energy of greater than 10^{18}eV has a flux of $10^{-11}m^{-2}s^{-1}$, but a small detector, at sea-level, would be hit once every few weeks by the secondaries of such a particle. However the price of this improvement in detection rate is the added complexity of interpreting the nuclear interactions of which the recorded secondaries are a result and therefore being able to deduce information about the initiating primary particle. This problem is compounded by the fact that accelerators have not yet reached the energies relevant to these problems, so one can only suggest models and try to fit these to observed shower data and existing theories.

In order to study EAS, large arrays of detectors have been built, which cover many square kilometres, eg. Volcano Ranch, USA ($8km^2$); Sydney, Australia ($34km^2$); Haverah Park, UK ($12km^2$); Yakutsk, USSR ($35km^2$) and these have detected showers due to primaries with energy up to about 10^{20}eV. Other methods used include observation of Cerenkov light and radio emission from showers to study shower development and particle detectors to study individual shower particles such as muons.

The following sections form a review of the most important aspects of EAS which have so far been revealed by the above methods. Results which are particularly relevant for the determination of air shower parameters are emphasised as are some of the implications for nuclear physics.

8.2 DESCRIPTION OF THE CASCADE PROCESS

Consider a proton primary of energy greater than 10^{13}eV (the minimum for an observable effect at sea-level to be produced). Collision with an air nucleus occurs with a mean free path of 70 to 80gcm^{-2} and produces many secondary particles of which the majority are pions both charged and neutral. ~~one or more are nuclear-active, of which one (the remains of the nucleus)~~ The surviving proton takes about half of the primary energy, ~~and some other hadrons~~. The neutral pions are unstable and decay within 10^{-15}s into pairs of gamma-rays, which can then initiate electron-photon cascades which grow by the process of bremsstrahlung and then decay away as the individual electron's energy falls and ionisation predominates (below 84MeV for an electron). Charged pions have a long lifetime due to the time-dilation effect and most, produced near the top of the atmosphere, will collide with air nuclei, producing yet more pions and feeding the nucleon cascade. However, in the later stages of a cascade, where the energies are lower and the lifetime shorter, they will decay into muons and neutrinos. The muon lifetime of 2 10^{-6}s, dilated by the relativistic effect, means that they are very unlikely to decay before they reach sea-level, but those that do, produce an electron and two neutrinos. Both muons and neutrinos are very weakly interacting and so have no problem in reaching sea-level. ~~Of course this makes them~~ The neutrinos are extremely difficult to detect. Finally there is the nuclear-active

component. They collide with further air nuclei or decay (in the case of unstable hadrons). Further collision will produce other cascades, similar to the initial one, the process continuing until the energy is too low. In addition to the processes already mentioned, there is also extensive cross-feeding between the components with the nuclear cascade dissipating energy to the other shower particles. A diagram of the cascade process is shown in figure 8.1.

Coulomb scattering spreads particles, depending on their mass, which results in the scattering of electrons being greater than muons which is, in turn, greater than for nucleons. However, the large distances travelled by muons, mean that they are found at great distances from the shower core.

The arrival at the ground of an air shower takes the form of a 'front' of electrons and photons, of about 2m thickness, spread over a circle of about 1km in diameter, their density falling away from the core. The core contains about 10% of the total shower energy and 90% of the particles at sea-level. The muons arrive more spread out in time (3 to 4m), due to their greater mass, and account for 60% of the energy and 10% of the number. Slower still is the nucleon component which forms a core along the shower axis of only a few metres in diameter. They have about 5% of the energy and 1% of the number. Finally the neutrinos take about 20% of the energy.

8.3 LATERAL STRUCTURE

8.3.1 Electron Lateral Distribution

The distribution of the particle density as a function of the distance from the core is an important characteristic of an

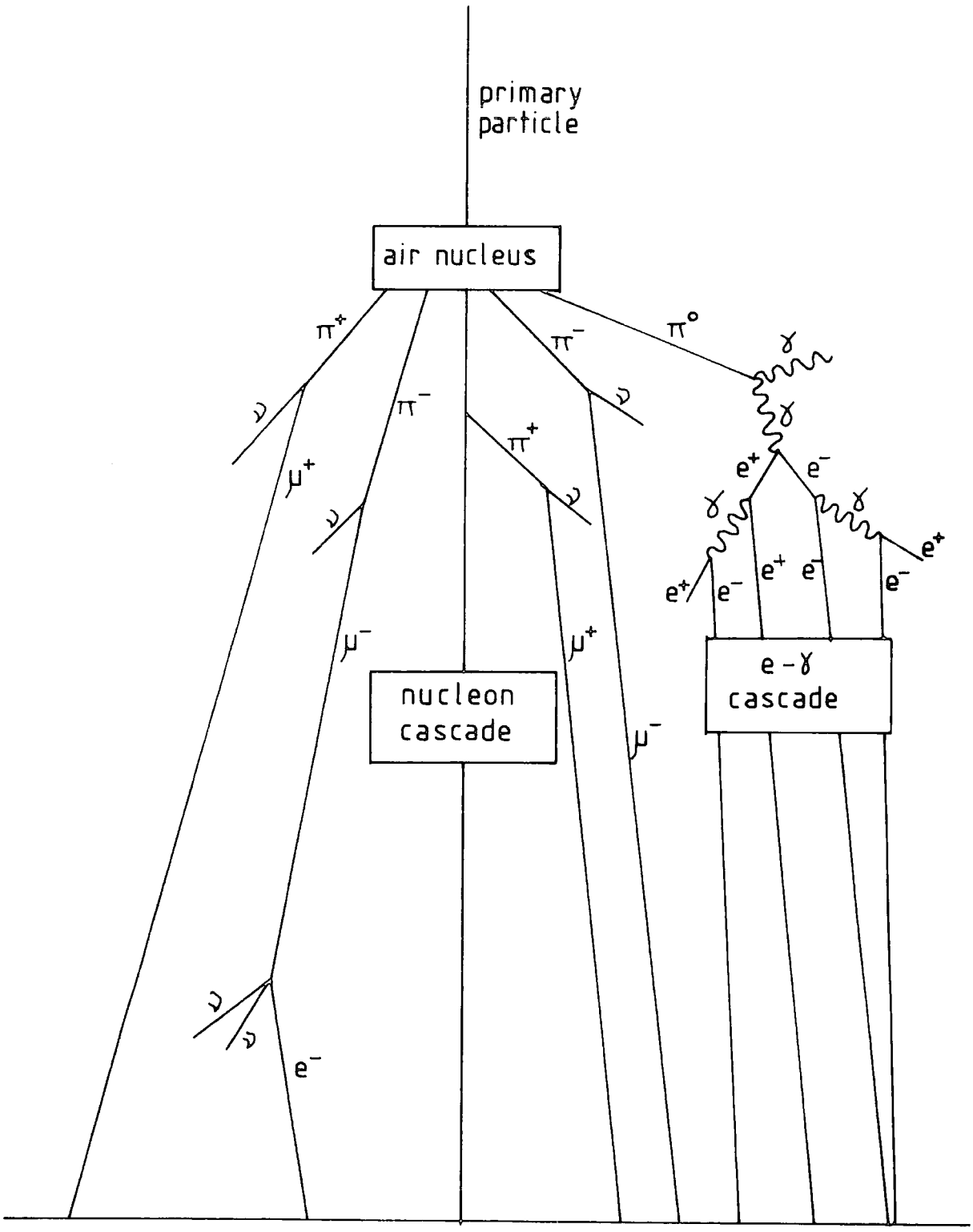

FIGURE 8.1 : Development of an extensive air shower

air shower. It has been investigated for each of the three components of the cascade. The most important of these is the electronic component which is the most numerous fraction and, in this case, the distribution is known as the lateral distribution function. This function has been shown to be remarkably invariant to different methods of measurement, shower size and observation altitude. Also, on average, it agrees with that obtained from theoretical determination using a pure electromagnetic cascade having coulomb scattering of electrons as the sole spreading agent. Greisen (1960) has combined a large number of results and produced a function which is claimed to hold good for shower sizes between $2\ 10^3$ and $2\ 10^9$ particles, atmospheric depths of 537 to 1800gcm^{-2}, radii from the axis of 5cm to 1500m and zenith angles less than 55°. This function is

$$\rho(N,r) = \frac{0.4N}{r_1^2}\left(\frac{r_1}{r}\right)^{0.75}\left(\frac{r_1}{r+r_1}\right)^{3.25}\left(1+\frac{r}{11.4r_1}\right)m^{-2} \qquad (8.1)$$

where ρ is the density of particles per square metre for a shower of size N at a radius r (m). r_1 is the Molière unit, a characteristic unit of length in scattering theory. Its similarity to the theoretical function of Nishimura and Kamata (1958), at distances less than 100m and an age parameter of 1.25, led Greisen to produce a simplified version.

$$f\left(\frac{r}{r_1}, s\right) = C(s)\left(\frac{r}{r_1}\right)^{s-2}\left(\frac{r}{r_1}+1\right)^{s-4.5} \qquad (8.2)$$

where C(s) is a normalisation factor and s is the age parameter which will be discussed later. This is known as the NKG function. The density is given by,

$$\rho(N,r) = \frac{N}{r_1^2}f(r)\ m^{-2} \qquad (8.3)$$

It has been found that the function does vary slightly for different detectors used. Those for scintillators being steeper than those determined using Geiger-Müller tubes, which represent the actual distribution well. This is due to the fact that the scintillator response depends on the energy spectrum of the electromagnetic component. An example of one determined in the former way is that of Hasegawa et al (1962) and is as follows,

$$\rho(N,r) = \frac{N}{4\pi\sqrt{30}} \frac{\exp(-r/120)}{r^{1.5}} \quad m^{-2} \qquad (8.4)$$

A more recent result is that of Catz (1975), again using scintillation counters.

$$\rho(N,r) = 0.015N \frac{\exp(-r/120)}{(r+1)^{1.62}} \quad m^{-2} \qquad (8.5)$$

where $2m < r \leq 70m$. Figure 8.2 shows the three structure functions mentioned above. It can be seen that agreement is good except at small radii and this is partly due to experimental errors in core location.

Recently, however, experimental results have cast doubt on the validity of using the NKG formula with a single age parameter, Khristianasen et al (1981) have measured the lateral structure and found a fit to NKG with s varying from 1.18 to 1.33 as r increases. This is similar to the results of Ashton et al (1977c). Other evidence is the conclusion of Abdrashitov et al (1981), using the Tien-Shan array. Their results are more in line with those determined by Monte-Carlo simulations (which avoid the approximations of analytic cascade theory) by Hillas (1981). These results are compared in figure 8.3. Thus it can be seen that there is still plenty of research to be carried out in the determination of a lateral structure function. However,

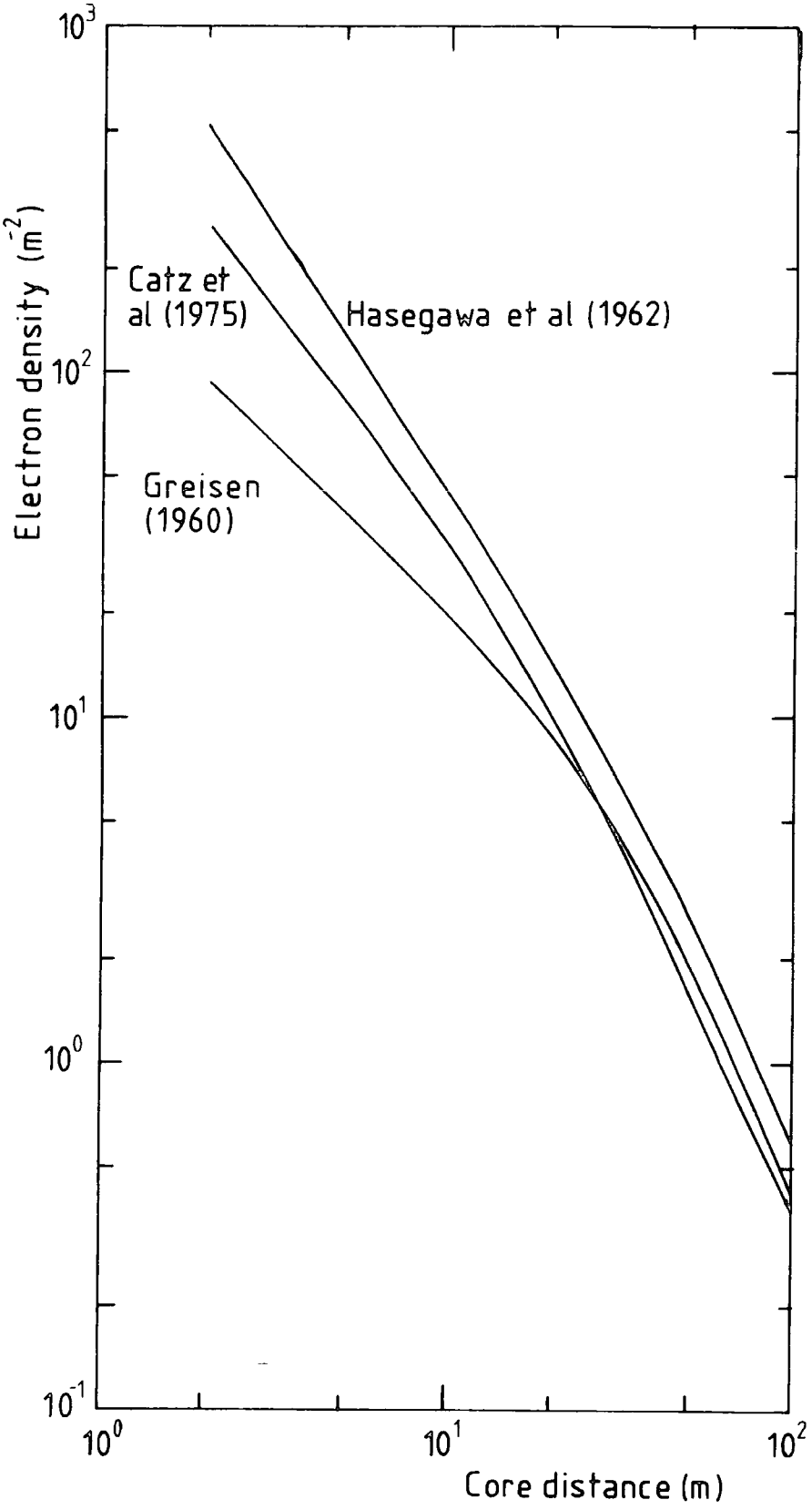

FIGURE 8.2 : Electron lateral distribution functions for showers of size 10^5.

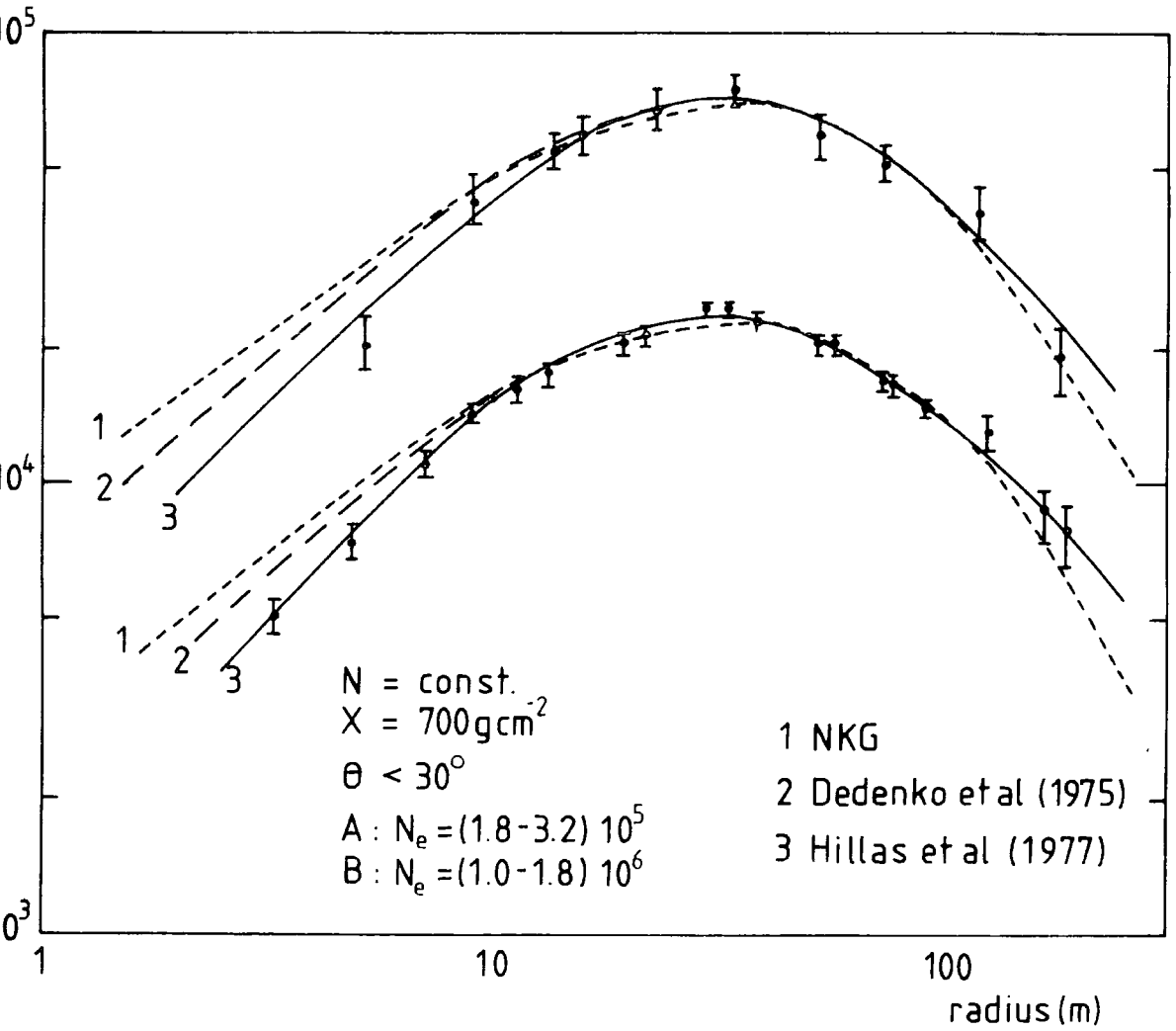

FIGURE 8.3 : Comparison of electron lateral distribution measured at Tien-Shan.
(after Abdrashitov et al, 1981)

in the range 10<r<100m agreement between all methods and experiments appears to be good.

8.3.2 Muon Lateral Distribution

Muons produced at high altitudes are spread by multiple scattering and geomagnetic deflection, the latter leading to asymmetry in the east-west direction. The spread can be as large as several tens of metres especially for inclined showers. However the most important cause is the angular divergence of their parent pions, which acquire transverse momentum at their generation.

It is convenient to determine the lateral distribution above a given energy threshold. Clark (1958) produced a result for showers of size $2\ 10^5$ to $2\ 10^8$ and muon energies greater than 1.2GeV. The results were reduced by Greisen (1960) to the following empirical form:

$$\rho(N,r) = 18\left(\frac{N}{10^6}\right)^{0.75} r^{-0.75}\left(1+\frac{r}{320}\right)^{-2.5} m^{-2} \qquad (8.5)$$

Later, Bennett and Greisen (1962) investigated the variation in structure with energy and produced the following relation,

$$\rho(N,r,>E_\mu) = 14.4\left(\frac{N}{10^6}\right)^{0.75} r^{-0.75}\left(1+\frac{r}{320}\right)\left(\frac{51}{E_\mu+50}\right)\left(\frac{3}{E_\mu+2}\right)^{0.14r^{0.37}} m^{-2} \qquad (8.6)$$

where E_μ is in GeV and $1 \leq E_\mu \leq 10$GeV.

These results are shown, along with more recent ones, in figure 8.4. All the data are normalised to a shower size of $2\ 10^7$ particles and the energy threshold is taken as 1GeV. The different determinations can be seen to be consistent except at radii less than about 20m which can partly be ascribed to errors in core location and also the normalisation procedure.

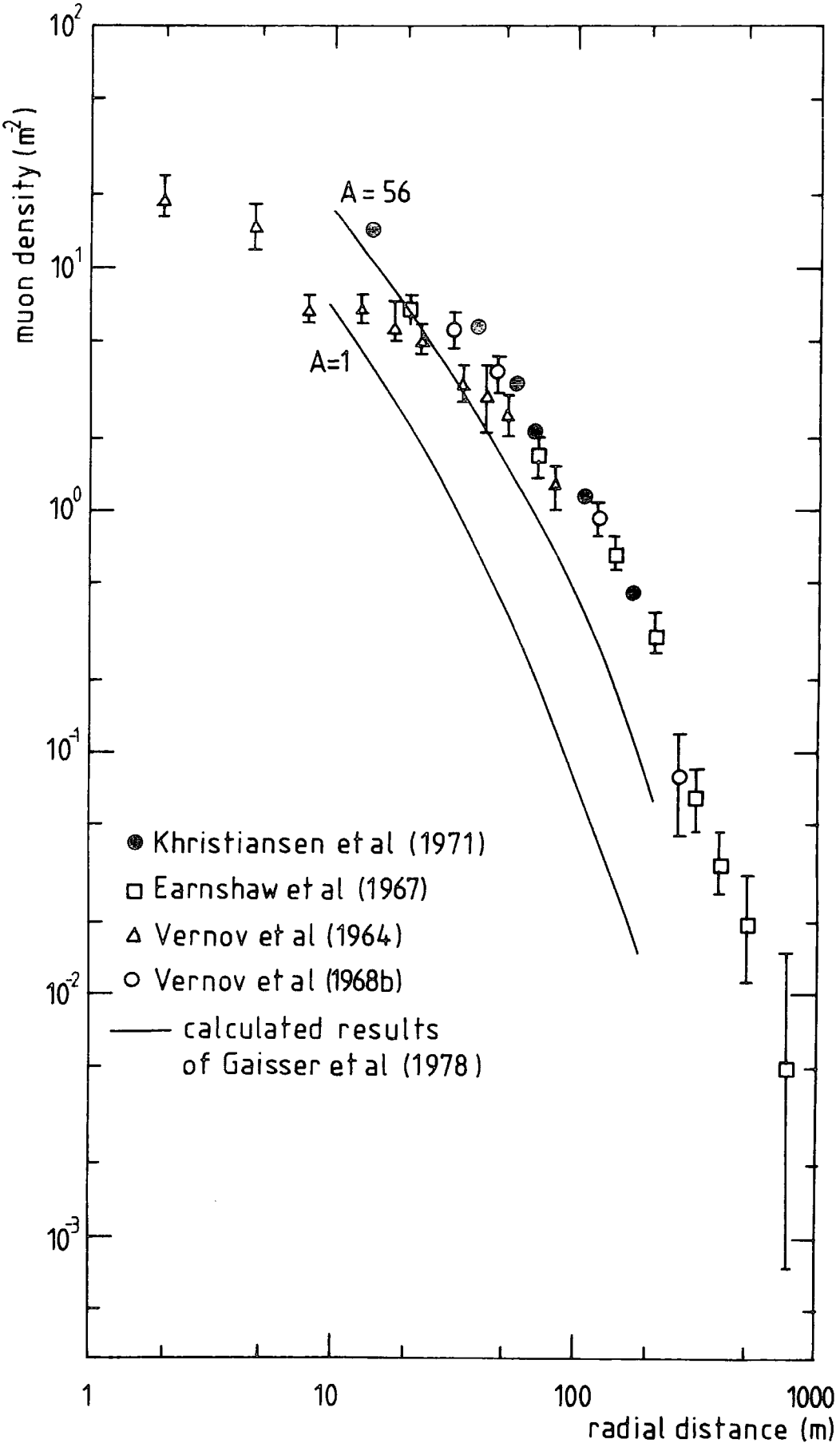

FIGURE 8.4 : Muon lateral distribution for a 10GeV energy threshold

Comparisons with theoretical distributions, using standard models, eg. scaling, reveal a steeper ~~spectrum~~ lateral distribution than is observed. This indicates that the particles have higher transverse momenta than predicted and therefore points to a need to revise the theory. It can be seen that the muon lateral distribution plays an important part in the understanding of the shower process and especially in the determination of the height of origin of the shower and the multiplicity of the first interactions.

8.3.3 Nuclear-active Lateral Distribution

The nuclear-active particles have small transverse momenta and so have only a small spread. Consequently the lateral density distribution is much narrower than that of either the muon or electron components. The differential lateral density distribution is given by Kamedo et al (1965) as,

$$\rho(E,r,N)\,dEdr = 0.35\ N^{0.35}\ E^{-1.2}\ e^{-r/r_o}\,dEdr \qquad (8.6)$$

where $r_o = 2.4\ N^{0.32}\ E^{-0.25}$ and N,E are measured in units of 10^5 particles and 100GeV respectively. The results from several workers are shown in figure 8.5.

8.4 LONGITUDINAL DEVELOPMENT

The longitudinal development of a shower can be determined by observing it at different heights in the atmosphere. An easier method is to observe showers, at a fixed level, with different zenith angles, since the air thickness traversed increases with zenith angle. However, for small depths, there is no substitute for mountain and aircraft observations, with particle detectors. Other methods have been developed such as the observation of the Cerenkov light, produced by the highly relativistic particles in

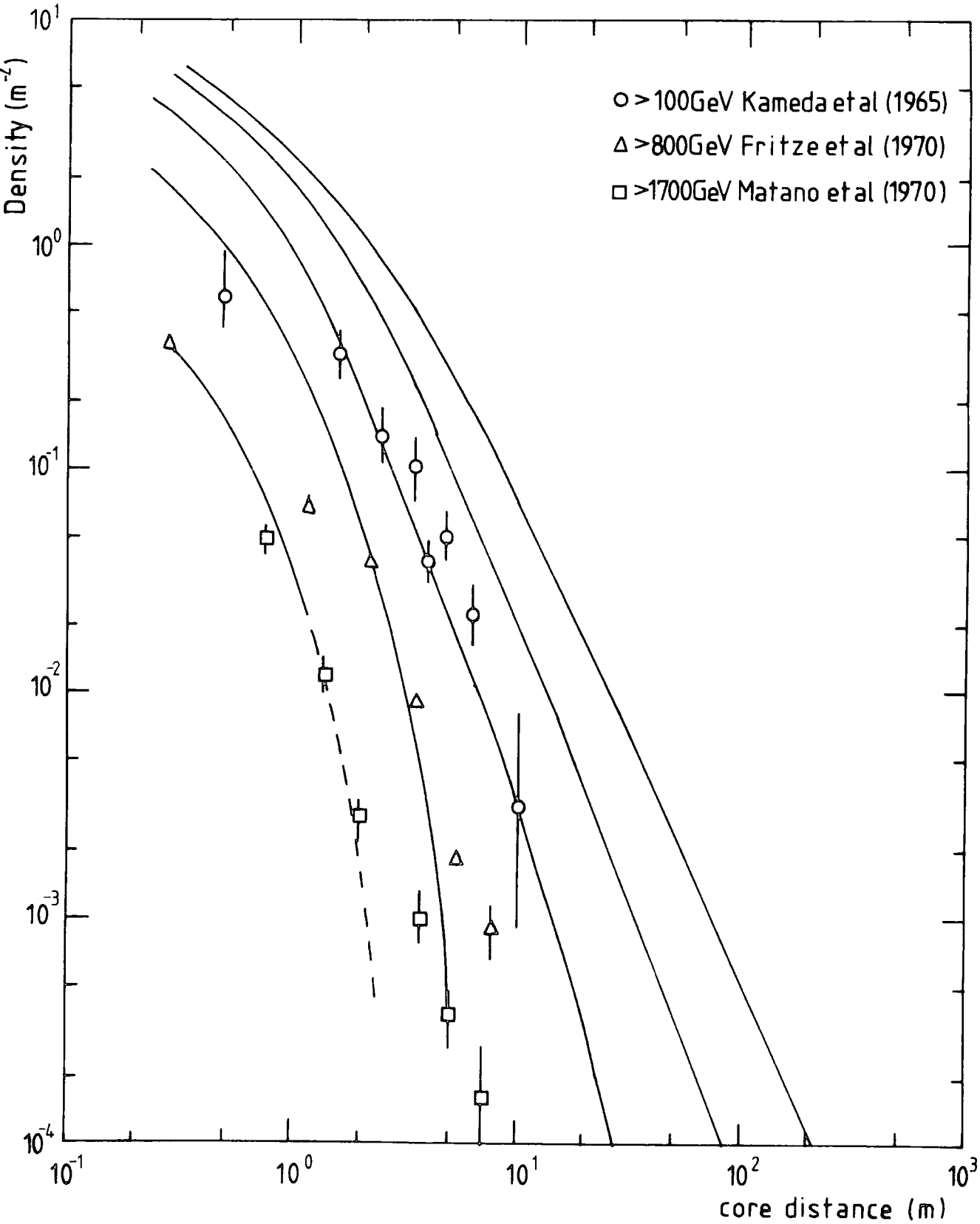

FIGURE 8.5 : Lateral distribution for hadrons of different energy, at sea-level. The lines are the simulated distributions for proton-initiated showers of energy 10^{6} GeV. Experimental data is normalised to $N_e = 10^{5}$. (after Grieder, 1977)

the atmosphere and scintillation light from the scattering of electromagnetic waves by the ionised column produced by the EAS.

The size of the shower depends on the primary energy, E_o, and the atmosperic depth, and is designated $N(E_o,x)$. This is subject to considerable fluctuations, due, in the main, to the depth of the first interaction, since in subsequent interactions the number of participating particles is so great that fluctuations at this point can be compensated for, approximately.

A detailed knowledge of the longitudinal development is, thus, very important for the understanding of the high energy interactions which occur in the early stages of a shower.

An example of the development of showers of two different energies is shown in figure 8.6 (after Hillas 1970). For depths, less than about $500gcm^{-2}$, the curves are derived theoretically, using cascade theory. The energy content of the showers is shown in table 8.1. The area under the curves gives the energy loss, by ionisation in the atmosphere, which can be added to the remaining energy of the particles at sea-level to give the total shower energy.

Since the vast majority of particles, in the shower, are electrons, the longitudinal development is well represented by the electromagnetic cascade model. Greisen (1956) produced an expression which describes the development of the cascade as it passes through the atmosphere which is as follows,

$$N(E_o,t) = \frac{0.31}{\beta_o^{1/2}} \exp\left[t(1-1.5\log(s))\right] \qquad (8.7)$$

where $t = x/x_o$ is the thickness of air in radiation units, $\beta_o = \log(E_o/E_c)$ where E_c is the electron critical energy in air (84.2MeV),

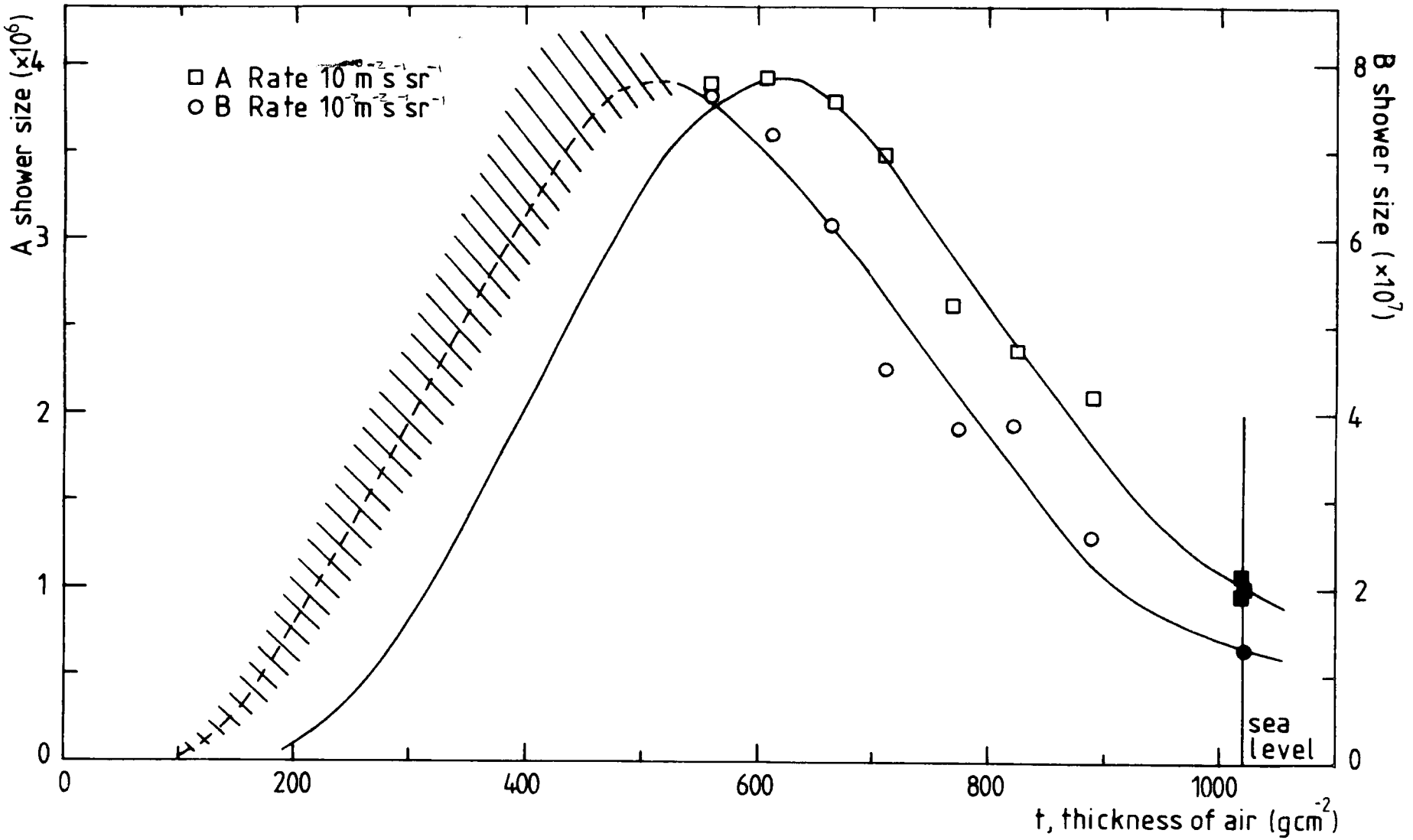

FIGURE 8. : Number of particles, N, in showers which are detected at a fixed rate (A or B) under different thicknesses, t, of air. (after Hillas, 1970)

Size, N, at shower maximum	$3.9\ 10^{6}$	$7.8\ 10^{7}$
Size, N, at sea-level	$6.3\ 10^{5}$	$2.0\ 10^{7}$
Ionisation above sea-level (eV)	$4.4\ 10^{15}$	$8.8\ 10^{16}$
Energy of soft component (eV)	$0.14\ 10^{15}$	$0.4\ 10^{16}$
Energy of nucleons and pions at sea-level (eV)	$0.08\ 10^{15}$	0.2 ?
Energy of muons at sea-level (eV)	$0.64\ 10^{15}$	$1.3\ 10^{16}$
Energy of neutrinos (estimated) at sea-level (eV)	$0.33\ 10^{15}$	$0.6\ 10^{16}$
Total Energy, E_p	$5.6\ 10^{15}$ eV	$11.3\ 10^{16}$ eV

TABLE 8.1 : Energy Content of Showers of two Selected Sizes (after Hillas, 1970)

$s = (3t)/(t+2\beta_o)$ is the age parameter and $x_o = 37.7 gcm^{-2}$ in air.

From this, the maximum development of the shower occurs when $s=1$ or $t_{max} = \beta_o = \log(E_o/E_c)$. Figure 8.7 shows the variation of the electron number with depth for various energies.

More detailed study of the cascade process has been done by computer simulation of shower development (eg. Grieder, 1977; Gaisser et al, 1978). Here, models of the cascade are utilised such as that due to Greisen (1956). This allows the development to be specified by the variation in the absorption length with electron size. Dixon et al (1974) give this shower attenuation length as,

$$\lambda_A = 47.7 \ln(N_e) + 32.0 \quad gcm^{-2}$$
$$\text{and} \quad \lambda_B = 25.0 \ln(N_e) + 95.0 \quad gcm^{-2} \qquad (8.8)$$

obtained under different approximations, the former taking into account the radiation loss of electrons and the gain in electron number due to pair-production from γ-rays, the latter also includes ionisation loss.

The results of several experiments on shower development are shown in figure 8.8 after Gaisser et al (1978). They were mainly conducted at Chacaltaya ($520 gcm^{-2}$) but include that carried out by Antonov (1974) at aircraft altitude. The data assumes that showers occurring at a given rate originate from primaries of similar energy. If this were true then the curves would correspond to the true average development of showers corresponding to the given integral density. However, because of fluctuations this is not the case and Gaisser and Hillas (1977) have shown that the curves correspond to N_{rms} rather than $\bar{N}$ of showers of fixed primary energy.

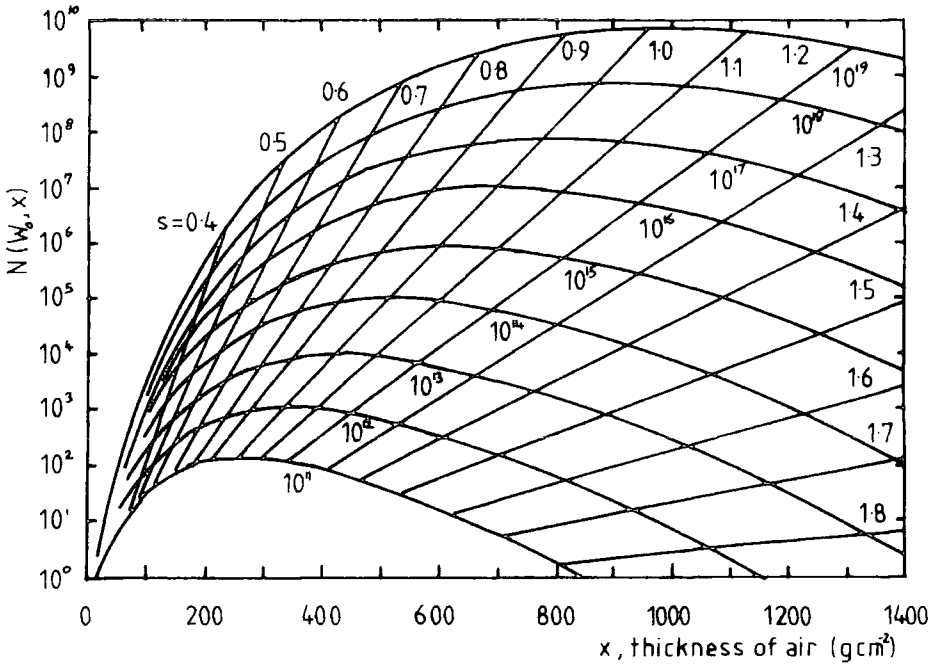

FIGURE 8.7 : The total number of electrons, as a function of the thickness of air crossed, produced by photons of various energies, W_o, in eV. The parameter s is the age parameter at different stages of its development. (after Cocconi, 1961)

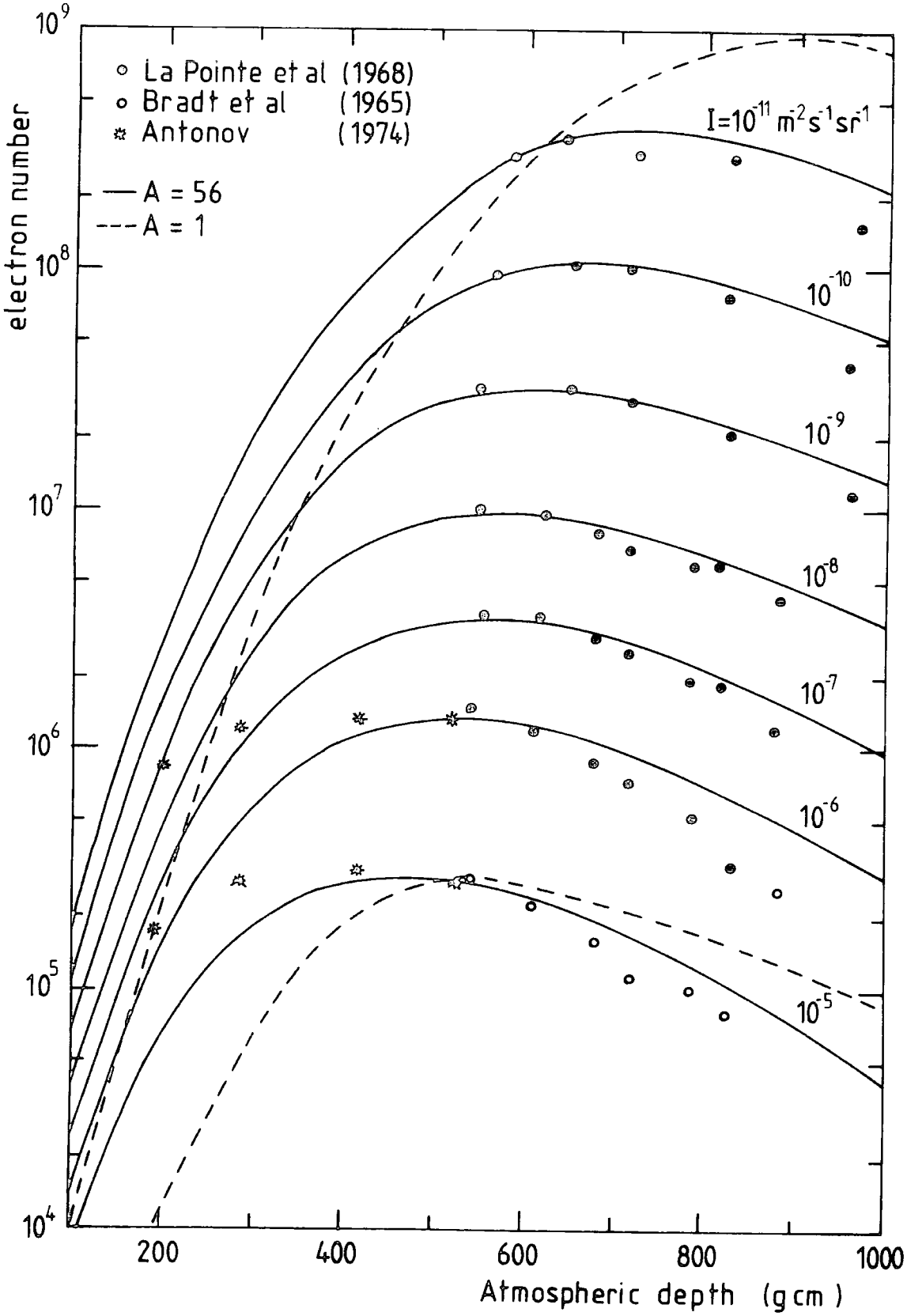

FIGURE 8.8 : Longditudinal development of electron c scades. Lines are computed results of Gaisser et al (1978)

The stage of development of a shower is determined by the age parameter, s. This increases as the shower develops, reaches one at shower maximum and, as the shower dies, s increases past one. The result of the theoretical prediction of the shower age parameter as a function of size, using the standard EAS model of deBeer et al (1966), is given in figure 8.9. The experimental data of Vernov (1970) is also included in the figure. The rise in the age parameter has been ascribed to two phenonema. The first is the flattening of the lateral structure function at large distances from the core, and the second is that large showers have greater mean core distances from the centre of the array. However, it can be concluded that $\bar{s}$ is nearly constant over the shower size range 10^5 to 10^7 at sea-level. This can be understood as a consequence of an equilibrium between the electromagnetic and nuclear-active components due to the continuous regeneration of the former by interactions of the latter which is attenuated in the atmosphere at a constant rate.

8.5 FLUCTUATIONS

As mentioned in the previous section, the air shower parameters are subject to fluctuation, particularly for proton initiated showers. The high fluctuations of the shower age parameter (~10%) indicate a high proportion of protons, but the expected fluctuation for proton initiated showers is only 4-8%, depending on the model. However measurements of fluctuations are complicated by the fact that experimental errors also cause fluctuations and these two are difficult to separate, leading to over-estimation. Catz et al (1973) have described a method for obtaining a lower limit on the width of the fluctuations. It is found that the age parameter is correlated to the muon content

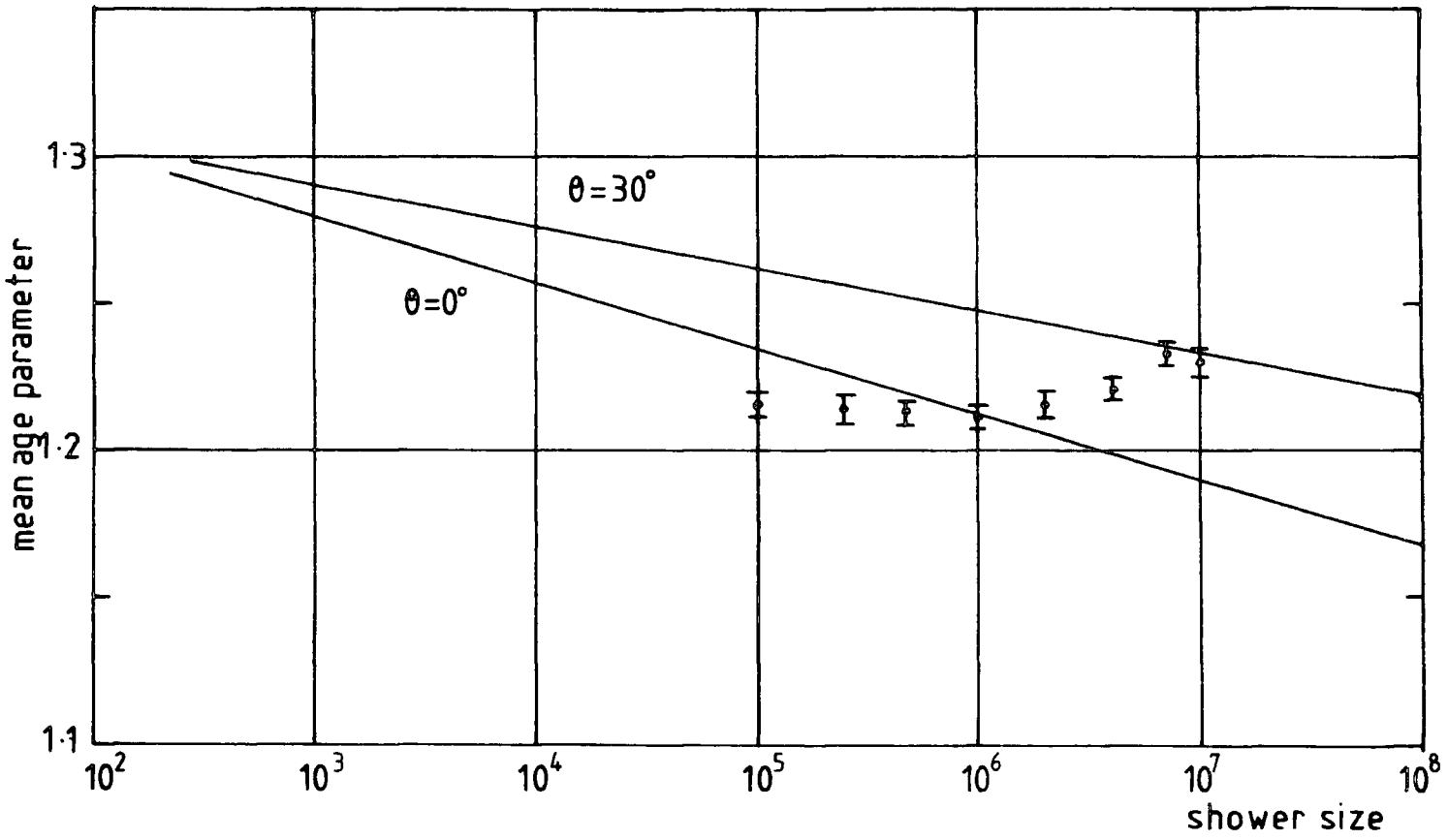

FIGURE 8.9 : The age parameter variation predicted on the basis of the standard EAS model. Data is that of Vernov et al (1970).

of the shower. Using this dependence, the age parameter distribution can be obtained from the N_μ/N_e ratio distribution. The result is a width of 5-6%, thus confirming proton domination at primary energies of around 10^{15}eV.

Fluctuations also occur in the muon component. Investigations of the variation of muon number for fixed shower sizes (eg. Gawin et al, 1968; Vernov et al, 1968), reveals that the width of the fluctuations of the muon number decreases with shower size and agrees with theoretical determinations. Though the agreement indicates the fluctuation model is reasonable, the difference between a proton and a mixed composition model is not large enough to allow the use of the data to determine primary composition. The larger fluctuations of electron to muon ratio indicate that it is the electron number which has the greater fluctuations and the fluctuation in the muon number is relatively small for fixed energy. Elbert et al (1976) used a scaling model to determine the fluctuations and these are plotted in figure 8.10. Though the standard composition deviates greatly from the data, Gaisser et al (1978) conclude, taking into account other evidence, that this indicates a breakdown of scaling.

8.6 THE MUON COMPONENT

The study of muons, especially at higher energies, in EAS is important due to the information they can provide on the early interactions, since their interactions are relatively weak. The lateral distribution allows the determination of the distribution of transverse momenta of their parent pions, while the total number of muons at sea-level is a better indicator of

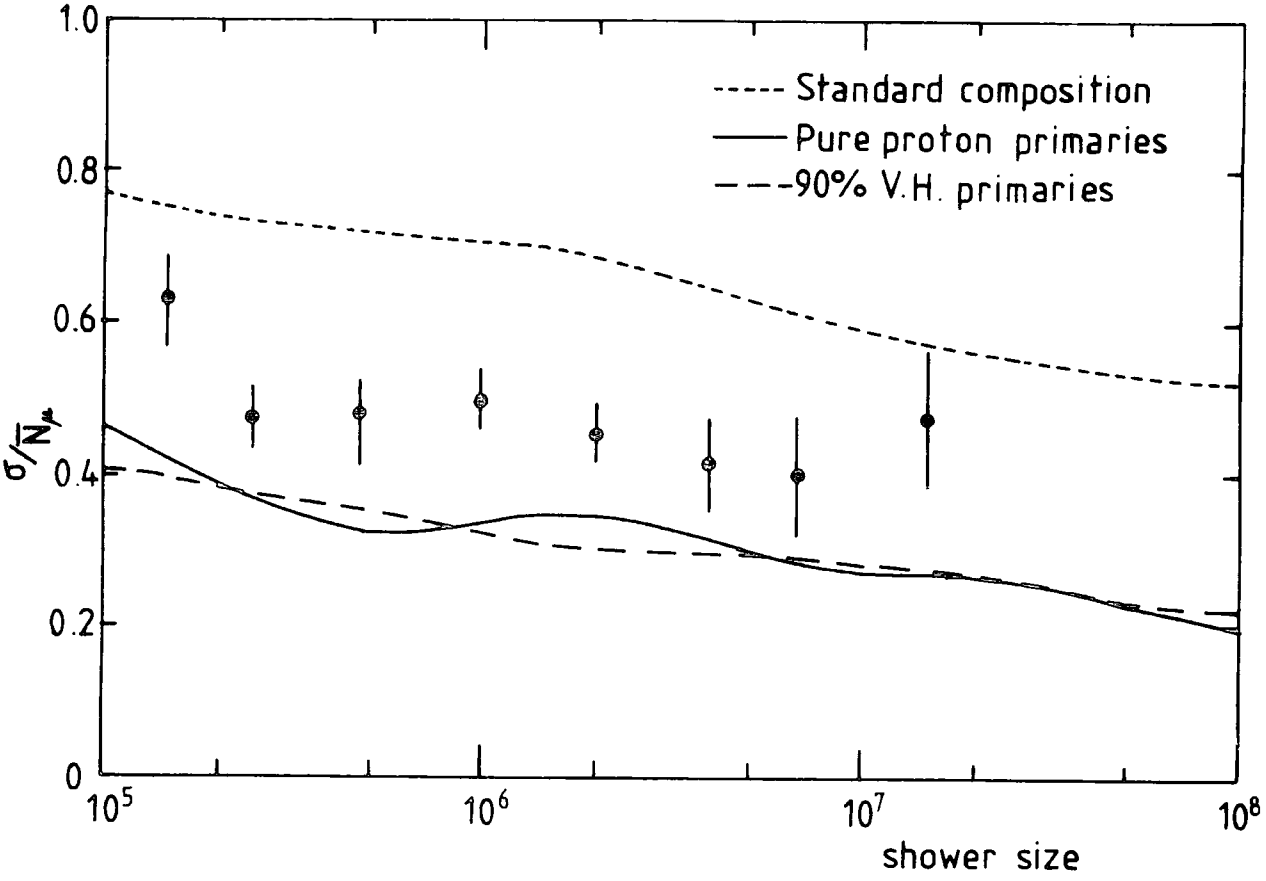

FIGURE 8.10 : Relative standard deviation of N_μ for fixed N_e. Data due to Vernov et al (1970) (after Elbert et al, 1976)

the primary energy than the electron number. However their density is much lower than electrons and this renders them difficult to detect. Detectors require to be well shielded, and have large area. A review of investigations into energetic muons is given by Thompson (1973).

8.7 THE NUCLEAR-ACTIVE COMPONENT

Hadrons in EAS are far less numerous than other particles and their separation from electrons is only possible on the basis of energy difference. However their energy dominates the shower and is responsible for sustaining its development.

The lateral distribution of hadrons, which has been discussed in §8.3.3, can be used to determine the energy spectrum. Modelling has shown that this spectrum can be well described by the standard model when allowance is made for an increase in transverse momentum of about 0.5GeV/c.

8.8 CERENKOV RADIATION

The observation of the Cerenkov radiation emitted by the shower particles as they pass through the atmosphere provides information on the development of a single shower, unlike normal ground-based methods. Work by Chudakov et al (1960) was confined to showers smaller than about 10^{17}eV. More recently attention has been given to larger showers using large arrays of detectors. The detectors are relatively cheap and very large arrays can easily be constructed, thus allowing improved statistics for large showers. Climatic conditions are, of course, a major problem in this type of investigation.

Efimov et al (1973) conducted investigations into the light pulse shape to see if it could be used as an indicator of shower development. Hammond et al (1977) conducted a more extensive study. It is indeed found that the shape is a useful parameter and Gaisser et al (1978) conclude that it is one of the best tests for shower models. A further measurement that is of use is the radius of the shower front which gives an indication of the depth of initiation of the electron cascade.

8.9 CONCLUSION

The basic tools for unravelling the mechanisms of the extensive air shower have been described. Research continues on three basic lines. The first is to improve measurement techniques in order to refine the results and to increase the range of measurement, especially at high energy, to allow better fitting of models. The second is to continue to develop shower models in order to try and fit them to results and hence deduce primary composition and high energy interaction characteristics. Finally, to develop new methods of observation such as atmospheric Cerenkov radiation studies which have been seen to have great potential.

CHAPTER 9

RESULTS

9.1 INTRODUCTION

Shower data from 126.2 hours of running, within the period 6th August 1981 to 2nd September 1981, have been processed, as previously described, to provide estimates for the shower size and core location. This data is held on floppy disc for further processing. Out of 2796 showers which triggered the array, 2101 were able to be processed. Of the unprocessable showers, 39 had too little information due to saturated detectors, 450 lacked sufficient timing information, in the main due to their being large showers, falling at great distances from the array, and 206 failed on core location.

The first part of the analysis of the results consists of checking the distributions of the individual shower data, in order to check on the operation of the array. Following this, the data is used to find the shape of the zenith angle distribution and determine the shower size spectrum.

9.2 DISTRIBUTIONS OF SHOWER DATA

A summary of the triggers is given in table 9.1. As described in chapter 6, simulation was used to proscribe cuts to be put on the data in order to maintain accuracy. The principal cut is on the zenith angle which is restricted to less than 30^{o}. Showers whose cores fall at a distance greater than 50m from detector C are also ignored. There is also a cut on showers whose core location has a high chi-square and thus have suspect accuracy. This cut is chosen to be 10 for reasons described below. The shower size distribution will be described in detail in §9.5.

	Number	Percentage of total
Triggers	2796	100
Axis obtained	2307	83
Core located	2101	75
After cuts	1389	50

TABLE 9.1 : Percentage of analysable showers

	χ^2 minimisation		$\log(I(\bar{\theta}))-\log(\cos(\bar{\theta}))$ plot	
	Restricted data	Extrapolation	Restricted data	Extrapolation
$N>2\ 10^5$	8.6	8.6	8.9±0.9	8.9±0.9
$N>1\ 10^5$	9.3	8.4	9.2±1.6	7.4±1.8
$N>7\ 10^4$	8.7	7.8	8.4±1.6	8.0±1.2
$N>5\ 10^4$	8.2	8.4	7.7±1.2	8.1±0.6
	This experiment	Ashton et al (1975)	This experiment	Ashton et al (1975)
$10^5>N\geq2\ 10^5$	8.6	8.7	9.1±2.0	8.9±1.1
$10^5>N\geq1\ 10^5$	8.3	8.7	8.0±1.0	8.6±1.3
$10^5>N\geq7\ 10^4$	7.8	8.2	7.9±1.4	8.4±1.1
$10^4>N\geq5\ 10^4$	7.2		8.4±2.0	

TABLE 9.2 : Determinations of n in $I(\theta) = I(0)\ \cos^n\theta$

9.2.1 Detector Density Distribution

The similarity of the distributions of recorded densities for each detector (figure 9.1) indicate that the detectors are in good calibration. The calculated saturation densities (C, $100m^{-2}$: 11, $114m^{-2}$: 31, $82m^{-2}$: 51 and 52, $90m^{-2}$) closely correspond to the peaks at the end of the relevant distributions (due to piling up of saturating pulses). For the purposes of processing, densities are cut just below this peak to avoid introducing errors.

9.2.2 Timing Distributions

Distributions of the timing information, for each of the timing detectors are given in figure 9.2. The importance of these distributions is fully described in appendix D. The mean of the distribution is equal to the time a signal takes to travel from the scintillator to the time-to-amplitude converter (ie. cable plus electronic delays) added to the vertical distance the detector is out of the array plane, divided by the velocity of light. For example, detectors 11 and 31 have similar cable lengths, but 11 is about 5m lower which corresponds to about 16ns. The means can be seen to differ by about this value. This figure is used to provide parameters for the program to determine the direction of the axis. The width of the distribution is related to n, the power index of the zenith angle distribution. However the variation of width with n is rather insensitive over the range of n expected so, though this cannot be used to determine n, it does allow a check to be made on the validity of the data. The widths, measured in terms of the standard deviation, assuming the distributions to be Gaussian, are given in the figure and these agree with the calculated n, which is in the region of 8 to 9.

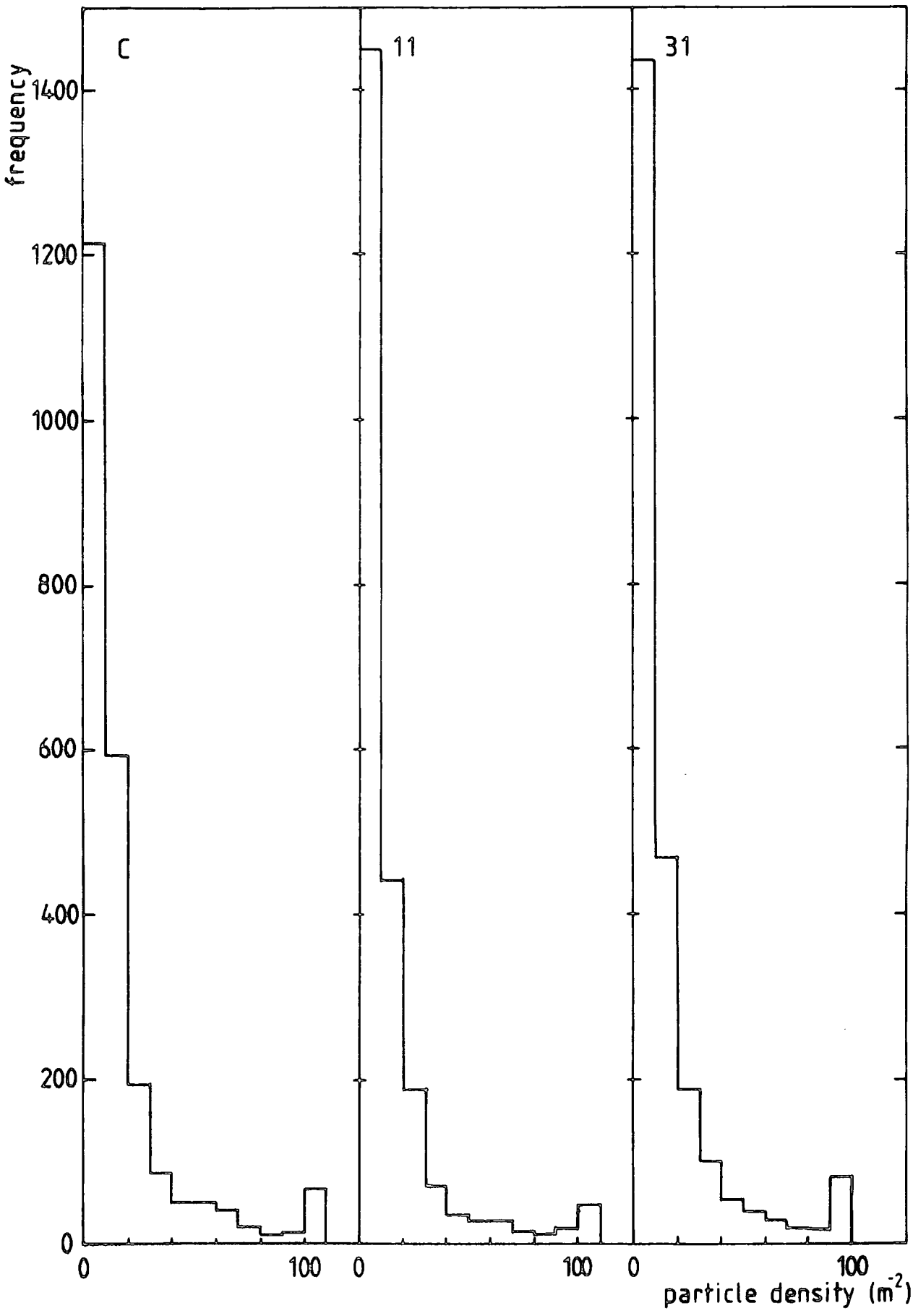

FIGURE 9.1 : Density distributions for the five array detectors.

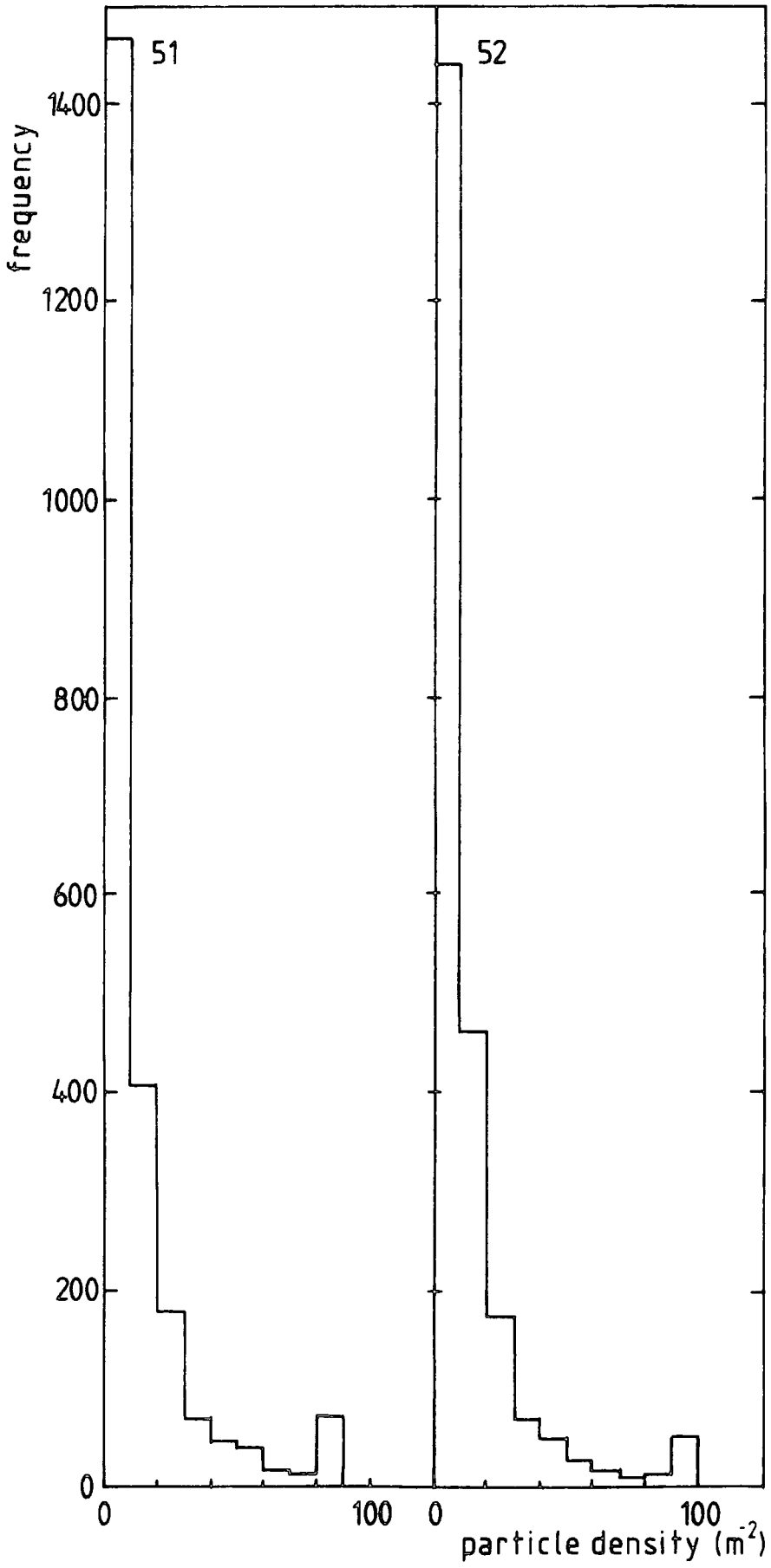

FIGURE 9.1 : continued

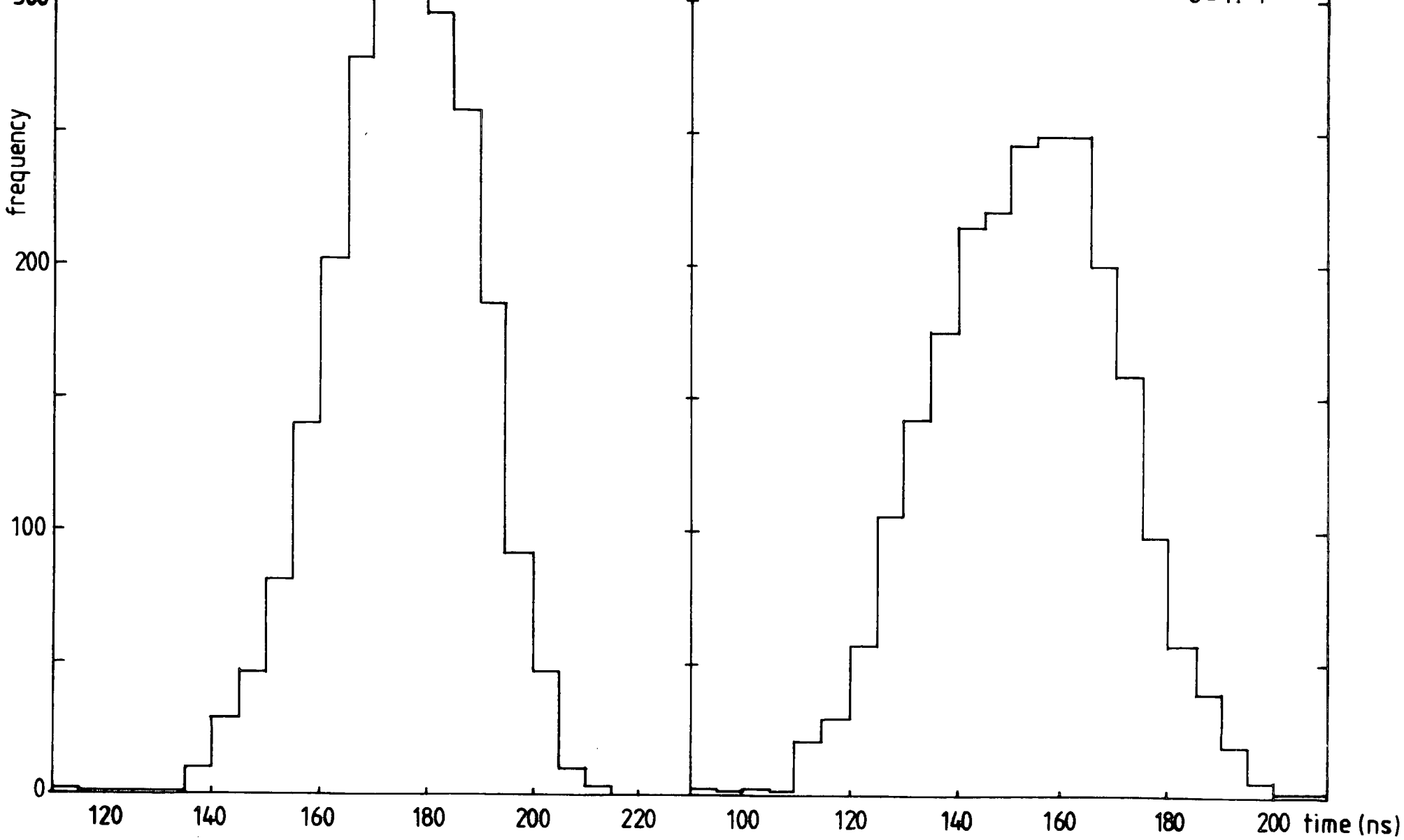

FIGURE 9.2 : Frequency distributions of the time difference between a shower front traversing detector C and each of the timing detectors for 2307 showers.

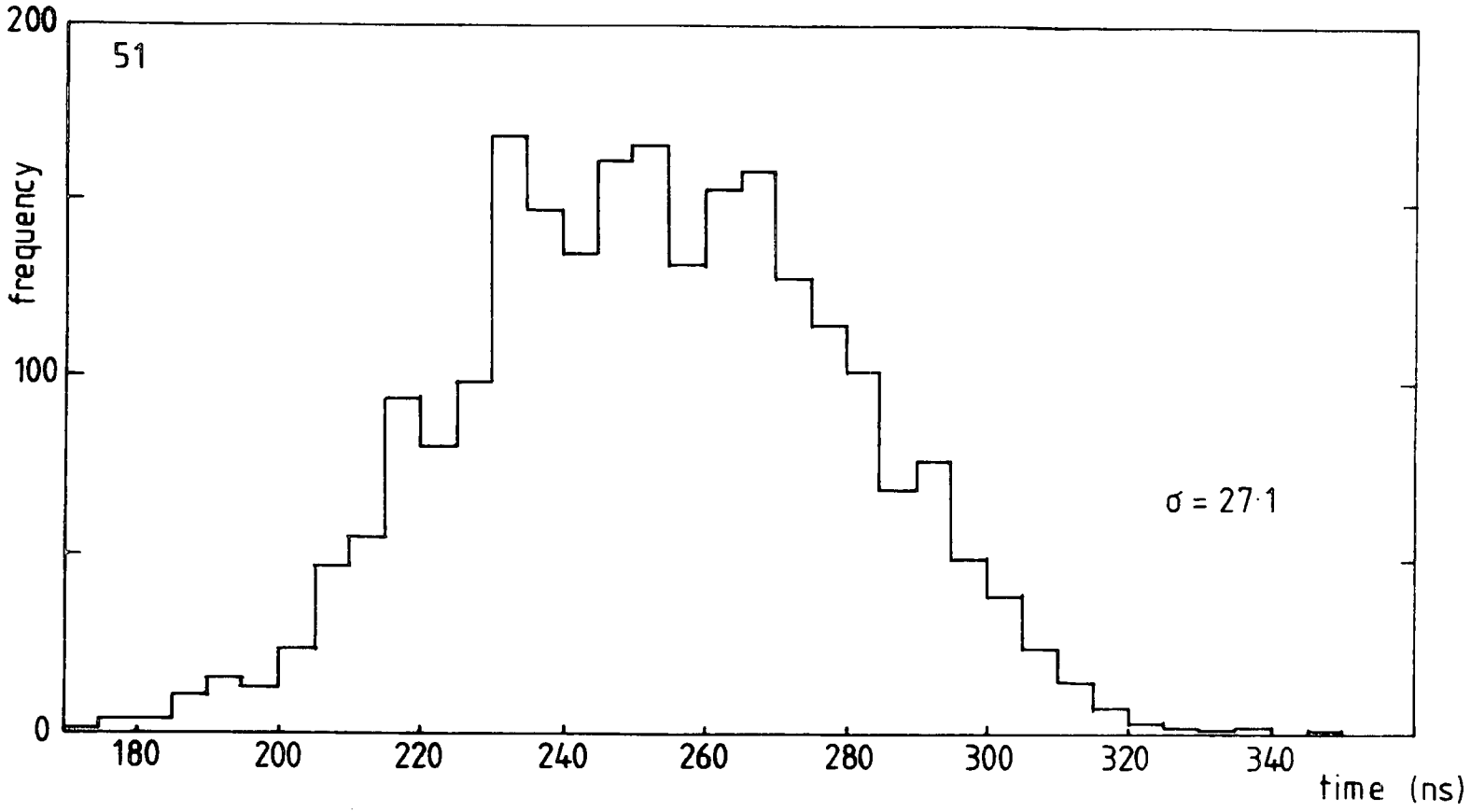

FIGURE 9.2 : continued

9.2.3 Axis Direction Distributions

The zenith angle distribution takes the form

$$I(\theta) = I(0) \cos^n\theta$$

However, for reasons explained in §9.3, the power, n, cannot be determined directly from the distribution shown in figure 9.3. The basic shape of the distribution is in line with that expected, with a peak at around 20°. The normalised, best fit, distribution for n equal to 8.3 is superimposed on the figure.

The azimuthal angle distribution is shown in figure 9.4a. An excess of showers is observed in the directions 90° and 270°. It has been noted that this corresponds to the larger collecting areas for these directions at lower shower sizes. However it can be seen from figures 9.4b to 9.4d that the excess does not vary significantly for different shower size ranges. It is thought more likely to be a result of local absorption since the phase of the distribution coincides with the phase of absorbers, ie. brick walls close to the detectors.

9.2.4 Time Interval between Showers

If showers arrive randomly in time, then an exponential distribution of time intervals is expected. A plot of log(frequency) versus the separation would then be a straight line (Ashton et al, 1977a). It has been, further suggested (Bhat, C.L. et al, 1979) that any structure in this distribution would indicate a non-uniformity of sources. Due to the lack of available data it is not possible to say anything about the fine scale structure, but the fact that the distribution (figure 9.5) is a good fit to an exponential indicates correct operation of the triggering, storage and time recording sections of the data capture system.

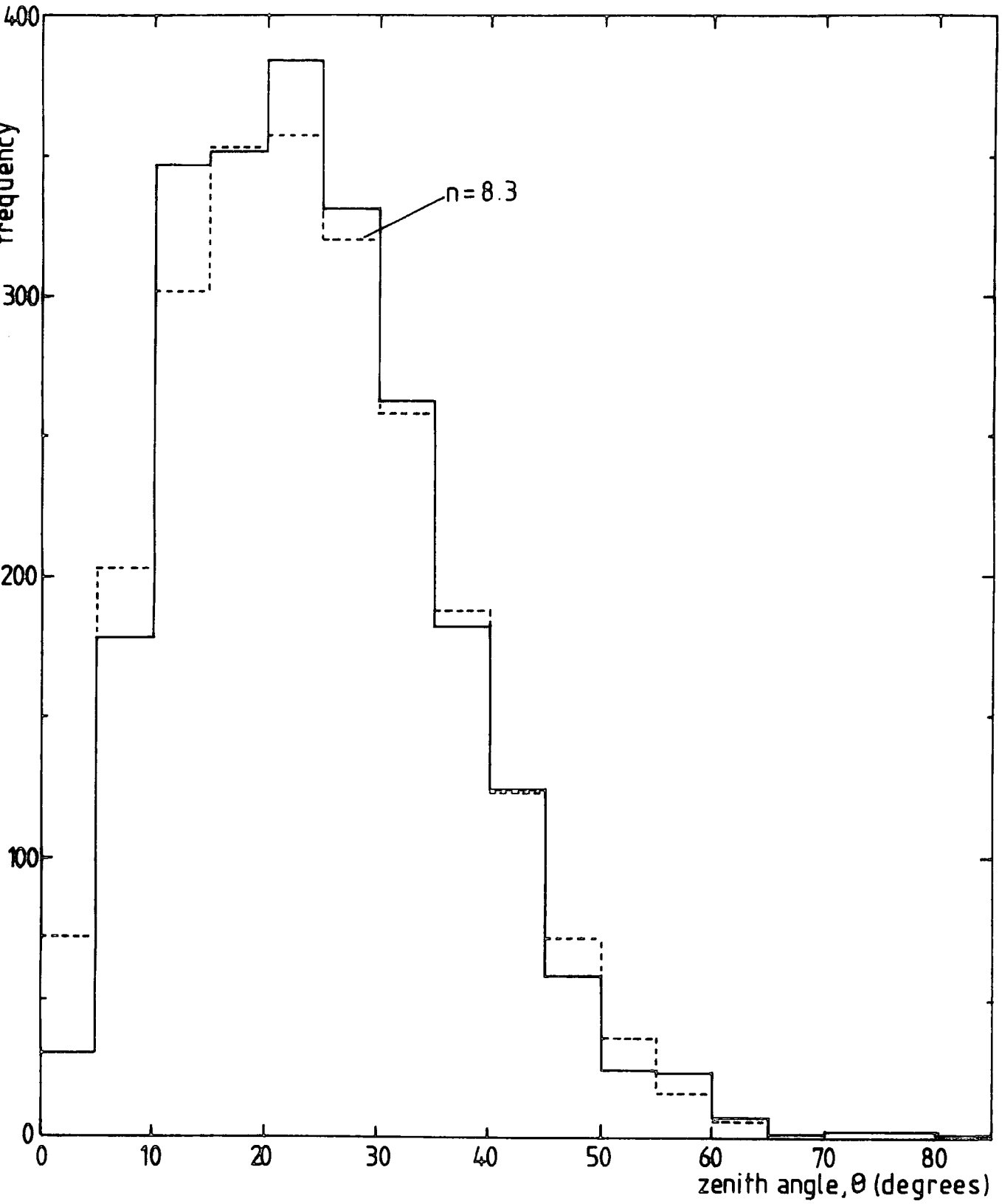

FIGURE 9.3 : Zenith angle distribution for 2307 showers. Dotted distribution shows best fit to $\cos^n\theta$ with n=8.3

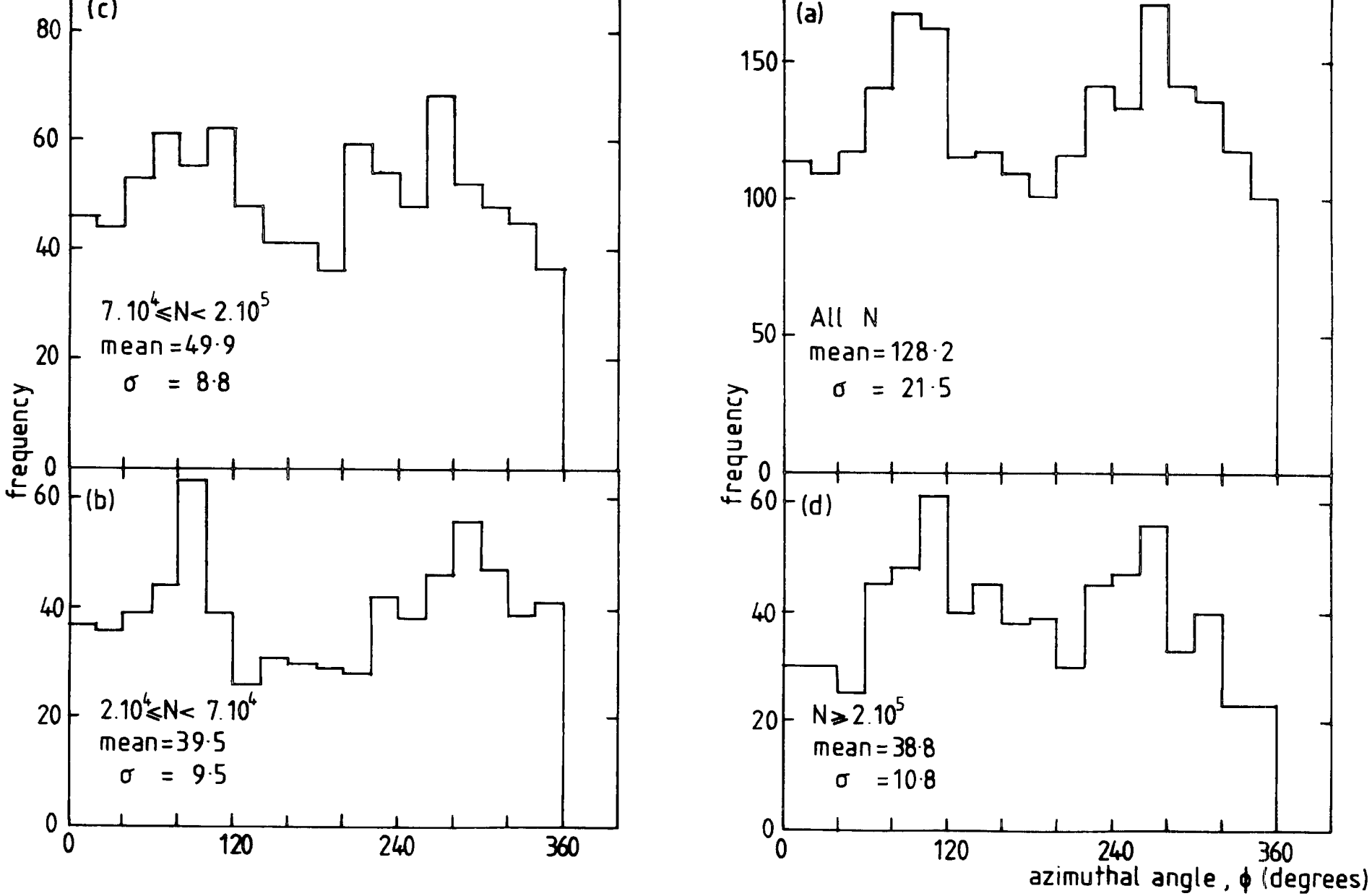

FIGURE 9.4 : Frequency distributions of azimuthal angle for various shower size ranges. 2307 showers.

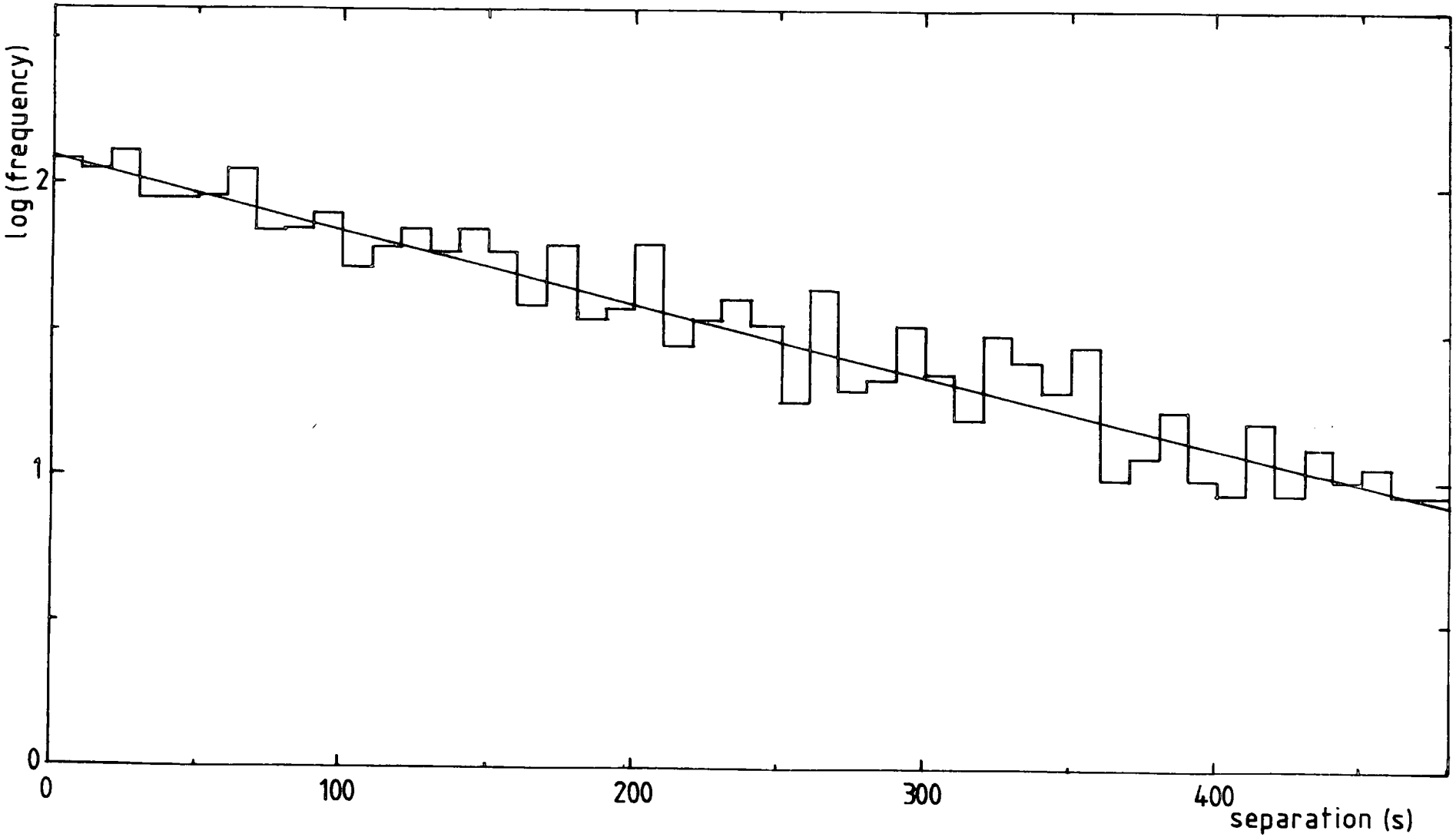

FIGURE 9.5 : Distribution of shower separation in time for 2307 showers.

9.2.5 Core Distributions

Figure 9.6 shows the distribution of shower cores for different shower size ranges. For each range, the array area is divided into squares, of side 10m, with the number of recorded showers in each. Superimposed on each plot is the acceptance area for vertical showers of the maximum size for that range. The close correlation between these two indicates that the core location procedure is working correctly. Although some of the showers falling outside the area can be accounted for by showers with high zenith angle, the majority are probably due to core location error.

9.2.6 Chi-square Distribution

The search routine relies on a chi-square minimising technique in order to locate the core. This allows the use of the final chi-square, obtained when the core has been found, to be used as a measure of the accuracy of location. In order to avoid using the more inaccurate data, a cut is imposed on showers which have large final chi-squares and this has been chosen, arbitrarily, to be equal to the mean plus one standard deviation, ie. equal to 10. This rejects some 5% of the data.

9.2.7 Distribution of Core Distances from Detector C

Figure 9.8 shows frequency histograms of the radius of the core location with respect to the central detector. Each plot is for a different shower size range. As expected, the mean distance of the cores rises as the shower size increases and this is clearly shown in figure 9.9. The variation of core distance with the zenith angle of the axis was also determined and the result shown in figure 9.10. This indicates a weak

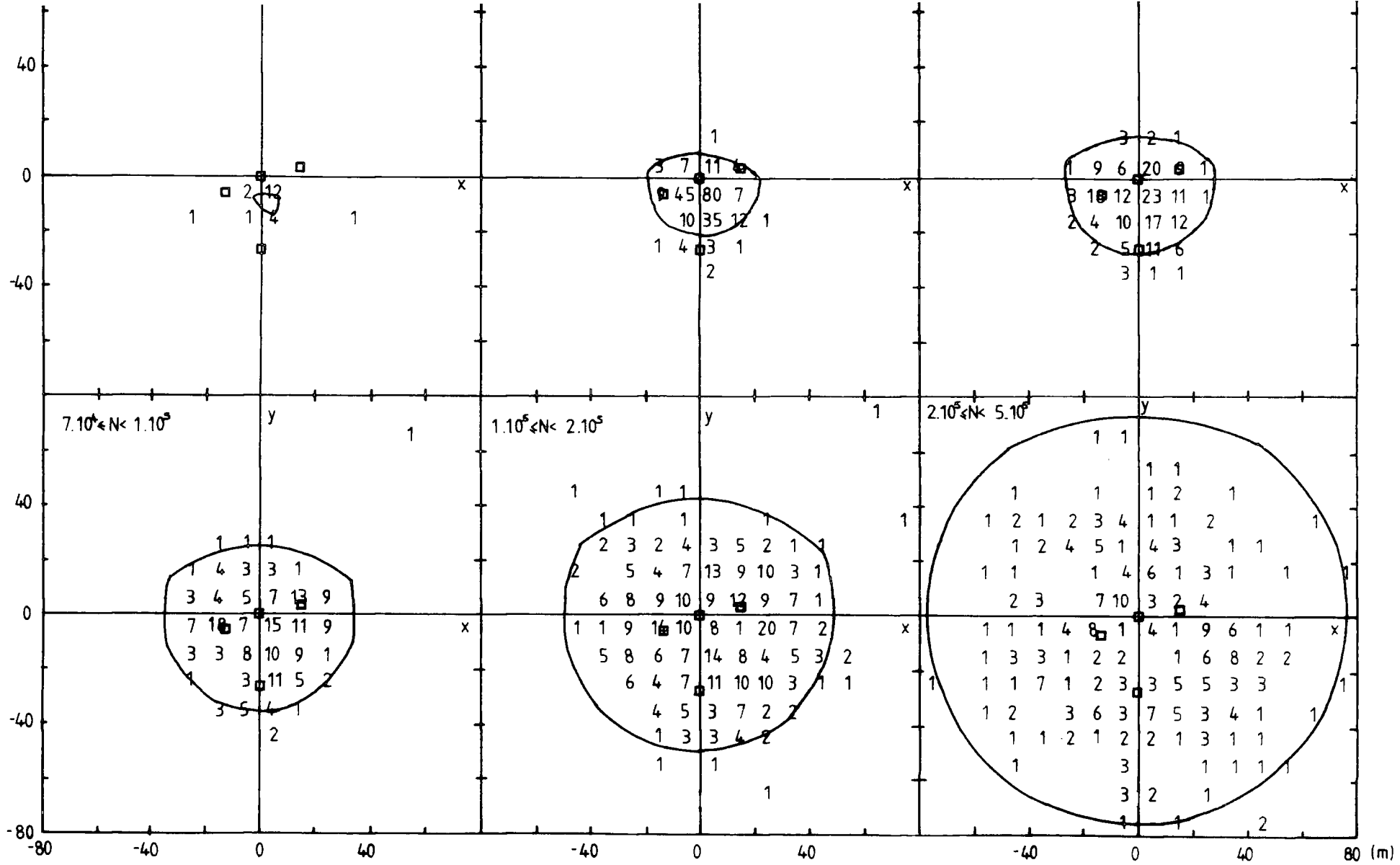

FIGURE 9.6 : Distribution of core positions for showers of $\theta < 30^{\circ}$ and $\chi^2 \leq 10$. Indicated area denotes the collecting area for vertical showers of size equal to the upper limit of the range.

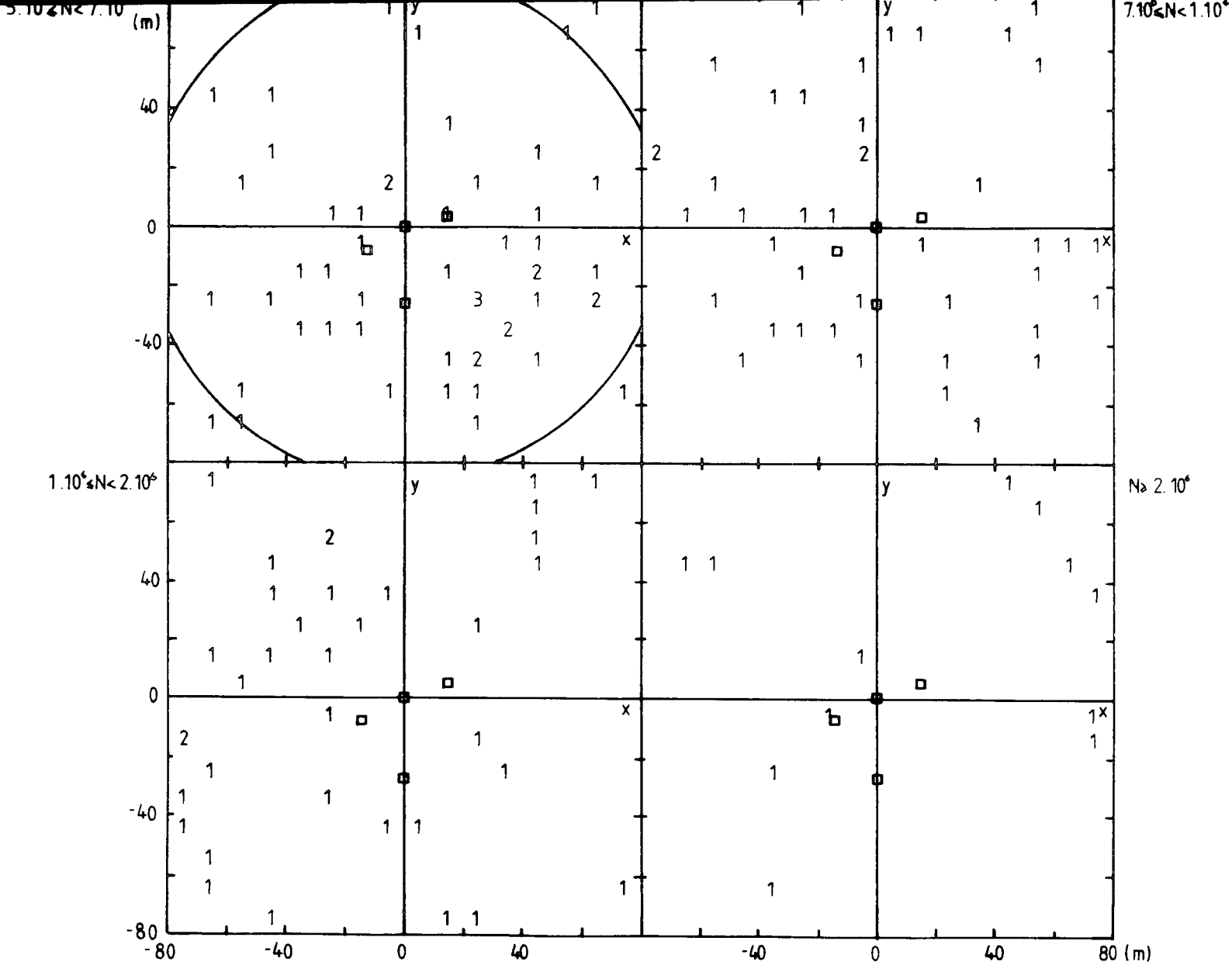

FIGURE 9.6 : continued

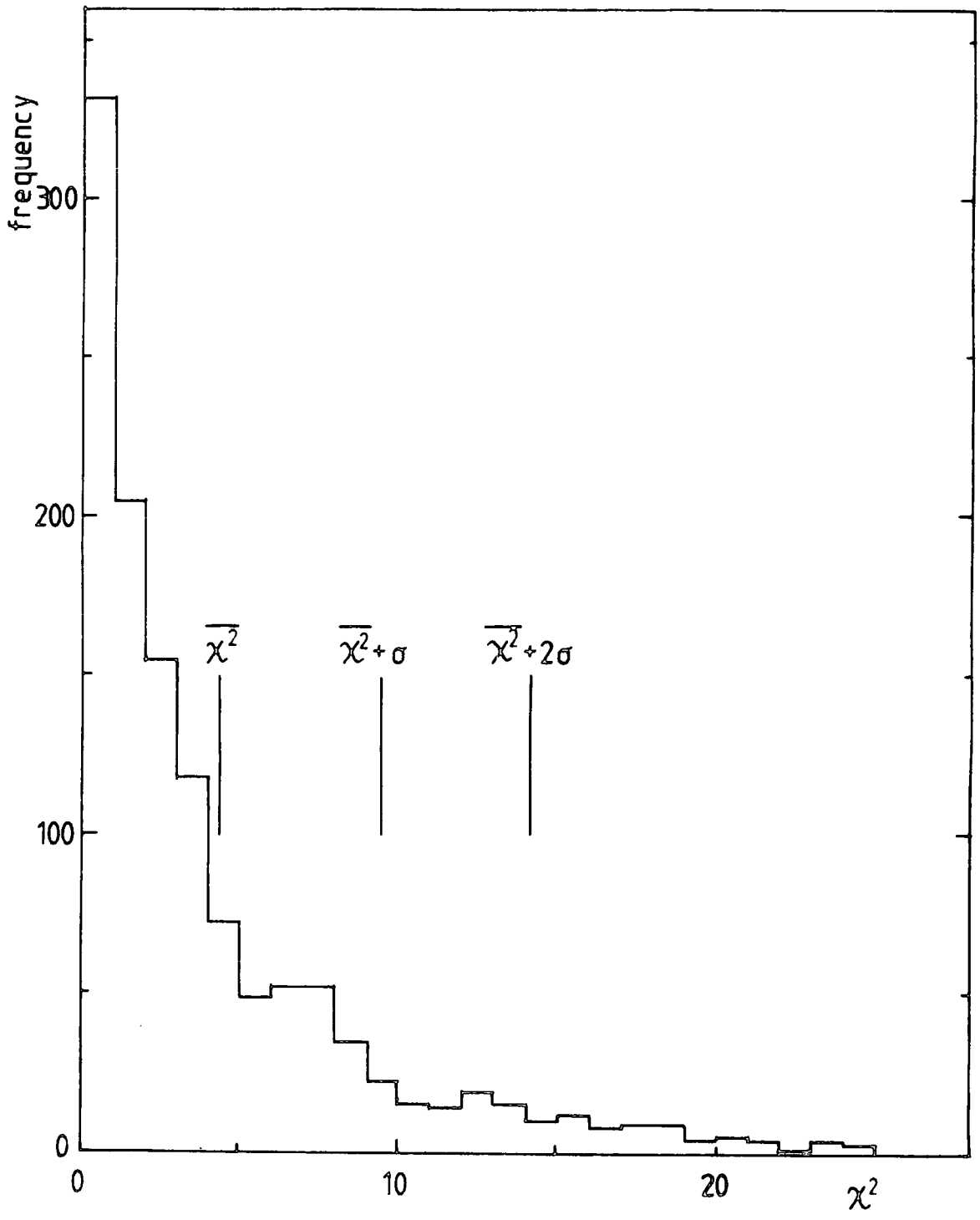

FIGURE 9.7 : Distribution of core location chi-squares for 1220 showers.

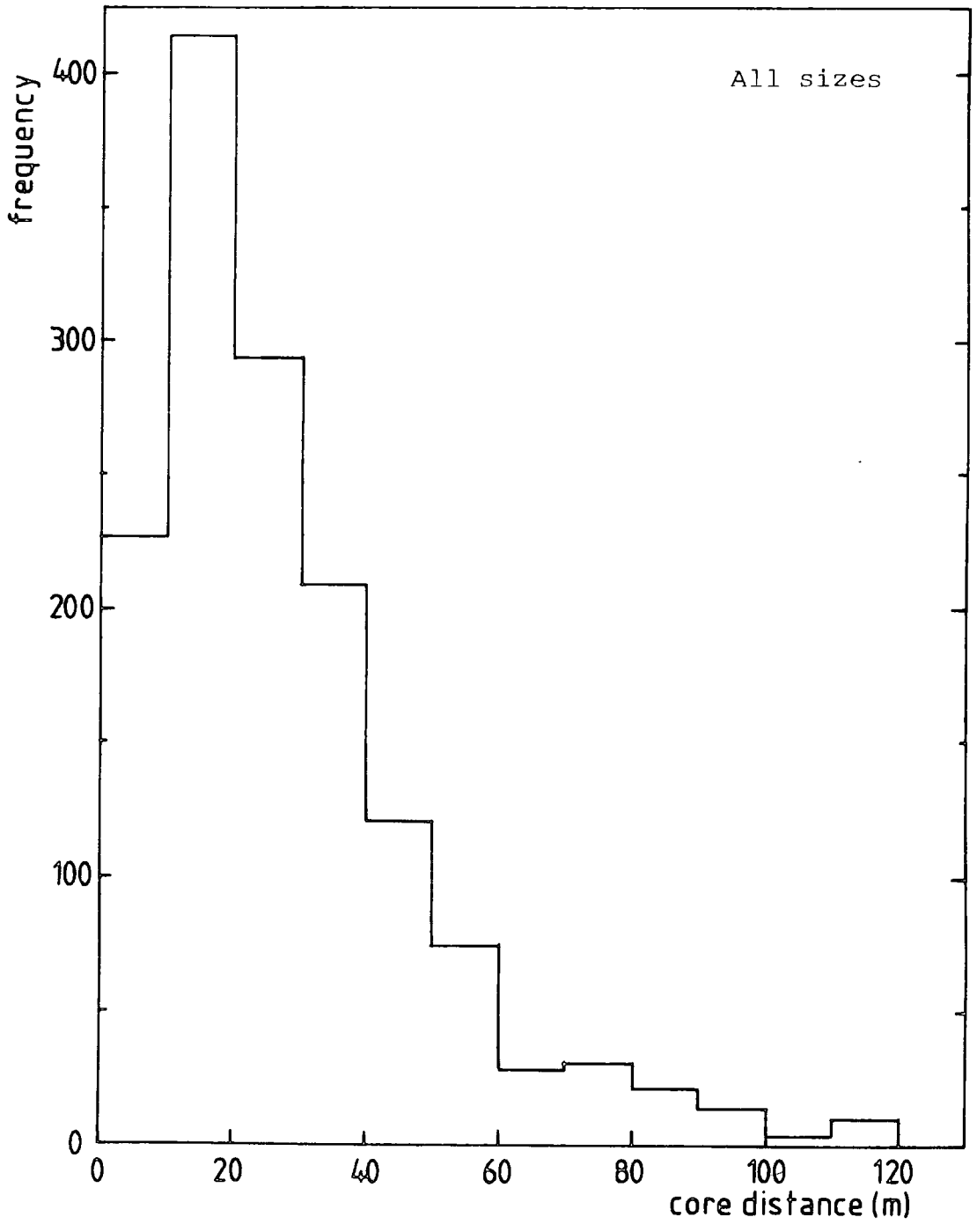

FIGURE 9.8 : Distribution of core distances for showers with $\theta < 30^{\circ}$ and $\chi^2 \leq 10$.

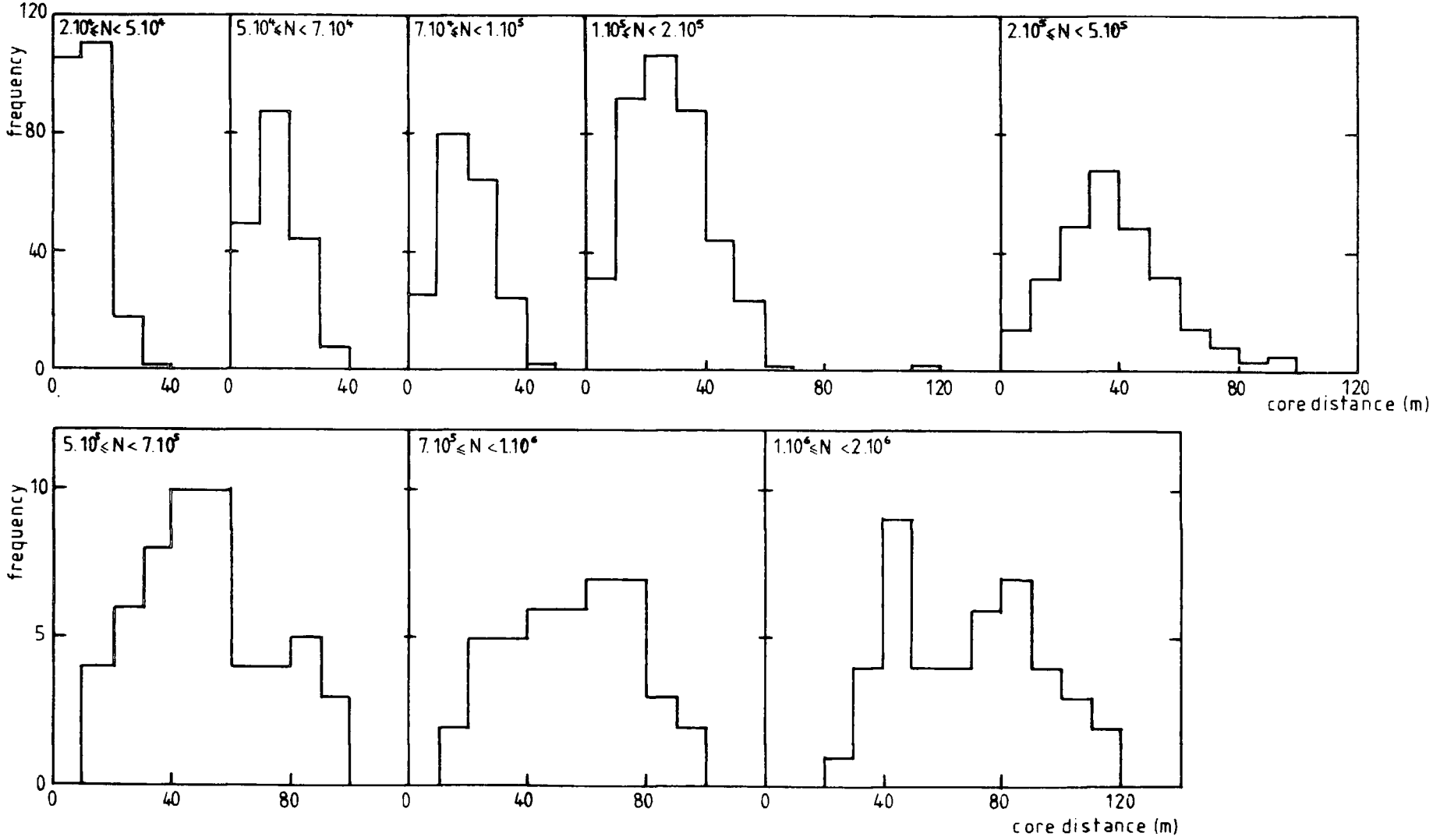

FIGURE 9.8 : continued

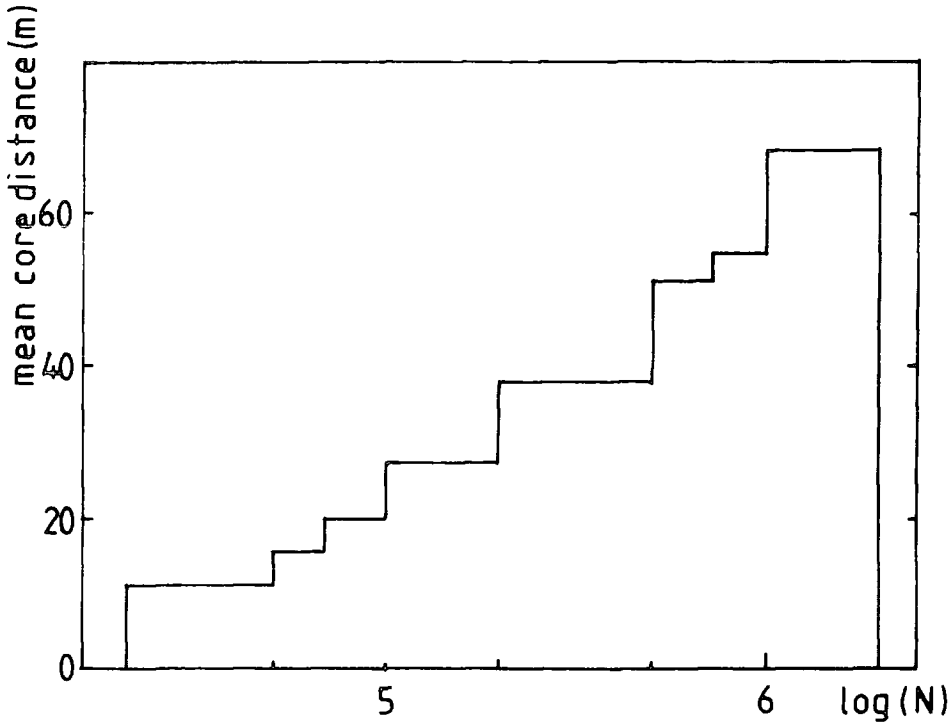

FIGURE 9.9 : Variation of mean, estimated, core distance with shower size, N.

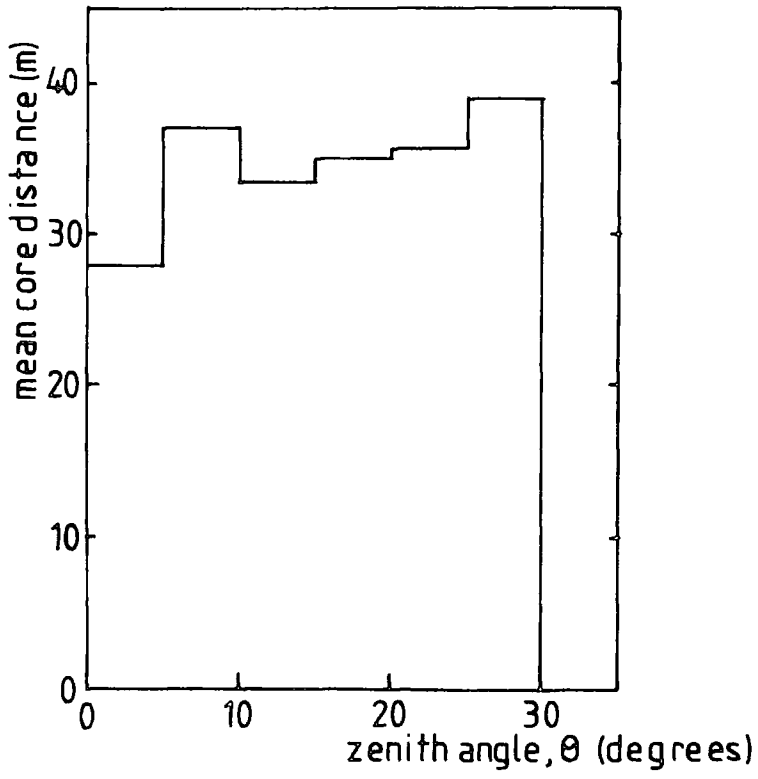

FIGURE 9.10 : Variation of mean, estimated, core distance with zenith angle, θ.

dependence of core distance on zenith angle, the distance rising as the angle increases, this being in line with the small increase in the shower collecting area as the zenith angle increases.

9.2.8 Conclusions on the Basic Shower Data

It is concluded, from the above, that the array, its data collection system and the data processing are performing satisfactorily . However a number of observations can be made about certain of the distributions which relate to possible improvements which can be made to the system. By far the largest cause of showers failing to be processed was lack of timing information. This occurred, mainly, with showers which gave low density readings. As previously mentioned, the thresholds on the timing channels have to be set reasonably high in order to avoid spurious triggering of the time-to-amplitude converters and hence erroneous axis determinations. Though it might be possible to improve matters slightly by more critical adjustment of these thresholds, it is felt the best way would be to add further timing detectors in order to build some redundancy into the timing system as well as improving the statistical accuracy of the axis direction.

9.3 DETERMINATION OF THE POWER OF THE ZENITH ANGLE DISTRIBUTION

The dependence of the shower intensity on zenith angle is given by,

$$I(\theta) = I(0) \cos^{n}\theta \quad m^{-2}s^{-1}sr^{-1} \qquad (9.1)$$

where the area is measured perpendicular to the shower axis. From this we can derive the number of showers, S, with zenith angle between θ and $\theta+d\theta$ falling in an area, one metre square, perpendicular to the shower axis, and in time t, as being;

$$S\ d\theta = 2\pi t\, I(0)\ \cos^{n}(\theta)\ \sin(\theta)\ d\theta \qquad m^{-2} \qquad (9.2)$$

This distribution cannot, however, be directly compared with that obtained from the shower data. This is because the collecting area is required and this is a function of shower size and zenith angle, the latter being particularly large at low shower sizes. The procedure for determining n is as follows.

For a given shower size, N_T, an area, A_{N_T} (perpendicular to the shower axis), can be found such that all showers of size N_T, or greater, that fall in the area will trigger the array. Therefore if we take a zenith angle distribution for showers of size greater than N_T, then it can be compared to,

$$S\ d\theta = 2\pi t\, A_{N_T}\, I(0)\ \cos^{n}(\theta)\ \sin(\theta)\ d\theta \qquad (9.3)$$

on the assumption that the shape of the distribution is independent of the shower size. For example, a cut has been put on the distance of a core, from the central detector, of 50m which is equivalent to a shower size of $2\ 10^5$. So if we count all showers of size greater than this, then a fit, using a chi-square test, can be made to (9.2) in order to obtain a value for n. To use more of the data, a lower shower size is taken and all showers of this size or above, which fall in the relevant collecting area are counted. There are two problems with this. The first is that for showers of size less than $5\ 10^4$ the zenith angle variation becomes significant. An attempt at correction has been made by multiplying the number in a bin by a factor $A_N(0)/A_N(\theta)$ derived from the calculated collecting areas. The second is that for lower shower sizes the area used is also reduced and so the data set is again restricted.

An alternative approach is to normalise all counts to an area equivalent to a radius of 50m by multiplying the data by a factor $A_{2.10^5}/A_{N_T}$. From the results it can be seen that this is reasonable except for small showers of less than about $5\ 10^4$, where the variation in the collecting area with size and zenith angle becomes much more rapid and hence the normalisation factor is much more uncertain.

The results of the analysis are given in table 9.2. For the reasons cited above and the lack of data, it is only possible to estimate n as being in the region 8 to 9. This agrees well with other quoted values, eg. n=8 at sea level (Cocconi, 1958). With the data for different size ranges there appears to be an increase in n with size as has been suggested by Ashton et al (1979). Their results are given in the table and the agreement can be seen to be good. However much more data is required to improve statistics.

Instead of a chi-square test, it is possible to derive a value of n graphically from the same data. From (9.1) it can be seen that a plot of $\log(I(\theta))$ versus $\log(\cos(\theta))$ will be a straight line of slope n. To find $I(\theta)$ from a set of data, suppose that N showers, with zenith angles between θ and $\theta+d\theta$, are observed to cross an area A (perpendicular to the shower axis) in time t. Suppose the θ range is from θ_1 to θ_2 where $d\theta = \theta_2-\theta_1$ and $\theta = (\theta_1+\theta_2)/2$. The intensity of showers is then given by,

$$I(\bar{\theta}) = N/(tA \int_{\theta_1}^{\theta_2} 2\pi \sin(\theta)\ d\theta\ )$$

$$\text{or} \quad I(\bar{\theta}) = N/(tA\ 2\pi\ (\cos(\theta_1)-\cos(\theta_2)) \qquad (9.4)$$

Using this equation and the corrections, mentioned above, values

of n can be determined from the plot of $\log(N/(\cos(\theta_1)-\cos(\theta_2)))$ versus $\log(\bar{\theta})$, an example of which is given in figure 9.11. The agreement with the other method is good.

9.4 DETERMINATION OF THE SIZE SPECTRUM

9.4.1 Previous Determinations

Determination of the size spectrum has been carried out by many workers, and at many altitudes ranging from sea-level to 10000m. Two methods are commonly used. The first is the direct determination of shower size from the air shower data and the second is by measurement of the density spectrum (which is the frequency of showers, $\rho(\Delta)d\Delta$, which give densities within the range Δ to $\Delta+d\Delta$ particles per unit area at a particular point and has the form $H(>\Delta)=k\Delta^{-\beta}$) which can then be converted to the number spectrum using theoretically derived relations.

A review of size spectra is given in figure 9.12, taken from Hillas (1972). This clearly shows the change in slope in the size region 10^5 to 10^6 and the confusion that exists for sizes above 10^8 (see chapter 8). From this it can be seen that two further types of investigation are required, firstly using very large arrays to investigate the spectrum for large showers and secondly small to medium size arrays to investigate the knee region. Table 9.3 gives the slopes of various size spectra determinations, at sea-level, made in recent years.

9.4.2 Determination of the Energy Spectrum

Measurement of the size spectrum at different altitudes can give an insight into the shower development, but the main purpose of determining the size spectrum is to enable the energy

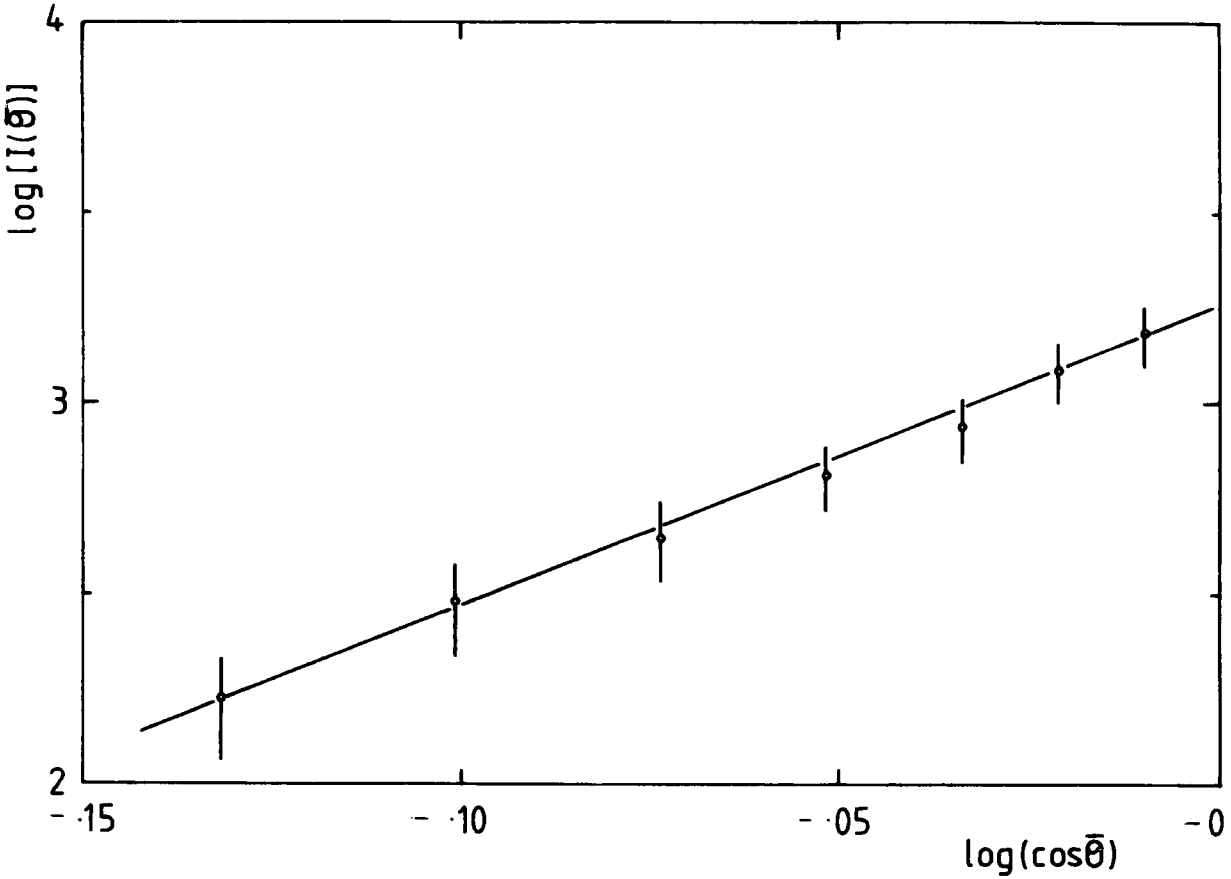

FIGURE 9.11 : Example of an log $I(\bar{\theta})$ - log(cos($\bar{\theta}$)) plot for determining n. Restricted data set with $N > 7\ 10^4$.

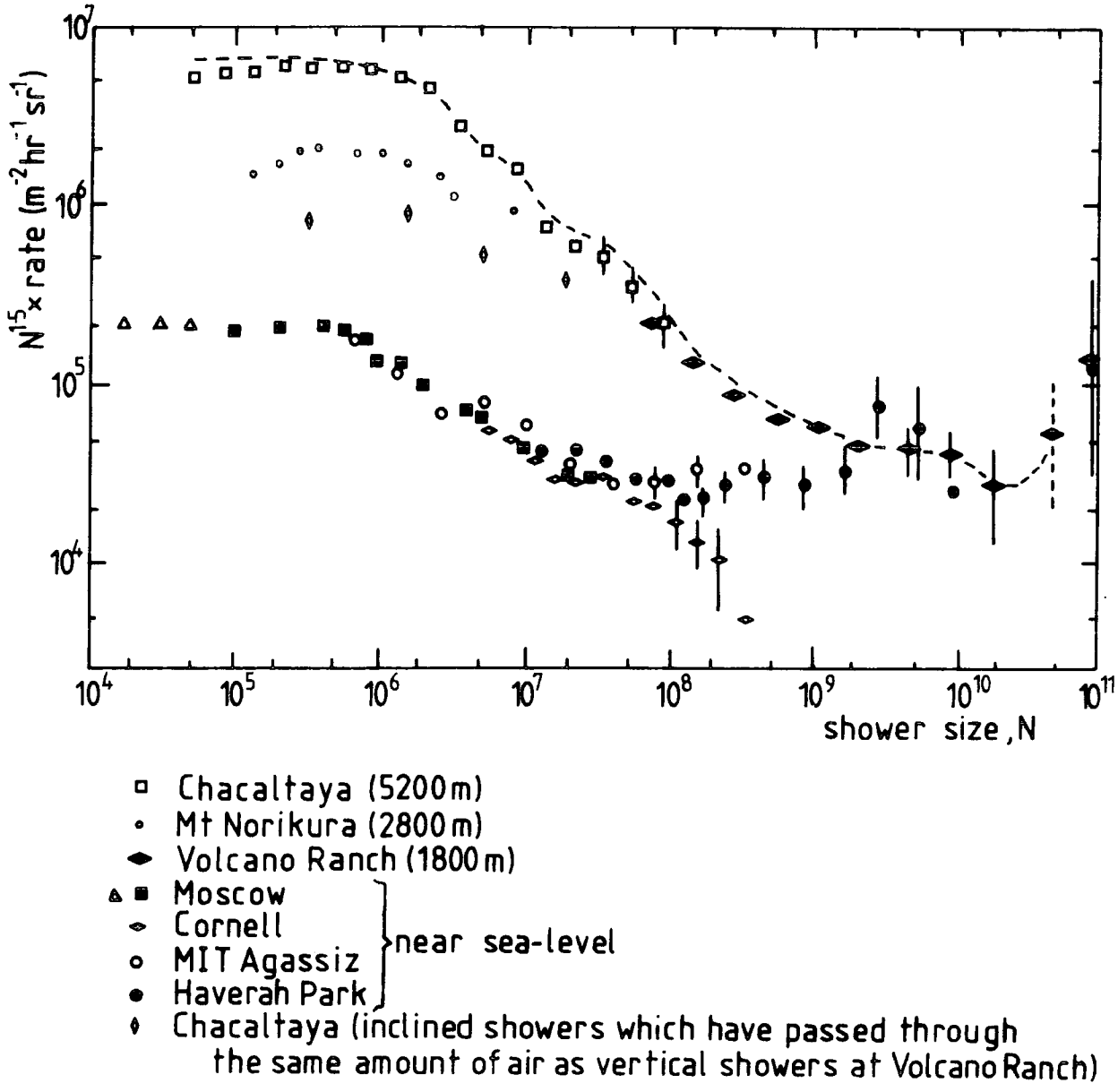

FIGURE 9.12 : Integral shower size spectrum for near vertical showers (after Hillas, 1972).
Dashed line represents the envelope of all such curves.

Reference	Slope	Size range
Hillas (1970)	1.47@	$N \leq 5\ 10^5$
	2.00@	$N > 5\ 10^5$
Ashton & Paveresh (1975)	1.3@	$N \leq 7\ 10^5$
	2.0@	$N > 7\ 10^5$
Catz et al (1975)	1.59±0.02	$5\ 10^4 < N \leq 10^6$
	2.19±0.02	$10^6 < N \leq 10^7$
Asakimori et al (1981)	1.85±0.06	$10^5 < N \leq 10^6$
	1.4@	$5\ 10^4 < N \leq 10^5$
Hara et al (1981)	1.55±0.1	$10^5 < N \leq 1.73\ 10^6$
	1.90±0.1	$1.73\ 10^6 < N \leq 10^8$
Crouch et al (1981) (differential)	2.01@	$N \leq 5\ 10^5$
	3.00±0.06	$5\ 10^5 < N < 10^7$
Clay & Gerhardy (1982) (differential)	2.90±0.05	$5\ 10^5 < N < 10^7$

@ slopes estimated

TABLE 9.3 : Recent sea-level determinations of the size spectrum slope. (The spectra are integral unless stated otherwise).

spectrum to be determined. Direct measurements of the energy have been made by balloon borne detectors, covering energies upto 10^{12}eV, and extended to 10^{15}eV by the satellite observations of Grigorov et al (1970). Above this energy, the low flux means that the energy spectrum has to be indirectly determined from air showers, either using the electron or muon number spectra.

The relationship between the electron number of a shower and the primary energy has been investigated by many workers, using calculation or simulation techniques. Reasonable agreement has been obtained between the different calculations, differences being due to the choice of interaction model. Figure 9.13 shows the results of the simulation of Dixon et al (1974) which uses a $n_s \propto E^{\frac{1}{4}}$ multiplicity law and the calculations of Kempa (1976) where multiplicity laws $n_s \propto E^{\frac{1}{4}}$ and $n_s \propto E^{\frac{1}{2}}$ are investigated. From these, a mean conversion function has been determined as,

$$E_p = 1.74\ 10^7\ N^{0.92}\ \text{eV} \qquad N \geq 10^5 \qquad (9.5)$$

9.5 PRESENT DETERMINATION OF THE SIZE SPECTRUM

9.5.1 Introduction

The cuts on the data are important when determining the size spectrum, since the absolute rate of showers has to be calculated, and thus certain corrections are required. A further restriction is as follows. The triggering probability, as a function of electron shower size has been given in figure 6.15. From this it has been decided to restrict the shower size range to that for which the triggering probability is greater than or equal to 90%. Due to the rapid fall-off of probability below this value, corrections will become increasingly inaccurate, thus the

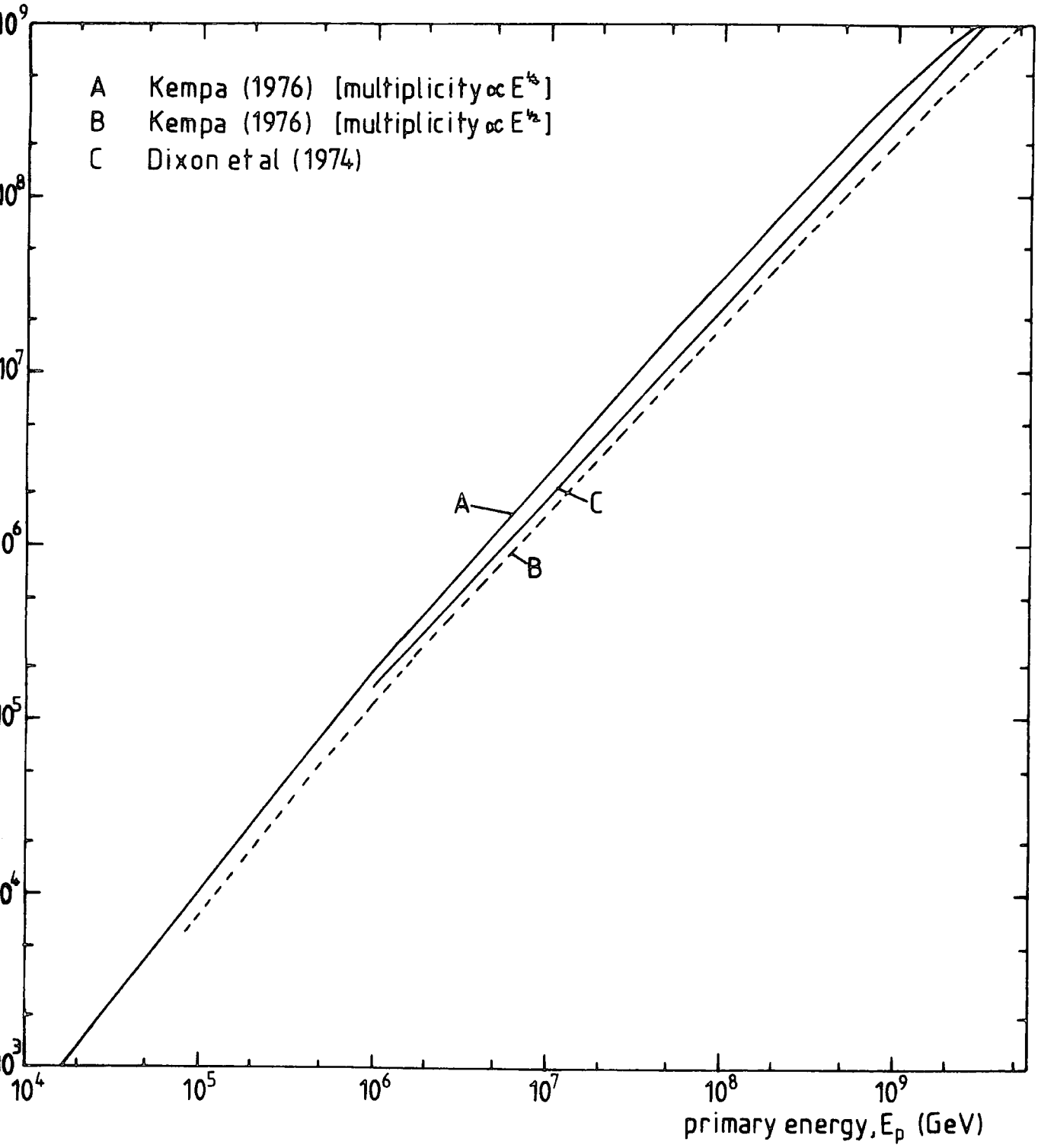

FIGURE 9.13 : The variation of shower size with primary energy calculated for sea-level.

cut-off has been chosen by trading off between maintaining a useful size range and accuracy of the result. This restriction on range is $3\ 10^5$ to $7.5\ 10^5$.

9.5.2 Calculation of the Size Spectrum

Table 9.4 contains the basic data used to determine the size spectrum. The data was initially binned by log(N)/50. Each number indicates the number of showers falling within the relevant collecting area, in the sensitive time, with zenith angle less than 30^o, having a search chi-square of less than 10 and a shower size within the bin range. To convert these to produce the differential spectrum requires the following corrections to be made.

(i) Time: The total sensitive time, t, was 454200s.

(ii) Collecting area, A_N: This could be determined from the plots of collecting area as a function of size given in appendix B. For shower sizes greater than $2\ 10^5$, the radius of this area exceeds 50m and therefore, since a cut is made at this distance, the area is taken as $7854m^2$ for these showers. In practice the triggering probability, P_N, (given in figure 6.15) is used as this accounts for fluctuations and axis direction as well as collecting area. However for small shower size, ie. below 10^5, P_N becomes less accurate and the collecting area correction is used, the area being taken as that for a zenith angle of 20^o.

(iii) Solid angle: The rate per steradian is required whereas the data is for a solid cone of angle 60^o. To correct for this, we first take intensity as a function of zenith angle.

$$I(\theta) = I(0)\ \cos^n(\theta) \quad m^{-2}s^{-1}sr^{-1}$$

log(shower size)	0.00	0.02	0.04	0.06	0.08	0.10
4.2	2	3	6	2	1	
4.3	3	3	11	9	5	
4.4	6	10	7	18	11	
4.5	15	11	12	14	16	
4.6	17	15	17	15	24	
4.7	13	16	25	25	23	
4.8	39	26	22	23	24	
4.9	25	32	33	24	25	
5.0	23	13	35	33	17	
5.1	30	14	37	32	11	
5.2	34	30	22	24	16	
5.3	16	22	21	19	22	
5.4	11	9	11	13	9	
5.5	6	7	6	5	5	
5.6	12	7	6	7	5	
5.7	0	6	5	2	5	
5.8	5	2	3	2	1	
5.9	2	2	3	2	2	
> 6.0	16					

TABLE 9.4 : Basic data for shower size spectrum determination $\theta < 30^{\circ}$, $R \leq 50$m, $\chi^2 < 10$.

The intensity of showers with zenith angle between θ and $\theta+d\theta$ is given by,

$$I(\theta)\ 2\pi \sin(\theta)\ d\theta \quad m^{-2}s^{-1}sr^{-1}\theta^{-1} \tag{9.6}$$

In this case only zenith angles up to 30° are considered, so that the intensity is given by,

$$I(\theta\rightarrow\theta+d\theta, \theta\leq 30) = I(0)\int_{0}^{30^{\circ}} 2\pi \cos^{n}(\theta) \sin(\theta)\ d\theta \quad m^{-2}s^{-1} \tag{9.7}$$

and taking n as 8 gives,

$$I(\theta\rightarrow\theta+d\theta, \theta\leq 30) = 0.51\ I(0) \quad m^{-2}s^{-1} \tag{9.8}$$

So we require to multiply the rate ($m^{-2}s^{-1}$) by 1.97.

(iv) Others: 5% of data is rejected due to high chi-square. This is assumed to be size independent and the rate is therefore multiplied by 1.05 to correct for this. The other main loss is due to showers whose axes cannot be determined due to lack of timing information. Although these number about 10%, this is not size independent since they are more likely to be large showers falling at great distances from the centre. Therefore this error is not taken into account.

Figures 9.14 and 9.15 show the calculated differential and integral rates of EAS at sea-level. Comparisons are made with the measurements of Paveresh (1975), Crouch et al (1980), Abdullah (1982) and the summary of Hillas (1970). The resulting slopes are as follows:

Differential spectrum	2.33±0.15	$2\ 10^{5} > N$
	2.99±0.20	$2\ 10^{5} \leq N$
Integral spectrum	1.44±0.06	$2\ 10^{5} > N$
	1.91±0.14	$2\ 10^{5} \leq N$

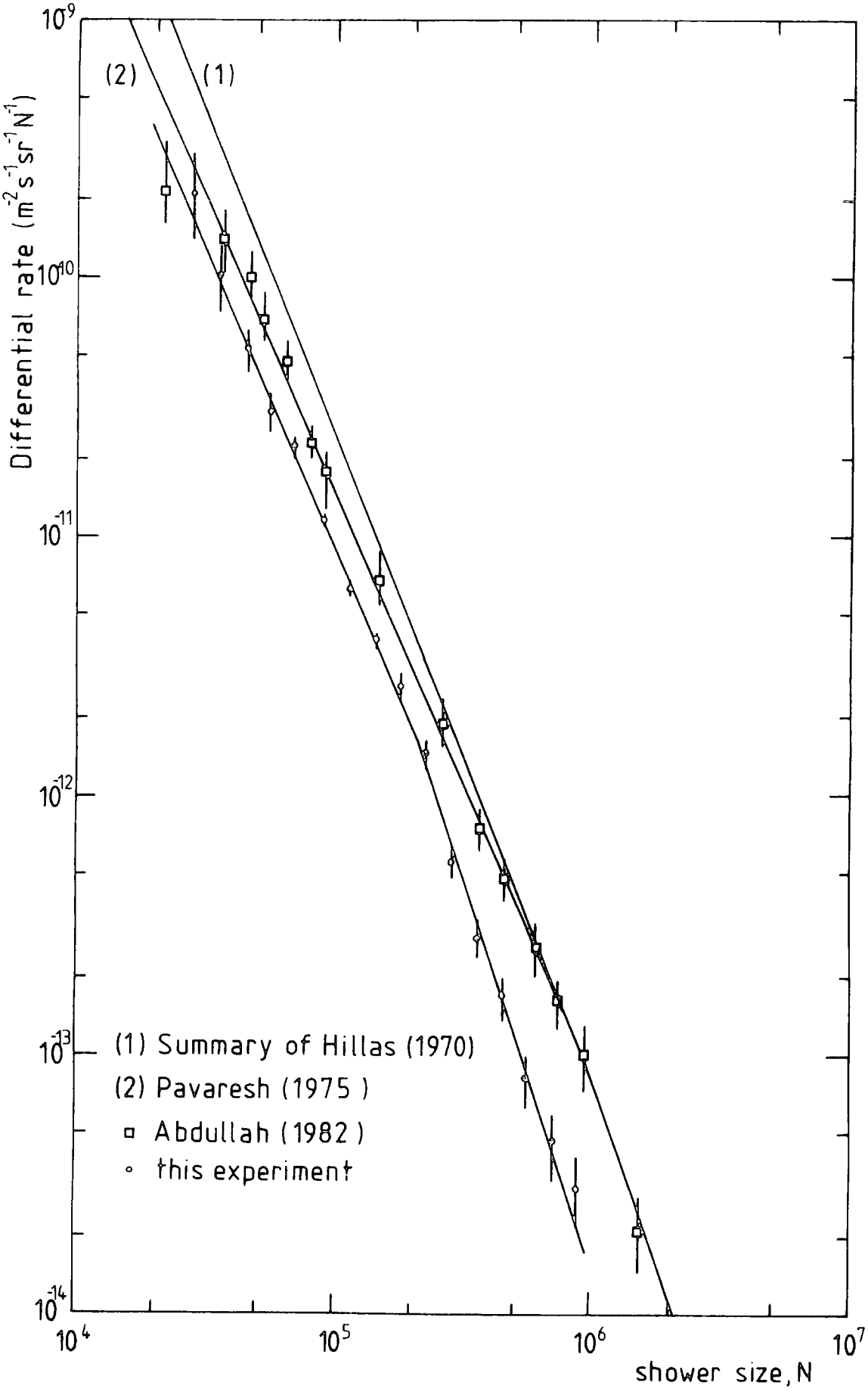

FIGURE 9.14 : The vertical differential size spectrum of EAS at sea-level.

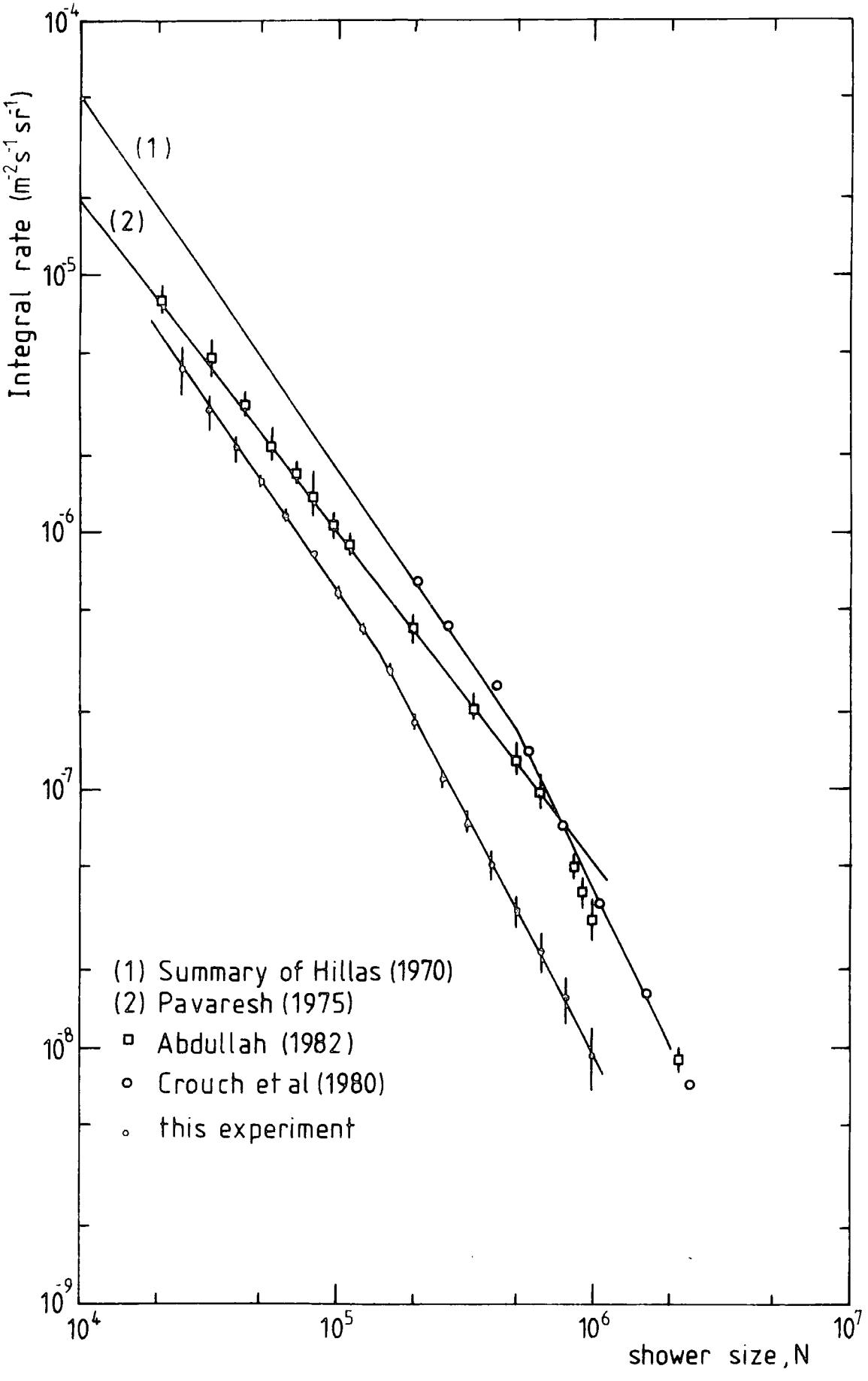

FIGURE 9.15 : The vertical integral size spectrum of EAS at sea-level.

These can be compared to the figures given in table 9.3. Though the slopes are in reasonably good agreement with previous measurements, the absolute rate is much lower. In the region of greatest sensitivity, ie. 3 10^5 to 7.5 10^5, it is down by a factor of three. This could, in part, be explained by showers with insufficient data for processing, as mentioned previously. Another explanation is inaccuracy in the shower size determination. Two factors influence this. These are the lateral structure function and the bias introduced by the core location procedure. This latter introduces the largest error and from figure 6.16 it can be seen that the correction required is uncertain. However the evidence from the data distributions, especially that of the core location, seem to indicate that the size is determined reasonably well.

9.6 CONCLUSIONS

These results indicate a number of modifications and investigations that need to be undertaken in order to improve the performance of the air shower array. In order to extend the useful shower size range, the effects of increasing the dynamic range of the density data electronics and changing trigger levels, on the probability of triggering need to be investigated. By doing this the shower size range of interest can be selected and optimised. Extra detectors will also help in this matter. The methods described in the chapter on data processing can be used for this work. The other problem is to minimise data losses, ie. to avoid many showers being lost due to their not being able to be processed. Many of these were due to lack of timing data due to signals from the timing detectors being below the threshold

set to eliminate noise and hence spurious timing data. The triggering could be raised but this would raise the minimum shower size detectable and reduce the shower rate. A more satisfactory solution would be to increase the number of detectors in the array and so build in an element of redundancy. The system described allows this to be done fairly easily.

Note added in proof

Two errors have been found in the calculation of the calibration coefficients for the detector density channels. These are as follows:

(a) The mode to mean ratios, R, have been found to be in error. New ratios have been calculated from the pulse height calibration curves and, on average, found to be 70% of those used previously.

(b) The ratio of the vertical flux to the global flux has been omitted. The average value for this has been determined as 0.8, for all detectors, by M. Treasure (private communication).

These two errors mean that the densities have been under-estimated by approximately 44%.

This has several effects,

(i) All densities should be increased by a factor of 1.8.

(ii) This has no effect on core locations but all shower sizes are increased by a factor of 1.8.

(iii) The trigger levels are increased by a factor of 1.8.

(iv) The shape of the number spectrum is altered.

The differential and integral number spectra have been recalculated and are shown in figures 9.14a and 9.15a. Two sets are shown. One includes the size correction due to the minimisation technique (§6.4.4) and the other is uncorrected for this.

It is seen that in the region of high confidence ($3\ 10^5$ to $7.5\ 10^5$) agreement of the former with the previous determination of Pavaresh (1975) is good. Above this region the simulation correction for N is uncertain. Below this region the uncertainties

in correcting for collecting area become large, as the area falls rapidly with shower size, and the asymmetry of the array also introduces error. However it appears that the corrections, determined from the simulation and collecting area analysis, also hold good for the size range 8 10^4 to 3 10^5.

Values of γ are:

Differential	2.47±0.06	1 $10^5 \leq N \leq 8$ 10^5
Integral	1.47±0.08	1 $10^5 \leq N \leq 8$ 10^5

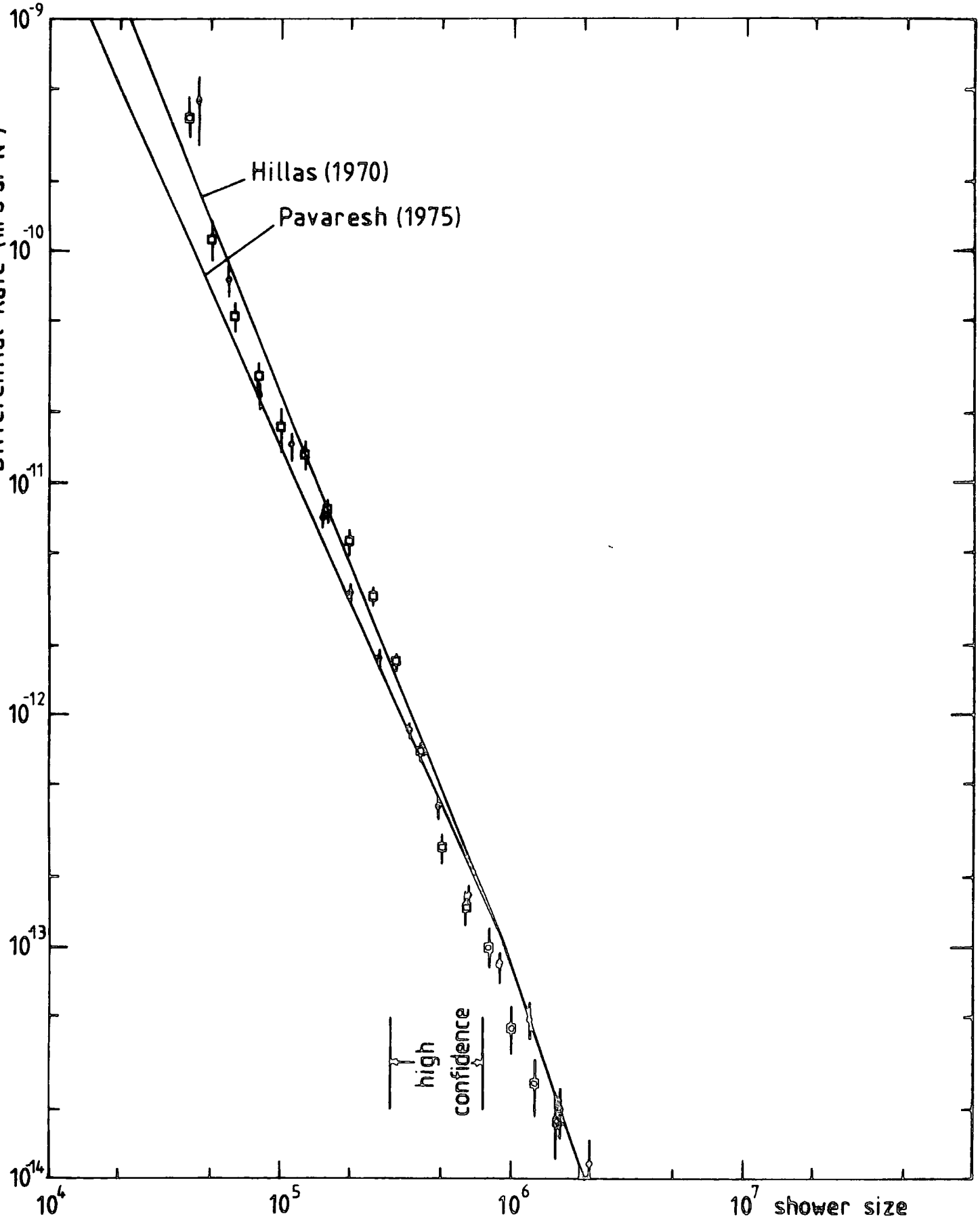

FIGURE 9.14a : The vertical differential size spectrum of EAS at sea-level. ⊡ without size correction, ∘ with size correction.

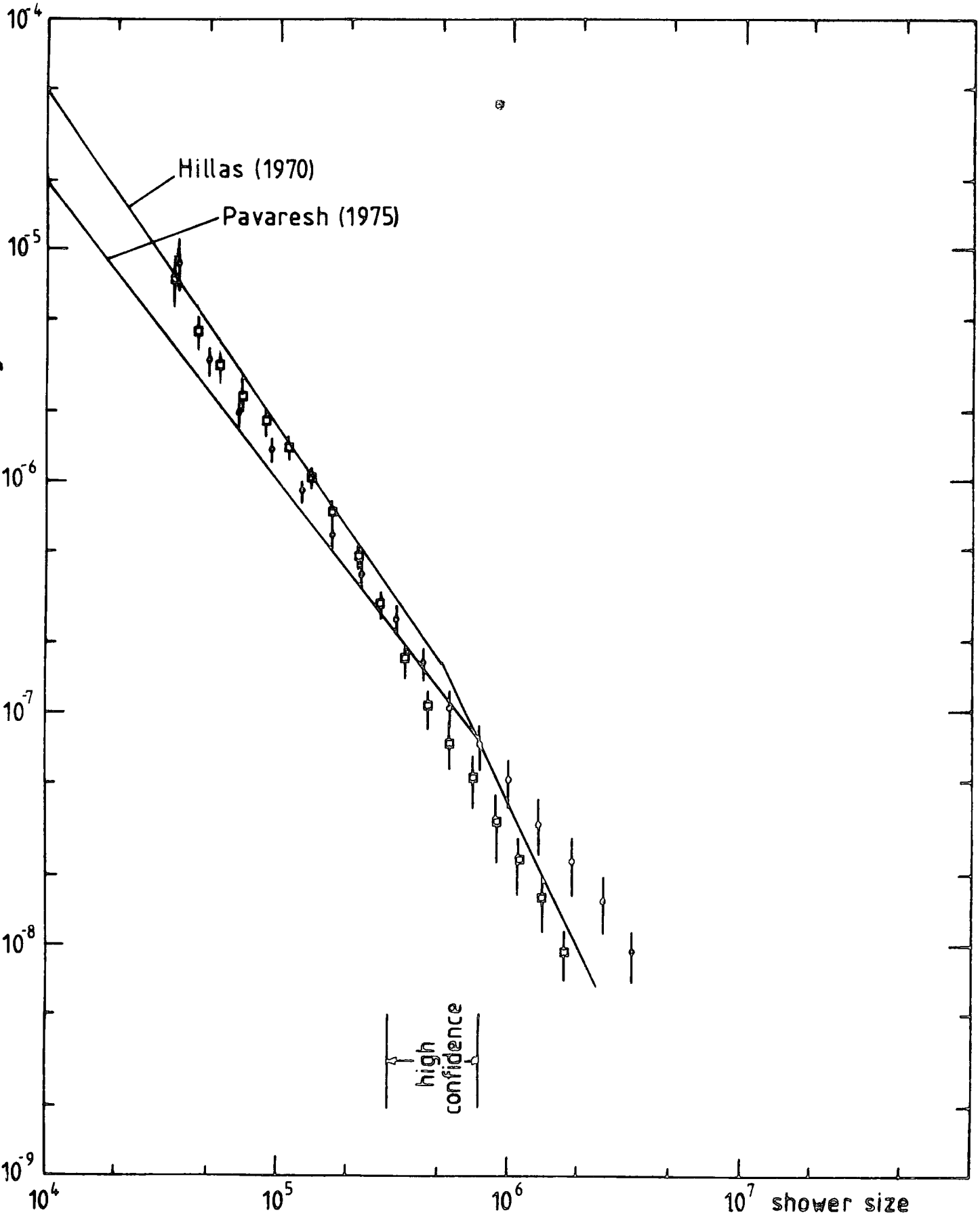

FIGURE 9.15a : The vertical integral size spectrum of EAS at sea-level. □ without size correction, ∘ with size correction.

CHAPTER 10

SUMMARY AND CONCLUSIONS

An experiment to search for tachyons has been described which involved looking for precursors to EAS on the basis that tachyons may be produced in the high energy interactions which occur when a primary cosmic ray particle makes its first interaction with a molecule in the upper atmosphere. No evidence for these precursors was found. However in the light of the fact that theories of their interactions with ordinary matter are still not well founded, it is suggested that further searches are worthwhile, especially in the cosmic radiation. These searches could take a similar form to that given here, with shielding of different types to provide a target for tachyons and the possible production of observable particles. The uncertainty of the forms of interaction, if any, also means that searches of different types, eg. time-of-flight measurements, and using different types of detectors, should be conducted.

The latter part of this thesis describes the improvements and modifications made to the Durham University Air Shower Array, in order to make it suitable as a trigger source and to provide air shower data for other cosmic ray experiments, eg. the flash tube chamber. The changes made included mechanical improvements, to enhance reliability, and the introduction of an automatic data recording system, using a PET microcomputer.

Various methods of checking the array data have been described, including the simulation of data from showers triggering the array. The data, from a short run, was found, in

the main, to be consistent with its correct operation. However two interesting discrepencies occurred. The first was the non-uniformity of the azimuthal angle distribution. A detailed examination of the array collecting area revealed that the observed structure could not be explained by the variation of collecting area with azimuthal angle. It is thus thought that it is due to local absorption by walls adjacent to certain detectors. The other discrepency is in the size spectrum. Although the slope is similar to previous determinations, the absolute rate is approximately three times too low. It is uncertain as to the cause of this and it is concluded that a further run of the experiment is required to determine whether this is a real effect or due to instrumental or processing biases.

From the simulations and data it is evident that a number of improvements are required to be made to the array. These include increasing the number of detectors, to improve the accuracy of core location and shower size determination, and to increase the dynamic range of the density channels in order to increase the efficiency of processing large showers of $N \gtrsim 10^6$. The former improvement has been allowed for in the data collection system, which has provision for upto a total of 24 detectors. Other improvements are detailed in chapter 9.

APPENDIX A

DATA COLLECTION AND PROCESSING PROGRAMS

The programs used in the collection and analysis of the data are listed in the following figures. The function of the programs are as follows:

Figure A.1 STORE.GO (§5.4.2) : This program reads data from the analogue to digital converter, stores it in memory and then transfers it to floppy disc.

Figure A.2 SET.GO (§5.4.2) : This program sets up parameters for use by STORE.GO.

Figure A.3 SETUP (§5.4.2) : This program sets up user supplied variables for use by STORE.GO.

Figure A.4 DATAPROC (§6.2) : This program converts the raw data, from disc, to give densities, times, axis direction and various other shower information.

Figure A.5 CORELOC (§6.3) : This program takes the density, timing and axis information and produces an estimate of the shower size and core location.

Figure A.6 SHOWERSIM (§6.4.3) : This program simulates showers falling on the array. Data is produced in a form suitable for processing by CORELOC.

Figure A.7 COLLECTAREA (Appendix B) : This program calculates the area of intersection of four circles, centred on the four triggering detectors. The radii of the circles are determined from the triggering conditions and the shower size, using the Greisen function. The resulting area is thus the collecting area for the relevant conditions.

GURE A.1 : Program STORE.GO

```
00  AD  B5  7F      LDA  $7FB5    /CHECK FLAG
03  F0  03          BEQ  $7E08
05  6C  B6  7F      JMP  ($7FB6)  /IF FLAG SET THEN INCREMENT CLOCK
08  AD  4D  E8      LDA  $E84D    /ELSE CHECK FOR ADC INTERRUPT
0B  29  02          AND  £$02
0D  C9  02          CMP  £$02
0F  D0  F4          BNE  $7E05    /IF NO ADC INTERRUPT THEN PERFORM RETRACE
11  78              SEI           /ELSE DISABLE INTERRUPT
12  EE  B5  7F      INC  $7FB5    /SET FLAG
15  A9  02          LDA  £$02
17  8D  4E  E8      STA  $E84E    /ENABLE INTERRUPT
1A  A5  E5          LDA  $E5      /SAVE BYTES, AT LOCATIONS TO BE USED BY
1C  48              PHA           /ROUTINE, ON STACK
1D  A5  E6          LDA  $E6
1F  48              PHA
20  A5  F7          LDA  $F7
22  48              PHA
23  A5  F8          LDA  $F8
25  48              PHA
26  A9  A4          LDA  £$A4     /SET RETRACE VECTOR TO PERFORM CLOCK
28  8D  B6  7F      STA  $7FB6    /INCREMENT ONLY
2B  A9  7F          LDA  £$7F
2D  8D  B7  7F      STA  $7FB7
30  A0  00          LDY  £$00
32  A9  C0          LDA  £$C0     /SET ADC OUTPUT MULTIPLEXER TO READ HIGH
34  8D  4C  E8      STA  $E84C    /ORDER BYTE
37  AD  41  E8      LDA  $E841    /LOAD DATA
3A  49  FF          EOR  £$FF     /EOR
3C  91  06          STA  ($06),Y  /STORE
3E  C8              INY
3F  A9  E0          LDA  £$E0     /LOOK AT LOW ORDER BYTE
41  8D  4C  E8      STA  $E84C
44  AD  41  E8      LDA  $E841
47  49  FF          EOR  £$FF     /EOR
49  29  0F          AND  £$0F     /AND NEGLECT 4 MSB
4B  91  06          STA  ($06),Y  /STORE
4D  C8              INY
4E  A2  07          LDX  £$07
50  AD  4D  E8      LDA  $E84D    /CHECK FOR NEXT INTERRUPT
53  29  02          AND  £$02
55  C9  02          CMP  £$02
57  F0  D9          BEQ  $7E32    /IF FOUND, READ NEXT DATA
59  CA              DEX           /ELSE COUNT OUT
5A  E0  00          CPX  £$00
5C  D0  F2          BNE  $7E50    /IF NO INTERRUPT OCCURS AFTER COUNT OUT
5E  58              CLI           /THEN CONTINUE
5F  EE  B1  7F      INC  $7FB1    /INCREMENT SHOWER NUMBER AND DISC SAVE
62  EE  B2  7F      INC  $7FB2    /COUNT
65  AD  00  02      LDA  $0200    /STORE TIME
68  91  06          STA  ($06),Y
6A  C8              INY
6B  AD  01  02      LDA  $0201
6E  91  06          STA  ($06),Y
70  C8              INY
71  AD  B1  7F      LDA  $7FB1    /STORE SHOWER NUMBER
74  91  06          STA  ($06),Y
76  C8              INY
```

GURE A.1 : continued

```
7  A9  FF          LDA  £$FF      /STORE TERMINATOR
9  91  06          STA  ($06),Y   /INCREMENT DATA BUFFER BASE ADDRESS FOR
B  A5  06          LDA  $06       /NEXT SHOWER
D  69  19          ADC  £$19
F  85  06          STA  $06
1  90  02          BCC  $7E85
3  E6  07          INC  $07
5  A5  07          LDA  $07
7  C9  6B          CMP  £$6B
9  D0  0C          BNE  $7E97
B  A5  06          LDA  $06       /IF BASE ADDRESS OCCURS IN AREA OF BAD
D  C9  E7          CMP  £$E7      /MEMORY THEN AVOID
F  90  06          BCC  $7E97
1  E6  07          INC  $07
3  A9  80          LDA  £$80
5  85  06          STA  $06
7  AD  B2  7F      LDA  $7FB2
A  C9  14          CMP  £$14
C  F0  07          BEQ  $7EA5     /CHECK IF DISC STORAGE REQUIRED
E  AD  B1  7F      LDA  $7FB1     /IE. DISC SAVE INTERVAL REACHED OR TRACK
1  C9  BF          CMP  £$BF      /FULL
3  D0  03          BNE  $7EA8
5  20  D1  7E      JSR  $7ED1     /STORE ON DISC ROUTINE
8  78              SEI            /SET INTERRUPT DISABLE
9  68              PLA            /RESTORE LOCATIONS FROM STACK
A  85  E5          STA  $E5
C  68              PLA
D  85  E6          STA  $E6
F  68              PLA
0  85  F7          STA  $F7
2  68              PLA
3  85  F8          STA  $F8
5  A9  AA          LDA  £$AA      /RESET RETRACE VECTOR
7  8D  B6  7F      STA  $7FB6
A  A9  7F          LDA  £$7F
C  8D  B7  7F      STA  $7FB7
F  AD  4D  E8      LDA  $E84D     /CLEAR INTERRUPT FLAG
2  8D  4D  E8      STA  $E84D
5  A9  82          LDA  £$82      /ENABLE INTERRUPT
7  8D  4E  E8      STA  $E84E
A  CE  B5  7F      DEC  $7FB5     /CLEAR FLAG
D  58              CLI            /CLEAR INTERRUPT DISABLE
E  4C  7E  E6      JMP  $E67E     /EXIT FROM INTERRUPT
1  AD  BA  7F      LDA  $7FBA     /SET ADDRESS OF FILE NAME
4  85  FD          STA  $FD
6  AD  BB  7F      LDA  $7FBB
9  85  FE          STA  $FE
B  AD  B3  7F      LDA  $7FB3     /GET FILE NUMBER
E  29  F0          AND  £$F0      /CONVERT TO ASCII AND INSERT IN FILE NAME
0  4A              LSR  A
1  4A              LSR  A
2  4A              LSR  A
3  4A              LSR  A
4  20  2E  7F      JSR  $7F2E
7  E6  FD          INC  $FD
9  AD  B3  7F      LDA  $7FB3
C  29  0F          AND  £$0F
E  20  2E  7F      JSR  $7F2E
1  20  40  7F      JSR  $7F40     /DISC SAVE
4  18              CLC
5  AD  B1  7F      LDA  $7FB1     /IF FULL TRACK THEN CONTINUE
8  C9  BF          CMP  £$BF      /ELSE RETURN
A  F0  01          BEQ  $7EFD
```

GURE A.1 : continued

```
FC  60                  RTS
FD  EE  B3  7F          INC  $7FB3      /INCREASE FILE NUMBER
00  AD  B3  7F          LDA  $7FB3
03  C9  15              CMP  £$15
05  30  17              BMI  $7F1E      /IF FULL DISC THEN JUMP
07  AD  B4  7F          LDA  $7FB4      /ELSE CHECK FOR DISC NUMBER = 2
0A  C9  32              CMP  £$32
0C  D0  08              BNE  $7F16      /IF DISC = 2 WRITE "CHANGE DISCS" AND
0E  20  8B  7F          JSR  $7F8B      /SET DISC TO 0
11  A9  30              LDA  £$30
13  8D  B4  7F          STA  $7FB4
16  EE  B4  7F          INC  $7FB4      /INCREMENT DISC NUMBER
19  A9  01              LDA  £$01
1B  8D  B3  7F          STA  $7FB3      /SET FILE NUMBER TO 1
1E  AD  B8  7F          LDA  $7FB8      /RESET BASE ADDRESS
21  85  06              STA  $06
23  AD  B9  7F          LDA  $7FB9
26  85  07              STA  $07
28  A9  00              LDA  £$00       /RESET SHOWER NUMBER
2A  8D  B1  7F          STA  $7FB1
2D  60                  RTS             /RETURN
2E  A0  00              LDY  £$00       /ASCII CONVERSION ROUTINE
30  C9  0A              CMP  £$0A
32  10  07              BPL  $7F3B
34  69  30              ADC  £$30
36  91  FD              STA  ($FD),Y
38  4C  3F  7F          JMP  $7F3F
3B  69  36              ADC  £$36
3D  91  FD              STA  ($FD),Y
3F  60                  RTS
40  A9  23              LDA  £$23       /DISC SAVE ROUTINE
42  8D  FA  AF          STA  $AFFA      /ENTER COMMAND MODE
45  AD  B4  7F          LDA  $7FB4
48  8D  FB  AF          STA  $AFFB      /SET DISC NUMBER
4B  20  13  B4          JSR  $B413      /CLEAR CURRENT FILE DATA AREA
4E  A2  06              LDX  £$06       /LOAD FILE NAME
50  BD  BC  7F          LDA  $7FBC,X
53  9D  E0  AF          STA  $AFE0,X
56  CA                  DEX
57  10  F7              BPL  $7F50
59  A9  00              LDA  £$00
5B  20  B8  B1          JSR  $B1B8      /OPEN DRIVE AND READ DIRECTORY RETURN
5E  A9  02              LDA  £$02
60  20  F7  B1          JSR  $B1F7      /ALLOCATE FILE TRACK
63  A9  00              LDA  £$00
65  8D  F1  AF          STA  $AFF1      /SET INDEX DATA
68  8D  B2  7F          STA  $7FB2      /CLEAR COUNTER FOR DISC SAVE
6B  85  F7              STA  $F7
6D  A9  56              LDA  £$56
6F  8D  F2  AF          STA  $AFF2      /RELOAD POINTERS IN AFF1 - AFF4
72  A9  6A              LDA  £$6A
74  85  F8              STA  $F8        /BLOCK POINTERS IN 00F7/8,00E5/6
76  38                  SEC
77  A5  06              LDA  $06
79  85  E5              STA  $E5
7B  8D  F3  AF          STA  $AFF3
7E  A5  07              LDA  $07
80  85  E6              STA  $E6
82  E9  14              SBC  £$14
84  8D  F4  AF          STA  $AFF4
87  20  5B  B1          JSR  $B15B      /SAVE RELOCATABLE PROGRAM
8A  60                  RTS
8B  A2  77              LDX  £$77       /PRINT "CHANGE DISCS" ROUTINE
```

RE A.1 : continued

```
A9  20          LDA  £$20
9D  00  80      STA  $8000,X  /CLEAR TOP OF SCREEN
CA              DEX
10  FA          BPL  $7F8F
BD  C3  7F      LDA  $7FC3,X
C9  FF          CMP  £$FF     /WRITE *** CHANGE DISCS ***
F0  07          BEQ  $7FA3
9D  00  80      STA  $8000,X
E8              INX
4C  95  7F      JMP  $7F95
60              RTS
20  36  F7      JSR  $F736    /CLOCK ROUTINE
4C  7E  E6      JMP  $E67E
AD  12  E8      LDA  $E812    /RETRACE ROUTINE
58              CLI
4C  85  E6      JMP  $E685
```

URE A.2 : Program SET.GO

```
A9 FF       LDA £$FF    /SET TOP OF BASIC TO PROTECT STORE.GO AND
85 86       STA $86     /DATA BUFFER
A9 69       LDA £$69
85 87       STA $87
A0 25       LDY £$25
A9 7F       LDA £$7F    /TRANSFERS INITIAL DATA FOR USE BY
85 EC       STA $EC     /STORE.GO FROM THIS ROUTINE TO END OF
A9 B0       LDA £$B0    /STORE.GO
85 EB       STA $EB
A9 03       LDA £$03
85 FE       STA $FE
A9 85       LDA £$85
85 FD       STA $FD
B1 FD       LDA ($FD),Y
91 EB       STA ($EB),Y
88          DEY
D0 F9       BNE $0354
A9 00       LDA £$00
85 06       STA $06     /INITIALISES BASE ADDRESS OF DATA BUFFER
A9 6A       LDA £$6A
85 07       STA $07
8C 43 E8    STY $E843   /SETS REGISTERS
AD 4D E8    LDA $E84D   /IE. DATA DIRECTION FOR INPUT
8D 4D E8    STA $E84D   /    INTERRUPT FLAG
8C 4C E8    STY $E84C   /    AUXILLIARY CONTROL FOR LATCHING ON
A9 00       LDA £$00    /    -VE INPUT
8D 4B E8    STA $E84B   /CLEAR INTERRUPT FLAG REGISTER
78          SEI
A9 00       LDA £$00    /ALTER INTERRUPT VECTOR
8D 19 02    STA $0219
A9 7E       LDA £$7E
8D 1A 02    STA $021A
58          CLI
A9 82       LDA £$82    /ENABLE INTERRUPT
8D 4E E8    STA $E84E
60          RTS
```

```
6  7  8  9  A  B  C  D  E  F  0  1  2  3  4  5

00 00 01 31 00 AA 7F 00 6A C1 7F 44 D 41 A 54 T 41 A 23 #
30 0 31 1 2A * 2A * 2A * 03 C 08 H 01 A 0E N 07 G 05 E 20  04 D 09 I 13 S 0B K
13 S 2A * 2A * 2A * FF
```

```
COUNTERS          0386-038A
RETRACE VECTOR    038B,038C
BUFFER BASE       038D,038E
FILENAME ADDRESS  038F,0390
```

GURE A.3 : Program SETUP

```
) REM PROGRAM SETUP
) REM --------------
. REM INITIALIZES VARIABLES USED BY STORE.GO
) INPUT"TIME (HMS)";TI$                          /INPUT TIME
) SYS826                                         /RUN SET.GO
) INPUT"NO OF FILES PER DISK";A                  /INPUT NUMBER OF FILES ON DISC
) IFA)39THENA=39                                 /(≤NUMBER OF FREE TRACKS)
) POKE32516,A+1
) INPUT"NO OF SHRS PER FILE";B                   /INPUT NUMBER OF SHOWERS PER
) IFB)191THENB=191                               /FILE (≤191)
) POKE32418,B:POKE32505,B
) INPUT"DISK£";D                                 /INPUT DISC NUMBER (1 OR 2)
) IFD<3GOTO240
) PRINT"DISK£ MUST BE 1 OR 2"
) GOTO200
) POKE32692,49
) IFA=2THENPOKE32692,50
) INPUT"FILE£";E                                 /INPUT INITIAL FILE NUMBER
) IFE=<AGOTO300                                  /(≤39)
) PRINT"FILE£ MUST BE =<";A
) GOTO260
) POKE32691,A
  INPUT"SHOWER£";A                               /INPUT INITIAL SHOWER NUMBER
) IFA<B+1GOTO350                                 /(≤NUMBER OF SHOWERS PER FILE)
) PRINT"SHOWER£ MUST BE =<";B
) GOTO310
  POKE32689,A-1                                  /BUFFER BASE ADDRESS SET SO, IF
) D=0                                            /REQUIRED, PREVIOUS SHOWERS
  B=(A-1)*26                                     /BELOW NUMBER OF INITIAL
) IFB<256GOTO420                                 /SHOWERS CAN BE KEPT
  B=B-256
) D=D+1
  GOTO380
  POKE6,B
  POKE7,106+D
) PRINT:INPUT"DISK SAVE INTERVAL";B              /INPUT SHOWER SAVE INTERVAL
  IFB)191THENB=191                               /(≤191). ENABLES FREQUENCY OF
) POKE32411,B                                    /SAVING DATA ON DISC TO BE
  POKE32690,0                                    /VARIED
  STOP
  END
```

URE A.4 : Program DATAPROC

```
0 REM PROGRAM DATAPROC
0 REM ----------------
1 REM CONVERTS RAW DATA TO SHOWER PARAMETERS
0 POKE134,255:POKE135,85
0 DIMAG(17),AH(35),D(4),DA(4),DB(4),DC(4),F(1,2),G(1,2),HF(2)
0 DIML(2),LF(2),P(2),SA(2),SB(2),T(2),TF(2,34),X(2),Y(2),Z(2)
0 DIMB$(4),BD$(99),R1(4),R2(2),AF(4,19),PH(1),TA(1)
0 OPEN1,4
0 PRINT"":INPUT"DATA TO BE WRITTEN TO DISK £";DD
0 PRINT:PRINT:PRINT:INPUT"FILENAME";F$
5 PRINT:PRINT:PRINT
0 PRINT"NO OF SHOWERS TO BE PROCESSED":INPUT"- PUT 0 IF ALL REQD";LI
5 IFLI=0THENLI=191
0 DE=1:F1=0:F2=0:NM=1:TG=0:FH=0
0 IFDD=1THENDE=2
5 PRINT:PRINT:PRINT
0 PRINT"ENSURE DISK IN CORRECT DRIVE - PRESS ANY KEY TO CONTINUE"
0 PRINT:PRINT"DATA INPUT  DISK IN";DE
1 PRINT"DATA OUTPUT DISK IN";DD
5 GETA$:IFA$=""GOTO1135
7 PRINT
9 PRINT"LOADING ";F$
0 $LOD;DE,F$
0 SA=5*4096+6*256
1 PRINT"OPTIONS REQUIRED":PRINT:PRINT:PRINT"0 = ALL":PRINT"1 = STATS ON3H"K
2 PRINT"2 = MAP & STATS":PRINT"3 = PRINT & STATS"
3 PRINT"4 = MAP & STATS & DISK":PRINT"5 = DATAPRINT & STATS & DISKS"
5 PRINT:PRINT:INPUT"OPTION";OP
6 IFOP)5GOTO1155
7 PRINT:PRINT:PRINT
0 INPUT"START DATE (DYMTYR)";D$
0 DD$=LEFT$(D$,2):DM$=MID$(D$,3,2):DY$=RIGHT$(D$,2)
0 D1=VAL(DD$):D2=VAL(DM$):D3=VAL(DY$)
0 IFSA)27110GOTO1335
5 ER=0
0 GOSUB2000
5 IFF2=0GOTO1250
6 F1=0:F2=0:GOTO1320
0 GOSUB3000
5 GOSUB3500
0 GOSUB4000
0 GOSUB5000
0 GOSUB6000
1 IFNL(3GOTO1285
2 ER=6
3 GOSUB2500
4 GOTO1320
5 FG=0
6 IFOP)3THENGOSUB1500
0 IFOP/2()INT(OP/2)THENGOSUB7500
0 IFOP/2=INT(OP/2)THENGOSUB7000
5 IFOP)3THENGOSUB8000
0 IFOP)1THENGOSUB4500
0 SA=SA+26
2 IFSA=22510THENSA=22656
5 IFNO=LIGOTO1335
0 GOTO1220
5 GOSUB8500
0 IFOP)1THENGOSUB9000
0 CLOSE1
0 STOP
```

GURE A.4 : continued

```
)0 END
'0 REM ----------
)0 REM SUBROUTINE RANDOMFORMAT
)5 REM ----------
.0 REM FORMATS OUTPUT DISK FILE
 5 PRINT:PRINT"CREATING OUTPUT FILE":PRINT
:0 DF$="P"+F$
)0 R$=""
·0 FORI=1TO55:R$=R$+" ":NEXTI
·0 A=190:GOSUB1650
·0 DI$=CHR$(L)+CHR$(H)
'0 A=55:GOSUB1650
)0 DI$=DI$+CHR$(L)+CHR$(H)+"    "
'0 $ODISK,DD,"W",DF$,DI$
)0 FORI=1TO190
 0 $WDISK,R$
'0 NEXTI
)0 $CDISK
·0 RETURN
·0 H=INT(A/256)
·0 L=A-(H*256)
 0 RETURN
)0 REM ----------
)0 REM SUBROUTINE DATAREAD
)5 REM ----------
.0 REM CONVERTS TIME TO HMS ABSOLUTE
30 IFPEEK(SA+25)=255THEN2110
)0 ER=1:NN=1:GOSUB2500
'0 RETURN
 0 IFPEEK(SA+24))NOGOTO2140
:0 ER=2:GOSUB2500
)0 RETURN
·0 NO=PEEK(SA+24)
·0 MA=PEEK(SA+12)*16+PEEK(SA+13)
·0 IFMA)400ANDMA(500GOTO2190
'0 ER=3:GOSUB2500
)0 RETURN
'0 J=PEEK(SA+10)+PEEK(SA+11)
 0 IFJ=0GOTO2240
:0 ER=4:GOSUB2500
)0 RETURN
·0 FORI=0TO2
·2 KZ=I*4
·4 IFI=0THENKZ=KZ+2
·0 T(I)=PEEK(SA+KZ)*16+PEEK(SA+KZ+1)
·0 NEXT
'0 IFT(0)+T(1)+T(2)=0THENF1=1
)0 IFT(0)=00RT(1)=00RT(2)=0THEN2360
)0 FORI=0TO3
.0 D(I)=PEEK(SA+14+2*I)*16+PEEK(SA+2*I+15)
:0 NEXT
30 D(4)=PEEK(SA+6)*16+PEEK(SA+7)
40 T1=PEEK(SA+22):T2=PEEK(SA+23)
·0 RETURN
·0 ER=5:GOSUB2500
'0 RETURN
30 REM ----------
)0 REM SUBROUTINE BADDATA
)5 REM ----------
.0 REM STORES BAD DATA AS CHAR STRING
.4 F2=1
.5 IFF1=1THENRETURN
20 BD$(II)="":X$="0123456789ABCDEF"
```

GURE A.4 : continued

```
30 FORI=SATOSA+25
40 BD$(II)=BD$(II)+MID$(X$,INT(PEEK(I)/16)+1,1)
50 BD$(II)=BD$(II)+MID$(X$,PEEK(I)-INT(PEEK(I)/16)*16+1,1)
60 NEXT
70 BD$(II)=RIGHT$(STR$(ER),1)+BD$(II)
80 II=II+1
85 IFII<100GOTO2590
86 PRINT"OVER 100 BADDATA - RUN TERMINATED":STOP
90 RETURN
00 REM ----------------
00 REM SUBROUTINE TICONV
05 REM ----------------
10 REM CONVERTS TIME TO HMS ABSOLUTE
15 TG=TH
20 T=(T1*65536+T2*256)/60
30 TH=INT(T/3600)
40 TM=INT((T-TH*3600)/60)
50 TS=INT((T-TH*3600-TM*60)+.5)
60 TH$=STR$(TH):TM$=STR$(TM):TS$=STR$(TS)
62 IFLEN(TH$)=2THENTH$=" 0"+RIGHT$(TH$,1)
64 IFLEN(TM$)=2THENTM$=" 0"+RIGHT$(TM$,1)
66 IFLEN(TS$)=2THENTS$=" 0"+RIGHT$(TS$,1)
70 RETURN
80 REM ----------------
00 REM SUBROUTINE DATE
05 REM ----------------
10 REM CALCULATION OF DATE (NOT LEAP YEARS)
20 IFTH>=TGTHENRETURN
40 D1=D1+1
50 IFD2>6GOTO3580
60 OND2GOTO3630,3590,3630,3610,3630,3630
80 OND2-6GOTO3630,3630,3610,3630,3610,3630
90 IFD1>=28GOTO3650
00 GOTO3660
10 IFD1>=30GOTO3650
20 GOTO3660
25 IFD2<>12GOTO3660
26 D3=D3+1:D2=1
30 IFD1>=31GOTO3620
40 GOTO3660
50 D1=1:D2=D2+1
60 DD$=STR$(D1):DM$=STR$(D2):DY$=STR$(D3)
61 IFLEN(DD$)=2THENDD$="0"+RIGHT$(DD$,1)
62 IFLEN(DM$)=2THENDM$="0"+RIGHT$(DM$,1)
63 IFLEN(DY$)=2THENDY$="0"+RIGHT$(DY$,1)
65 DD$=RIGHT$(DD$,2):DM$=RIGHT$(DM$,2):DY$=RIGHT$(DY$,2)
70 RETURN
80 REM ----------------
00 REM SUBROUTINE FPCONV
05 REM ----------------
 0 REM CONVERSION OF TIMING DATA
20 F(0,0)=.152:F(0,1)=.158:F(0,2)=.156
30 F(1,0)=.144:F(1,1)=.149:F(1,2)=.148
60 G(0,0)=4.645:G(0,1)=-2.962:G(0,2)=-1.159
70 G(1,0)=11.43:G(1,1)=7.681:G(1,2)=8.104
00 FORI=0TO2
30 IFT(I)>1500GOTO4160
40 T(1)=F(0,I)*T(I)+G(0,I):GOTO4180
60 T(I)=F(1,I)*T(I)+G(1,I):GOTO4180
80 IFT(I)<0THENT(I)=0
90 NEXT
00 RETURN
10 REM ----------
```

GURE A.4 : continued

```
00 REM SUBROUTINE STATS
05 REM ------------------
10 REM GENERATES STATISTICS
20 LF(0)=130:LF(1)=110:LF(2)=140:HF(0)=230:HF(1)=200:HF(2)=400
30 P(0)=5:P(1)=5:P(2)=10
40 FF=INT(TA/5)
50 IFFF(18GOTO4570
55 NG=NG+1:GOTO4580
70 AG(FF)=AG(FF)+1
80 FF=INT(PH/10)
90 AH(FF)=AH(FF)+1
00 FORI=0TO2
10 IFT(I)(LF(I)ORT(I))HF(I)GOTO4640
20 FF=INT((T(I)-LF(I))/P(I))
30 TF(I,FF)=TF(I,FF)+1
40 NEXT
50 FORI=0TO2
60 IFT(I)(500RT(I))500GOTO4680
70 SA(I)=SA(I)+T(I):SB(I)=SB(I)+1
80 NEXT
90 FORI=0TO4
00 FF=INT(D(I)/5)
10 IFFF)19GOTO4730
20 AF(I,FF)=AF(I,FF)+1
30 NEXT
40 RETURN
00 REM ----------------
00 REM SUBOUTINE SPCONV
05 REM ----------------
10 REM CONVERSION OF DENSITY DATA
20 DA(0)=.00284:DA(1)=.00272:DA(2)=.00272:DA(3)=.00281:DA(4)=.00274
30 DB(0)=.1659:DB(1)=.1412:DB(2)=.1284:DB(3)=.1411:DB(4)=.1456
40 DC(0)=10.8:DC(1)=10.7:DC(2)=10.1:DC(3)=9.1:DC(4)=10.
45 DD=D(0)
50 FORI=0TO4
60 D(I)=D(I)*DA(I)+DB(I)
72 D(I)=D(I)*DD/(.9305*DD-.0246)
84 D(I)=D(I)*DC(I)
96 D(I)=(INT(D(I)*100+.5))/100
00 NEXT
10 RETURN
00 REM ----------------
00 REM SUBROUTINE AXIS
05 REM ----------------
10 REM DETERMINES DIRECTION OF AXIS
20 PH=0:TA=0:ER=0:NL=0
30 X(0)=-12.3:X(1)=14.8:X(2)=.3
40 Y(0)=-5.64:Y(1)=3.1:Y(2)=-26.8
50 Z(0)=-4.83:Z(1)=.16:Z(2)=.18
60 L(0)=159.1:L(1)=153.3:L(2)=253.5
70 FORJ=0TO1
80 T0=.3*(T(J)-L(J)):T1=.3*(T(2)-L(2))
90 E=X(2)*Y(J)-X(J)*Y(2)
40 A=(Y(J)*T1-Y(2)*T0)/E
50 B=(Y(J)*Z(2)-Y(2)*Z(J))/E
60 C=(X(2)*T0-X(J)*T1)/E
70 D=(X(2)*Z(J)-X(J)*Z(2))/E
80 F=A*B+C*D
90 G=B*B+D*D+1
00 H=(F*F-G*(A*A+C*C-1))
10 IFH(0THEN6275
40 H=SQR(H)
50 TA=(H-F)/G:S=(-H-F)/G
```

GURE A.4 : continued

```
60 IFTA(0GOTO6510
70 IFS(0GOTO6340
75 NL=NL+J+1
25 GOSUB2500
30 GOTO6510
40 W=C+D*TA:V=A+B*TA
50 IFTA()1GOTO6380
60 TA=0:PH=0:GOTO6490
80 IFV()0GOTO6415
90 PH=1.571
00 IFW(0THENPH=4.713
10 GOTO6480
15 PH=W/V
20 Q=3.142
30 IFV(0GOTO6460
40 Q=0
50 IFW(0THENQ=6.284
60 PH=ATN(PH)+Q
80 TA(J)=(-ATN(TA/SQR(-TA*TA+1))+1.5708)*57.296
90 PH(J)=PH*57.296
95 IFPH(J))=360THENPH(J)=PH(J)-360
10 NEXT
20 IFNL=3THENRETURN
30 IFNL=0THEN6550
40 PH=INT(PH(2-NL)+.5):TA=INT(TA(2-NL)+.5):RETURN
50 TA=(TA(0)+TA(1))/2
60 PH=(PH(0)+PH(1))/2
70 IFABS(PH(0)-PH(1)))180THENPH=PH-180
80 IFPH(0THENPH=PH+360
85 PH=INT(PH+.5):TA=INT(TA+.5)
90 RETURN
00 REM ---------------
00 REM SUBROUTINE MAP
05 REM ---------------
 0 REM HARD COPY DATA OUTPUT
20 IFJJ=2GOTO7040
30 PRINT£1,CHR$(12):JJ=2:GOTO7050
40 JJ=1
50 PRINT£1,TAB(19)"XI_10"TAB(19)"SHOWER NO: "NO:PRINT£1,TAB(20)"I"
60 PRINT£1,TAB(20)"I"TAB(22)"DATE: "DD$+DM$+DY$
70 PRINT£1,TAB(20)"I"TAB(4)"31("D(2)")":PRINT£1,TAB(20)"I"TAB(14)"*";
80 PRINT£1,TAB(7)"TIME: "TH$+TM$+TS$:PRINT£1,"-20"TAB(6)"-10"TAB(8)"I";
90 PRINT£1,TAB(8)"10"TAB(8)"20"
00 FORI=0TO40:PRINT£1,"_";:NEXT
 0 PRINT£1,CHR$(13)"L"TAB(9)"L"TAB(9)"*"TAB(9)"L"TAB(9)"L"
20 PRINT£1,TAB(20)"IC("D(0)")"CHR$(13)TAB(40)"Y  AXIS:"ER$
30 PRINT£1,TAB(20)"I"TAB(22)"THETA="TA:PRINT£1,TAB(8)"11("D(1)")";
40 PRINT£1,CHR$(13)TAB(20)"I"TAB(22)"PHI="PH:PRINT£1,TAB(7)"*"TAB(12)"I"
50 PRINT£1,TAB(20)"I"TAB(22)"T11="T(0)"NS":PRINT£1,TAB(20)"I_-10";
60 PRINT£1,TAB(18)"T31="T(1)"NS":PRINT£1,TAB(20)"I"TAB(22)"T51="T(2)"NS"
70 PRINT£1,TAB(20)"I":PRINT£1,TAB(9)"52("D(4)")"CHR$(13)TAB(20)"I"
80 PRINT£1,TAB(19)"*I":PRINT£1,TAB(20)"I":PRINT£1,TAB(20)"I_-20"
90 FORI=1TO3:PRINT£1,TAB(20)"I":NEXT:PRINT£1,TAB(9)"51("D(3)")"CHR$(13);
00 PRINT£1,TAB(20)"I":PRINT£1,TAB(19)"*I":PRINT£1,TAB(20)"I_-30"
05 FORI=1TO4:PRINT£1,:NEXT
 0 RETURN
20 REM --------------------
00 REM SUBROUTINE DATAPRINT
05 REM --------------------
 0 REM PRINTS RESULTS
20 IFFH=1GOTO7580
30 FH=1
35 PRINT£1,CHR$(12),F$:PRINT£1
```

GURE A.4 : continued

```
40 PRINT£1,TAB(28)"DENSITIES"TAB(18)"TIMES"
50 PRINT£1,"SHR.NO. DATE   TIME    C    11    31    51    52    ";
60 PRINT£1,"11   31   51 THETA PHI"
70 PRINT£1
80 FORI=0TO4
90 R1(I)=INT(D(I)*10+.5)/10
00 IFR1(I))=100THENR1(I)=INT(D(I)+.5)
10 NEXT
11 PRINTR1(0);R1(1);R1(2);R1(3);R1(4)
20 FORI=0TO2:R2(I)=INT(T(I)+.5):NEXT
30 PH=INT(PH+.5):TA=INT(TA+.5)
40 IFTA>90THENTA=99
50 PRINT£1,TAB(2)NO;TAB(4-LEN(STR$(NO)))DD$+DM$+DY$" ";
60 PRINT£1,RIGHT$(TH$,2)+RIGHT$(TM$,2)+RIGHT$(TS$,2);
70 PRINT£1,TAB(5-LEN(STR$(R1(0))))R1(0)TAB(5-LEN(STR$(R1(1))));
80 PRINT£1,R1(1)TAB(5-LEN(STR$(R1(2))))R1(2)TAB(5-LEN(STR$(R1(3))));
90 PRINT£1,R1(3)TAB(5-LEN(STR$(R1(4))))R1(4)R2(0)R2(1)R2(2)TA;
00 PRINT£1,TAB(3-LEN(STR$(TA)))PH
10 RETURN
20 REM ----------------
30 REM SUBROUTINE STORE
35 REM ----------------
40 REM STORES PROCESSED DATA ON DISK
45 DF$="P"+F$
20 $ODISK,DD,"D",DF$,CHR$(170)+CHR$(0)+CHR$(55)+CHR$(0)+"      "
30 R$=RIGHT$("  "+STR$(NO),3)+DD$+DM$+DY$+RIGHT$(TH$,2)+RIGHT$(TM$,2)
40 R$=R$+RIGHT$(TS$,2)
50 FORI=0TO4
60 R$=R$+RIGHT$("   "+STR$(INT(10*D(I)+.5)/10),4)
70 NEXT
80 FORI=0TO2
90 R$=R$+RIGHT$("    "+STR$(INT(10*T(I)+.5)/10),5)
00 NEXT
10 R$=R$+RIGHT$(STR$(INT(TA)),2)+RIGHT$("  "+STR$(INT(PH)),3)
20 $WDISK;NM,R$
25 $CDISK
30 NM=NM+1
40 RETURN
50 REM ---------------------
60 REM SUBROUTINE BADDATAOUT
65 REM ---------------------
70 REM PRINTS BAD DATA
80 IFII=0THENRETURN
90 PRINT£1,:PRINT£1,"BAD DATA"
00 FORI=0TOII-1:PRINT£1,BD$(I):NEXT
10 PRINT£1,:PRINT£1,"ERROR CODES":PRINT£1,
20 PRINT£1,"1: NO TERMINATOR"
30 PRINT£1,"2: SHR NO ERROR"
40 PRINT£1,"3: MASTER HEIGHT OUT OF RANGE"
50 PRINT£1,"4: TIMING DATA SHIFT"
60 PRINT£1,"5: TIME ZERO ERROR"
70 PRINT£1,"6: TH,PH UNOBTAINABLE"
80 RETURN
90 REM ---------------
00 REM SUBROUTINE PLOT
05 REM ---------------
10 REM PRINTS SUMMARY OF DATA
20 B$(0)="11":B$(1)="31":B$(2)="51"
30 PRINT£1,CHR$(12)
35 PRINT£1,F$," SUMMARY OF DATA":PRINT£1
40 PRINT£1,"NO OF SHOWERS";NO
45 PRINT£1,"NO WITH THETA>90";NG
47 PRINT£1,"NO WITH -VE G";NQ
```

IGURE A.4 : continued

```
050 PRINT&1,"NO WITH BAD DATA";II
060 FORI=0TO2
065 IFSB(I)=0GOTO9160
070 IFB$(I)="51"THENPRINT&1,CHR$(12)
080 PRINT&1,:PRINT&1,"T";B$(I);"DISTRIBUTION - MEAN";SA(I)/SB(I)
090 FORIK=0TO(HF(I)-LF(I))/P(I)
100 K=IK*P(I)+LF(I)
110 U$=STR$(K)
120 IFINT(IK/2)()IK/2THENU$="     "
140 IJ=TF(I,IK)
150 GOSUB9500
160 NEXT
165 NEXT
170 PRINT&1,:PRINT&1,"THETA DISTRIBUTION"
180 FORI=0TO17
190 K=I*5
200 U$=STR$(K)
210 IFINT(I/2)()I/2THENU$="     "
230 IJ=AG(I)
240 GOSUB9500
250 NEXT
260 PRINT&1,CHR$(12):PRINT&1,"PHI DISTRIBUTION"
270 FORI=0TO35
280 K=I*10
290 U$=STR$(K)
300 IFINT(I/2)()I/2THENU$="     "
320 IJ=AH(I)
330 GOSUB9500
340 NEXT
350 B$(0)=" C":B$(1)="11":B$(2)="31":B$(3)="51":B$(4)="52"
360 FORI=0TO4
370 IFI=0ORI=2ORI=4THENPRINT&1,CHR$(12)
380 PRINT&1,"DETECTOR "B$(I)" DENSITY DISTRIBUTION"
390 FORL=0TO19
400 K=L*5:U$=STR$(K)
410 IFINT(L/2)()L/2THENU$="     "
420 IJ=AF(I,L)
430 GOSUB9500
440 NEXTL
445 FORKI=1TO2000:NEXTKI
450 PRINT&1,:PRINT&1,
460 NEXTI
470 PRINT&1,U$;TAB(5-LEN(U$));"I";
480 ONIJ+1GOTO9560,9540
490 FORIM=1TOIJ-1
500 PRINT&1,"X";
505 NEXT
510 PRINT&1,"X"
520 GOTO9570
530 PRINT&1," "
540 RETURN
Y.
```

GURE A.5 : Program CORELOC

```
00 REM ---------------------
10 REM MAIN PROGRAM CORELOC
20 REM ---------------------
21 REM DETERMINES CORE LOCATION & SHOWER SIZE
30 DIMA(4),AM(4),D(4,255),S(4),X(4),Y(4),Z(4),E(12),A$(255)
40 DE$=" C11315152":AL=1:DJ=10:SD=150
50 AM(0)=100:AM(1)=114:AM(2)=82:AM(3)=90:AM(4)=90
60 X(0)=0:X(1)=-12.3:X(2)=14.8:X(3)=.3:X(4)=-.5
70 Y(0)=0:Y(1)=-5.64:Y(2)=3.1:Y(3)=-26.8:Y(4)=-17
80 Z(0)=0:Z(1)=-4.83:Z(2)=.16:Z(3)=.18:Z(4)=.67
90 A(0)=.75:A(1)=2:A(2)=2:A(3)=2:A(4)=1
95 INPUT"NO OF SHOWERS";MM
00 GOSUB3000
01 PRINT""
10 FORM=0TOMM
11 BL=0:JK=0
15 GOSUB4000
16 IFTA>30THEN1700
17 TA=TA/180:PH=PH/180
20 MD=D(0,M):MI=0
30 FORJI=1TO4
40 IFD(JI,M)<MDGOTO1160
50 MD=D(JI,M):MI=JI
60 NEXTJI
70 G1=X(MI)+1:G2=Y(MI)+1
80 FORKI=1TONR
90 DI=DJ:CT=0:ST$="":SZ$=""
10 K=0
20 XM=G1+SD/2:XL=XM-SD:YM=G2+SD/2:YL=YM-SD
30 GOSUB2000
35 IFJK>2THEN1696
40 NM=NS:CM=C:H1=G1:H2=G2:G3=G1:G4=G2
70 J=1
80 IFG1<XLORG1>XMORG2<YLORG2>YMGOTO1540
90 PRINT"SHOWER £ ";SN
95 PRINT:PRINT"PRESENT SEARCH INCREMENT IS ";DI;"     "
00 CT=CT+1
10 IFCT>20GOTO1690
20 G1=G1-DI:G2=G2+DI
30 GOSUB2000
40 IFC>CMGOTO1360
50 H1=G1:H2=G2:NM=NS:CM=C
60 IFJ<>8GOTO1420
70 IFH1<>G3ORH2<>G4GOTO1410
80 DI=DI/2
90 IFDI<ALGOTO1500
00 G1=G3:G2=G4:GOTO1270
10 G3=H1:G4=H2:G1=H1:G2=H2:GOTO1270
20 IFJ>2GOTO1440
30 G1=G1+DI:GOTO1490
40 IFJ>4GOTO1460
50 G2=G2-DI:GOTO1490
60 IFJ>6GOTO1480
70 G1=G1-DI:GOTO1490
80 G2=G2+DI
90 J=J+1:GOTO1330
00 H1=INT(H1*10+.5)/10:H2=INT(H2*10+.5)/10
20 CM=INT(CM*10+.5)/10
30 GOTO1570
40 BL=1
70 FORI=0TO4
```

GURE A.5 : continued

```
80 IFD(I,M)(AM(I)GOTO1600
90 ST$=ST$+" "+MID$(DE$,I*2+1,2)
00 NEXTI
10 IFST$=""GOTO1630
30 FORI=0TO4
40 IFD(I,M )()0GOTO1660
50 SZ$=SZ$+" "+MID$(DE$,I*2+1,2)
60 NEXTI
70 IFSZ$=""GOTO1690
90 NEXTKI
95 GOSUB5000
96 GOSUB6000
00 NEXTM
04 STOP
05 GOSUB6091
10 CLOSE1
20 STOP
30 END
00 REM ------------------
10 REM SUBROUTINE SEARCH
20 REM ------------------
21 REM MINIMISATION ROUTINE
30 REM DETERMINES NEW CORE GUESS
60 K=K+1:S1=0:S2=0:C=0
70 FORI=0TO4:IA(I)=0:S(I)=0:NEXTI
80 FORI=0TO4
90 IFD(I,M)(=0ORD(I,M))AM(I)GOTO2240
00 AX(I)=X(I)-G1:AY(I)=Y(I)-G2
10 R=SIN(TA)*(AX(I)*COS(PH)+AY(I)*SIN(PH))
20 R=(R+Z(I)*COS(TA))^2
30 R=SQR(AX(I)^2+AY(I)^2+Z(I)^2-R)
40 IFR(.5GOTO2240
50 S(I)=.000064*(79/R)^.75
60 S(I)=S(I)*(79/(R+79))^3.25
70 S(I)=S(I)*(1+R/900.6)
80 S1=S1+S(I)*A(I)
90 S2=S2+S(I)^2*A(I)/D(I,M)
00 GOTO2250
40 IA(I)=1
45 JK=JK+1
50 NEXTI
55 IFJK)2THENRETURN
60 NS=INT(S1/S2)
70 FORI=0TO4
80 IFIA(I)=1GOTO2310
90 F=S(I)*NS
95 FF=SQR(F*A(I))
00 C=C+(F-D(I,M))^2*A(I)*A(I)/(FF*FF+FF+.25)
10 NEXTI
20 RETURN
00 REM ----------------------
10 REM SUBROUTINE DISK INPUT
20 REM ----------------------
21 REM SHOWER DATA INPUT
30 INPUT"FILE  *    ";F$
40 INPUT"INPUT DRIVE £";D
45 INPUT"OUTPUT DRIVE £";DD
50 $ODISK,D,"R",F$,DI$
60 IFPEEK(44976)()255THEN3090
80 INPUT"REPLACEMENT FILE";F$:GOTO3050
90 REM
00 FORII=0TOMM:$RDISK,R$:A$(II)=R$:NEXTII
10 $CDISK
```

GURE A.5 : continued

```
20 RETURN
00 REM -----------------
10 REM SUBROUTINE DECODE
20 REM -----------------
30 REM DECODE DATA FROM DISK
40 J=0:C$=""
50 A$(M)=A$(M)+"-"
60 FORL=2T071
70 B$=MID$(A$(M),L,1)
80 IFB$=" "ORB$="-"THEN4095
90 C$=C$+B$:GOTO4150
95 IFJ=1THENDA$=C$
96 IFJ=2THENTT$=C$
00 E(J)=VAL(C$)
10 C$=""
30 J=J+1
40 IFB$="-"THENL=71
50 NEXTL
60 SN=E(0):TA=E(11):PH=E(12)
70 D(0,M)=E(3):D(1,M)=E(4):D(2,M)=E(5):D(3,M)=E(6):D(4,M)=E(7)
90 RETURN
00 REM -----------------
10 REM SUBROUTINE OUTPUT
20 REM -----------------
21 REM OUTPUT RESULTS TO SCREEN
22 PRINT"HOWER £ ";M+1:PRINT
23 PRINT"DATE:";DA$;"    TIME:";TT$
25 PRINT"0@@@@@@2@@@@@@@@@@@@@@@@."
30 PRINT"]       ]      OUTPUT"TAB(23)"]"
35 PRINT"+@@@@@@[@@@@@@@@@@@@@@@@3"
40 PRINT"]SIZE  ]";TAB(8);NM;TAB(23)"]"
50 PRINT"]THETA ]";TAB(8);TA;TAB(23)"]"
60 PRINT"]PHI   ]";TAB(8);PH;TAB(23)"]"
70 PRINT"]X CORE]";TAB(8);H1;TAB(23)"]"
80 PRINT"]Y CORE]";TAB(8);H2;TAB(23)"]"
85 PRINT"-@@@@@@1@@@@@@@@@@@@@@@@="
90 PRINT:PRINT"CHISQ FOR SEARCH",CM
95 IFBL=1THENPRINT"BOUNDARY OVERRUN"
00 RETURN
00 REM ----------------
10 REM SUBROUTINE STORE
20 REM ----------------
21 REM OUTPUT RESULTS TO DISK
30 A$(NN)=STR$(SN)+" "+DA$+" "+TT$+STR$(NM)
40 A$(NN)=A$(NN)+STR$(H1)+STR$(H2)+STR$(CM)
50 IFBL=1THENA$(NN)=A$(NN)+"BL"
55 IFJK)2THENA$(NN)=A$(NN)+"SA"
60 A$(NN)=A$(NN)+"-"
65 NN=NN+1
90 RETURN
91 F$=F$+"*"
00 $ODISK,DD,"W",F$,I$
10 FORI=0TONN:$WDISK,A$(I):NEXT
20 $CDISK
30 RETURN
```

GURE A.6 : Program SHOWERSIM

```
00 REM SHOWER SIMULATION PROGRAM
10 REM ------------------------
11 REM SIMULATES SHOWERS FALLING ON ARRAY
20 DIMX(4),Y(4),Z(4),A(4),RO(4),RA(4),AM(4),XR(4),TL(4),R$(255)
25 DIMF$(4),C(4),MM(4),MO(4),YR(4),        T(3),TA(3),PH(3)
30 DEFFNA(V)=2.772*NS*(900.6+V)/((V^.75)*(V+79)^3.25)
34 L(1)=159.1:L(2)=153.3:L(3)=253.5
35 C(0)=.01:C(1)=.0045:C(2)=.0045:C(3)=.0045:C(4)=.011
36 MM(0)=1.53:MM(1)=1.83:MM(2)=1.83:MM(3)=1.83:MM(4)=1
37 MO(0)=10.6:MO(1)=11.7:MO(2)=8.8:MO(3)=10.1:MO(4)=9.6
40 X(0)=0:X(1)=-12.3:X(2)=14.8:X(3)=.3:X(4)=-.5
45 END
50 Y(0)=0:Y(1)=-5.64:Y(2)=3.1:Y(3)=-26.8:Y(4)=-17
60 Z(0)=0:Z(1)=-4.83:Z(2)=.16:Z(3)=.18:Z(4)=.67
70 A(0)=.75:A(1)=2:A(2)=2:A(3)=2:A(4)=1
75 F$(0)="SIM0":F$(1)="SIM1":F$(2)="SIM2":F$(3)="SIM3":F$(4)="SIM4"
80 AM(0)=100:AM(1)=114:AM(2)=82:AM(3)=90:AM(4)=90
90 TL(0)=4:TL(1)=2:TL(2)=2:TL(3)=2
00 CL=75:GL=30:L=0:LL=0
10 INPUT"NO OF SHOWERS";NN
12 INPUT"TRIGGER SAVE INTERVAL";NZ
15 INPUT"DISK £";DD
20 FORK=1TONN
30 GOSUB8000
40 NS=X:GOSUB7000
50 TG=RT:PG=2*RND(1)
55 GOSUB9000
70 XC=CL*(RND(1)-.5):YC=CL*(RND(1)-.5)
80 FORI=0TO4
90 XR(I)=X(I)-XC:YR(I)=Y(I)-YC
00 NEXTI
10 SI=SIN(TH)
20 FORI=0TO4
30 D=XR(I)*XR(I)+YR(I)*YR(I)+Z(I)*Z(I)
40 D=D-(XR(I)*SI*COS(PH)+YR(I)*SI*SIN(PH)+Z(I)*COS(TH))^2
50 D=SQR(D)
55 IFD).05THEN1260
56 RA(I)=AM(I)+1
57 GOTO1310
60 RA(I)=FNA(D):RO(I)=RA(I)*A(I)*COS(TH)
70 IFRO(I)(GLTHEN1280
71 SG=SQR(RO(I)):ME=RO(I)
72 GOSUB6000
73 GOTO1290
80 GOSUB5000
90 RA(I)=X/(A(I)*COS(TH))
91 ME=RA(I)/(MM(I)*MO(I))
92 SG=C(I)
93 GOSUB6000
94 RA(I)=X*MM(I)*MO(I)
00 IFRA(I))AM(I)THENRA(I)=AM(I)+1
10 NEXTI
20 FL=1
30 FORI=0TO3
40 IFRA(I)(TL(I)THENFL=0
50 NEXTI
70 IFFL=1THENGOSUB3000
75 PRINT"£ SHOWERS ";K
77 PRINT" TRIGGERS ";L+LL*NZ
80 NEXTK
85 GOSUB3095
```

FIGURE A.6 : continued

```
00 STOP
10 REM ----------------------
00 REM SUBROUTINE DATA STORE
10 REM ----------------------
11 REM STORES SIMULATED SHOWERS ON DISK
20 NS=INT(NS+.5):TH=INT(TH*1000+.5)/1000:PH=INT(PH*1000+.5)/1000
25 TG=INT(TG*1000+.5)/1000:PG=INT(PG*1000+.5)/1000
30 XC=INT(XC*100+.5)/100:YC=INT(YC*100+.5)/100
40 FORI=0TO4:RA(I)=INT(RA(I)*100+.5)/100:NEXT
50 R$(L)=STR$(NS)+STR$(TH)+STR$(PH)+STR$(XC)+STR$(YC)
60 FORI=0TO4:R$(L)=R$(L)+STR$(RA(I)):NEXT
65 R$(L)=R$(L)+STR$(TG)+STR$(PG)+"-"
70 L=L+1
90 IFL<NZTHENRETURN
95 I$=STR$(L)
00 $ODISK,DD,"W",F$(LL),I$
10 FORI=0TOL:$WDISK,R$(I):NEXT
20 $CDISK
30 L=0:LL=LL+1
40 IFLL>4THENSTOP
50 RETURN
60 REM --------------------
00 REM SUBROUTINE POISSGEN
10 REM --------------------
11 REM GENERATES POISSONIAN FLUCTUATIONS
20 X=0
30 B=EXP(-RO(I))
40 TR=1
50 R=RND(1)
60 TR=TR*R
70 IFTR<BGOTO5090
80 X=X+1:GOTO5050
90 RETURN
00 REM --------------------
00 REM SUBROUTINE GAUSSGEN
10 REM --------------------
11 REM GENERATES GAUSSIAN FLUCTUATIONS
20 V1=2*RND(1)-1:V2=2*RND(1)-1
30 S=V1*V1+V2*V2
40 IFS>=1GOTO6020
50 X=V1*SQR(-2*LOG(S)/S)
60 X=SG*X+ME
70 RETURN
80 REM --------------------
00 REM SUBROUTINE THETAGEN
10 REM --------------------
11 REM GENERATES ZENITH ANGLE
15 N=8
20 RT=(1-RND(1))^(1/(N+1))
30 RT/2-ATN(RT/SQR(-RT*RT+1))
40 RETURN
50 REM ---------------
00 REM SUBROUTINE NGEN
10 REM ---------------
11 REM GENERATES SHOWER SIZE
20 G1=-1.5:G2=-2:A1=52:A2=36920
30 NL=1.8E4:NB=5E5:NU=1E9
40 B=A1*(NB^G1-NL^G1)
50 C=B+A2*(NU^G2-NB^G2)
60 R=RND(1)
70 IFC*R<BTHEN8100
80 X=(C*R/A1+NL^G1)^(1/G1)
90 GOTO8110
```

GURE A.6 : continued

```
00 X=((C*R-B)/A2+NB^G2)^(1/G2)
10 RETURN
00 REM ------------------
10 REM SUBROUTINE TIMEVAR
20 REM ------------------
21 REM FLUCTUATES TIMING DATA
30 SG=5
40 FORI=1TO3
50 D=X(I)*SIN(TG)*COS(PG)+Y(I)*SIN(TG)*SIN(PG)+Z(I)*COS(TG)
60 ME=D/.3+L(I)
70 GOSUB6000
80 T(I)=X
90 NEXTI
00 PH=0:TA=0:NL=0
10 FORJ=1TO2
20 T0=.3*(T(3)-L(3)):T1=.3*(T(J)-L(J))
30 E=X(J)*Y(3)-X(3)*Y(J)
80 A=(Y(3)*T1-Y(J)*T0)/E
90 B=(Y(J)*Z(3)-Y(3)*Z(J))/E
00 C=(X(J)*T0-X(3)*T1)/E
10 D=(X(3)*Z(J)-X(J)*Z(3))/E
20 F=A*B+C*D
30 G=B*B+D*D+1
40 H=(F*F-G*(A*A+C*C-1))
50 IFH<0THEN9300
60 H=SQR(H)
70 TA=(H-F)/G:S=(-H-F)/G
80 IFTA<0GOTO9490
90 IFS<0GOTO9330
00 NL=NL+J
20 GOTO9490
30 W=C+D*TA:V=A+B*TA
40 IFTA<>1GOTO9360
50 TA=0:PH=0:GOTO9470
60 IFV<>0THEN9400
70 PH/2
80 IFW<0THENPH=4.713
90 GOTO9460
00 PH=W/V

20 IFV<0GOTO9450
30 Q=0
40 IFW<0THENQ=2
50 PH=ATN(PH)+Q
60 TA(J)=-ATN(TA/SQR(-TA*TA+1))+1.5708
70 PH(J)=PH
80 IFPH(J)>=2THENPH(J)=PH(J)-2
90 NEXT
00 IFNL=3THENRETURN
10 IFNL=0THEN9530
20 PH=PH(3-NL):TH=TA(3-NL):RETURN
30 TH=(TA(1)+TA(2))/2:PH=(PH(1)+PH(2))/2
40 IFABS(PH(1)-PH(2))/2THENPH=PH/2
50 IFPH<0THENPH=PH+2
70 RETURN
```

GURE A.7 : Program COLLECTAREA

```
00 REM PROGRAM COLLECT AREA
10 REM ---------------------
20 REM DETERMINES COLLECTING AREA OF ARRAY
30 DEFFNA(V)=-ATN(V/SQR(-V*V+1))+1.5708
40 DEFFNB(V)=ATN(V/SQR(-V*V+1))
50 DEFFNQ(V)=2.772*NS*(900.6+V)/((V^.75)*(V+79)^3.25)
60 DIMX(3),Y(3),XM(3),YM(3),XR(3),YR(3),DC(3),M(3),B(3),C(3)
70 DIMDI(3),XS(2),XC(3),YC(3),XD(3),YD(3)
80 X(1)=.3:X(2)=14.8:X(3)=-12.3:Y(1)=-26.8:Y(2)=3.1:Y(3)=-5.64
90 PH=45
00 INPUT"THETA OF SHR AXIS";TH
10 TH=TH/180:PH=PH/180
20 INPUT"SHR SIZE";NS
30 L1=4:L2=2
40 L=L1:GOSUB4000
50 RC=R:L=L2:GOSUB4000
60 FORI=1TO3
70 XM(I)=X(I)*SQR(1-SIN(TH)*SIN(TH)*COS(PH)*COS(PH))
80 YM(I)=Y(I)*SQR(1-SIN(TH)*SIN(TH)*SIN(PH)*SIN(PH))
90 NEXT
00 FORI=1TO3
.0 DC(I)=SQR(XM(I)*XM(I)+YM(I)*YM(I))
20 NEXT
30 GOSUB5000
40 IFR)=RC+DC(1)THEN1370
50 K=1:F=DC(1):GOSUB2000
60 IFR)=RC+DC(2)THEN1370
70 K=2:F=DC(2):GOSUB2000
00 GOSUB6000
10 IFDI(1))=RCTHEN1310
00 K=1:GOSUB3000
.0 IFR)=RC+DC(3)THEN1370
20 K=3:F=DC(3):GOSUB2000
30 IFDI(2))=RCTHEN1350
40 K=2:GOSUB3000
50 IFDI(3))=RCTHEN1370
60 K=3:GOSUB3000
70 A=0
80 IFC(3)()0THEN1400
90 IFO)-2*(XC(3)*XM(1)+YC(3)*YM(1))THENB(3)=0
00 IFC(1)()0THEN1420
10 IFO)-2*(XC(1)*XM(1)+YC(1)*YM(1))THENB(1)=0
20 FORI=1TO3:A=A+C(I)-B(I):NEXT
30 A=A*RC*RC
40 PRINTA
50 END
60 REM -----------------
70 REM SUBROUTINE AREA B
80 REM -----------------
91 REM DETERMINE AREA B
00 T=(R*R-F*F-RC*RC)/(2*F*RC):P=(F*F+R*R-RC*RC)/(2*F*R)
10 B(K)=RC*RC*FNA(T)-R*R*FNA(P)+F*RC*SIN(FNA(T))
20 RETURN
30 REM -----------------
40 REM SUBROUTINE AREA C
50 REM -----------------
61 REM DETERMINE AREA C
70 XX=XC(K)-XD(K):YY=YC(K)-YD(K):GOSUB3500
80 G=W/2
90 FORI=0TO3
00 XT=XM(I)-XC(K):YT=YM(I)-YC(K)
```

GURE A.7 : continued

```
50 XR(I)=YT*SIN(G)+XT*COS(G)
70 YR(I)=YT*COS(G)-XT*SIN(G)
80 NEXTI
90 AA=-1
00 FORI=1TO2
10 IFI=2THENAA=1
20 L=I+K-1:IFL=4THENL=1
30 E=SQR((XR(L)-XR(0))^2+(YR(L)-YR(0))^2)
40 T=(E*E+RC*RC-R*R)/(2*E*RC)
50 T=FNA(T)
60 XX=XR(L)-XR(0):YY=YR(L)-YR(0):GOSUB3500
70 P=W:DE=P+AA*T
80 XS(I)=XR(0)+RC*COS(DE)
90 NEXTI
00 C1=-XS(1)+XR(K):C2=XS(2)-XR(L):C3=R*R/2:C4=RC*RC/2
10 C5=XS(2)-XR(0):C6=XS(1)-XR(0)
20 C(K)=C4*FNB(C5/RC)+(C5/2)*SQR(RC*RC-C5*C5)+YR(0)*XS(2)
30 C(K)=C(K)-C4*FNB(C6/RC)-(C6/2)*SQR(RC*RC-C6*C6)-YR(0)*XS(1)
40 C(K)=C(K)+(XR(K)/2)*SQR(R*R-XR(K)^2)
50 C(K)=C(K)-C3*FNB(-XR(K)/R)-(C1/2)*SQR(R*R-C1*C1)
60 C(K)=C(K)+C3*FNB(-C1/R)+YR(K)*XS(1)-(C2/2)*SQR(R*R-C2*C2)
70 C(K)=C(K)-C3*FNB(C2/R)-YR(L)*XS(2)-(XR(L)/2)*SQR(R*R-XR(L)^2)
80 C(K)=C(K)+C3*FNB(-XR(L)/R)
90 RETURN
00 REM --------------
10 W=ATN(YY/XX)
20 IFXX<0THENW=W
30 IFXX>=0ANDYY<0THENW=W+2
40 RETURN
50 REM -------------------
00 REM SUBROUTINE GREISEN
10 REM -------------------
11 REM DETERMINE DENSITIES FROM GREISEN FN
20 I=0:J=200:K=10
30 FORR=ITOJSTEPK
40 IFR=0THENR=.01
50 AN=FNQ(R)
60 IFAN>LTHEN4080
70 I=R:R=J:J=I:I=I-K:K=K/2
80 NEXT
90 IFK>=.05THEN4030
00 R=I+2*K
.0 RETURN
20 REM -----------------
00 REM SUBROUTINE ORDER
10 REM -----------------
.1 REM PUT DISTANCES IN DESCENDING ORDER
20 MX=DC(1)
30 FORI=1TO3:M(I)=I:NEXT
40 IFDC(2)<MXTHEN5060
50 M(1)=2:M(2)=1:MX=DC(2):DC(2)=DC(1):DC(1)=MX
60 IFDC(3)<MXTHEN5100
70 M(3)=M(2):M(2)=3:MX=DC(3):DC(3)=DC(2):DC(2)=MX
80 IFMX<DC(1)THEN5100
90 M(2)=M(1):M(1)=3:DC(2)=DC(1):DC(1)=MX
00 FORI=1TO2
 0 IFI=2ANDM(2)=1THENM(2)=3
20 MX=XM(I):XM(I)=XM(M(I)):XM(M(I))=MX
30 MY=YM(I):YM(I)=YM(M(I)):YM(M(I))=MY
40 NEXT
50 RETURN
60 REM --------------------
00 REM SUBROUTINE INTERSECT
```

GURE A.7 : continued

```
10 REM ---------------------
11 REM DETERMINES INTERSECTIONS OF DENSITY CONTOURS
20 FORI=1TO3
30 J=I+1
40 IFJ>3THENJ=1
50 D=SQR((XM(I)-XM(J))^2+(YM(I)-YM(J))^2)
60 T=FNA(D/(2*R)):P=FNA((XM(I)-XM(J))/D)
70 IF(YM(I)-YM(J))<0THENP=2-P
80 DE=P-T
90 DF=P+T
00 XC(I)=XM(J)+R*COS(DE)
10 XD(I)=XM(J)+R*COS(DF)
20 YC(I)=YM(J)+R*SIN(DE)
30 YD(I)=YM(J)+R*SIN(DF)
40 DI(I)=SQR(XC(I)*XC(I)+YC(I)*YC(I))
50 NEXT
60 RETURN
```

APPENDIX B

CALCULATION OF ARRAY ACCEPTANCE

B.1 CALCULATION OF THE COLLECTING AREA

The calculation of the area in which a shower of size N must fall, in order to trigger the array, is a complex problem, even for symmetrical arrays. A solution is described for an array of four triggering detectors, in which one is central and triggers on a different, higher, level to the other three. The detectors need not be in the ground plane but the central one is taken as the origin.

The collecting area for a single detector is given by a circle of radius, R, which is determined by a lateral structure function, with the appropriate triggering density and shower size inserted. For a system of several detectors, the problem is to find the area common to the circles about each detector. The more detectors, the more complex the problem becomes.

The structure function used is that due to Greisen (1960),

$$\Delta(N,r) = \frac{0.4N}{r_1^2}\left(\frac{r_1}{r}\right)^{0.75}\left(\frac{r_1}{r+r_1}\right)^{3.25}\left(1+\frac{r}{11.4r_1}\right) \text{ m}^{-2} \qquad \text{(B.1)}$$

where r_1 = 79m at sea level. This assumes an age parameter of 1.25.

Consider four detectors C, 1, 2, 3. The triggering density for C is such that the radius of the single detector acceptance area is r_c. Similarly for the others the radius r. The areas are in the plane perpendicular to the shower axis so the perpendicular distances of each detector from the axis are required. The coordinate system is, therefore, first transformed so the z-axis is parallel to the shower axis.

$$x' = x\cos\theta\cos\phi + y\cos\theta\sin\phi - z\sin\theta$$
$$y' = y\cos\phi - x\sin\phi \qquad (B.2)$$

The detectors are placed in descending order of distance from the shower axis. There are eight cases of intersection as shown in figure B.1. It is seen that the intersection points of the outer three circles, areas B and areas C have to be determined.

B.1.1 Determination of Intersection Points

Referring to figure B.2,

$$\cos\theta = \frac{d}{2r} \quad : \quad \cos\alpha = \frac{d_x}{d} \quad : \quad \delta = \alpha \pm \theta$$
$$\underline{c} = \underline{b} + \underline{r}_1 \quad : \quad x_c = x_b + r\cos\delta \; : \; y_c = y_b + r\sin\delta \qquad (B.3)$$

The required intersection point of the pair is that closest to the median point of the three detectors.

B.1.2 Areas B

Referring to figure B.3,

$$\theta_i = \cos^{-1}\left(\frac{r^2 - f_i^2 - r_c^2}{2f_i r_c}\right) \; : \quad \alpha_i = \cos^{-1}\left(\frac{r^2 + f_i^2 - r_c^2}{2f_i r}\right)$$
$$B_i = r_c^2\theta_i - r^2\alpha_i + f_i r_c\sin\theta_i \quad (\text{where } f_i = d_{ci}) \qquad (B.4)$$

B.1.3 Areas C

The axes are first transformed so that the point of intersection is at the origin and the line through the pair of relevant intersections forms the y-axis (ie. a rotation through an angle G, figure B.4).

Referring to figure B.5,

Conditions		Collecting Area
$r \geq r_c + d_{c_i}$	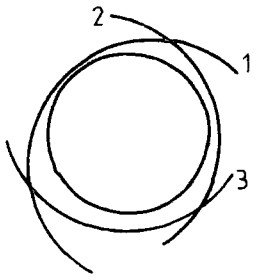	πr_c^2
$r < r_c + d_{c_i}$ $r \geq r_c + d_{c_j}$	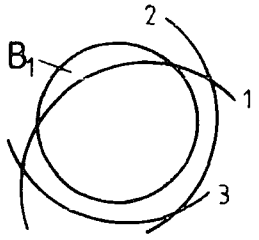	$\pi r_c^2 - B_1$
$r < r_c + d_{c_i}$ $r \geq r_c + d_{c_k}$ $d_{c_{ij}} \geq r_c$	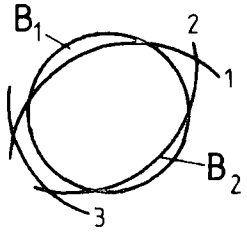	$\pi r_c^2 - B_1 - B_2$
$r < r_c + d_{c_k}$ $d_{c_{ij}}, d_{c_{ik}}, d_{c_{kj}} \geq r_c$	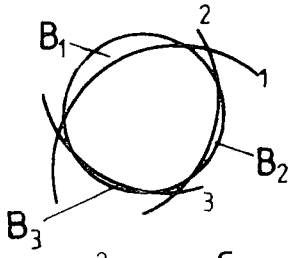	$\pi r_c^2 - \sum_{i=1}^{3} B_i$
$r < r_c + d_{c_j}$ $r \geq r_c + d_{c_k}$ $d_{c_{ij}} < r_c$	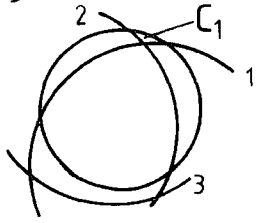	$\pi r_c^2 - B_1 - B_2 + C_1$
$r < r_c + d_{c_k}$ $d_{c_{ij}} < r_c$ $d_{c_{jk}}, d_{c_{ik}} \geq r_c$	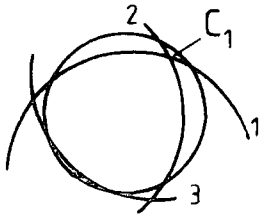	$\pi r_c^2 - \sum_{i=1}^{3} B_i + C_1$
$r < r_c + d_{c_k}$ $d_{c_{jk}}, d_{c_{ik}} < r_c$ $d_{c_{ij}} \geq r_c$	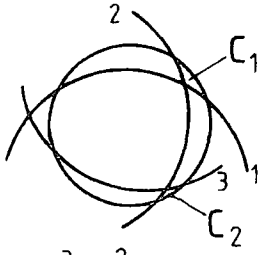	$\pi r_c^2 - \sum_{i=1}^{3} B_i + C_1 + C_2$
$r < r_c + d_{c_k}$ $d_{c_{ij}}, d_{c_{ik}}, d_{c_{jk}} < r_c$	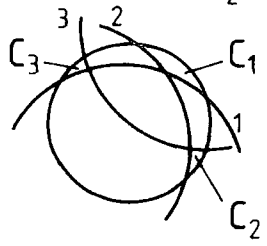	$\pi r_c^2 + \sum_{i=1}^{3} (C_i - B_i)$

FIGURE B.1 : Intersection of the collecting areas of four detectors $d_{c_{ij}}$ is the distance from C to the intersection of circles about detectors i and j.

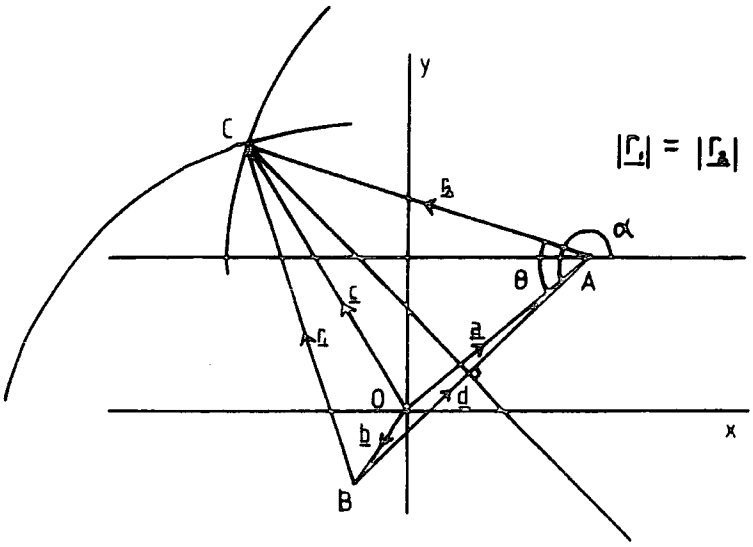

FIGURE B.2 : Determination of the intersection points of 2 circles of equal radii, with centres at A and B. (0 is the central detector, A,B are any two others)

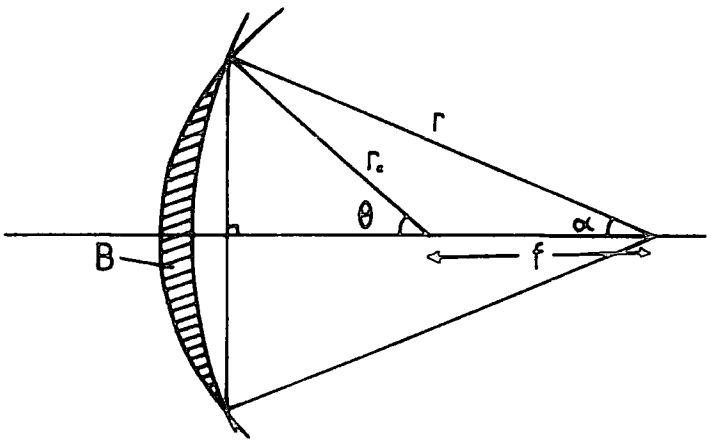

FIGURE B.3 : Determination of area B (hatched area).

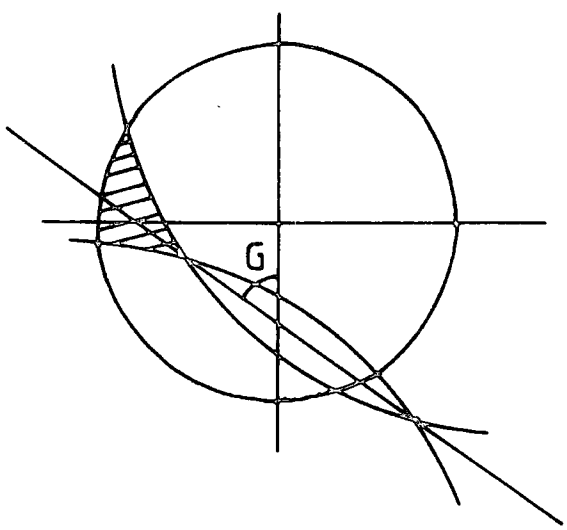

FIGURE B.4 : Definition of angle G used in the determination of area C (hatched area)

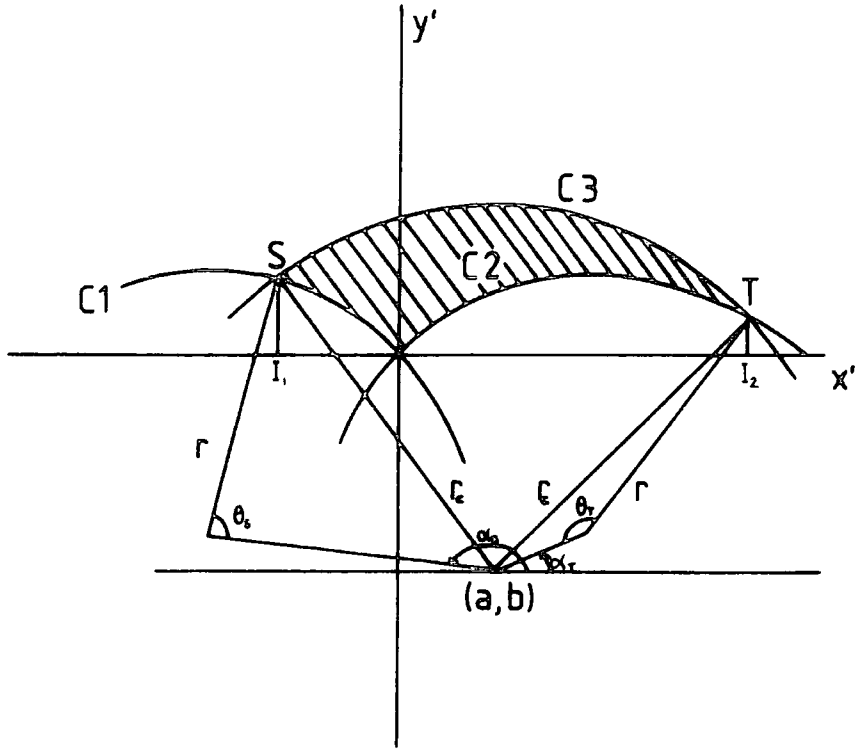

FIGURE B.5 : Determination of area C (hatched area)

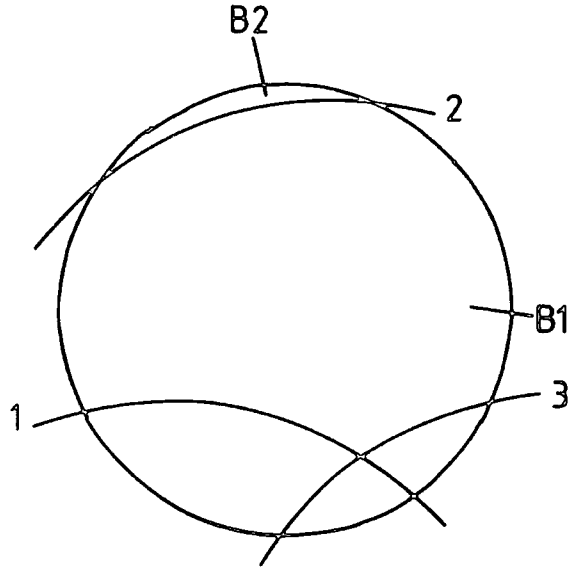

FIGURE B.6 : Enclosed areas (this problem only arises close to the minimum shower size trigger threshold)

two solutions are obtained,

$$I_1 = a - r_c \cos(\theta - \alpha)$$
$$I_2 = a + r_c \cos(\theta - \alpha - \pi) \qquad (B.5)$$

The required point is that on the same side of the y-axis as the centre of the particular detector's circle. The area can then be calculated by integration over each circle between the relevant limits.

$$C = \int_{I_2}^{I_1} C3 - \int_{I_2}^{0} C1 - \int_{0}^{I_1} C2 \qquad (B.6)$$

The relevant integral, with respect to x, for a circle of centre (a,b) and radius r is,

$$I = \int \left[b + \sqrt{r^2 - (x-a)^2} \right] dx$$
$$= \frac{r^2}{2} \sin^{-1}\left(\frac{x-a}{r}\right) + \left(\frac{x-a}{2}\right)\left(r^2 - (x-a)^2\right)^{\frac{1}{2}} + bx \qquad (B.7)$$

which must be evaluated between the relevant limits of x.

B.1.4 Special Cases

In some cases, an area B is totally enclosed by another area B, figure B.6. Because of the ordering of detectors, the possibilities are restricted to B_3 in B_2, B_2 in B_1, B_2 in B_1. The existance of any of these is determined by calculating the angle subtended at the central detector by each area B and testing if one is contained in the other. The relevant area B is set to zero as is any associated area C.

The resulting area can then be projected onto the ground plane by dividing by cosθ. Table B.1 gives collecting areas, perpendicular to the shower axis, for various combinations of shower size and axis direction for the inner ring trigger with

N	θ	AZIMUTHAL ANGLE															
		0	π/8	π/4	3π/8	π/2	5π/8	3π/4	7π/8	π	9π/8	5π/4	11π/8	3π/2	13π/8	7π/4	15π/8
2E4	0	3.8															
	30	7.3	12.4	22.5	30.2	25.9	16.9	10.1	6.9	7.1	12.2	21.1	28.1	28.8	22.6	12.7	7.5
	60	12.5	28.3	90.3	149	109	64.6	36.4	19.2	12.5	29.1	83.4	124	108	91.7	43.7	20.0
5E4	0	865															
	30	902	922	966	1004	1009	976	933	902	894	917	960	997	1009	990	948	913
	60	913	973	1143	1330	1365	1258	1127	980	912	975	1149	1325	1334	1286	1143	983
7E4	0	1694															
	30	1718	1742	1805	1862	1879	1851	1795	1743	1718	1745	1810	1867	1886	1860	1804	1748
	60	1718	1793	1998	2220	2265	2205	2010	1801	1718	1796	2004	2228	2260	2214	2018	1805
1E5	0	2992															
	30	2993	3020	3095	3173	3208	3177	3100	3024	2992	3024	3102	3183	3219	3187	3107	3028
	60	2993	3081	3316	3536	3548	3542	3332	3091	2992	3084	3324	3541	3548	3546	3339	3095
3E5	0	11117															
	30	11117	11151	11236	11312	11340	11315	11241	11155	11117	11155	11243	11321	11348	11324	11249	11159
	60	11117	11220	11372	11372	11372	11372	11372	11231	11117	11224	11372	11372	11372	11372	11372	11236
7E5	0, 30, 60	24274	(independent of azimuthal angle)														
1E6	0, 30, 60	32561	(independent of azimuthal angle)														

TABLE B.1 : Collecting area, perpendicular to the shower axis (m^2). Inner ring trigger ($\Delta_c > 4m^2, \Delta_{1,2,3,5} \geq 2m^2$)

levels of four and two particles. Figure B.7 shows how the area varies with azimuthal angle, while figures B.8 and B.9 display the variation with shower size.

B.2 ARRAY TRIGGERING RATES

In order to estimate the triggering rate, the differential number spectrum of EAS at sea level is required. This was taken from Ashton et al (1975) and is as follows:

$$\begin{aligned} R(N) &= 78 \quad N^{-2.5} \; m^{-2} \; s^{-1} \; sr^{-1} \; N^{-1} && N<9\ 10^5 \\ R(N) &= 73840 \; N^{-3.0} \; m^{-2} \; s^{-1} \; sr^{-1} \; N^{-1} && 9\ 10^5 \leq N < 5.3\ 10^7 \\ R(N) &= 10.14 \; N^{-2.5} \; m^{-2} \; s^{-1} \; sr^{-1} \; N^{-1} && N \geq 5.3\ 10^7 \end{aligned} \qquad (B.8)$$

This rate is then multiplied by the collecting area calculated for a zenith angle of 20^{o} (the mode of the intensity as a function of zenith angle) and averaged over all azimuthal angles. This results in the differential triggering rate.

This rate is per steradian, so to find the total array triggering rate showers arriving over the hemisphere have to be taken into account. The zenith angle dependence is given by,

$$I(\theta) = I(0) \cos^{n}\theta \; m^{-2} \; s^{-1} \; sr^{-1} \qquad (B.9)$$

where $n \simeq 8$ at sea-level.

The intensity of showers with zenith angles between θ and $\theta+d\theta$ is,

$$I(\theta \rightarrow \theta+d\theta) = = I(0) \; 2\pi \; \cos^{n}\theta \; \sin\theta \; d\theta \; m^{-2} \; \theta^{-1} \qquad (B.10)$$

Integrating between 0 and $\frac{\pi}{2}$ gives,

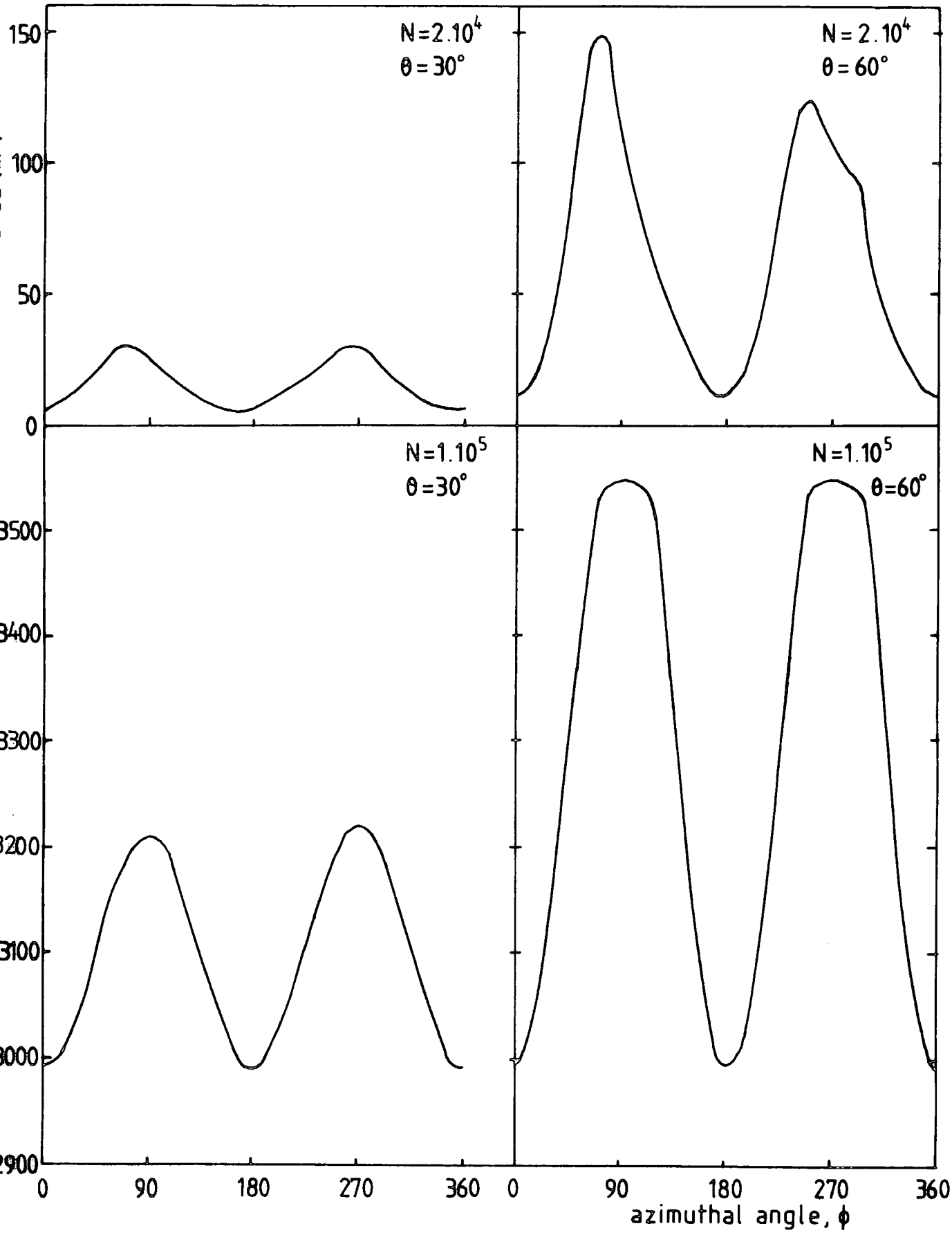

FIGURE B.7 : Collecting areas, perpendicular to the shower axis (m^2)
Inner ring trigger ($\Delta_c \geq 4m^{-2}$, $\Delta_{\text{outer}} \geq 2m^{-2}$)

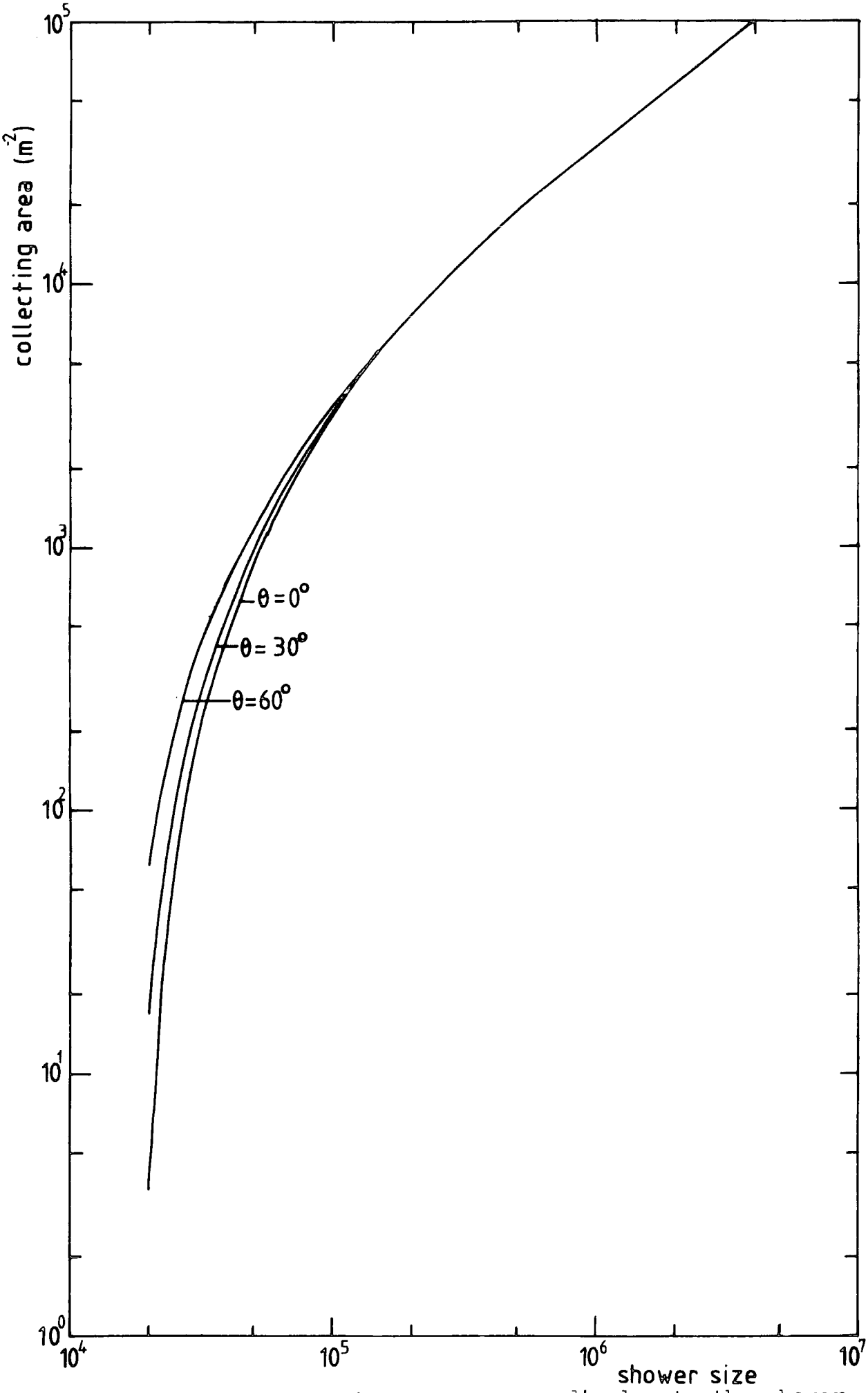

FIGURE B.8 : Mean collecting area, perpendicular to the shower axis. Inner ring trigger ($A_c \geq 4m^2; A_{II,SI,SI} \geq 2m^{-2}$)

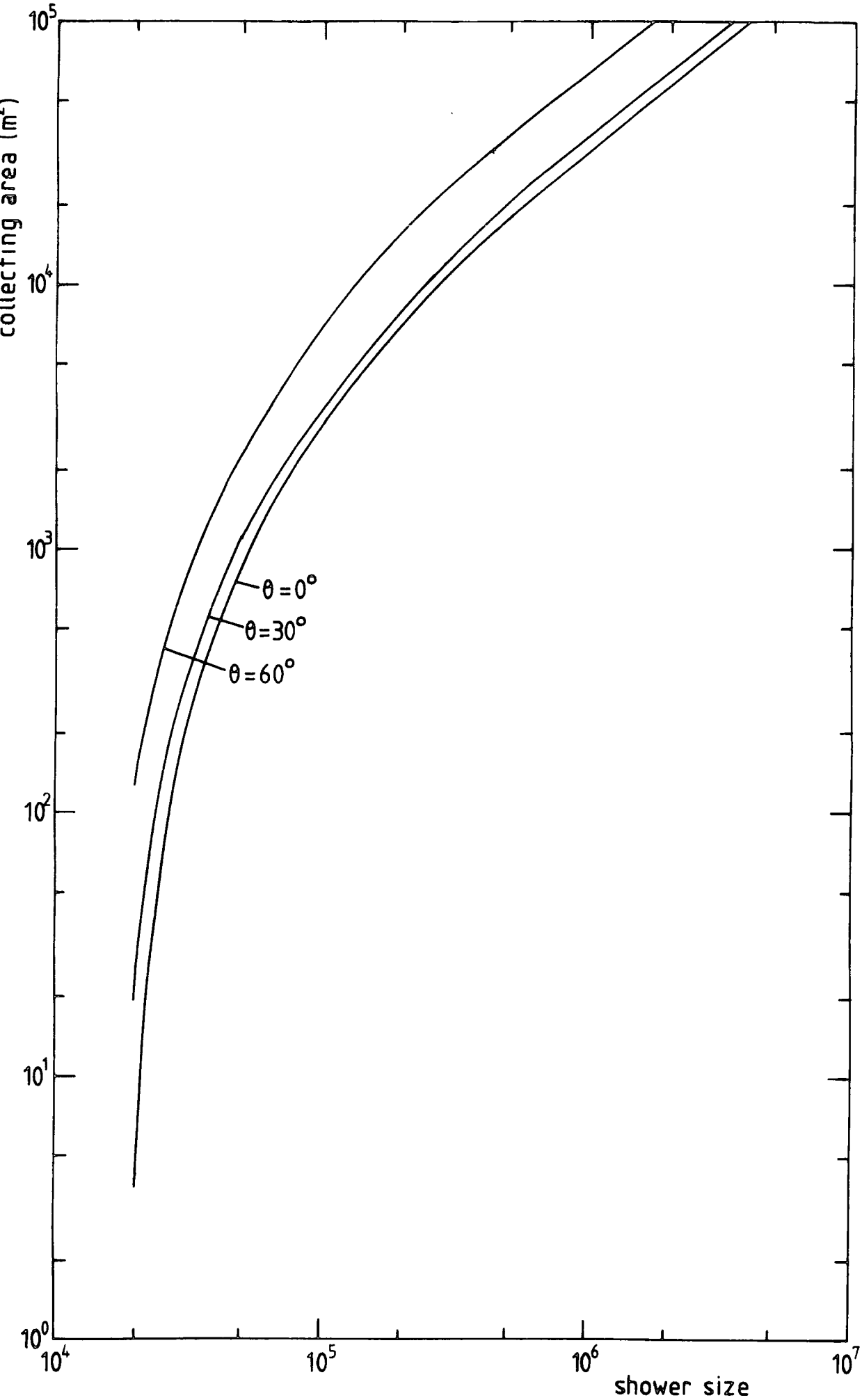

FIGURE B.9 : Mean collecting area, in the ground plane for the inner ring trigger ($\Delta_c \geq 4m^{-2}, \Delta_{n,\mu,\beta} \geq 2m^{-2}$)

$$I(0 \rightarrow \frac{\pi}{2}) = \frac{2\pi I(0)}{n+1} \qquad (B.11)$$

So the differential rate is multiplied by $\frac{2}{9}\pi$ to give the trigger rate per second per unit shower size. The resulting plot can be integrated to give the integral trigger rate per second (see figures 4.3 and 5.9).

It is also useful to estimate the rate of showers, triggering the array, which fall at a distance greater than r from the centre of the array. To estimate this, the collecting area is taken as being a circle of area equal to the collecting area calculated for the given shower size. Thus for a given r there is a shower size, N_{T_r}, below which a shower, falling outside this radius, will not trigger the array.

The differential rate is obtained by determining how many showers of size greater than N_{T_r} fall in a ring of radius r and width 1. The resulting graph can then be integrated to give the rate, greater than r, per second as a function of r.

$$R(>r) = \frac{R_T(>N_{T_r})}{\pi r^2} \int_r^\infty R(>N_{T_r}) 2\pi r dr \qquad (B.12)$$

Examples of the integral rate, greater than r, are given in figures 4.4 and 5.10.

APPENDIX C

AXIS DIRECTION DETERMINATION

At the minimum, three detectors are required in order to determine the direction of the shower axis. Let T_2, T_1 be the time difference between the shower front passing through detectors 2, 1 with respect to detector 0. Let $\hat{u}$ be the unit vector in the, upward, direction of the shower axis. In figure C.1, A1, A2 are the positions of detectors 1 and 2 respectively. B1 is a point on the line projected through A1, parallel to the shower axis, a distance cT_1. B2 is produced similarly for A2. B1, B2, 0 thus lie in the shower plane.

$$\underline{0,A1} = \underline{0,B1} + cT_1\hat{u} \qquad \underline{0,A2} = \underline{0,B2} + cT_2\hat{u} \tag{C.1}$$

$$\underline{0,A1}.\hat{u} = cT_1 \qquad \underline{0,A2}.\hat{u} = cT_2$$

$\underline{0,A1}$, $\underline{0,A2}$ are the distances of detectors 1, 2 relative to 0, ie. $\underline{r}_1, \underline{r}_2$.

$$\underline{r}_1.\hat{u} = cT_1 \qquad \underline{r}_2.\hat{u} = cT_2$$

$$\text{or} \quad \underline{r}_1.\hat{u} - cT_1 = 0 \qquad \underline{r}_2.\hat{u} - cT_2 = 0 \tag{C.2}$$

$$\therefore \; x_1\ell + y_1m + z_1n - cT_1 = 0 \qquad x_2l + y_2m + z_2n - cT_2 = 0$$

where ℓ, m, n are the components of the unit vector.

$$\therefore \quad \begin{bmatrix} x_1 & y_1 \\ x_2 & y_2 \end{bmatrix} \begin{bmatrix} \ell \\ m \end{bmatrix} = \begin{bmatrix} cT_1 - z_1n \\ cT_2 - z_2n \end{bmatrix}$$

$$\ell = \begin{vmatrix} cT_1 - z_1n & y_1 \\ cT_2 - z_2n & y_2 \end{vmatrix} \Big/ \begin{vmatrix} x_1 & y_1 \\ x_2 & y_2 \end{vmatrix} \qquad m = \begin{vmatrix} x_1(cT_1 - z_1n) \\ x_2(cT_2 - z_2n) \end{vmatrix} \Big/ \begin{vmatrix} x_1 & y_1 \\ x_2 & y_2 \end{vmatrix}$$

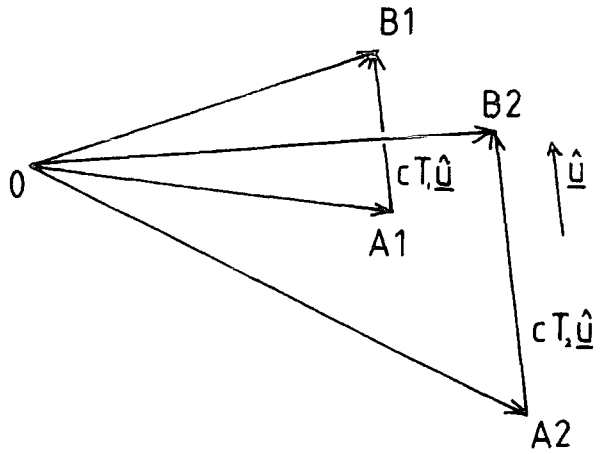

FIGURE C.1 : Axis direction determination.
0 is the central detector
A1, A2 are two other detectors
$\hat{u}$ is in the direction of the shower axis

sign		correction (radians)
W	V	
+	+	+0
+	-	+π
-	+	+2π
-	-	+π

TABLE C.1 : Corrections used in the calculation of the azimuthal angle, ϕ.

$$\therefore \quad \ell = \frac{1}{E}\begin{vmatrix} cT_1 & y_1 \\ cT_2 & y_2 \end{vmatrix} + \frac{1}{E}\begin{vmatrix} -z_1 & y_1 \\ -z_2 & y_2 \end{vmatrix}.n$$

$$m = \frac{1}{E}\begin{vmatrix} x_1 & cT_1 \\ x_2 & cT_2 \end{vmatrix} + \frac{1}{E}\begin{vmatrix} x_1 & -z_1 \\ x_2 & -z_2 \end{vmatrix}.n$$

where $$E = \begin{vmatrix} x_1 & y_1 \\ x_2 & y_2 \end{vmatrix}$$

let $A = (cT_1y_2 - cT_2y_1)/E$; $B = (y_1z_2 - y_2z_1)/E$

$C = (x_1cT_2 - x_2cT_1)/E$; $D = (x_2z_1 - x_1z_2)/E$

Now $$\hat{\underline{u}} = \begin{bmatrix} \ell \\ m \\ n \end{bmatrix} = \begin{bmatrix} \sin\theta\cos\phi \\ \sin\theta\sin\phi \\ \cos\theta \end{bmatrix}$$

$$\therefore \quad V = A + B\cos\theta \qquad W = C + D\cos\theta$$

Combining these gives,

$$\cos\theta = \frac{-(AB+CD)+((AB+CD)^2-(A^2+C^2-1)(B^2+D^2+1))^{\frac{1}{2}}}{(B^2+D^2+1)} \qquad (C.3)$$

and $$\tan\phi = \frac{W}{V} = \frac{C+D\cos\theta}{A+B\cos\theta} \qquad (C.4)$$

To ensure ϕ is in the correct quadrant, the signs of W and V have to be taken into account. The angles which require to be added to ϕ, evaluated between $-\frac{\pi}{2}$ and $+\frac{\pi}{2}$, are shown in table C.1.

In the array, as presently formed, are three timing detectors. This means it is possible to produce three values of θ and ϕ, due to statistical fluctuations in the timing information. However only two of these are independent, so θ,ϕ are determined for two detector pairs and then averaged.

APPENDIX D

TIME DELAY DISTRIBUTIONS

In order to check the operation of the fast timing measurements of the array, the distribution of the relative time differences between the shower front passing through a given detector to that through detector C was investigated. A two-fold coincidence requirement between C and the detector being investigated was used to select EAS. This distribution can be theoretically determined as follows.

The perpendicular distance from the detector to the plane of the shower front, at the time it passes through C, divided by the velocity of light, gives the time delay, D. In figure D.1, $\underline{r}$ is the vector of the detector, $\underline{s}$ is a vector in the plane of the shower front and $\hat{\underline{u}}$ is the unit vector perpendicular to the shower front.

Now
$$\underline{r} = \underline{s} + k\hat{\underline{u}} \tag{D.1}$$

$$\therefore \quad \hat{\underline{u}}.\underline{r} = k \tag{D.2}$$

Since $\hat{\underline{u}} = \begin{bmatrix} \sin\theta\cos\phi \\ \sin\theta\sin\phi \\ \cos\theta \end{bmatrix}$ and $\underline{r} = \begin{bmatrix} x \\ y \\ z \end{bmatrix}$

where x,y,z are the coordinates of the detector relative to C we get,

$$K = x \sin\theta \cos\phi + y \sin\theta \sin\phi + z \cos\theta$$

and
$$D = K/c \tag{D.3}$$

The equation is plotted for each inner ring trigger detector in figures D.2a-c. The measured delay is given by subtracting from

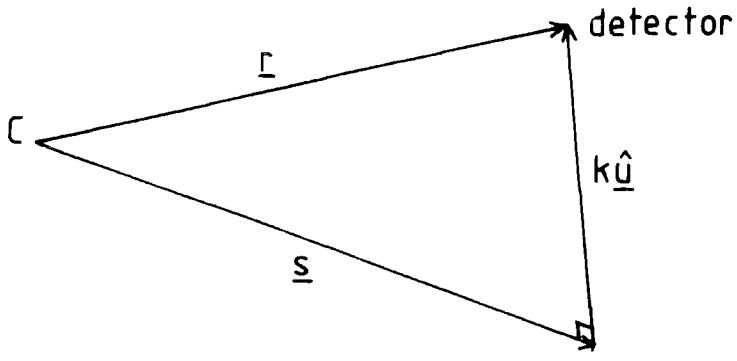

FIGURE D.1 : Calculation of the perpendicular distance of a detector to the plane of the shower front. C is the central detector and $\hat{u}$ is the unit vector in the direction of the shower axis.

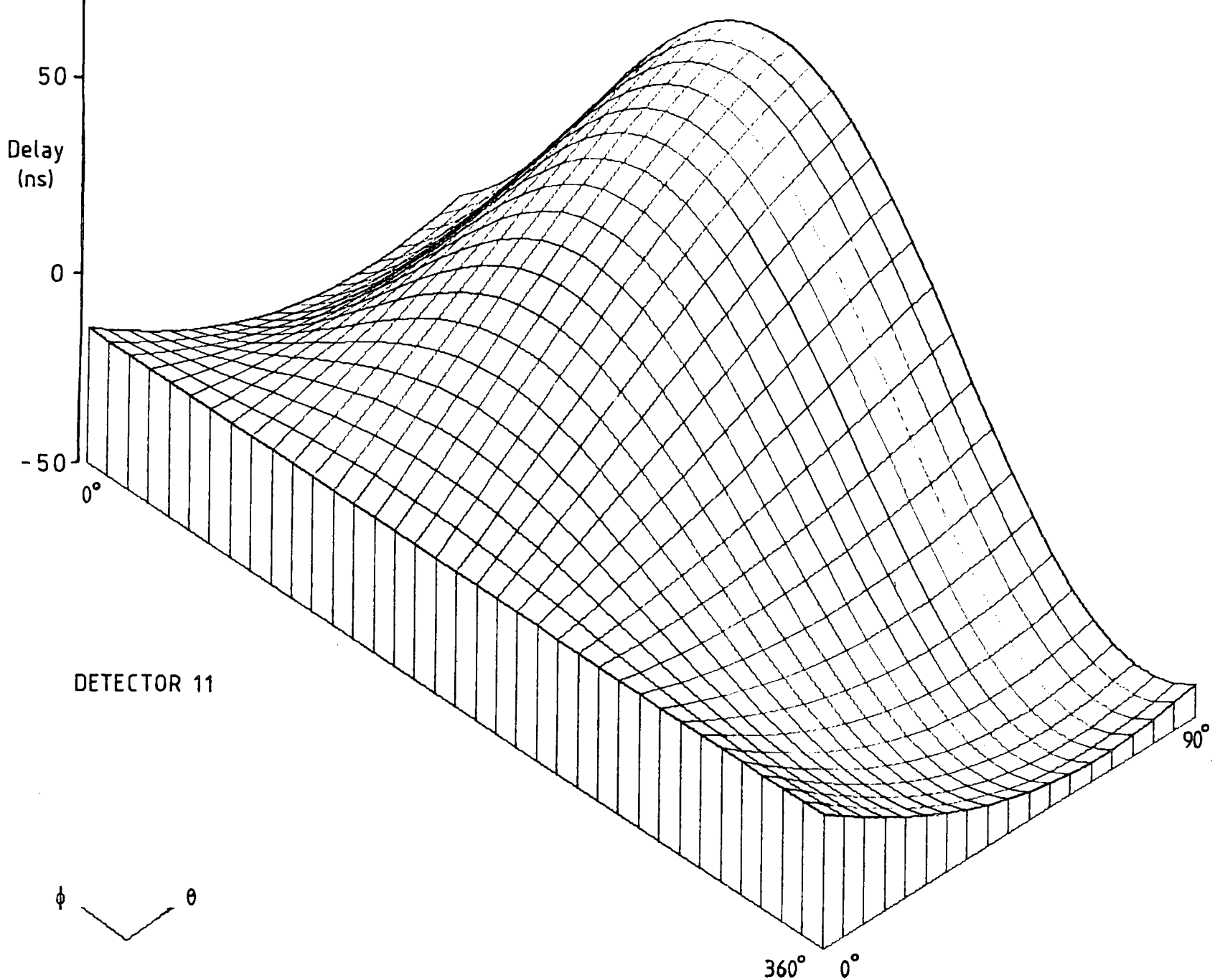

FIGURE D.2a : Calculated time delay distribution for detector 11.

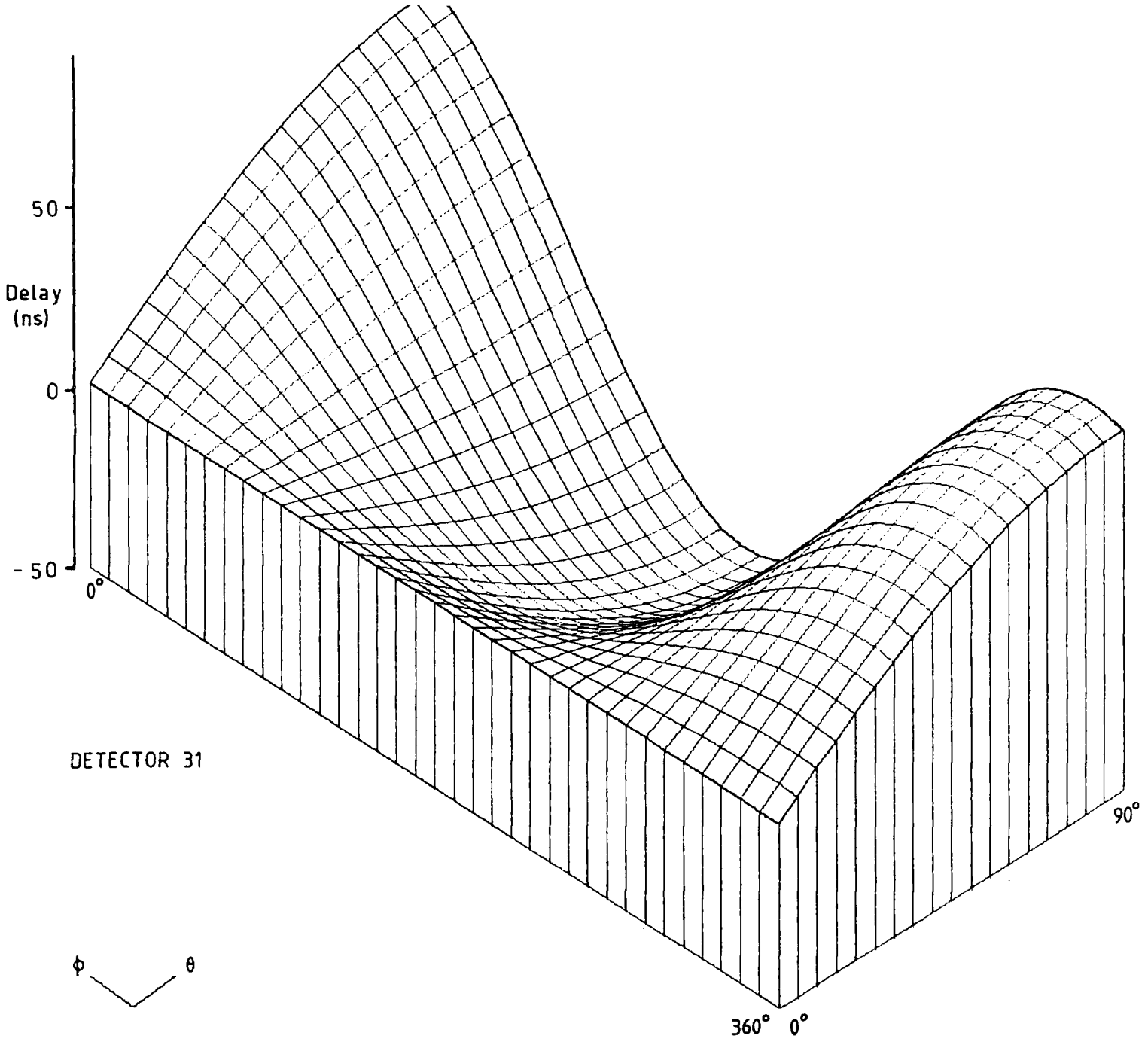

FIGURE D.2b : Calculated time delay distribution for detector 31.

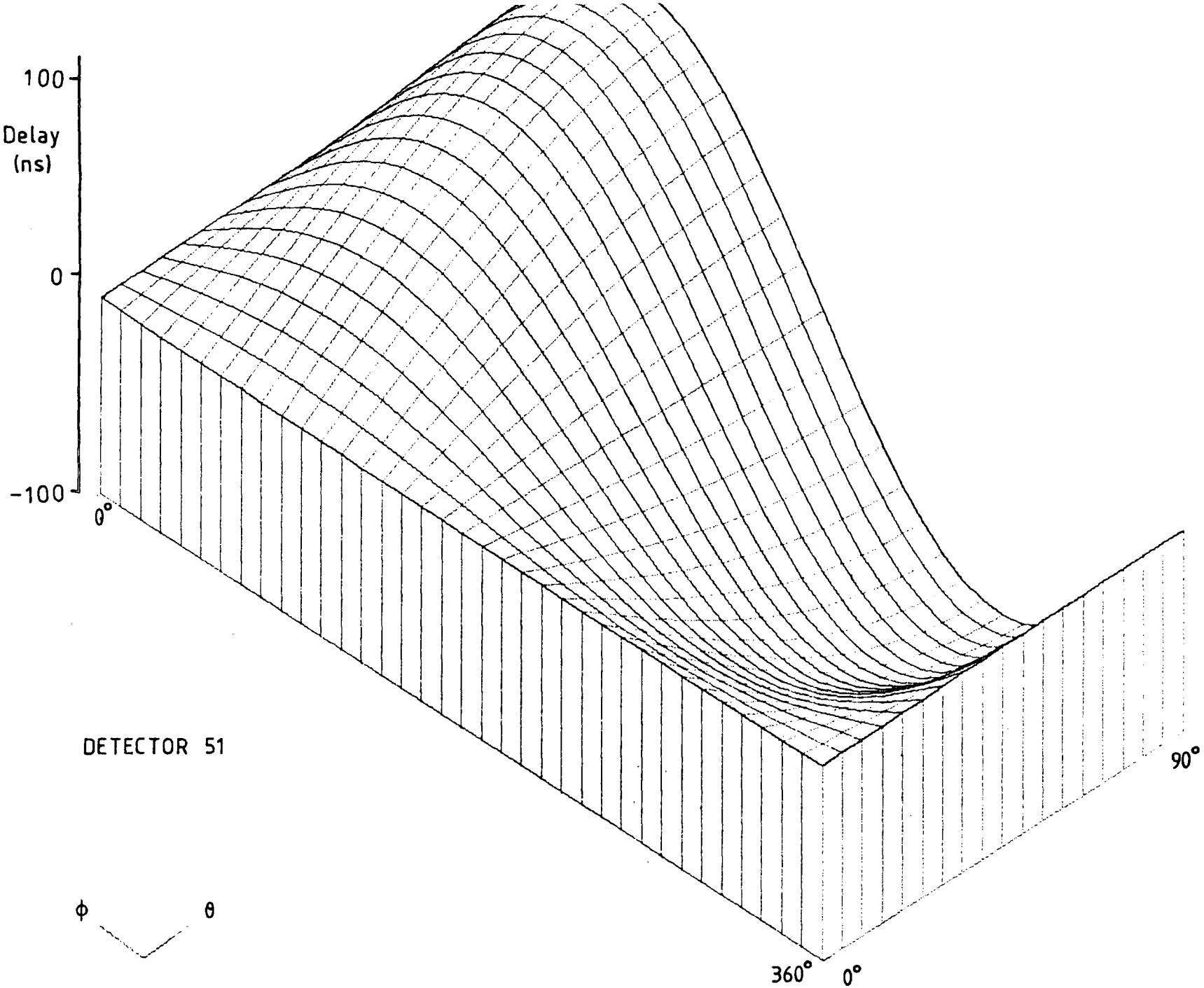

FIGURE D.2c : Calculated time delay distribution for detector 51.

D the relative difference in the cable and electronics delays for the two detectors.

A simulation program (figure D.3) was written which produces time delay distributions by generating random zenith angles, modulated by $\cos^n\theta$. Examples of these distributions are shown in figures D.4a-d. The main features are a broad peak, which is centred on the delay corresponding to a vertical shower, ie. the z-coordinate divided by the velocity of light. For detector 11, this is -16ns and for 31 and 51, 0.5ns. The large offset of the distribution for 11 also produces a slight assymmetry.

Thus, from the data, it is possible to calculate the relative cable and electronic delays and allow those directly measured to be checked. Also the variation of width (as measured by the standard deviation about the mean) with n was investigated (figure D.5). As can be seen, the width increases as n decreases, the variation being most rapid for small n. Unfortunately this is not a particularly reliable method for determining n since it lies in the 7 to 10 region where variation of n is small. The large width for 51 when compared to those for 11 and 31 is due to the fact that it is further from C than the other two detectors.

```
      DIMENSION ND(200),NU(100),NP(72),NT(45)
      REAL*8 G05CAF
      REAL FMT(1)/'*'/
      DO50 I=1,200
   50 ND(I)=0
      DO 60 I=1,45
   60 NT(I)=0
      DO 65 I=1,72
   65 NP(I)=0
      DO 70 I=1,100
   70 NU(I)=0
      X1=0.
      X2=1.
      CALL G05CCF
      READ(5,FMT)X,Y,Z,NN,N,J
      N=N+2
      AN=1./N
      DO 10 I=1,NN
      PH=G05CAF(XX)*2.*3.142
      U=G05CAF(XX)
      TR=1.-U
      TR=TR**AN
      TH=ARCOS(TR)
      IT=INT(TH*57.296/2)+1
      IP=INT(PH*57.296/5)+1
      IU=INT(U*100)+1
      IF(IP.EQ.73)THENIP=72
      NT(IT)=NT(IT)+1
      NP(IP)=NP(IP)+1
      NU(IU)=NU(IU)+1
      D=(X*SIN(TH)*COS(PH)+Y*SIN(TH)*SIN(PH)+Z*COS(TH))/.3
      ID=INT(2*(D+50.))+1
      IF(J.EQ.1)GOTO15
      ID=INT(D+100.)+1
   15 ND(ID)=ND(ID)+1
   10 CONTINUE
      WRITE(7,900)(ND(I),I=1,200)
  900 FORMAT('ND=',20I4)
      WRITE(7,910)(NU(I),I=1,100)
  910 FORMAT('NU=',20I4)
      WRITE(7,920)(NT(I),I=1,45)
  920 FORMAT('NT=',20I4)
      WRITE(7,930)(NP(I),I=1,72)
  930 FORMAT('NP=',20I4)
      STOP
      END
```

FIGURE D.3 : Program to simulate time delay distributions. G05CAF and G05CCF are NAG routines.

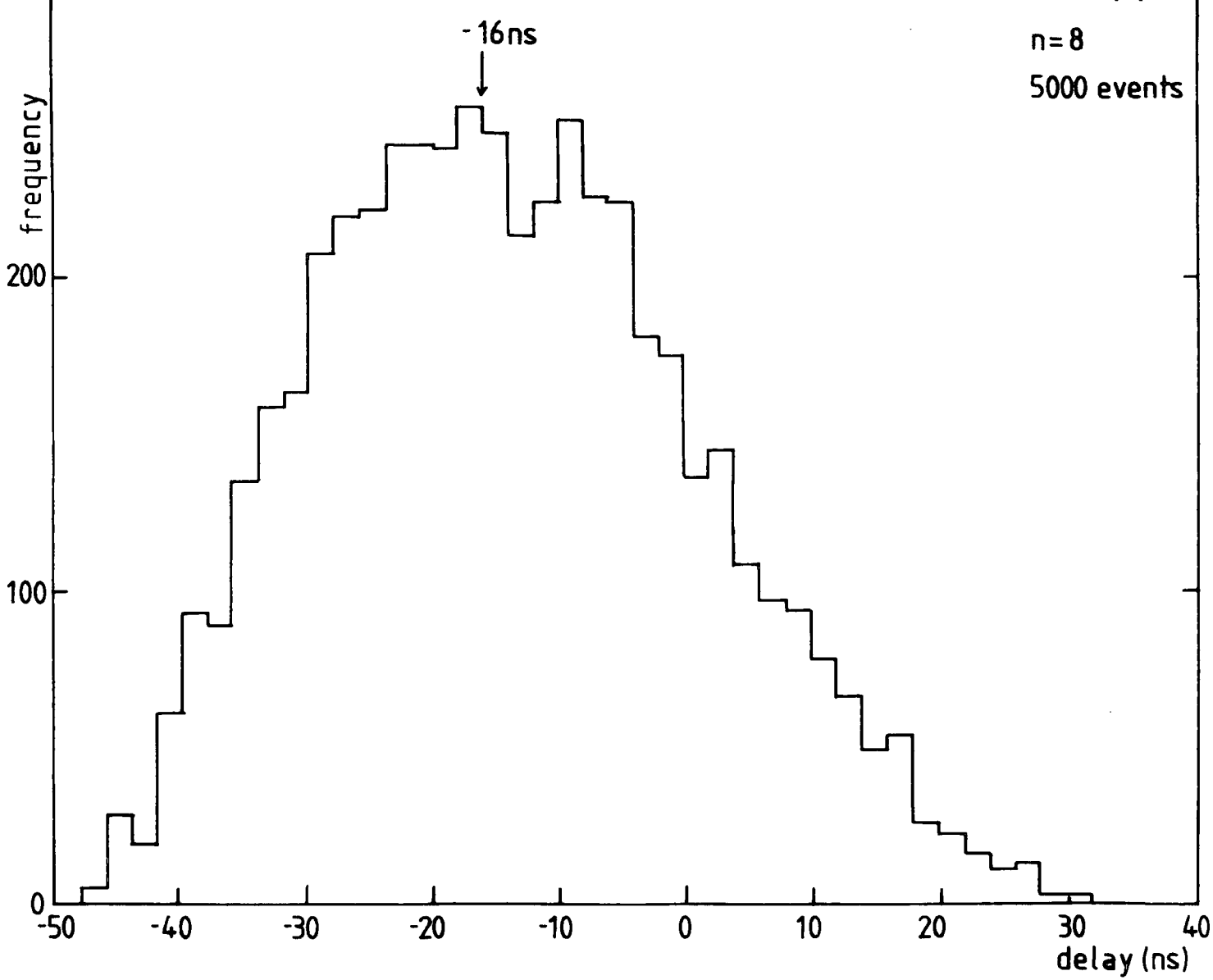

FIGURE D.4a : Time delay distribution for detector 11 with respect to detector C. (z-coordinate = -4.83m, D = -16ns)

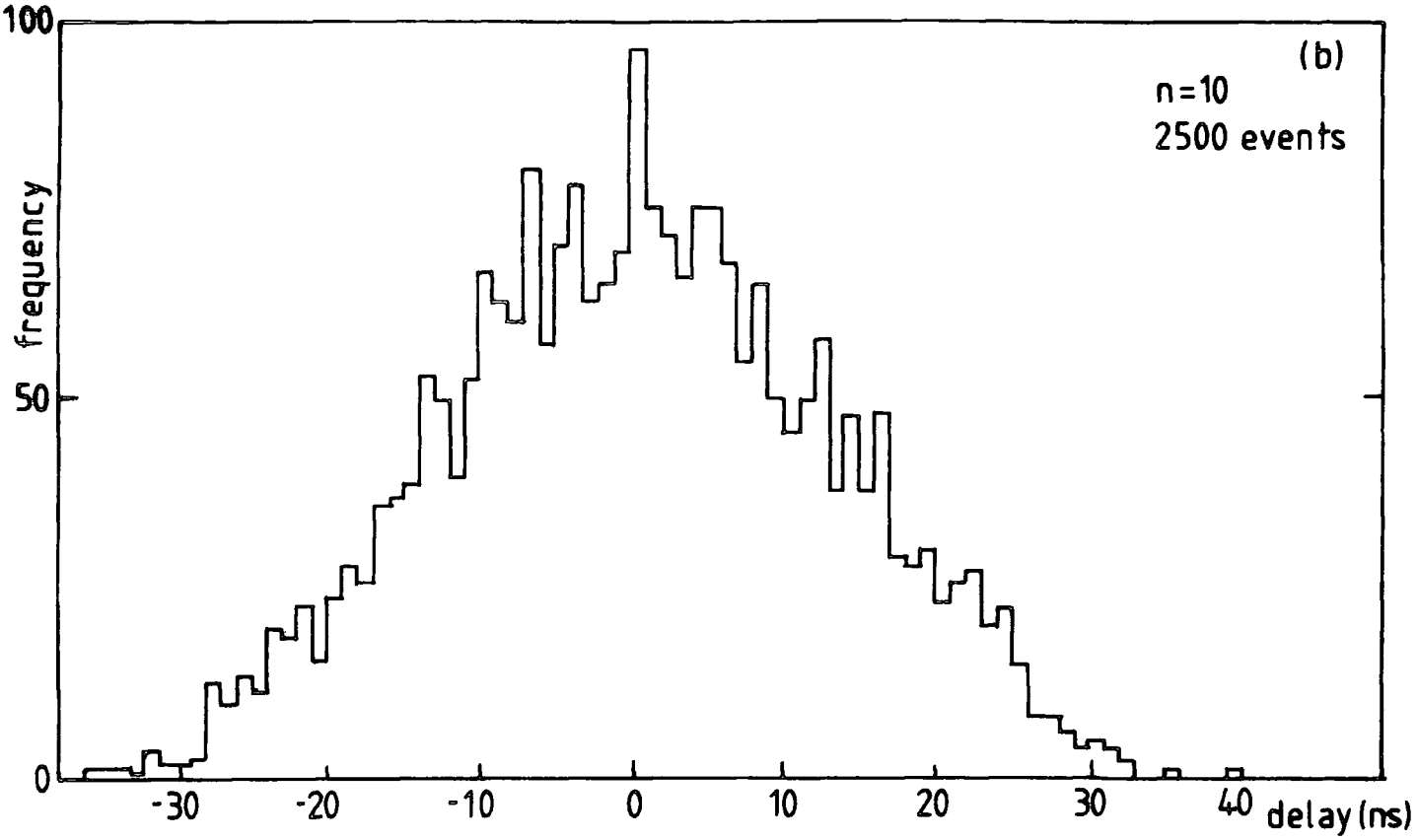

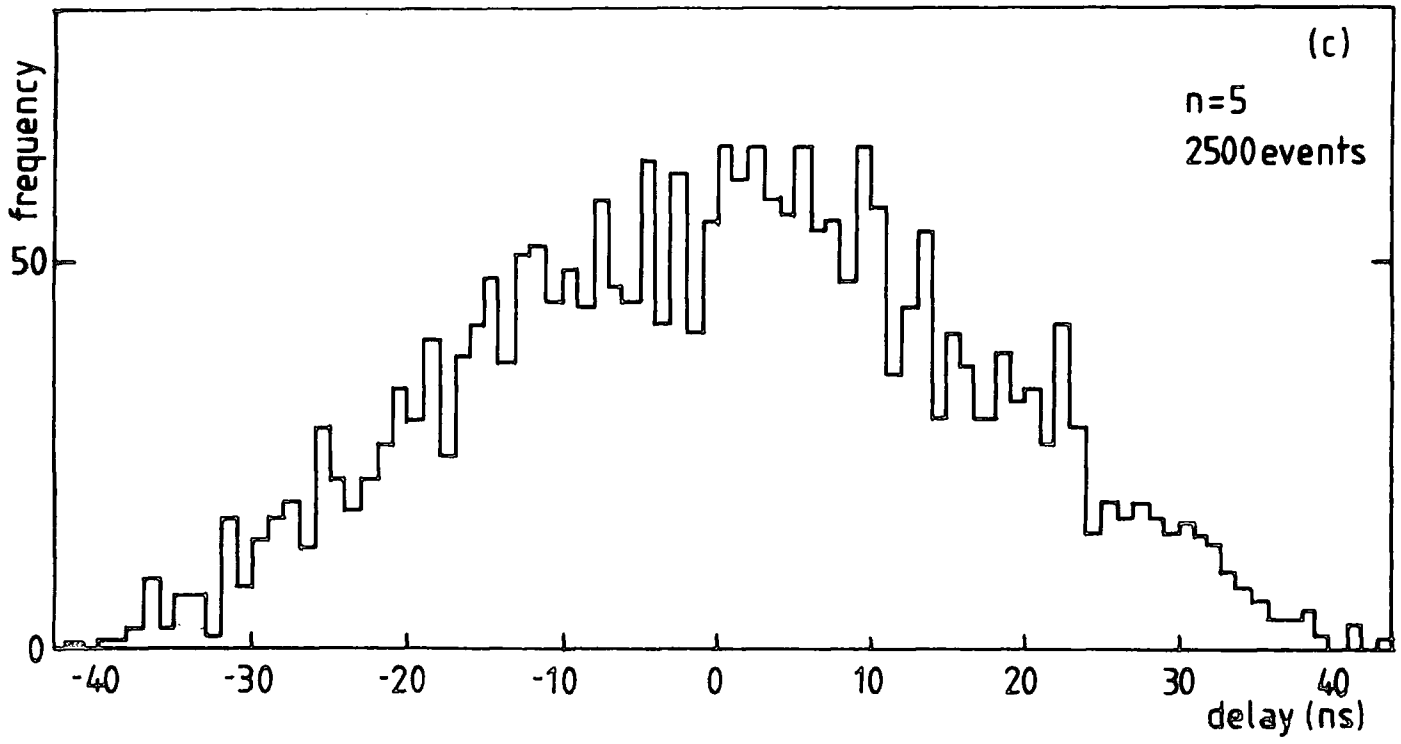

FIGURE D.4b,c : Time delay distribution for detector 31 with respect to detector C showing variation in width with varying n. (z-coordinate = 0.16m, D = 0.5ns)

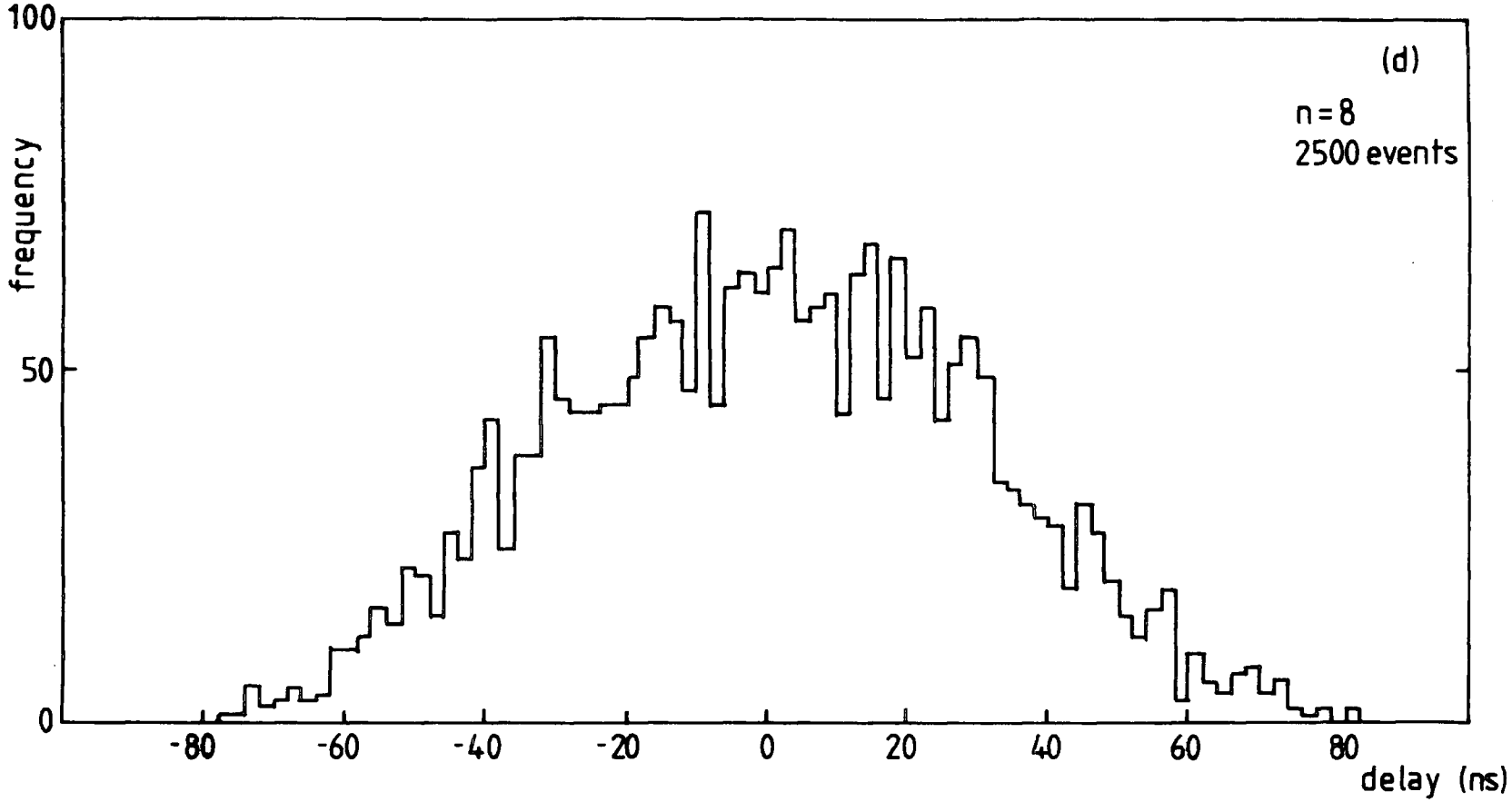

FIGURE D.4d : Time delay distribution for detector 51 with respect to detector C.
(z-coordinate = 0.18m, D = 0.5ns)

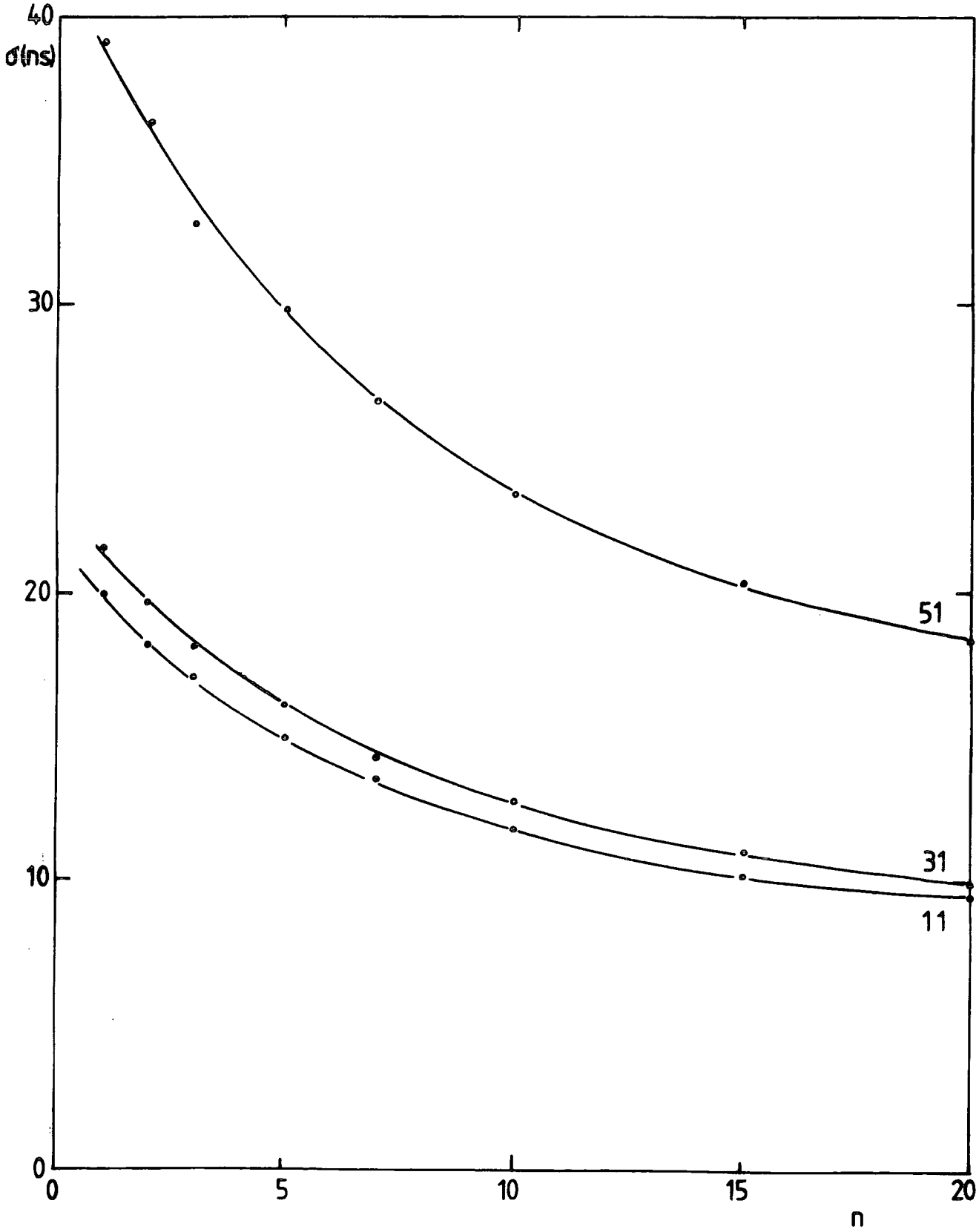

FIGURE D.5 : Variation of the width of the time distributions (as measured by the standard deviation) as a function of n.

REFERENCES

(PICCR = Proceedings of the International Conference on Cosmic Rays)

Abdrashitov, S.F., et al (1981), PICCR, Paris, 6, 156

Abdullah, M.M., et al (1979), PICCR, Kyoto, 13, 254

Abdullah, M.M. (1982), Ph.D. Thesis, University of Durham

Allan, H.R., et al (1965), PICCR, London, 2, 678

Alväger, T., et al (1963), Nature, 197, 1191

Alvåger, T. and Kreisler, M.N. (1968), Phys.Rev., 171, 1357

Andreyev, Yu.M., et al (1979), PICCR, Kyoto, 10, 184

Antippa, A.F. and Everett, A.E. (1971), Phys.Rev., D4, 2198

Antippa, A.F. (1972), Nuov.Cim A, 10, 389

Antippa, A.F. and Everett, A.E. (1973), Phys.Rev., D8, 2352

Antonov, R.A. (1974), Sov.J.Nucl.Phys., 19, 1053

Aarons, M.E. and Sudarshan, E.C.G. (1968), Phys.Rev., 173, 1622

Asakimori, K., et al (1981), PICCR, Paris, 6, 301

Ashton, F. and Pavaresh, A. (1975), PICCR, Munich, 8, 2719

Ashton, F., et al (1977a), PICCR, Plovdiv, 12, 172

Ashton, F., et al (1977b), PICCR, Plovdiv, 7, 370

Ashton, F., et al (1977c), PICCR, Plovdiv, 8,2

Ashton, F., et al (1979), PICCR, Kyoto, 13, 238

Auger, P., et al (1939), Rev.Mod.Phys., 11, 288

Baltay, C., et al (1970), Phys.Rev., D1, 759

Bartlett, D.F. and Lahana, M.D. (1972), Phys.Rev., D6, 1817

Bartlett, D.F., et al (1978), Phys.Rev., D18, 2253

Basano, L. (1980), Found.Phys., 10, 937

Bennett, S., et al (1962), J.Phys.Soc.Japan.Suppl.AIII, 17, 196

Bethe, H.A. and Heitler, W. (1934), Proc.Roy.Soc., A146, 83

Bhat, C.L., et al (1979), PICCR, Kyoto, 8, 57

Bhat, P.N., et al (1979), J.Phys.G., 5, L13

Bilaniuk, O.M.P. and Sudarshan, E.C.G. (1962), Am.J.Phys., 30, 718

Blackett, P.M.S. and Occhialini, G.P.S. (1933), Proc.Roy.Soc., A139, 699

Blandford, R.D., et al (1977), Nature, 267, 211

Bludman, S.A. and Ruderman, M.A. (1968), Phys.Rev., 170, 1176

Bothe, W. and Kolhörster, W. (1928), Naturwiss, 16, 1044

Bothe, W. and Kolhörster, W. (1929), Zeit.fur Physik, 56, 751

Bower, A., et al (1981), PICCR, Paris, 9, 166

Bradt, H., et al (1965), PICCR, London, 2, 715

Brecher, K. (1977), Phys.Rev.Lett., 39, 1051

Brodio, M.M. and Taylor, J.G. (1968), Phys.Rev., 174, 1606

Camerini, U., et al (1951), Phil.Mag., 42, 1241

Catz, P., et al (1973), PICCR, Denver, 4, 2495

Catz, P., et al (1975), PICCR, Munich, 12, 4329

Chamberlain, O., et al (1955), Phys.Rev., 100, 947

Chudakov, A.G., et al (1960), PICCR, Moscow, 2, 50

Clark, G.W., et al (1958), Nuov.Cim.Supp., 8, 623

Clay, J. (1927), Proc.Roy.Acad.Amsterdam, 30, 1115

Clay, J. (1932), Proc.Roy.Acad.Amsterdam, 35, 1282

Clay, R.W. and Crouch, P.C. (1974), Nature, 248, 28

Clay, R.W. and Gerhardy, P.R. (1982), Aust.J.Phys., 35, 59

Cocconi, G. (1961), Handbuch der Physik, 46i, 215

Cohen, M.H., et al (1977), Nature, 268, 405

Cooper, J.C. (1979), Found.Phys., 9, 461

Crouch, P.C., et al (1981), Nucl.Ins.Meth., 179, 467

Danburg, J.S., et al (1971), Phys.Rev., D4, 53

Danburg, J.S. and Kalbfleisch, G.R. (1972), Phys.Rev., D5, 1575

Davis, M.B., et al (1969), Phys.Rev., 183, 1132

De, A.K., et al (1971), Il Nuov.Cim., 3B, 115

DeBeer, J.F., et al (1966), Proc.Phys.Soc., 89, 567

Dedenko, L.G., et al (1975), PICCR, Munich, 8, 2731

DeSitter, W. (1913), Proc.Amsterdam Acad., 16, 395

Delvaille, J., et al (1960), PICCR, Moscow, 2, 101

Dhar, J. and Sudarshan, E.C.G. (1968), Phys.Rev., 174, 1808

Dixon, H.E., et al (1974), Proc.Roy.Soc.London A, 337, 133

Earnshaw, J.C., et al (1967), Proc.Phys.Soc., 90, 91

Efimov, N.N., et al (1973), PICCR, Denver, 4, 2378

Elbert, J.W., et al (1976), J.Phys.G, 2, 971

Elster, J. and Geitel, H. (1899), Physik.Z., 1, 11

Emery, M.W., et al (1975), PICCR, Munich, 7, 2486

Everett, A.E. (1976), Phys.Rev., D13, 795

Fegan, D.J., et al (1975), PICCR, Munich, 7,2480

Fegan, D.J. (1981), PICCR, Paris, 5, 55

Feinberg, G. (1967), Phys.Rev., 159, 1089

Feinberg, G. (1978), Phys.Rev., D17, 1651

Fermi, E. (1949), Phys.Rev., 75, 1169

Feynman, R.P. (1949), Phys.Rev., 76, 749

Filippas, T.A. and Fox, J.G. (1964), Phys.Rev., 135, 1071

Fox, J.G. (1965), Am.J.Phys., 33, 1

Fritze, R., et al (1970), Acta.Phys.Acad.Sci.Hung., 29, Supp3, 439

Gaisser, T.K. and Hillas, A.M. (1977), PICCR, Plovdiv, 8, 353

Gaisser, T.K., et al (1978), Rev.Mod.Phys., 50, 859

Gawin, J., et al (1968), Can.J.Phys., 46, 5104

Gerasimova, N.M. and Zatsepin, G.T. (1960), Sov.Phys.JETP, 11, 899

Ginzburg, V.L. and Syrovatskii, S.I. (1964), "The Origin of Cosmic Rays", Pergamon Press, New York

Goldoni, R. (1972), Lett.Nuov.Cim., 5, 495

Goldoni, R. (1973), Il Nuov.Cim., 14A, 501

Green, J.R. and Barcus, J.R. (1959), Il Nuov.Cim., 14, 1356

Greisen, K. (1956), Prog.in Cosmic Ray Phys., III, Ch3

Greisen, K. (1960), Ann.Rev.Nucl.Phys., 10, 63

Greisen, K. (1966), Phys.Rev.Lett., 16, 748

Grieder, P.K.F. (1977), Rev.Nuov.Cim., 7, 1

Grigorov, N.L., et al (1970), Sov.J.Nucl.Phys, 11, 588

Hammond, R.T., et al (1977), PICCR, Plovdiv, 8, 281

Hara, T., et al (1981), PICCR, Paris, 6, 250

Hasegawa, H., et al (1962), J.Phys.Soc.Japan, AIII, 17, 189

Hazen, W.E., et al (1975), Nucl.Phys., B96, 401

Hess, V.F. (1911), Physik.Z., 12, 998

Hess, V.F. (1912), Physik.Z., 13, 1084

Hillas, A.M. (1970), Acta.Phys.Hung., 29, Supp3, 355

Hillas, A.M. (1975), Phys.Reports (Phys.Lett.C), 20C, 61

Hillas, A.M. and Lapikens, J. (1977), PICCR, Plovdiv, 8, 460

Hillas, A.M. (1979), PICCR, Kyoto, 8, 7

Hillas, A.M. (1981), PICCR, Paris, 6, 244

Johnson, T.H. (1935), Phys.Rev., 48, 287

Juliusson, E. (1975), PICCR, Munich, 8, 2689

Kameda, T., et al (1965), PICCR, London, 2, 681

Karakula, S., et al (1974), J.Phys., A1, 437

Kempa, J. (1976), Nuov.Cim., 31A, 568

Khristianasen, G.B., et al (1971), PICCR, Hobart, 3, 1074

Khristianasen, G.B., et al (1981), PICCR, Paris, 6, 39

Knuth, D.E. (1981), "The Art of Computer Programming, Vol.2", Addison Wesley

Kolhörster, W. (1913), Phys.Zeits., 14, 1153

Kowalczynski, J.K. (1978), Phys.Lett., 65A, 269

Kowalczynski, J.K. (1979), Phys.Lett., 74A, 157

La Pointe, M., et al (1968), Can.J.Phys., 46, 568

Lattes, C.M.G., et al (1947), Nature, 160, 453

LeMaitre, G. and Vallarta, M.S. (1933), Phys.Rev., 43, 87

Lemke, H. (1975), Nuov.Cim., 27A, 141

Lemke, H. (1976a), Nuov.Cim., 35A, 181

Lemke, H. (1976b), Lett.Nuov.Cim., 17, 209

Longair, M.S. (1981), "High Energy Astrophysics", Cambridge

McCaughan, J.B.T. (1982), J.Phys.G., 8, 413

Maccarrone, G.D. and Recami, E. (1980), Found.Phys., 10, 949

Matano, T. (1970), Acta.Phys.Hung., 29, suppl, 451

Marchildon, L., et al (1979), Il Nuov.Cim., 53B, 253

Masline, G.C., et al (1968), Can.J.Phys., 46, S1116

Millikan, R.A. and Cameron, G.H. (1926), Phys.Rev., 28, 851

Miyake, S., et al (1962), J.Phys.Soc.Japan, 17, AIII, 240

Narlikar, J.V. and Sudarshan, E.C.G. (1976), MNRAS, 175, 105

Nishimura, J. and Kamata, K. (1958), J.Suppl.Prog.Theo.Phys., 6, 93

Pavaresh, A. (1975), Ph.D Thesis, Durham University

Pavlopoulus, T.G. (1967), Phys.Rev., 159, 1106

Prescott, J.R. (1975), PICCR, Munich, 7, 2474

Ramana Murthy, P.V. (1971), Lett.Nuov.Cim., 1, 908

Recami, E. and Mignani, R. (1974), Riv.Nuov.Cim., 4, 209

Recami, E. (1978), (ed), "Tachyons, Monopoles and Related Topics", North Holland

Ritz, W. (1911), "Oeuvres", Gauthier-Villars, Paris

Robinett, L. (1978), Phys.Rev., D18, 3610

Rossi, B. (1935), Proc.Int.Conf.Phys., I, 238

Rutherford, E. and Cooke, H.L. (1903), Phys.Rev., 16, 1st ser., 183

Sadeh, D. (1963), Phys.Rev.Lett., 10, 271

Santilli, R.M. (1982), Il Nuov.Cim., 33, 145

Schwartz, C. (1982), Phys.Rev., D25, 356

Skobeltzyn, D. (1927), Zs.f.Phys., 43, 371

Smith, A.C. (1976), Ph.D Thesis, Durham University

Smith, G.R. and Standil, S.,(1977), Can.J.Phys., 55, 1280

Street, J.C. and Stevenson, E.C. (1937), Phys.Rev., 52, 1003

Størmer, C. (1930), Z.Astrophys., 1, 237

Tanaka, S. and Inove, T. (1979), PICCR, Kyoto, 2, 277

Teucher, M. (1952), Zeits.f.Naturfor., 7a, 61

Thompson, M.G. (1973), "Cosmic Rays at Ground Level", ed. Wolfendale, A.W., Inst.of Physics, London

Tolman, R.C. (1917), "The Theory of Relativity of Motion", Univ. California Press

Vernov, S.N., et al (1964), Izvest.Akad.Sci.,USSR, 28, 1886

Vernov, S.N., et al (1968a), Can.J.Phys., 46, S110

Vernov, S.N., et al (1968b), Izvest.Akad.Sci.,USSR, 32, 458

Vernov, S.N., et al (1970), Acta.Phys.Hung., 3, 429

Walstad, A. (1979), Found.Phys., 9, 371

Wdowczyk, J. and Wolfendale, A.W. (1979), PICCR, Kyoto, 2, 154

Wilson, C.T.R. (1901), Proc.Roy.Soc., 68, 151

Wolfendale, A.W. (1973), "Cosmic Rays at Ground Level", Inst. of Physics

Yukawa, H. (1935), Proc.Phys.-Math.Soc.Japan, 17, 48